Transplantation for Microglia Replacement:
Grafting Therapeutic Strategies for RNASET2-deficient Leukodystrophy in a Zebrafish Model

Holly Ann Rutherford

Supervised by Prof. Stephen Renshaw, Dr Noémie Hamilton,
Dr Andrew Grierson, Dr Christopher Duncan and Prof. Sophie Hambleton

A thesis submitted in partial fulfilment of the requirements
for the degree of Doctor of Philosophy

The University of Sheffield
School of Medicine & Population Health
Division of Clinical Medicine

1st October 2024

Acknowledgments

My first and most resounding thank you must go to my incredibly supportive supervisory team, without whom I would never have even started this PhD, let alone finished it. To Noémie, thank you for inspiring a love of research that will stay with me for the rest of my life. Your continuous support, encouragement and advice – in and outside of the lab – has been invaluable throughout the last few years, and your commitment to my development as both a scientist and an individual has shaped my outlook on the future. To Steve, thank you for always making time to share your wisdom and guidance, and for cultivating such a wonderful place to work. Thank you all for continuously sharing my excitement about this research and reminding me to celebrate the wins when all I could see was hurdles.

An endless thank you to the entire D31 extended family, past and present – you have truly felt like family to me over the last six years. A particular thank you to Cat and Dave, for sharing your immeasurable expertise, tolerating my endless questions and always doing it with a smile. Together, you have provided me with so many wonderful memories, laughter and friendships, and I will miss you all dearly. Thank you also to the core facilities that made this work possible: Darren and Nick in the LMF, Sue in the Flow Cytometry Facility, and the entire BSU Aquarium team. A special mention must go to Susie and Mike, who have dealt with any number of queries and crises of confidence over the last four years.

I am truly indebted to the wonderful patients and families who have so generously and courageously shared their time and experiences with me throughout my PhD. The community's optimism and excitement about my research was genuinely inspiring, and I thought of your kind words and questions every time I felt like giving up. A huge thank you to the teams at Alex TLC, the United Leukodystrophy Foundation and a Sisters' Hope Foundation for welcoming me into the community and allowing me to share my work.

I am fortunate to have had wonderful friends in Sheffield and beyond, who have supported – and occasionally dragged – me through the last four years. Jelle, thank you for bringing so much laughter to every PhD milestone from start to finish; I am so happy we got to share this journey. Jess, Topher, Tom, Zoë, Nils and Ibrahim – thank you for ensuring I laughed at the back of the lab a lot more than I cried. Becca, Shammah, Lucy and George – thank you for always making space for me amidst so many life events and changes, and for being the very definition of friends that fill your cup.

A huge thank you to Stuart Gaines, who has been the most amazing partner – in the lab, and in life – over the last five years. Thank you for celebrating every transplant, qPCR result and TUNEL with me. Thank you for letting me talk about exciting experiments (or, more often, very boring troubleshooting) at 10pm when the working day was long since finished. Thank you for reminding me when it's time to come home for the day, and most importantly, for making home such a wonderful place to come back to. I could not have asked for a better person to share this chapter of my life with.

And finally, overwhelming thanks to my wonderful, endlessly supportive family. To Connor, Kaitlin, Shaun and Debbie, thank you for creating so many moments of pure laughter, dancing and joy – I will always treasure our family madness. To my Dad, for always inspiring the scientist within me, ever since I was a little girl determined to become a marine biologist (I did end up working with fish, in the end!). To Les, for always being there and never ever doubting me – whether it was a GCSE mock exam or my Oxford finals, your unwavering belief that my best would always be good enough has driven me through the last decade (as have you, to be fair – thank you also for the thousands of miles of lifts). To my dear Nan, who was always so vocally proud of me despite having very little idea what it was I actually did – you continue to be with me every step of the way. And finally, but most importantly, to my amazing, inspiring, unstoppable Mum – thank you for creating a world for us where I could be whatever I wanted to be, despite all the hurdles in our way. I have never been afraid to chase my dreams knowing I could come home to you. Thank you for being my therapist, my proof-reader, my sounding board, my biggest cheerleader and my best friend. I am eternally grateful for your endless love and advice, and for being such a pillar of strength when I've struggled. You have always, and will always, be my ultimate role model.

Summary

As the principle immune cells of the central nervous system, microglia have critical roles in neurodevelopment and homeostasis. However, aberrant microglial function has also been associated with a variety of neurodevelopmental and neurodegenerative disorders. One such condition is Ribonuclease T2 (RNASET2)-deficient leukodystrophy; a rare, heritable white matter disorder characterised by psychomotor impairments, neuroinflammation and infantile onset. Research using the *rnaset2* mutant zebrafish – one of the few animal models to recapitulate patient phenotypes – has demonstrated that microglial dysfunction is one of the earliest signs of neuropathology in this disorder, with *rnaset2*-deficient microglia failing to clear apoptotic cells during development. As such, I hypothesised that microglia are the cellular drivers of RNASET2-deficient leukodystrophy, and that replacing these dysfunctional cells will have therapeutic benefits in this disease. I therefore aimed to further characterise the contribution of microglial dysfunction to *rnaset2* mutant pathology, establish a methodology for the replacement of these deficient cells and assess the impact of this intervention on pathogenesis. To address these aims, I developed a novel strategy for microglia depletion and replacement in zebrafish larvae through transplantation of haematopoietic stem cell (HSC)–derived macrophages into embryonic hosts. Using live imaging and tissue clearing, I demonstrated that transplant-derived cells engraft within the brains of zebrafish larvae and persist into juvenile stages. In *rnaset2* mutants, transplantation was able to clear the apoptotic cell burden, and rescue overactivation of the antiviral immune response, as confirmed by RNA sequencing. Finally, this reduction in neuroinflammation resulted in behavioural rescue in transplanted animals – restoring *rnaset2* mutant motor function. Together, this data demonstrates that microglia are key cellular drivers of pathogenesis in *rnaset2* mutants, and that transplantation of HSC-derived macrophages is a viable strategy for microglial replacement in zebrafish hosts. As such, future therapies for RNASET2-deficient leukodystrophy may seek to explore microglia-targeted interventions.

Abbreviations

AAV	adeno-associated virus
AGS	Aicardi–Goutières syndrome
ALD	Adrenoleukodystrophy
ALSP	Adult-onset leukoencephalopathy with axonal spheroids and pigmented glia
ANOVA	Analysis of variance
ASD	autism spectrum disorders
ASO	antisense oligonucleotides
CADASIL	cerebral autosomal dominant arteriopathy with subcortical infarcts and leukoencephalopathy
CDCA	chenodeoxycholic acid
cDNA	complementary DNA
CFSE	carboxyfluorescein succinimidyl ester
CHT	caudal haematopoietic tissue
CMV	cytomegalovirus infection
CNS	central nervous system
CRISPR	clustered regularly interspaced short palindromic repeats
CSF	cerebrospinal fluid
CTX	Cerebrotendinous xanthomatosis
CUBIC	clear, unobstructed brain/body imaging cocktails and computational analysis
DAM	disease-associated microglia
DAPI	4’,6-diamidino-2-phenylindole
DEGS	differentially expressed genes
DEPC	Diethyl pyrocarbonate
DNA	deoxyribonucleic acid
dpf	days post-fertilisation
dpt	days post-transplant
EBV	Epstein-Bar virus
EMA	European Medicines Agency
ENU	N-ethyl-N-nitrosourea
ERT	enzyme replacement therapy
ERV	endogenous retrovirus
FACS	fluorescent-activated cell sorting
FBS	foetal bovine serum
FDA	Food and Drug Administration
FXTAS	Fragile X-Associated Tremor/Ataxia Syndrome
gDNA	genomic DNA
GFP	green fluorescent protein
GO	gene ontology
GSEA	gene set enrichment analysis

GWAS	genome wide association studies
HIV	Human immunodeficiency virus
HLA	human leukocyte antigen
HSC	haematopoeitic stem cell
HSCT	haematopoeitic stem cell transplant
IFN	interferon
ISG	interferon-stimulated gene
ISKNV	infectious spleen and kidney necrosis virus
LBSL	Leukoencephalopathy with brainstem and spinal cord involvement and lactate elevation
LoF	loss of function
MeOH	methanol
MLD	Metachromatic leukodystrophy
mpf	months post-fertilisation
MRI	magnetic resonance imaging
MS	Multiple Sclerosis
NHD	Nasu-Hakola disease
NPC1	Niemann–Pick disease, type C1
OPC	oligodendrocyte progenitor cells
PCA	principal component analysis
PCR	polymerase chain reaction
PET	Positron emission tomography
PFA	paraformaldehyde
PMD	Pelizaeus-Merzbacher disease
PPAR	peroxisome proliferator-activated receptors
PVP	polyvinylpyrrolidone
qRT-PCR	quantitative reverse transcription polymerase chain reaction
RIN	RNA integrity number
RNA	ribonucleic acid
rRNA	ribosomal RNA
RT-PCR	reverse transcription polymerase chain reaction
RTI	reverse transcriptase inhibitor
SFM	serum free media
SSM	serum supplemented medium
STAR	Spliced Transcripts Alignment to a Reference
TALEN	Transcription activator-like effector nucleases
TEM	transmission electron microscopy
TUNEL	terminal deoxynucleotidyl transferase dUTP nick end labeling
VLCFA	very long chain fatty acid
VWM	Vanishing White Matter

WKM	whole kidney marrow
wpf	weeks post-fertilisation
ZSD	Zellweger spectrum disorders

Table of Contents

List of Tables

List of Figures

Declaration

I, the author, confirm that the Thesis is my own work. I am aware of the University's Guidance on the Use of Unfair Means (www.sheffield.ac.uk/ssid/unfair-means). This work has not previously been presented for an award at this, or any other, university.

The work discussed in this thesis has been published in various publications, listed below:

- Rutherford *et al.* Macrophage transplantation rescues RNASET2-deficient leukodystrophy by replacing deficient microglia in a zebrafish model. PNAS. 2024;121(21):e2321496121.
- Rutherford *et al.* A zebrafish reporter line reveals immune and neuronal expression of endogenous retrovirus. DMM. 2022;15(4):dmm048921.
- Rutherford *et al.* Dirty Fish Versus Squeaky Clean Mice: Dissecting Interspecies Differences Between Animal Models of Interferonopathy. Front Immunol. 2021;11:623650.

Chapter 1. Introduction

1.1 Leukodystrophies – a family of rare white matter disorders

Rare diseases – disorders that affect fewer than 1 in 2,000 individuals – are emerging as a global health priority (Nguengang Wakap *et al.*, 2020; EURORDIS, 2021). While individually rare, surveys of international databases have begun to reveal the true cumulative burden of these disorders – with over 300 million people living with rare diseases worldwide (Nguengang Wakap *et al.*, 2020). Particularly devastating, over 50% of rare diseases manifest in childhood (The Lancet Diabetes Endocrinology, 2019). Despite this, the impact of such disorders is often magnified by a lack of understanding of pathogenesis and, accordingly, limited treatments.

The leukodystrophies are a family of over four hundred rare, heritable disorders – collectively affecting up to 1 in 4500 live births (Bonkowsky *et al.*, 2010; Stellitano *et al.*, 2016; Shih, Raas and Bonkowsky, 2024). Although the genetic causes and clinical presentation are highly heterogeneous, the leukodystrophies are distinctly characterised by selective loss of white matter – manifesting most frequently as myelin abnormalities, psychomotor impairments and often reductions in survival (Vanderver *et al.*, 2015; van der Knaap and Bugiani, 2017a; United Leukodystrophy Foundation, 2021). Devastatingly, as many as 30% of children diagnosed with leukodystrophy die before the age of eight (Shih, Raas and Bonkowsky, 2024). As such, these disorders are truly debilitating to the families and patients affected by them.

For most leukodystrophies, there remain no disease modifying treatments, meaning clinical outcomes for affected individuals are poor and often devastating. However, the last decade has brought significant advances in the leukodystrophy field. As monogenic disorders, each leukodystrophy is often defined by the underlying genetic cause of pathology – with patients with a particular disorder possessing pathogenic variants in a single gene (or, occasionally, a small subset of related genes). The growing use of whole exome sequencing has therefore led to an explosion in the number of genetically identified leukodystrophies and a revolution in the way leukodystrophies are classified (van der Knaap and Bugiani, 2017b). Leukodystrophy pathogenesis is now classified based on the expected impact of a given genetic mutation on various cellular components of white matter and has paved the way for the development of increasingly targeted therapies. As such, while the unmet clinical need remains immense, it is currently an exciting and dynamic time for leukodystrophy research.

1.2 Treatments for leukodystrophy

1.2.1 Haematopoietic stem cell transplantation

In the clinic, one of the most widely used treatments for most leukodystrophies is allogenic (donor-derived) haematopoietic stem cell transplantation (HSCT). For around three decades, this has remained the only option for clinical intervention in many of these disorders, with engraftment of healthy donor haematopoietic stem cells (HSCs) derived from umbilical cord blood, bone marrow or peripheral blood thought to provide variable functional recovery in some patients (Page *et al.*, 2019). In this section, I will discuss the evidence for HSCT across leukodystrophies, as well as the proposed mechanism by which this intervention may provide clinical benefits.

1.2.1.1 Evidence for HSCT efficacy in the leukodystrophies

Although efficacy is variable across the leukodystrophies, HSCT remains the recommended treatment for patients with three of the most common leukodystrophies – adrenoleukodystrophy (ALD), metachromatic leukodystrophy (MLD) and Krabbe disease – based on observations of clinical efficacy (Page *et al.*, 2019). In MLD, patients who are transplanted before substantial disease progression are more likely to maintain cognitive function (Martin *et al.*, 2013). Evidence also suggests that HSCT may have benefits in children with early-stage cerebral ALD, with improvements in survival relative to non-transplanted controls (Peters *et al.*, 2004; Mahmood *et al.*, 2007; Miller *et al.*, 2011). Similarly, HSCT significantly improves survival and symptoms in patients with early infantile Krabbe disease, with several treated children developing age-appropriate cognitive function (albeit with some motor delays) (Escolar *et al.*, 2005). Although not as widely studied, reports of clinical efficacy have also been reported for HSCT in adult-onset leukoencephalopathy with axonal spheroids and pigmented glia (ALSP), whereby transplantation has been shown to stabilise cognitive decline and even improve some motor outcomes (Bergner *et al.*, 2023). Modest cognitive improvements and stabilisation of functional decline have also been reported in a small number of patients with Pelizaeus-Merzbacher disease, accompanied by arrest of myelin pathology (Wishnew *et al.*, 2014). Finally, reports of HSCT efficacy have been reported in preclinical models in a breadth of further leukodystrophies, including Vanishing White Matter disease and Canavan Disease (Feng *et al.*, 2020; Hillen *et al.*, 2022). As such, there is a robust body of evidence suggesting HSCT may be a useful intervention for some patients with leukodystrophies.

1.2.1.2 Proposed mechanism of HSCT rescue in leukodystrophy

It is widely accepted that the mechanism by which HSCT is able to rescue pathology in patients with leukodystrophy is achieved by the infiltration of donor-derived macrophages into the brain, where

they adopt a microglia-like identity (Krivit, 1995; Priller *et al.*, 2001; Asheuer *et al.*, 2004; Yamada *et al.*, 2004; Schönberger *et al.*, 2007; Cronk *et al.*, 2018). In mouse models, elegant studies taking advantage of genetically-modified HSCs expressing green fluorescent protein (GFP) have demonstrated that, following transplantation, up to 30% of the microglial population are transplant-derived within 4–8 weeks of transplantation in mouse models (Priller *et al.*, 2001; Biffi *et al.*, 2004). Comparable findings have been reported following transplantation of human HSCs (derived from umbilical cord or peripheral blood) into immunocompromised mice, with up to 50% of human cells engrafted in host brains expressing microglia markers (Asheuer *et al.*, 2004). Strikingly, murine transplant-derived cells appear to be preferentially engrafted around sites of neuronal damage, including following focal ischemia or axon transection (Priller *et al.*, 2001). Accordingly, brain engraftment of transplant-derived cells has been reported to be increased in animal models of leukodystrophy, with robust expression of microglial markers (Biffi *et al.*, 2004; Miyake *et al.*, 2010). As such, there is consensus across the field that HSCT acts by replacing, or at least supplementing, microglia in host brains.

The mechanism by which these transplant-derived microglia/macrophages provide therapeutic rescue remains up for debate. The first mechanism by which these cells may provide therapeutic relief is through enzymatic cross correction – whereby these healthy cells provide a source of functioning enzyme to the central nervous system (CNS). Indeed, this is a well characterised mechanism across lysosomal storage disorders, including leukodystrophies like MLD and Krabbe disease, with co-culturing experiments revealing transfer of lysosomal enzymes from competent- to enzymatically deficient cells, with similar reports following HSCT *in vivo* (Fratantoni, Hall and Neufeld, 1968; Beck, 2010; Harrison *et al.*, 2013; Page *et al.*, 2019). However, several studies have questioned the contribution of cross correction to transplant success in these disorders. In a conditional mouse model of Krabbe Disease, no evidence of transfer of galactosyl ceramidase (GALC) from GALC-competent macrophages to GALC-deficient myelinating cells was found, even following recruitment of healthy macrophages to sites of axonal degeneration (Weinstock *et al.*, 2020). Furthermore, histological analysis of post-mortem tissue from transplanted MLD patients failed to identify the presence of arylsulfatase A (ARSA) – the enzyme deficient in this disorder – in the astrocytes or oligodendrocytes surrounding transplant-derived cells, providing no evidence of cross-correction (Wolf *et al.*, 2020). It should be noted that, in this study, just two transplanted patients were included and, sadly, for both of these, transplantation was not sufficient to rescue pathology – making it difficult to interpret whether lack of enzymatic cross correction is simply a marker of unsuccessful transplantation. As such,

evidence for cross-correction as a mechanism of pathology rescue by transplant-derived glia is conflicting in MLD and Krabbe disease.

It also remains unclear the extent to which cross-correction contributes to HSCT success for disorders which are not characterised by loss of soluble enzymes, but rather membrane proteins such as ABCD1 – defective in ALD (Kemp *et al.*, 2001). In post-mortem tissue from a single transplanted ALD patient, ABCD1 expression was observed in blood, endothelial and glial cells of the brain, with additional punctae in neurons – suggesting potential transfer from transplant-derived cells (Schönberger *et al.*, 2007). In support, co-culture of ALD-derived fibroblasts with healthy cells has been demonstrated to reduce the accumulation of ABCD1 substrates (Yamada *et al.*, 2004). Interestingly, this correction was not seen when the two cell populations were separated by a filter membrane – suggesting possible cell-to-cell transfer of ABCD1 rather than release into the media. Transfer of membrane proteins has been reported to occur by lysosomal exchange via projecting nanotubules by HSC-derived macrophages following transplantation in mice, although this has only been reported in the kidney *in vivo* (Naphade *et al.*, 2015). Therefore, although much remains to be understood about potential mechanisms, cross-correction may also contribute to the clinical success of HSCT in ALD.

However, growing consensus suggests that transplant-derived microglia may exert beneficial effects through cell autonomous functions beyond simple enzyme replacement (Page *et al.*, 2019). In addition to reporting no enzyme exchange between transplant-derived microglia and other glial cells, analysis of post-mortem MLD tissue revealed an increased expression of anti-inflammatory markers in the macrophages and microglia of transplanted patients, relative to non-transplanted controls, which was accompanied by increased numbers of oligodendrocytes and some evidence of remyelination (Wolf *et al.*, 2020). Thus, this work suggests that the presence of anti-inflammatory transplant-derived microglia is sufficient to support myelin integrity, without transferring enzyme to neighbouring cells. Indeed, microglia are known to have a host of critical roles in supporting white matter integrity – from supporting oligodendrocyte progenitor cell survival and differentiation, responding to demyelination and inducing oligodendrocyte apoptosis in response to white matter injury (Hamilton and Rome, 1994; Nicholas, Wing and Compston, 2001a; Yeo *et al.*, 2012a). For example, in a conditional mouse model of Krabbe disease, healthy macrophages are thought to aid in myelin turnover and ameliorate pathology through phagocytosis of myelin debris (Weinstock *et al.*, 2020). More broadly, microglia are essential in restoring the brain to homeostasis due to their interactions with other glial cells, phagocytosis of apoptotic debris and response to inflammation ((Nicholas, Wing and Compston, 2001a; Fuhrmann *et al.*, 2010a; Yeo *et al.*, 2012a; Healy *et al.*, 2016a; Hickman *et al.*, 2018a). As such,

a combination of enzymatic cross-correction and cell autonomous microglial functions, including phagocytosis, likely contributes to the clinical success of HSCT in the leukodystrophies.

1.2.1.3 Limitations of HSCT in the leukodystrophies

However, despite the relatively widespread use of HSCT in the clinic, there remain several key limitations for transplantation in the treatment of leukodystrophies. Firstly, HSCT is associated with substantial mortality risk. Particularly in young children, intense chemotherapy regimens and inherent risks of transplantation itself leads to mortality rates of approximately 20% throughout the leukodystrophies, with potentially higher mortality in some patient populations (Bonkowsky *et al.*, 2021). Strikingly, studies in MLD have reported that transplantation was associated with mortality up to half of patients, due to infection, chemotherapy-related toxicity, graft-versus-host disease or further disease progression (Martin *et al.*, 2013; Boucher *et al.*, 2015; Armstrong *et al.*, 2023). Therefore, the risks of HSCT remain a key clinical consideration, and limit the number of patients who may benefit from this intervention.

Secondly, transplantation is only indicated in a small population of patients, with highly variable efficacy – particularly in patients who have already experienced symptom onset (Page *et al.*, 2019). Systematic review of transplantation studies in MLD has suggested that HSCT does not induce robust improvements in motor function or survival in late infantile or juvenile patients, although some cognitive function may be maintained if HSCT was performed pre-symptomatically (Armstrong *et al.*, 2023). Similarly, in Krabbe disease, many patients present with ongoing neurological deterioration – although along a slower time course than might be expected in non-transplanted individuals (Duffner *et al.*, 2009). Sadly, transplantation remains most successful in patients who receive treatment at extremely young ages (less than 30 days old). Given the rarity of the leukodystrophies, diagnosis is often delayed – making it unlikely that suitable patients would be identified at this early age, particularly before the onset of symptoms. Additionally, challenges finding suitable donors may also delay transplantation (Page *et al.*, 2019). As such, many patients develop progressive disease prior to transplantation that cannot be rescued by this intervention.

Finally, there is a widely reported delay between transplantation and development of any clinical benefit, attributed to the time needed for donor-derived cells to engraft in hosts and reach the brain – thought to be the mechanism of therapeutic efficacy (Bonkowsky *et al.*, 2021). Clinical observations have suggested that clinically meaningful stabilisation is unlikely to occur until approximately one-year post-transplant (Page *et al.*, 2019). This delay is thought to be due to the time needed for HSCs to engraft within and repopulate the haematopoietic niche, before giving rise to donor-derived

macrophages which can infiltrate the brain and adopt a microglial identity (Krivit, 1995; Priller *et al.*, 2001; Asheuer *et al.*, 2004; Yamada *et al.*, 2004; Schönberger *et al.*, 2007; Cronk *et al.*, 2018). Furthermore, the intense myeloablation regimes needed prior to transplant may themselves cause clinical deterioration, delaying the development of any observable improvements for these patients. As such, this delay in efficacy reflects an inherent limitation of both the methodology and mechanism by which HSCT is thought to work.

Therefore, although HSCT provides clinically meaningful benefits for some patients with specific leukodystrophies, there is a clear need for more effective therapies which have better safety profiles and can reach the brain more quickly across this family of disorders.

1.2.1.4 Macrophage transplantation as an alternative to HSCT

Given the delay between HSCT and therapeutic benefit – and the number of intermediate steps between transplantation and brain engraftment – it has been suggested that transplantation of macrophages may provide quicker replacement of microglia and, therefore, disease stabilisation in the leukodystrophies (Sieweke and Allen, 2013; Cronk *et al.*, 2018). Indeed, preclinical studies have demonstrated that transplant-derived macrophages can engraft within the CNS and adopt a microglial phenotype in a relatively short time window following transplantation (Suzuki *et al.*, 2014; Haideri *et al.*, 2017; Bennett *et al.*, 2018; Cronk *et al.*, 2018). Furthermore, in a mouse model of CSF1R-deficient paediatric-onset leukodystrophy, transplanted macrophages were able to engraft in the CNS and express microglia-specific markers, suggesting this approach may be a viable strategy for microglial replacement (Bennett *et al.*, 2018). However, the ability of transplanted macrophages to rescue pathology in this mouse model – or indeed, any other leukodystrophy animal model – is yet to be published, and macrophage transplantation has yet to be trialled in the clinic for leukodystrophies. To our knowledge, there are two reported clinical trials of macrophage transplantation in neurological disorders. Intrathecal transplantation of macrophages polarised to promote tissue repair led to functional improvements in patients who had suffered acute ischemic and haemorrhagic stroke, and led to increased motor function in patients with cerebral palsy (Chernykh *et al.*, 2014, 2016; Na, Kim and Seok, 2023). Therefore, macrophage transplantation is clinically feasible, and has robust rationale for use in disorders where HSCT efficacy is hindered by delayed arrival of donor-derived cells to the brain, including leukodystrophies. Nonetheless, macrophage transplantation in leukodystrophies is yet to be explored. Instead, emerging therapies are targeting the genetic and molecular mechanisms of pathogenesis in these disorders through gene therapy and pharmacological approaches, rather than cell-based therapies.

1.2.2 Emerging therapies in clinical development

For many years, therapy development for the leukodystrophies was sparse – hindered by the rarity of these disorders, minimal understanding of pathogenesis and limited animal models. However, in recent years, there has been huge growth in preclinical and clinical research in these diseases, culminating in the approval of two novel therapies for the treatment of MLD and ALD, in 2020 and 2021 respectively (see Section 1.2.2.3). There are now over fifteen therapies in clinical trials for the treatment of various leukodystrophies, as summarised in Table 1.1. In this section, I will provide an overview of these upcoming therapies and the animal studies from which they emerged, in order to establish future directions and gaps within the treatment of these disorders.

Table 1.1. Treatments for leukodystrophy currently in therapeutic development.
AAV, adeno-associated virus; CSF, cerebrospinal fluid; HSCT, haematopoietic stem cell transplant; LoF, loss of function.

Disease (and causal gene)	Treatment	Mode of action	**Clinical** or *preclinical* evidence	Trials
Enzyme replacement therapies				
Cerebrotendinous Xanthomatosis (*CYP27A1*)	Chenodeoxy-cholic acid (CDCA)	Orally-dosed bile acid; directly replaces CDCA (which is deficient due to CYP27A1 LoF)	*Replacement of CDCA inhibits flux of cholesterol into bile acid synthesis pathway and reduces accumulation of toxic metabolites* **Treated patients showed reduced accumulation of bile alcohols (which are known to accumulate and cause neurotoxic accumulation of cholestanol in this disorder)**	NCT04270682 **(Phase 3; complete)**
Metachromatic leukodystrophy (*ARSA*)	TAK-611 (HGT 1110)	recombinant human arylsulfatase A enzyme replacement therapy	**Pharmacokinetics revealed TAK-611 penetrates the CNS, but failed to meet primary and secondary endpoints (patients continued to show decline in motor function)**	NCT03771898 **(Phase 2 extension)**
In vivo gene therapies				
Krabbe disease (*GALC*)	FBX-101	AAV rh10 vector designed to deliver functioning *GALC* alongside HSCT (within 21 days)	**Interim analysis suggests no adverse infusion reactions in patients. Gross motor development improved relative to HSCT alone, and were within the normal range for age**	NCT05739643 **(Phase 1b)**
Krabbe disease (*GALC*)	PBKR03	AAV hu68 designed to deliver functioning *GALC*	*Increased GALC activity, reduced microglial activation and improved motor function in mouse and canine model*	NCT04771416 **(Phase 1/2)**
Canavan disease (*ASPA*)	BBP-812	rAAV9 vector engineered to deliver functioning *ASPA*	**Interim analysis suggests no adverse events leading to hospitalization to date, increased ASPA activity in CSF and promising clinical signs in patients**	NCT04998396 **(Phase 1/2)**
Canavan disease (*ASPA*)	MYR-101	rAAV9 vector engineered to deliver functioning *ASPA* specifically to oligodendrocytes	**Interim analysis demonstrates increased overall white matter and myelin volume, alongside improvements in gross motor and language function in patients 1 year post-treatment**	NCT04833907 **(Phase 1/2)**
Metachromatic leukodystrophy (*ARSA*)	TG-MLD	AAV rh10 vector designed to deliver functioning *ARSA*	*Intracranial delivery reduced sulfatide accumulation in oligodendrocytes, reduced astrogliosis and microglial activation in mouse model*	NCT01801709 **(Phase 1/2)**

Pelizaeus-Merzbacher Disease (*PLP1*)	ION356	Antisense oligonucleotide designed to decrease production of PLP1	*In mouse model, ION356 restored oligodendrocyte numbers, increased myelination, and improved motor function and survival*	NCT06150716 **(Phase 1b)**
Alexander disease (*GFAP*)	Zilganersen	Antisense oligonucleotide designed to suppress production of GFAP	*Reduced GFAP expression, accompanied by reduced microglia activation, inflammatory cytokine levels and stress response in mouse model*	NCT04849741 **(Phase 1–3)**
Ex vivo gene therapies				
Metachromatic leukodystrophy (*ARSA*)	Libmeldy (atidarsagene autotemcel)	Autologous HSC-based gene therapy; patient's own cells are lentivirally transduced with functioning *ARSA*	**Treated patients showed elevation of ARSA levels, improved survival (100% vs 36.8% untreated) and improved gross motor function 24 months post-treatment**	NCT01560182 **(Phase 1/2; completed)** **FDA + EMA approved**
Adrenoleuko-dystrophy (*ABCD1*)	Skysona (elivaldogene autotemcel)	Autologous HSC-based gene therapy; patient's own cells are lentivirally transduced with functioning *ABCD1*	**74% of patients were alive and did not exhibit signs of major functional disability (including loss of communication or voluntary movement, tube feeding, wheelchair dependence) 24 months post-therapy**	NCT03852498 **(Phase 3; completed)** **FDA + EMA approved**
Pharmacological approaches				
Adrenoleuko-dystrophy and adrenomyelo-neuropathy (*ABCD1*)	Leriglitazone	PPAR gamma agonist, represses NF-κB activity and reduces oxidative stress	*Reduced oxidative stress, production of inflammatory cytokines and microglial activation in mouse model, alongside improved motor function. Increased phagocytosis of myelin debris thought to promote remyelination.* **Reduced progression to cerebral disease in patients with adrenomyeloneuropathy; stabilised clinical decline and reduced lesion load in patients with cerebral disease**	NCT03231878 **(Phase 2/3, complete);** NCT05819866 **(Phase 3);** NCT04528706 **(Phase 3)**
Adrenoleuko-dystrophy (*ABCD1*)	VK0214	thyroid beta receptor (TRβ) agonist; increases expression of ABCD2 (to compensate for ABCD1 LoF)	**After 14 days treatment, patients showed reduced accumulation of very long chain fatty acids and other lipids known**	NCT04973657 **(Phase 1; complete)**

Vanishing white matter disease (*eIF2B*)	Guanabenz	α2-adrenergic agonist; independently prolongs eIF2B phosphorylation	*Single dose of guanabenz rescues integrated stress response in treated mice. Treatment reduced astrocyte activation, increased oligodendrocyte number and myelin protein synthesis and improved clinical signs in this model*	Ongoing at Amsterdam Medical Centre **(Phase 2)**
Vanishing white matter disease (*eIF2B*)	Fosigotifator	eIF2B activator; stabilises eiF2B complex formation	*Treatment of mouse model reduced integrated stress response throughout brain and spinal cord, and corrected motor deficits*	NCT05757141 **(Phase 1b/2)**
Sjögren-Larsson syndrome (*ALDH3A2*)	ADX-629	aldehyde trapping agent; thought to reduce toxic accumulation of fatty aldehydes	None published so far	NCT05443685 **(Phase 1/2)**
Aicardi-Goutieres Syndrome (multiple)	Abacavir, lamivudine, and zidovudine	Reverse transcriptase inhibitors	**Reduced expression of interferon stimulated genes in 8 patients, which returned to pretreatment levels after treatment cessation. Limited evidence of increased cerebral blood flow. No other clinal outcomes assessed.**	NCT02363452 **(Phase 2)**
Aicardi-Goutieres Syndrome (multiple)	Baricitinib	JAK1/2-inhibitor	**Improvement in parent-reported outcomes, with treated individuals achieving more key developmental milestones than natural history. Reduced expression of interferon stimulated genes across 35 patients.**	NCT01724580 **(Expanded access)**
Adult-onset leukoencephalo-pathy with axonal spheroids and pigmented glia (*CSF1R*)	Iluzenabart	TREM2 agonist	**Interim analysis demonstrates increases in soluble CSF1R, alongside reductions in neurofilament light chain (marker of neuronal death) and slowed brain volume loss**	NCT05677659 **(Phase 2)**

1.2.2.1 Enzyme replacement therapy

Various studies have suggested that the mechanism by which HSCT exerts therapeutic benefits is by replacing deficient enzymes in the CNS (Fratantoni, Hall and Neufeld, 1968; Harrison *et al.*, 2013; Wolf *et al.*, 2020). As such, enzyme replacement therapy (ERT) seeks to increase the levels of absent and/or dysfunctional proteins in leukodystrophy patients, without the need of the highly invasive procedures required for HSCT. However, at the time of writing, ERT has shown limited success across the leukodystrophies.

ERT has particularly strong theoretical rationale in lysosomal storage disorders – with this therapy being used with striking clinical efficacy in Gaucher disease (a non-leukodystrophy storage disorder) since the early 1990s (Barton *et al.*, 1991). Yet, in lysosomal storage leukodystrophies, ERTs have been largely unsuccessful. A recent phase 2 trial exploring the efficacy of recombinant ARSA in patients with MLD failed to achieve its primary or secondary outcomes and was discontinued due to poor efficacy (MLD Support Association UK, 2024). This was despite promising findings in mouse models, where administration of this enzyme reduced lysosomal markers in the brain indicative of reduced number and size of lysosomes, and from human pharmacokinetic studies which showed penetration and persistence of this compound into the CNS (Wright *et al.*, 2018; Troy *et al.*, 2020). However, it should be noted that no evidence of the effect of this compound on further markers of MLD in animal models has been published thus far. As such, there is limited evidence for the treatment of MLD by ERT.

Nonetheless, there are some leukodystrophies were ERT may have benefits. Cerebrotendinous xanthomatosis (CTX) is an ultra-rare leukodystrophy caused by deficiency of an enzyme required for the conversion of cholesterol into the bile acid chenodeoxycholic acid (CDCA) (Björkhem, 2013). In the absence of this enzyme, cholestanol and bile alcohols begin to accumulate, with neurotoxic effects (Verrips *et al.*, 2020). Treatment of CTX by CDCA replacement in a phase 3 trial has shown early indications of efficacy, with reduced accumulation of bile alcohols in patients, mirrored by previous retrospective studies which showed improvements in clinical symptoms following treatment across several years (Verrips *et al.*, 2020). This success may reflect the somewhat unique pathophysiology of CTX – whereby pathogenesis begins with defective bile acid processing in the liver, leading to build up of toxins which can make their way into the brain. As such, oral treatment with CDCA may act in the periphery, rather than the CNS, to restore this pathway and reduce toxic metabolites. Thus, these studies demonstrate that ERT may have a role in the treatment of leukodystrophies, but that this may require careful consideration of the disease-specific pathogenetic mechanisms involved and may not be suitable for all disorders.

1.2.2.2 In vivo gene therapy

Other therapeutic strategies have aimed to go one step beyond ERT – targeting the affected gene rather than protein, with a view to restoring enzymatic function in the CNS. As such, gene therapies in the leukodystrophies have explored two main routes: gene delivery and gene targeting.

1.2.2.2.1 Gene delivery

The most commonly explored gene therapy in leukodystrophies is gene delivery, in which viral vectors (most frequently adeno-associated viruses [AAVs]) are used to deliver healthy copies of a dysfunctional gene into the CNS. This strategy is particularly appealing in leukodystrophies associated by loss-of-function in a particular protein, and is currently undergoing clinical trials in Krabbe disease, Canavan disease and MLD (Table 1.1).

In Krabbe disease, intravenous delivery of AAVs encoding *GALC* in parallel with umbilical cord blood transplantation has yielded particularly positive findings thus far. Interim analysis of a small patient population suggests this treatment restores GALC enzymatic activity and, crucially, rescues white matter integrity and gross motor function to levels seen in healthy age-matched controls (Escolar *et al.*, 2023). These benefits supersede those achieved by HSCT alone. This is paralleled by promising findings from mouse and canine models of Krabbe disease, in which the administration of various AAV-GALC vectors induced robust increases in GALC activity, reduced microglial activation, improved motor function and mild reductions in demyelination (Rafi *et al.*, 2015; Marshall *et al.*, 2018; Hordeaux *et al.*, 2022). A variety of experimental set-ups have demonstrated that the combination of AAV-mediated gene delivery and HSCT shows greater efficacy than either treatment alone – with almost complete rescue of pathology in several mouse models (Rafi *et al.*, 2015; Karumuthil-Melethil *et al.*, 2016; Marshall *et al.*, 2018). This has been attributed to the widespread effects of HSCT in modulating the inflammatory consequences of disease combined with the efficient increase in GALC activity mediated by AAV-vectors (greater than that seen in HSCT alone) (Rafi *et al.*, 2015). Thus, this work has laid the foundations for the ongoing combination therapy trial in Krabbe disease, with promising effects thus far.

However, there remain some limitations of this intervention. Firstly, gene therapy trials in Krabbe disease and MLD are currently only enrolling presymptomatic patients, or those at the very earliest stages of disease. Animal studies have demonstrated that AAV-mediated therapies – like HSCT – are unlikely to have therapeutic effects after the onset of symptoms, with minimal increases in enzymatic activity and potential induction of antibodies against the functioning protein (Hironaka *et al.*, 2015).

As discussed previously, the rarity of this disorder, along with rapid progression in affected children, makes pre-symptomatic diagnosis highly unlikely, such that most patients are ineligible for these treatments at the point of diagnosis. As such, there remains a need for disease modifying therapies for patients at more advanced disease stages.

1.2.2.2.2 Gene targeting

A further gene therapy strategy emerging into clinical trials is the use of antisense oligonucleotides (ASOs) to target dysfunctional genes in leukodystrophies. ASOs are short nucleotide sequences which bind to complementary DNA or RNA sequences to silence a gene of interest. As such, ASOs can be used to either block translation of a dysfunctional protein or prevent silencing of an under-expressed protein, by either preventing premature gene splicing or targeting other genes which may be involved in its regulation. ASOs have emerged as an exciting therapeutic area following the success of two such therapies in clinical trials and their subsequent approval: tofersen in amyotrophic lateral sclerosis and nusinersen in spinal muscular atrophy (Mercuri *et al.*, 2018; Miller *et al.*, 2022). As such, ongoing clinical research is investigating the utility of ASOs in the leukodystrophies.

There are currently two ASO therapies in clinical trials for leukodystrophies, both of which aim to decrease expression of overactive or abundant genes: *proteolipid protein-1 (PLP1)* in Pelizaeus-Merzbacher Disease (PMD), and *glial fibrillary acidic protein (GFAP)* in Alexander Disease. To date, no results have been shared from these clinical trials, but data from preclinical models is encouraging. In mouse model of Alexander Disease, intracerebral injection of ASOs targeting GFAP reduced levels of both *GFAP* transcripts and protein and was mirrored by reductions in microglial activation and pro-inflammatory cytokines in the brain (Hagemann *et al.*, 2018). Similarly, *PLP1*-targeting ASOs also reduced markers of microglial activation in a PMD mouse model, resulting in restored oligodendrocyte numbers, increased myelination, and improved motor function and survival (Elitt *et al.*, 2020). Future work will establish whether the preclinical promise of ASOs can translate into clinical efficacy.

There are notable caveats to the use of ASOs which may limit their therapeutic potential. Firstly, ASOs are most easily employed in disorders caused by gain-of-function mutations, while most leukodystrophies are associated with loss-of-function of a key protein or enzyme. For example, in PMD, ASO therapy is only suitable for patients with *PLP1* duplications, and not the not the subset of patients which have *PLP1* loss-of-function mutations (Elitt *et al.*, 2020). Although increasing levels of a dysfunctional protein may be possible through mediating gene splicing or targeting other regulators of gene expression, these approaches require an even greater understanding of gene function and are

not currently under investigation in any leukodystrophies. Furthermore, ASO delivery to the CNS is particularly challenging, as these oligonucleotides typically cannot cross the blood brain barrier and so must be delivered intracranially, a highly invasive route (Phillips *et al.*, 1997). Therefore, the clinical promise of ASOs is likely to be limited to only a subset of leukodystrophies, and further research is needed to reduce the burden of treatment-associated procedures for this intervention.

1.2.2.3 Ex vivo gene therapy

By far the most promising therapeutic strategy of recent years, *ex vivo* gene therapy involves harvesting bone marrow-derived HSCs from a patient, genetically correcting these cells to introduce functional copies of a specific gene (often using lentiviral vectors) and then re-administering these cells to the patient via bone marrow transplant (Wu *et al.*, 2022). To date, two *ex vivo* gene therapies have been approved by the Food and Drug Administration (FDA) and European Medicines Agency (EMA): Libmeldy for MLD and Skysona for ALD. Clinical trial results demonstrated that 74% children with cerebral ALD treated with Skysona were living without major functional disability at two years post-treatment, compared with just 43% of untreated patients in a natural history study (Skysona, 2024). Even more strikingly, treatment with Libmeldy improved two-year survival of MLD patients from 36.8% in untreated patients to 100% in treated individuals, accompanied by drastic improvements in gross motor function (Libmeldy, 2024). Subsequently, compelling evidence from a recent systematic review has suggested that patients who received Libmeldy have better gross motor and cognitive function versus traditional allogenic HSCT, mirrored by improvements in survival (Armstrong *et al.*, 2023). As such, for eligible patients, these therapies have a truly transformative impact and demonstrate that leukodystrophies are, potentially, curable.

One of the great appeals of *ex vivo* gene therapy is the removal of a need for a donor, with transplantation of a patient's own cells thought to be better tolerated by the immune system (Wu *et al.*, 2022). However, there remain some safety concerns about the transplantation of lentivirus-transfected HSCs in infantile patients. In infants treated with Skysona, several cases of myelodysplastic syndrome have been reported, thought to be the result of integration of the lentiviral vector into proto-oncogenes (BluebirdBio, 2024). As such, careful, lifelong monitoring of patients is required to ensure early diagnosis of any haematologic malignancies. However, causes of myelodysplastic syndrome are relatively rare (occurring in just three patients out of over sixty individuals who have been treated with Skysona) and, as such, the risk-benefit profile remains in favour of this treatment.

However, the major limitations of *ex vivo* gene therapies are cost and patient identification. These interventions are among the most expensive treatments ever approved in the United States and

Europe, with a single dose of Skysona or Libmeldy costing around $3 million (BluebirdBio, 2022; Walsh, 2023). Additionally, these interventions are only indicated in patients who are asymptomatic or have very mild disease. Identifying these patients is hugely challenging, and previously has only been possible in instances where an older sibling has been affected by the same disorder. This can lead to devastating instances where a younger sibling may be cured, but treatment is unavailable for older children (Walsh, 2023). There is a growing push for newborn screening for leukodystrophies – particularly in light of these approved therapies – which could facilitate earlier identification of patients; however, this is not routinely employed in the clinic (Hong *et al.*, 2021). As such, these life-altering treatments remain available to only a proportion of patients with specific leukodystrophies, and at huge financial cost - therefore, the broader application of this therapy to other leukodystrophies, and more advanced patients, remains to be seen.

1.2.2.4 Pharmacological approaches

The gene- and enzyme-focussed strategies discussed above began to emerge as whole exome sequencing identified the specific mutations causing specific leukodystrophies – demonstrating how an early understanding of the genetics of disease can facilitate therapeutic target development. However, as our understanding of leukodystrophy disease mechanisms has grown, pharmaceutical strategies targeting affected signalling cascades, or even the function of specific cell types, have progressed to clinical development (Table 1.1). In this section, I will highlight several such approaches with clinical evidence in later stage trials (Phase 2 onwards).

1.2.2.4.1 PPARγ agonists

Understanding the specific signalling pathways which are affected in leukodystrophies can lead to the identification of novel targets beyond the gene or protein implicated in a given disorder. One such example is the development of leriglitazone for ALD, one of the most common leukodystrophies. As previously discussed, ALD is caused by loss-of-function mutations in the peroxisomal membrane transporter ABCD1, which is required for the transportation of very long chain fatty acids (VLCFAs) into the peroxisome for degradation (Contreras *et al.*, 1994). In the absence of functioning ABCD1, VLCFAs build up in white matter of the brain and spinal cord, resulting in mitochondrial dysfunction and oxidative stress, microglial activation and apoptosis, and, ultimately, demyelination (Eichler *et al.*, 2008). The ongoing trials of leriglitazone in ALD seek to prevent these neurotoxic effects, not by directly targeting ABCD1 itself, but by ameliorating the effects of very long chain fatty acid (VLCFA) accumulation. Leriglitazone is a peroxisome proliferator–activated receptor gamma (PPARγ) agonist with a variety of cellular effects (Rodríguez-Pascau *et al.*, 2021)). *In vitro* studies have demonstrated

that leriglitazone is able to minimise oxidative stress and improve mitochondrial function, alongside decreased activation of the NF-κB pathway. *In vivo* studies subsequently revealed that these changes were mirrored by reduced activation of microglia and increased microglial phagocytosis of myelin debris in a mouse model, ameliorating demyelination and motor dysfunction. Accordingly, published results from one clinical trial has shown that leriglitazone can prevent progression of cerebral disease in patients with an adult-onset form of ALD – however, this study failed to meet its primary endpoint (increased motor function) (Köhler *et al.*, 2023). Subsequent clinical trials have revealed that leriglitazone may have a more prominent therapeutic effect in patients with more severe ALD, with treatment inducing clinical stabilisation and preventing further lesion growth with a similar efficacy to HSCT (Minoryx Therapeutics, 2023). As such, these findings demonstrate the benefits of targeting downstream of gene dysfunction to rescue cellular signalling and function – in this instance, mitochondrial dysfunction and microglial activation – for therapeutic interventions in leukodystrophy.

1.2.2.4.2 Reverse transcriptase and Janus Kinase (JAK) inhibitors

Another pathway-centric approach being explored in the leukodystrophies is the use of reverse transcriptase inhibitors (RTIs) and JAK inhibitors in Aicardi-Goutières Syndrome (AGS) – a disorder characterised by striking upregulation of the interferon response which is thought to contribute to pathology (Liu and Ying, 2023).

The rationale for the use of RTIs in AGS emerged from the finding that multiple genes implicated in this disorder are involved in the sensing and metabolism of nucleic acids, and particularly in restricting reverse transcription of transcripts derived from invading viruses or endogenous retroelements (Benitez-Guijarro *et al.*, 2018; Rutherford and Hamilton, 2019a; Crow, Shetty and Livingston, 2020; Rutherford, Kasher and Hamilton, 2021). As such, several groups have hypothesised that AGS is triggered by the uncontrolled reverse transcription of these endogenous retroelements which may trigger the antiviral immune response – explaining why AGS patient phenotypes so closely mimic viral infection (Crow *et al.*, 2006). Both clinical and preclinical studies have investigated the efficacy of RTIs – a class of antiretroviral drugs used to prevent reverse transcription in human immunodeficiency virus (HIV) – in AGS. Studies in animal models have shown limited success, with RTI treatment failing to reliably increase survival of AGS mouse models (Stetson *et al.*, 2008; Beck-Engeser, Eilat and Wabl, 2011; Achleitner *et al.*, 2017). However, these studies were vastly limited in that the mouse model used – the *Trex1*$^{-/-}$ mouse – does not develop neuropathology, despite sharing similar genetic underpinnings to patients and showing prominent upregulation of the interferon response (Morita *et al.*, 2004; Gall *et al.*, 2012). RTIs have shown arguably more success in patients, with a small clinical

trial showing that a combination of three RTIs reduced expression of interferon stimulated genes in 8 patients, which returned to pretreatment levels after treatment cessation (Rice *et al.*, 2018). However, the authors reported no further clinical outcomes, so it is unclear whether this intervention led to recovery of neuropathology or symptoms. Thus, the efficacy of RTIs in AGS remains unclear.

Rather than targeting potential triggers of the interferon response, interventions aiming to block downstream effects of interferon signalling may have greater impacts in AGS. The JAK/STAT pathway acts downstream of both IFN-α/β and -γ receptors and may therefore reduce interferon signalling in AGS (Sanchez *et al.*, 2018). An open-label trial of the JAK1/2 inhibitor baricitinib revealed that treatment reduced expression of interferon stimulated genes across 35 patients (Vanderver *et al.*, 2020). Most strikingly, treatment was associated with improvement in parent-reported outcomes, with treated children achieving more key developmental milestones than they had obtained prior to treatment. These findings have been mirrored across several case studies of AGS patients with different mutations (Cattalini *et al.*, 2021; Mura *et al.*, 2021; Li *et al.*, 2022). Therefore, the clinical use of JAK inhibitors demonstrates a role for targeting of immune pathways in this leukodystrophy.

1.2.2.4.3 TREM2 agonism

Finally, pharmacological therapies targeting the overall function of specific cell types are emerging in leukodystrophies, with early clinical success. In ALSP, therapeutic developments aimed at increasing function of microglia are showing benefits in patients and animal models. Iluzanebart, a TREM2 agonist, is thought to increase microglial function to promote the survival and proliferation of microglia, as well as the ability of these cells to respond to neuronal injury, migrate to sites of cellular damage and phagocytose myelin or other protein debris (Deczkowska, Weiner and Amit, 2020; Larson *et al.*, 2024). Interim analysis from an ongoing Phase 2 trial indicates that treatment of patients with ALSP with iluzanebart increased microglia function, alongside slowing of disease progression (as characterised by reduced grey matter loss and reduced ventricular enlargement) (Lynch *et al.*, 2024). Biomarkers of neuronal death were also reduced, suggesting a possible halting of neuropathology in treated patients. Due to the rarity of this disorder and early stage of this trial, these results reflect changes in just six patients treated across six months: publication of the full trial results with longer treatment durations and increased patient numbers will elucidate the true effect of iluzanebart in ALSP. Nonetheless, this encouraging data demonstrates that pharmacological manipulation of cellular function – particularly microglia function – may be beneficial in leukodystrophies.

1.2.2.5 Common themes in emerging therapies for leukodystrophy

As discussed above, novel strategies for the treatment of leukodystrophies are currently exploring a wide range of therapeutic modalities, targeting a variety of genetic, molecular, and cellular disease mechanisms. While different strategies may have benefits in specific leukodystrophies owing to the unique pathogenic mechanisms underpinning each disorder, there are several common themes emerging from these new therapies.

Firstly, the majority of treatments discussed above show efficacy only in patients at the very earliest stages of disease and are often most effective when employed pre-symptomatically. This is certainly true for HSCT, and both *in vivo* and *ex vivo* gene therapy (Hironaka *et al.*, 2015; Page *et al.*, 2019). While earlier diagnosis may increase the number of patients who can access these treatments, there remains a huge gap in the treatment landscape for therapies which may slow more advanced disease, which must be addressed.

Secondly, while therapies are in clinical development for a range of leukodystrophies, there remain a huge number for which no treatment is available. Out of over 400 leukodystrophies, clinical trials are currently ongoing for just eleven (Table 1.1). Many of these neglected disorders are ultra-rare, challenging research due to small patient populations and limited funding. As such, future research may wish to investigate common mechanisms underpinning the pathogenesis of multiple leukodystrophies, to develop treatments that may be more widely employed across the patient community (Halley *et al.*, 2022).

Finally, it is notable that rescue of the neuroimmune response – and particularly microglial function – appears to be a central feature of many successful therapies. The finding that many *in vivo* gene therapies have greater efficacy in combination with HSCT demonstrates that simply restoring enzymatic activity is insufficient to rescue disease – instead, the broader impact of stabilisation of the immune response following HSCT seems to be necessary (Rafi *et al.*, 2015; Karumuthil-Melethil *et al.*, 2016; Marshall *et al.*, 2018). Furthermore, both approved *ex vivo* gene therapies also likely rely on the infiltration of donor-derived cells into the brain where they may become microglia, restore enzyme levels and support white matter health (Hamilton and Rome, 1994; Nicholas, Wing and Compston, 2001a; Yeo *et al.*, 2012a; Page *et al.*, 2019). Additionally, multiple pharmacological strategies in advanced clinical trials are thought to exert their beneficial effects, at least in part, by restoring microglial and immune functioning, with secondary effects on oligodendrocyte and myelin integrity (Vanderver *et al.*, 2020; Rodríguez-Pascau *et al.*, 2021; Lynch *et al.*, 2024). Therefore, the microglia

reflect a common cellular target in several treatment modalities across multiple leukodystrophies and may represent a useful lead for the development of further therapies.

1.3 Microglia – possible cellular drivers of leukodystrophy

For many years, the central dogma of leukodystrophy research remained focussed on myelin and the cells which produce it – the oligodendrocytes – driven by the observation of white matter lesions being central to leukodystrophy clinical presentation (Morell, 1984). However, several lines of research have driven the field away from this purely oligodendrocyte-focussed view of this family of white matter diseases. As discussed in Section 1.2, almost none of the emerging therapies in ongoing trials directly target the oligodendrocytes. Instead, many treatments showing promise in the clinic may exert their beneficial effects by modulating the function of microglia, or the neuroimmune axis, in some way. This is supported by the growing use of next generation sequencing and advanced magnetic resonance imaging (MRI) pattern recognition in the clinic, which has facilitated the identification of over four hundred genetically distinct leukodystrophies – many of which are caused by mutations in genes associated with white matter components beyond oligodendrocytes, such as microglia and astrocytes (van der Knaap and Bugiani, 2017a; Rutherford and Hamilton, 2019b). As such, in this section, I will provide an overview of the current evidence for microglial dysfunction across the leukodystrophies in order to better understand how these cells may be implicated in pathogenesis, and if these could be targeted for effective treatment.

1.3.1 A brief overview of microglia in health and disease

Given the prominent role of microglia in neuroinflammation, it is perhaps unsurprising that this cell type has been identified as a target of interest for therapeutic interventions in leukodystrophy. As the principal immune cell of the CNS, these highly specialised brain-resident macrophages have a host of functions in both health and disease. Recent literature has begun to consider the microglia as performing three distinct roles within the brain: the sentinel, the housekeeper and the warrior (Hickman *et al.*, 2018b). As the sentinels of the CNS, microglia extend cellular processes throughout their environment, searching for any disruptions that may threaten homeostasis (Nimmerjahn, Kirchhoff and Helmchen, 2005). In their housekeeping role, microglia respond to any such perturbations by phagocytosing dying neurons or extracellular debris, interacting with other glial cells and promoting synaptic remodelling (among others) (Nicholas, Wing and Compston, 2001b; Fuhrmann *et al.*, 2010b; Yeo *et al.*, 2012b; Healy *et al.*, 2016b). Finally, as the so-called “warriors” of the brain, microglia serve to protect the CNS from potentially deleterious stimuli, including pathogens or protein

aggregates (Hatton and Duncan, 2019a). As such, microglia are well positioned to protect from disease, but also to exacerbate – or even drive – neuropathology.

Accordingly, microglia have been linked to a variety of neurodevelopmental and neurodegenerative diseases – with complex interactions with pathogenesis. For example, in Alzheimer's disease, microglia are thought to be protective against some aspects of pathology, while exacerbating others. As the "housekeepers" of the brain, the microglia are well positioned to phagocytose and clear amyloid plaques, yet, in their "warrior" role, their subsequent release of pro-inflammatory cytokines is thought to be neurotoxic (Salter and Stevens, 2017). The central role of microglia in Alzheimer's disease pathology is further demonstrated by genome-wide association studies (GWAS) of patients, which have demonstrated that many genes involved in core microglial functions increase risk of disease (Efthymiou and Goate, 2017). A similar dual role for microglia is thought to occur in Parkinson's disease, whereby microglia release reactive oxygen species following engulfment of alpha-synuclein – clearing protein aggregates, while also promoting inflammation (Glass *et al.*, 2010). In multiple sclerosis – a disorder characterised by both inflammation and demyelination – microglia are thought to contribute to the inflammatory environment which induces myelin loss, but also be essential for myelin repair (Distéfano-Gagné *et al.*, 2023). Microglial abnormalities have even been reported in neurodevelopmental disorders such as autism-spectrum disorders (ASD), with increased microglial density and activation visible in post-mortem tissue, and several microglial-specific genes implicated in GWAS of individuals with ASD (Morgan *et al.*, 2010; Suzuki *et al.*, 2013). As such, whether simply responding to or directly driving pathology, microglia are implicated in a wide variety of neurological disorders and, therefore, are likely to be involved in leukodystrophy pathogenesis in some way.

1.3.2 Microglia in leukodystrophy

1.3.2.1 Primary microgliopathies

The growing use of next generation sequencing in the clinic has led to the finding that loss-of-function mutations in microglia-associated genes are directly causal in several leukodystrophies, often referred to as 'primary microgliopathies' (van der Knaap and Bugiani, 2017b). These include ALSP and Nasu-Hakola Disease (NHD): both of which are caused by mutations in proteins critical for the survival, differentiation or activation of microglia (Paloneva *et al.*, 2000; Oosterhof *et al.*, 2019).

NHD is caused by homozygous pathogenic variants in *TREM2* – a microglia-specific receptor essential for maintenance of microglial homeostasis and response to disease – or *TYROBP*, which encodes the TREM2-adaptor protein DAP12 (Ulland and Colonna, 2018; Bennett, 2023). Patients with NHD develop

early-onset dementia – sometimes as early as adolescence – and present with general cerebral atrophy and sclerosing leukoencephalopathy (Ulland and Colonna, 2018; Bennett, 2023). Post-mortem studies have confirmed microglial abnormalities in patients, with evidence of variable microgliosis in the limited number of cases which have been studied, while single cell RNA sequencing of NHD microglia show a striking upregulation of genes involved in proliferation in response to injury and tissue repair (Zhou *et al.*, 2023). In contrast, *Trem2*$^{-/-}$ knockout mice show reduced microglia number from around 1 year old, with microglia appearing less responsive to demyelination and unable to phagocytose and metabolise myelin debris (Poliani *et al.*, 2015). Single cell RNA sequencing of microglia from *DAP12* loss-of-function knock-in mice also demonstrated reduced reactivity, lipid metabolism and lysosomal dysfunction – in alignment with findings from the *Trem2*$^{-/-}$ mouse but showing minimal overlap with NHD patients (Zhou *et al.*, 2023). Strikingly, these animal models develop only very mild – if any – hypomyelination, failing to recapitulate this key patient phenotype (Poliani *et al.*, 2015; Zhou *et al.*, 2023). It has been suggested that this divergence in mouse and patient phenotype may be due to a compensatory response present in mice, but not humans. Alternatively, it is possible that additional challenge is needed to trigger NHD-like pathology in mice, such as the presence of another demyelinating stimuli (Poliani *et al.*, 2015). Nonetheless, although microglia are somehow implicated in NHD, their role in pathogenesis remains unclear.

Another primary microgliopathy in which the role of microglia is better understood is ALSP. This disorder is among the few autosomal dominant leukodystrophies, caused by mutations in *CSF1R*, a key receptor known to regulate microglia number and distribution (Oosterhof *et al.*, 2018). Patients with ALSP present with progressive cognitive, neuropsychiatric, and motor decline, with a mean age of onset of 43 years old and death within an average of 6–7 years after symptom presentation (Rademakers *et al.*, 2012; Konno *et al.*, 2018). Like NHD, early research yielded conflicting reports regarding the number and activation states of microglia in ALSP patients (Tada *et al.*, 2016; Oyanagi *et al.*, 2017). For example, one earlier study has reported a reduction in the number of activated microglia in the cortex of individuals with end-stage ALSP, while further research suggested an increase in activated microglia in patients with prelesional early-stage disease (Tada *et al.*, 2016; Oyanagi *et al.*, 2017). This variation may be in part due to the intrinsic limitations of rare disease research, whereby small patient numbers were used in each of these studies – suggesting any correlations reported may simply have been due to chance. Even within the same patient, substantial variations of microglia density have been reported across the brain suggesting it is possible such results are skewed by the exact regions analysed (Tada *et al.*, 2016). Similarly, transcriptomic analysis has revealed variable expression of several microglia markers throughout brain regions in patients versus controls –

demonstrating the importance of assessing brain tissue as a whole when assessing cell number and distribution (Kempthorne *et al.*, 2020). However, this discrepancy likely reflects the inclusion of patients at different disease states and suggests a mechanism whereby microglial activation is indicative of early disease stages, followed by widespread reduction in microglia as disease progresses. Indeed, a growing body of research has demonstrated a reduction in microglia number in the brains of ALSP patients (Oosterhof *et al.*, 2018; Kempthorne *et al.*, 2020; Papapetropoulos *et al.*, 2022). Perhaps most strikingly, homozygous mutations in *CSF1R* have been linked to an ultra-rare paediatric leukodystrophy, whereby one patient has been reported to develop a complete absence of microglia, resulting in fatality by 10 months of age (Oosterhof *et al.*, 2019; Daghagh *et al.*, 2022). These findings have been mirrored in Csfr1-deficient mice and zebrafish models, resulting in reduced microglia number, increased ventricular size, oligodendrocyte abnormalities and impaired survival (Dai *et al.*, 2002; Erblich *et al.*, 2011; Nandi *et al.*, 2012; Hagemeyer *et al.*, 2017; Oosterhof *et al.*, 2018). Finally, the most compelling evidence for a causal role of microglial dysfunction in ALSP is the emerging clinical evidence that microglia-targeted therapies – such as TREM2 agonists – may reduce disease progression in ALSP (see 1.2.2.4.3) (Lynch *et al.*, 2024). Together these developments demonstrate a clear role for microglia in the pathogenesis of ALSP and raise further questions about the impact of these neuroimmune cells on leukodystrophies more broadly.

1.3.2.2 A broader role for microglia in leukodystrophies

While ALSP and NHD are useful case studies in which to observe the role of microglia in leukodystrophy pathology, a growing number of studies have evidenced microglial abnormalities beyond primary microgliopathies in patients and animal models.

Histological staining of post-mortem tissue has revealed microglial abnormalities in a wealth of leukodystrophies, summarised in

Table 1.2. In many cases, widespread microglial activation is reported close to sites of white matter lesions and, in some instances, even in normal appearing white matter (Wada, Tifft and Proia, 2000; Eichler *et al.*, 2008; Cologna *et al.*, 2014; Wolf *et al.*, 2014; Bugiani *et al.*, 2018; Martínez Cerdeño *et al.*, 2018; Bergner *et al.*, 2019; Robinson *et al.*, 2020; Panahi *et al.*, 2023). These post-mortem findings have been corroborated using positron emission tomography (PET) imaging of tracers marking activated microglia – showing regional and widespread microglial activation in white matter in patients with the rare leukodystrophies CADASIL (cerebral autosomal dominant arteriopathy with subcortical infarcts and leukoencephalopathy) and Niemann Pick type C, respectively (Walterfang *et al.*, 2020; Walsh *et al.*, 2021). However, due to the highly reactive nature of microglia, it is difficult to establish whether this increase in microglial activation is causal in the pathogenesis of these disorders, or simply due to the broader pathogenic changes happening in the brain. As such, several studies have performed lesion staging in an attempt to track the pathological changes which may precede white matter injury. This work has identified microglial abnormalities in prelesional areas of patients with ALD and MLD, albeit with slightly different courses of progression (Eichler *et al.*, 2008; Bergner *et al.*, 2019). In MLD patients, microglia display an ameboid phenotype in prelesional areas, resulting in eventual microglial loss due to cell membrane lysis in more advanced lesions (Bergner *et al.*, 2019). In patients with ALD, microglial loss is observed even in prelesional areas, and is surrounded by a border of microglia apoptosis (Eichler *et al.*, 2008; Bergner *et al.*, 2019). Strikingly, in both disorders, microglial loss occurred prior to oligodendrocyte damage and myelin degeneration (Bergner *et al.*, 2019). As such, microglial abnormalities – whether that be increased activation, or cell death – may be among the early events driving disease beyond primary microgliopathies.

Table 1.2. Post-mortem evidence of microglial abnormalities in leukodystrophy beyond primary microgliopathies. Colours denote subclassification of white matter disorders.

Disease	No. of patients	Microglial alterations	Reference
Cerebral autosomal-dominant arteriopathy with subcortical infarcts + leukoencephalopathy (CADASIL)	16	Increased numbers of activated microglia in perivascular areas	(Panahi *et al.*, 2023)
Adrenoleukodystrophy (ALD)	4	Loss of microglia in prelesional areas, (prior to significant changes in oligodendrocytes)	(Bergner *et al.*, 2019)
	10	Loss of microglia in perilesional white matter; surrounded by clusters of activated and apoptotic microglia	(Eichler *et al.*, 2008)
Fragile X-Associated Tremor/Ataxia Syndrome (FXTAS)	13	Dystrophic senescent microglia in half of patients; other half show increased numbers of activated microglia	(Martínez Cerdeño *et al.*, 2018)
	1	Widespread microglial activation throughout brain	(Robinson *et al.*, 2020)
Niemann–Pick disease, type C1 (NPC1)	3	Increased numbers of activated microglia in cortex	(Cologna *et al.*, 2014)
Metachromatic leukodystrophy (MLD)	3	Ameboid phenotype in prelesional areas; eventual loss of microglia loss due to cell membrane lysis	(Bergner *et al.*, 2019)
4H Syndrome	1	Mild microglial activation	(Wolf *et al.*, 2014)
	1	Mild-to-moderate microglial activation	(Vanderver *et al.*, 2013)
Sandhoff disease	1	Increased numbers of activated microglia, alongside increased TNF-α expression	(Wada, Tifft and Proia, 2000)
Vanishing white matter disease (VWM)	1	Microglia activation observed in white matter of patients with infantile-onset VWM	(Bugiani *et al.*, 2018)
Krabbe disease (or globoid cell leukodystrophy)	-	Characterised by presence of large, multinucleated phagocytes (globoid cells) throughout CNS; thought to be microglial in origin	(Nicaise, Bongarzone and Crocker, 2016)

Myelin disorder	Leuko-vasculopathy	Lysosomal storage disorder
Leuko-axonopathy	Astrocytopathy	Not characterised

A second line of evidence for the role of microglia in leukodystrophy pathology is the success of therapies thought to target these cells – either directly, or indirectly, in the clinic. HSCT is thought to work the infiltration of donor-derived macrophages into the CNS, where they can adopt a microglial-like function, provide functioning enzyme to the tissue and provide support to damaged neurons and oligodendrocytes (Krivit, 1995; Priller *et al.*, 2001; Asheuer *et al.*, 2004; Yamada *et al.*, 2004; Schönberger *et al.*, 2007; Cronk *et al.*, 2018; Page *et al.*, 2019; Wolf *et al.*, 2020). The efficacy of HSCT is thought to be greater when combined with gene therapy – either by *ex vivo* correction of a patient's own cells, or by delivery of AAV vectors containing functioning copies of a deficient gene alongside HSCT (Wu *et al.*, 2022; Escolar *et al.*, 2023). However, HSCT is still needed for maximum therapeutic impact, with *in vivo* gene therapy alone failing to completely rescue neuropathology (Rafi *et al.*, 2015; Karumuthil-Melethil *et al.*, 2016; Marshall *et al.*, 2018). Finally, promising pharmacological strategies have demonstrated that supporting microglial survival and proliferation, as well as restoring of microglial function, may have downstream impacts on myelin health translating into the clinic (Rodríguez-Pascau *et al.*, 2021; Larson *et al.*, 2024; Lynch *et al.*, 2024). Together, the findings that therapeutic targeting of microglia may have benefits in leukodystrophies implicates these cells as potential drivers – or at least moderators – of pathogenesis across this family of disorders.

Finally, among the greatest indications of the involvement of microglia in pathogenesis are the growing number of animal models of leukodystrophy which, too, show microglial abnormalities. As summarised in Table 1.3, animal models of at least twenty leukodystrophies develop abnormal microglia, with a general trend toward increased numbers of microglia and/or increased microglial activation across these studies. Extending the findings from human post-mortem studies, changes in microglia precede other markers of pathology across many of these models, including synapse loss, astrogliosis, cytokine elevation, and neuronal death (Wada, Tifft and Proia, 2000; Baudry *et al.*, 2003; Kondagari, Yang and Taylor, 2011; Snook *et al.*, 2014; Aradjanski *et al.*, 2017; Gong *et al.*, 2017; Liu *et al.*, 2021). The early emergence of these phenotypes, along with the integral role of microglia in supporting brain homeostasis, suggests that microglial changes may be among the early triggers for pathology in at least some of these leukodystrophies. Accordingly, several experimental approaches targeting the microglia have demonstrated disease modifying effects across animal models. For example, in a mouse model of Niemann Pick Type C, a rare lysosomal disorder, depletion of microglia by targeting of the transcription factor *Irf8* led to modest improvements in survival alongside delayed onset of neurological impairments and neuronal loss (Cougnoux *et al.*, 2018). Other approaches have sought to restore the functioning of microglia. In murine model of Wilson disease, blockade of the NLRP3 inflammasome – thought to be activated in this disease, due to accumulation of copper – was

sufficient to inhibit widespread microglial activation and subsequent cognitive decline, reversing behavioural deficits in this model (Dong *et al.*, 2021). Similarly, restoring microglial activation state by prevention of innate immune activation (through knockout of the immune receptor *FcRγ*) rescues lifespan in a mouse model of Sandhoff disease – further demonstrating the potent role of the neuroimmune response in this disorder (Ogawa *et al.*, 2017). Finally, studies of a zebrafish model of Ribonuclease T2 (RNASET2)-deficient leukodystrophy – a disorder which sits at the intersection of leukodystrophies and interferonopathies – demonstrated that, not only is microglial dysfunction one of the earliest markers of pathogenesis in this disorder, microglia-specific restoration of *rnaset2* expression is sufficient to rescue neuropathology (Hamilton *et al.*, 2020a)

Thus, there is a growing body of evidence that microglia may be a potential driver of leukodystrophy pathology – rather than simply being activated downstream – in leukodystrophies beyond those considered primary microgliopathies.

Table 1.3. Animal models showing evidence of microglial abnormalities in leukodystrophies beyond primary microgliopathies. Colours denote subclassification of white matter disorders.

Disease	Animal model	Microglial alterations	Reference
Adrenomyeloneuropathy	*Abcd1*$^{-/-}$ mouse	Upregulation of microglial phagocytosis markers in spinal cord precedes synapse loss	(Gong *et al.*, 2017)
Canavan disease	*Aspa*$^{-/-}$ mouse	Increased proportion of activated microglia, alongside elevated markers of apoptosis	(Ahmed *et al.*, 2016)
Cerebral autosomal dominantarteriopathy with subcortical infarcts and leukoencephalopathy (CADASIL)	*TgNotch3*^{R169C} mouse	Increased overall number of microglia (but no change in number of activated microglia)	(Rajani *et al.*, 2021)
	TgN3R182C^{150} mouse	Activating microglia reduces NOTCH3 deposition	(Oliveira *et al.*, 2023)
Cockayne Syndrome	*Csa*$^{-/-}$/*Xpa*$^{-/-}$ mouse	Age dependent increase in overall number, and activation state, of microglia	(Kajitani *et al.*, 2021)
Fucosidosis	*Fuca1*$^{-/-}$ mouse	Increased numbers of activated microglia at early and late symptomatic stages	(Wolf *et al.*, 2016)
	Naturally occurring canine fucosidosis	Increased numbers of resting and activated microglia preceding onset of clinical signs	(Kondagari, Yang and Taylor, 2011)
Glutaric Acidemia type 1	*Gcdh*$^{ki/ki}$ rat	Widespread microglial activation, thought to trigger astrogliosis	(Gonzalez Melo et al., 2021)(Gonzalez Melo et al., 2021)
GM1 gangliosidosis	*Glb1*^{G455R} mouse	Microglial activation and proliferation precede onset of pathology	(Liu et al., 2021)(Liu et al., 2021)
Krabbe disease	Twitcher mouse	Activation of microglia prior to astrogliosis and cytokine elevation	(Snook et al., 2014)(Snook et al., 2014)
	Galc^{twi-5J} mouse	Increase in microglia throughout white matter in brain and spinal cord	(Potter et al., 2013)(Potter et al., 2013)
	Galc$^{-/-}$ mouse	Increase in microgliosis	(Weinstock et al., 2020)(Weinstock et al., 2020)
	Galc$^{+/-}$ mouse	Microglia impaired in their ability to clear myelin debris after cuprizone challenge	(Scott-Hewitt, Folts and Noble, 2018)(Scott-Hewitt, Folts and Noble, 2018)

L-2-hydroxyglutaric aciduria	*L2hgdh*$^{-/-}$ mouse	Increased numbers of activated microglia prior to astrocyte proliferation	(Ma et al., 2017)(Ma et al., 2017)
Leukoencephalopathy with brainstem and spinal cord involvement and lactate elevation (LBSL)	*Dars2*^{NEKO} mice (neuron-specific Dars2 KO)	Microglia activation precedes neuronal loss	(Aradjanski et al., 2017)(Aradjanski et al., 2017)
MTHFR deficiency	*mthfr*$^{-/-}$ zebrafish	Reduced numbers of microglia during early development, alongside accumulation of apoptotic cells	(Simonian et al., 2023)(Simonian et al., 2023)
Mucolipidosis type IV	*Mcoln1*$^{-/-}$ mouse	Activated microglia with a mixed neuroprotective/neurotoxic expression profile	(Cougnoux et al., 2019)(Cougnoux et al., 2019)
Multiple sulfatase deficiency	*Sumf1*$^{-/-}$ mouse	Microglia activation beginning during early development	(Settembre et al., 2007)(Settembre et al., 2007)
	sumf1$^{-/-}$ zebrafish	Increased numbers of microglia at 3dpf, which do not persist to 5–7dpf	(Fleming et al., 2022)(Fleming et al., 2022)
Niemann-Pick disease, type C	*NPC1*$^{-/-}$ mouse	Activated microglia throughout the CNS, thought to precede neuronal death and astrogliosis	(Baudry et al., 2003)(Baudry et al., 2003)
		Microglia become increasingly rounded in a manner that correlates with disease progression, with increased chemokine and proinflammatory mediator expression Depletion of microglia improves neuropathology and overall survival	(Cougnoux et al., 2018)(Cougnoux et al., 2018)
Ornithine transcarbamylase deficiency	*spf/Y* mouse	Increased numbers of activated microglia	(Robinson et al., 1995)(Robinson et al., 1995)
Pelizaeus–Merzbacher-like disease	*Cx47*$^{M282T/M282T}$ and *Cx47*$^{-/-}$ mouse	Increased microglia activation	(Tress et al., 2011)(Tress et al., 2011)
RNASET2-deficient leukodystrophy	*rnaset2*$^{-/-}$ zebrafish	Highly vacuolar microglia	(Weber *et al.*, 2020)
	rnaset2^{sh532} zebrafish	Increased number of microglia during development; microglia display highly vacuolar, rounded morphology with accumulating apoptotic cells	(Hamilton *et al.*, 2020a)

		Microglia-specific restoration of *rnaset2* expression is sufficient to rescue neuropathology	
Sandhoff Disease	*Hexb*$^{-/-}$ mouse	Microglia activation precedes neuronal apoptosis	(Wada, Tifft and Proia, 2000)
		Restoring microglial activation state by prevention of innate immune activation through knockout of *FcRγ* rescues lifespan	(Ogawa *et al.*, 2017)
Vanishing white matter disease (VWM)	*eif2b5*$^{zc102/zc102}$ + *eif2b5*$^{zc103/zc103}$ zebrafish	Mild increase in number of microglia undergoing cell division	(Keefe *et al.*, 2020)
	eif2b3$^{-/-}$ zebrafish	Decrease in overall microglia number	(Lee *et al.*, 2021)
Wilson Disease	*Atp7b*$^{-/-}$ mouse	Blockade of NLRP3 inflammasome prevents microglial activation and improves cognition	(Dong *et al.*, 2021)

Myelin disorder	Leuko-vasculopathy	Lysosomal storage disorder
Leuko-axonopathy	Astrocytopathy	Interferonopathy
Inherited metabolic disorder	Not characterised	

1.4 RNASET2-deficient leukodystrophy

Among the leukodystrophies, those characterised by prominent upregulation of the interferon response – referred to as interferonopathies – may be particularly susceptible to microglia-driven pathogenic changes relative to the broader white matter disease family. Given the essential role of microglia in orchestrating the antiviral response, such interferonopathies are characterised by widespread neuroinflammation, with microglial dysfunction implicated in some disorders (Hatton and Duncan, 2019b; Hamilton *et al.*, 2020a).

RNASET2-deficient cystic leukoencephalopathy (hereafter referred to as RNASET2-deficient leukodystrophy) is one such disorder: an ultrarare autosomal recessive neurogenetic disease. Radiological presentations of affected patients typically include white matter lesions, micro- or normo-cephaly, subcortical cysts (often in the temporal lobe) and intracranial calcification presenting during childhood (Henneke *et al.*, 2009a). Affected patients typically present with variable intellectual disability, spasticity, and delay in acquiring motor and speech milestones which results in many patients never gaining the ability to walk or talk (Medline Plus, 2024). Symptom onset typically occurs within the first few months of life and, although this disorder is typically non-progressive, the resulting impacts on quality of life for affected children and their families are devastating (Henneke *et al.*, 2009b; Kameli *et al.*, 2019). As with many interferonopathies, clinical phenotypes mimic that of patients with congenital cytomegalovirus infection – with some RNASET2-deficient patients also showing upregulation of several antiviral genes, including type 1 interferon response (although this, too, is highly variable) (Henneke *et al.*, 2009a; Tonduti *et al.*, 2016a; Garau *et al.*, 2019).

To date, approximately 50 cases of confirmed RNASET2-deficient leukodystrophy have been reported, meaning – like with many rare diseases – our understanding of the pathogenesis of RNASET2-deficient leukodystrophy remains limited (Medline Plus, 2024). Due to the small number of patients and variability in clinical phenotypes, it remains difficult to fully characterise the clinical phenotype of this disorder. For example, some patients present with developmental delay during early life and never achieve developmental milestones (Kameli *et al.*, 2019; Medline Plus, 2024). In contrast, other patients have been followed into adulthood, and are able to speak and walk without aids – demonstrating relatively subtle disability (Kameli *et al.*, 2019). This variability in clinical presentation may be explained by differences in mutations thought to underpin this disorder. Linkage analysis has revealed this disorder is caused by biallelic loss-of-function mutations in the ribonuclease RNASET2 – a lysosomal hydrolase involved in the metabolism of single-stranded RNA (Haud *et al.*, 2011a). Such mutations may either be homozygous (where a patient has two copies of the same mutated allele) or compound

heterozygous (where a patient inherits distinct mutations from each parent) (summarised in Table 1.4) (Kameli *et al.*, 2019). Each of these mutations is thought to result in a loss of RNASET2 mutation – however, the genotype-phenotype relationship remains unclear. Even patients with predicted null mutations are able to develop some speech, motor, cognitive and social skills, albeit with severe difficulties – demonstrating that biallelic null mutations are not only compatible with life, but also with neurodevelopment (Tonduti *et al.*, 2016b; Kameli *et al.*, 2019). Finally – and crucially – it remains unclear how loss of functioning RNASET2 causes the strikingly selective white matter pathology observed in patients – demonstrating the need for a greater understanding of the cellular drivers of RNASET2-deficient leukodystrophy.

Table 1.4. Mutations associated with RNASET2-deficient leukodystrophy.

Nucleotide position change	Zygosity	Predicted functional consequence	Reference
c.2delT/p.Met1	Homozygous	frameshift initiator codon variant (potentially null)	Tonduti *et al.,* 2016
c.2delT/p.Met1	Homozygous	frameshift initiator codon variant (potentially null)	Tonduti *et al.,* 2016
c.50_64del; 567G4A	Compound heterozygous	Deletion (both)	Henneke *et al.,* 2009
c.233C > A; p.Ser78Ter	Homozygous	Nonsense	Kameli *et al.,* 2019
c.262–2 A > G	Homozygous	Splicing - induces deletion and frameshift	Henneke *et al.,* 2009
c.332 + 1delG	Homozygous	Splicing - induces deletion	Henneke *et al.,* 2009
c.397_399delAAG/p.Lys133del; c.145G > T/p.Glu49	Compound heterozygous	Nonsense and deletion	Tonduti *et al.,* 2016
c.550 T > C/p.Cys184Arg	Homozygous	Missense	Tonduti *et al.,* 2016
c.550 T > C/p.Cys184Arg	Homozygous	Missense	Henneke *et al.,* 2009
c.550 T > C/p.Cys184Arg	Homozygous	Missense	Tonduti *et al.,* 2016
c.550 T > C/p.Cys184Arg	Homozygous	Missense	Tonduti *et al.,* 2016
c.87-1341_147 + 1181del2583	Homozygous	Deletion	Henneke *et al.,* 2009
c.87-1341_147 + 1181del2583	Homozygous	Deletion	Henneke *et al.,* 2009

1.4.1 Function of RNASET2

RNASET2 is a highly conserved ribonuclease, present in bacteria and plants through to invertebrates (MacIntosh, 2011). In humans, RNASET2 is thought to be ubiquitously expressed, albeit at low levels, with particular enrichment in the spleen, lymph nodes and colon (Acquati *et al.*, 2019). At a subcellular level, RNASET2 is localised within acidified lysosomes, as well as on the outer mitochondrial membrane and within the intermembrane space (Huang, Liu and Wang, 2018; Greulich *et al.*, 2019; Ostendorf *et al.*, 2020; Bérouti *et al.*, 2024). As such, various studies have demonstrated a key role for RNASET2 in metabolizing pathogenic, ribosomal and mitochondrial ribonucleotide structures (Huang, Liu and Wang, 2018; Greulich *et al.*, 2019; Ostendorf *et al.*, 2020; Bérouti *et al.*, 2024).

Accordingly, a growing body of literature has revealed the complex immunomodulatory role of RNASET2. As a ribonuclease, RNASET2 has long since been understood to essential in the degradation of foreign RNA, acting as a so-called “alarmin” to alert the immune system to the presence of pathogenic material (Schwartz et al., 2018; Rutherford, Kasher and Hamilton, 2021). Accordingly, in the absence of RNASET2, ribonucleic material of various origins is thought to accumulate within lysosomes and/or mitochondria which may spill into the cytoplasm and trigger antiviral signalling (Huang, Liu and Wang, 2018; Rutherford, Kasher and Hamilton, 2021). Indeed, recent research has demonstrated that a loss of RNaseT2 in mice triggers autoinflammatory signalling via activation of the murine-specific pattern recognition receptor (PRR) toll-like receptor TLR13 (Gomez-Diaz *et al.*, 2025). As such, in wild type mice, RNaseT2 may restrict TLR13-mediated autoinflammation, whereas TLR13-driven signalling may contribute to the widespread inflammation seen in RNaseT2-deficient animals.

However, several studies have since demonstrated that RNASET2 also plays an essential role in activating inflammatory signalling through preparation RNA ligands for PPR activation, acting upstream of the toll-like receptors TLR7 and TLR8. During infection, RNASET2 is thought to act synergistically with other nucleases, such as RNASE2 and phospholipase exonucleases, to release PRR ligands from pathogenic oligoribonucleotides (Greulich *et al.*, 2019; Ostendorf *et al.*, 2020). One such PRR ligand is uridine, which then binds to the pattern recognition receptor TLR8, facilitating downstream T helper-1 (Th1) cell signalling, cytokine release and interferon-γ response (Ostendorf et al., 2020). RNASET2 is also thought to act on complex RNA molecules to expose new 5’ ends, which may then activate the PRR TLR7 and trigger a type I interferon response (Bérouti *et al.*, 2024). Accordingly, RNASET2-deficient cells – including peripheral blood mononuclear cells derived from patients – are severely impaired in their TLR7/8-mediated response to RNA oligonucleotides, particularly those derived from bacteria, but are still able to respond to TLR7/8 ligands – confirming the role of RNASET2 upstream of these PRRs (Greulich *et al.*, 2019; Ostendorf *et al.*, 2020).

As such, the impact of a loss of RNASET2 function in human patients likely leads to complex changes in RNA metabolism – with a reduction in the RNA-derived metabolites thought to activate TLR7 and TLR8, alongside an accumulation of undigested RNA species which act as ligands for other RNA receptors (Greulich *et al.*, 2019; Ostendorf *et al.*, 2020). Further work is needed to understand the identity of these RNA receptors, and why the brain is so severely affected given the ubiquity of RNASET2 expression.

1.4.2 Mammalian models of RNASET2-deficient leukodystrophy

Despite the ultra-rare nature of this disorder, several animal models of RNASET2-deficient leukodystrophy have been published, including rat, mouse and zebrafish models. The ability of these animal models to recapitulate patient phenotypes is highly variable, both in terms of the neuropathology and behaviour displayed by these animals (summarised in Table 1.5). Strikingly, mammalian models have showed severe limitations in mirroring the human condition across RNASET2-deficient- and other leukodystrophies (Sinkevicius *et al.*, 2018; Rutherford and Hamilton, 2019a; Kettwig *et al.*, 2021; Rutherford, Kasher and Hamilton, 2021). As such, in this section, I will review these mammalian models and their utility in studying the human disease.

1.4.2.1 RNaseT2 knockout rat

From a clinical perspective, the pathological changes most frequently identified in patients are white matter lesions observable with MRI (Henneke *et al.*, 2009b). As such, the formation of such lesions – or at least, some white matter-associated pathology – is essential in any animal model of this disorder. However, the first rodent model of RNASET2-deficient leukodystrophy – the *RNaseT2*$^{-/-}$ rat – failed to develop any observable white matter pathology (Sinkevicius *et al.*, 2018). At three months of age, both MRI and histopathology indicated no changes in overall brain or white matter volume, and an absence of white matter hyperintensities and cysts. Diffusion weighted imaging indicated altered grey matter architecture in the hippocampus, which was accompanied by an increase in the number of reactive astrocytes observable with immunohistochemistry in this region – suggesting neurodegeneration of the hippocampus at 3 months old. Investigation of brain architecture at 12 months revealed enlargement of the hippocampus and prefrontal cortex – although, again, these were not accompanied by the formation of white matter lesions. At both 3- and 12 months old, *RNaseT2*$^{-/-}$ rats showed abnormal episodic memory, with 12-month-old animals also showing a modest deficit in spatial memory. However, crucially, this model did not model develop any motor impairments, as assessed using a battery of basic motor performance tasks. Psychomotor impairments are among the

most devastating features of RNASET2-deficient leukodystrophy, in terms of impact on patients' day-to-day lives (Medline Plus, 2024). As such, the failure of the RNaseT2 knockout rat to develop both white matter pathology and motor dysfunction limits its utility as a model of this disorder.

Table 1.5. Phenotypes of animal models of RNASET2-deficient leukodystrophy.
[a]Generated by ENU-mutagenesis. [b]Generated by CRISPR-Cas9. OPC, oligodendrocyte progenitor cell; MRI, magnetic resonance imaging.

Animal model	Macroscopic neuropathology	Microscopic neuropathology	Behavioural phenotype	Reference
Zebrafish				
rnaset2^{AO127} zebrafish[a]	White matter abnormalities adjacent to ventricles and focal lesions throughout tissue observable with MRI	Accumulation of amyloid precursor protein and reactive astrocytes around lesion sites	None reported	(Haud *et al.*, 2011b)
sa138 (rnaset2$^{-/-}$*)* zebrafish	No characterisation of white matter structure or lesions	Highly vacuolar microglia at 5dpf Normal neuron and OPC development	None reported	(Weber *et al.*, 2020)
rnaset2^{sh532} zebrafish[b]	White matter lesions observable with MRI	Dysfunctional microglia at 5dpf Uncleared apoptotic inclusions within microglia at 5dpf	Hypoactive during development (5dpf) Repetitive stereotyped movements, impaired exploratory phenotype and tilted swimming behaviour in adulthood	(Hamilton *et al.*, 2020a)
Mouse				
Rnaset2$^{-/-}$ mouse[b]	No characterisation of white matter structure or lesions Blood brain barrier leakage Enlarged brain ventricles (indicative of brain volume loss) Hippocampal atrophy	None reported	Defect in spatial and episodic learning and memory at 4-months-old No evidence of motor impairments at 4-months-old	(Kettwig *et al.*, 2021)
Rat				
RNaseT2$^{-/-}$ rat[b]	No evidence of abnormal white matter structure or lesions Enlarged hippocampus and prefrontal cortex	Increased reactive astrocytes in hippocampus	Defect in episodic learning and memory at 3-months-old which does not worsen with age No evidence of motor impairments at 12-months-old	(Sinkevicius *et al.*, 2018)

1.4.2.2 Rnaset2 knockout mice

Following the failure of the *RNaseT2*$^{-/-}$ rat to develop key disease hallmarks, subsequent research has investigated mouse models of disease. The *Rnaset2*$^{-/-}$ mouse does indeed develop many of the phenotypes displayed by RNASET2-deficient patients (Kettwig *et al.*, 2021). *Rnaset2* knockout mice show reduced survival emerging at 10 weeks of age, reduced brain volume and prominent antiviral response, with interferon response-associated transcripts elevated over 20-fold. Accordingly, knockout mice showed evidence of widespread neuroinflammation, characterised by infiltration of peripheral immune cells, microglial activation throughout the grey and white matter and localised sites of blood brain barrier leakage observable with contrast-enhanced cerebral MRI. Volumetric MRI also revealed ventricular enlargement suggesting brain volume loss and, in direct opposition to *RNaseT2* knockout rats, atrophy of the hippocampus. Nonetheless, *Rnaset2* knockout mice also showed impaired spatial and episodic memory which – like in the rat model – was not mirrored by motor defects. However, once again, neither MRI nor histopathology observed any white matter lesions in this rodent model – with immunohistochemistry against myelin basic protein showing normal myelination throughout the cortex, even close to sites of T-cell infiltration. Interestingly, single cell RNA sequencing revealed that oligodendrocytes and their precursors were transcriptionally disturbed in this model, with upregulation of transcripts associated with the type I interferon signalling and defence response to virus pathways. However, these changes were not reflected at a macroscopic level in white matter structure or lesion formation. Therefore, the *Rnaset2* knockout mice is also limited in its ability to recapitulate key patient phenotypes – highlighting the need for additional models to understand pathogenesis and develop treatments for RNASET2-deficient leukodystrophy.

1.4.3 The rnaset2 mutant zebrafish

While mammalian models of RNASET2-deficient leukodystrophy are lacking, recent research has demonstrated that zebrafish (*Danio rerio*) are a powerful model of this disorder – recapitulating core pathological hallmarks (Haud *et al.*, 2011b; Hamilton *et al.*, 2020a; Weber *et al.*, 2020). In this section, I will review the broad advantages for the use of zebrafish as a tool to study neurodevelopmental disorders, before assessing their utility specifically as a model of microglial function and white matter pathology – both of which are essential for any model of leukodystrophy. Finally, I will review existing zebrafish models of the broader leukodystrophy family and describe published fish models of RNASET2-deficient leukodystrophy to assess their utility as models of disease.

1.4.3.1 Introducing the zebrafish

The unique advantages of the zebrafish make it an increasingly popular model in biomedical research – with zebrafish research consistently representing a greater proportion of publications than mouse models each year since 2016 (Doszyn, Dulski and Zmorzynska, 2024). Despite their evolutionary divergence, zebrafish have a striking genetic similarity with humans – with over 70% of human genes having at least one zebrafish homolog (Howe *et al.*, 2013). Furthermore, the transparent, *ex utero* development of zebrafish embryos in combination with a wealth of available reporter lines allows observation of live cellular function in real time (Traver *et al.*, 2003). This is particularly useful in a developmental context, allowing researchers to visualise cellular interactions from a synapse to circuit level, to understand how brain architecture may develop (Doszyn, Dulski and Zmorzynska, 2024). Additionally, zebrafish have high fecundity – producing many hundreds of embryos per breeding pair – and develop rapidly, allowing high throughput screening of pathology and potential treatments in rapidly developing embryos. In particular, zebrafish display a complex repertoire of behaviours, from simple motor function to learning and memory, which can be tracked using automated systems – further increasing throughput. Finally, the genetic tractability of the zebrafish, along with a growing number of increasingly specific genetic tools, allows for careful manipulation of target gene expression to further understand the molecular mechanisms of pathogenesis. As such, these general strengths demonstrate the value of the zebrafish as a model of neurodevelopmental disorders, including the leukodystrophies.

1.4.3.2 The zebrafish as a tool to study microglial function

There are many advantages to the use of zebrafish as a tool to study microglial function, particularly in a neurodevelopmental context. Firstly, zebrafish microglia emerge during early development and form an integral part of a complete nervous system within just a few days post-fertilisation. Similar to their mammalian counterparts, zebrafish embryonic microglia arise from primitive yolk sac-derived macrophages, which begin colonising the brain from as early as 35 hours post-fertilisation, with robust colonisation of the midbrain by 72hpf (Herbomel, Thisse and Thisse, 2001; Ginhoux *et al.*, 2010; Ferrero *et al.*, 2018). Infiltration of microglia precursors occurs independently of circulation, and is thought to be triggered by developmental apoptosis, mediated by the release of nucleotides and phospholipids released by these dying cells (Casano, Albert and Peri, 2016a; Xu *et al.*, 2016). After colonisation, these cells begin to alter their gene expression profile, adopt an increasingly ramified morphology and show decreases in motility – all phenotypes which may differentiate microglia from macrophages – from 3- to 5dpf, suggesting differentiation into a comprehensive microglial phenotype occurs around these ages (Svahn *et al.*, 2013; Mazzolini *et al.*, 2020).

Secondly, the transparency of zebrafish during larval stages, in combination with their genetic tractability, has facilitated the generation of several transgenic reporters which allow the visualisation of microglia function in real time in the developing brain. These include *Tg(fms:GFP)* and *Tg(mpeg:mCherryCAAX)* lines, which label all macrophages and microglia in the zebrafish embryo (although the ability of the mpeg-reporter to reliably label macrophage-derived cells in the adult brain has been questioned), as well as the *TgBAC(p2ry12:p2ry12-GFP*) line, which drives GFP expression under control of the purinergic receptor p2ry12 and is expressed specifically in microglia (Sieger *et al.*, 2012; Bojarczuk *et al.*, 2016; Dee *et al.*, 2016; Rovira *et al.*, 2023; Nguyen *et al.*, 2024). These reporters have facilitated real-time observation of several key microglial functions including: microglial activation following exposure to damage- or disease-associated stimuli; migration to sites of neuronal injury; extension and retraction of cellular processes; phagocytosis of apoptotic debris; activity-dependent interactions with neurons; and remodelling of myelin sheaths (Sieger *et al.*, 2012; Svahn *et al.*, 2013; Mazaheri *et al.*, 2014; Blume *et al.*, 2020; Hughes and Appel, 2020). These live imaging studies demonstrate conservation of core microglial functions in the zebrafish and demonstrate the power of this model in live imaging of cellular behaviour which may be more challenging in other models.

Finally, transcriptomic studies have demonstrated that zebrafish microglia share many similarities with their mammalian counterparts. RNA sequencing has revealed that zebrafish microglia gene expression correlates strongly with that of mouse and human microglia, including conservation of genes involved in cellular, metabolic, immune and developmental processes as identified by gene ontology analysis (Svahn *et al.*, 2013; Oosterhof *et al.*, 2017; Mazzolini *et al.*, 2020). These findings suggest the zebrafish is a valid model in which to study microglial function.

However, there are several key differences between zebrafish and mammalian microglia. In zebrafish, it is now widely understood that there are two distinct populations of microglia present throughout life. Zebrafish embryonic microglia – as mentioned above – arise from yolk sac progenitors, colonise the brain from around 2dpf and persist to juvenile stages (~90dpf) (Ferrero *et al.*, 2018, 2021). However, in a phenomenon that has not been robustly reported in mammals, these embryonic microglia are gradually replaced by a distinct, second wave of adult microglia which are derived from haematopoietic stem cells in the whole kidney marrow (WKM) – with replacement beginning around 20dpf until these WKM-derived cells are the only microglia persisting in host brains (Ferrero *et al.*, 2018, 2021). In addition to arising from different precursors, these two populations are also transcriptionally distinct (Mazzolini *et al.*, 2020). It remains unclear whether the two populations are functionally different, or whether these changes in gene expression simply reflect the differing

environment between the larval and adult CNS. If this replacement is truly specific to the zebrafish, this may highlight a possible fundamental evolutionary difference between zebrafish and mammals, and call into question the validity of the study of microglia in this model. Consensus is that murine microglia derive from yolk sac progenitor macrophages, and that the CNS microglial pool self-renews throughout life with no involvement of peripheral cells (Ajami et al., 2007a; Mildner et al., 2007a; Ginhoux et al., 2010). However, there are some observations which suggest that multiple sources may give rise to murine microglia. For example, in mouse studies, up to 40% of adult microglia have been reported to express markers otherwise found in the HSCs and peripheral blood and arise from cells migrating into the CNS after birth – suggesting these cells may be haematopoietic in origin (Chen *et al.*, 2010). Furthermore, depletion of yolk sac macrophages during early development does not entirely deplete the postnatal microglial population – suggesting another potential source for microglia in this instance (Squarzoni *et al.*, 2014; Hoeffel *et al.*, 2015). Finally, evidence has suggested that HSC-derived cells are able to infiltrate the brain and produce microglia-like cells in instances of blood brain barrier disturbance or in disease models, including models of leukodystrophy (Priller *et al.*, 2001; Biffi *et al.*, 2004; Miyake *et al.*, 2010; Capotondo *et al.*, 2017). As such, it is entirely possible that there are indeed multiple sources of mammalian microglia, but inherent limitations of this model have thus far not been able to robustly identify them. Indeed, there is disagreement in the murine field about which specific yolk sac-derived population gives rise to microglia – whether these cells emerge from primitive macrophages emerging at embryonic day 7.5 or erythro-myeloid progenitors which emerge at embryonic day 8.25 – demonstrating the challenges of unpicking cellular ontogeny in overlapping populations, in an animal model where longitudinal live imaging is challenging (Ginhoux *et al.*, 2010; Kierdorf *et al.*, 2013; Gomez Perdiguero *et al.*, 2015; Ferrero *et al.*, 2018). Therefore, the use of zebrafish as a model of microglial function should not be ruled out based on these observations.

There are also some technical limitations to consider when studying microglia in zebrafish. Perhaps the most significant of these are the limited number of antibodies available to study microglia via immunohistochemistry in zebrafish models. In mammalians, whole panels of antibodies are available to detect and study microglia. Among the most common are antibodies against Iba1 (also expressed by some macrophages), PU.1 (a marker of yolk sac-derived macrophages), CD45 and CD11b (where CD11b-positive, CD45-low cells may indicate microglia, albeit not entirely specifically), Tmem119 (exclusively expressed in mature microglia) and P2ry12 (which is microglia-specific in homeostatic brains, but may be downregulated on microglia following activation and/or expressed on infiltrating macrophages) (Jurga, Paleczna and Kuter, 2020). In combination with others, relative levels of these antibodies can not only detect microglia, but also infer their activation state. In contrast, few microglial

antibodies are available in the zebrafish due to limited cross-reactivity with mammalian proteins. Arguably, there is only one robust, well-characterised and widely published antibody – the 7.4.C4 monoclonal antibody (hereafter referred to as 4C4). This antibody is generated from a hybridoma line inoculated with proteins from the optic nerve of freshwater fish and has since been discovered to be highly specific for microglia (Becker *et al.*, 1998; Becker and Becker, 2001). For many years, this antibody was widely used despite poor characterisation of its protein target – however, recent work has demonstrated that this antibody targets Galectin 3 binding protein (Lgals3bp), a scavenger receptor expressed ubiquitously across zebrafish microglia with a wealth of immune-related functions (Rovira *et al.*, 2023). As such, this antibody provides one tool to visualise microglia, but cannot infer the functional state of these cells. Nonetheless, the lack of antibodies available to study microglia in zebrafish are somewhat circumvented by the wealth of reporter lines available, which allow visualisation of these cells and assessment of expression of several markers of interest. Furthermore, assessment of microglial state by looking at a single marker alone – as is often performed by immunohistochemistry – is highly limited (Jurga, Paleczna and Kuter, 2020). Arguably the most comprehensive way to assess microglial function is through "omics" approaches – such as single cell- or bulk RNA sequencing, or proteomics – which have now been widely explored in zebrafish (Svahn *et al.*, 2013; Oosterhof *et al.*, 2017; Mazzolini *et al.*, 2020; Dumas, Borst and Prinz, 2021) As such, despite these limitations, the zebrafish provides a useful tool to study the microglial function in the context of leukodystrophies.

1.4.3.3 The zebrafish as a tool to study white matter

The hallmark characteristic of RNASET2-deficient leukodystrophy – and leukodystrophies in general – are white matter lesions observable with MRI (Henneke *et al.*, 2009b). Observation of these lesions is necessary for the diagnosis of this disorder – and other leukodystrophies – demonstrating how central this pathology is to this family of disease. Yet, as previously discussed, mammalian models have failed to sufficiently advance our understanding of the mechanism of lesion formation due to a failure accurately recapitulate the white matter defects seen in patients – demonstrating the need for further models of disease (Kettwig *et al.*, 2021).

Despite the evolutionary divergence to humans, the zebrafish remains a useful model in which to study myelination. Firstly, the protein composition of zebrafish myelin is well conserved from mammals. The complex structure of myelin is comprised predominantly of lipids – giving white matter structures the colour that forms their name – with around 30% formed of a multitude of proteins. In the zebrafish, many of these proteins are conserved across species, including the three most abundant proteins: myelin basic protein (encoded by two zebrafish orthologues, *mbpa* and *mbpb*), myelin protein zero

(analogous to mammalian P_0) and proteolipid protein 1a (Preston and Macklin, 2015; Siems *et al.*, 2021). Secondly, the resulting structure of zebrafish myelin seems to be comparable to that seen in mammals, with similar G ratios (the conserved relationship between axon diameter and sheath thickness) and periodicity (Hildebrand and Hahn, 1978; Avila *et al.*, 2007). Furthermore, the transcriptional cascades that control maturation of oligodendrocytes from oligodendrocyte progenitor cells (OPCs) are shared between zebrafish and mammals, including *sox2*, *sox10* and *olig2* (Ackerman and Monk, 2016). In addition, zebrafish myelination begins early in their transparent, *ex utero* development – with terminal differentiation of myelinating oligodendrocytes beginning at around 3dpf, and formation of mature myelinated tracts by 7–8dpf – allowing visualisation of myelin proteins and oligodendrocytes in live embryos using transgenic reporters (D'Rozario, Monk and Petersen, 2017). Finally, behavioural assays have been developed to allow functional assessment of myelination, exploiting simple circuitry known to underpin embryonic behaviours as a measure of axon potential conduction velocity (a correlate of myelination) (Madden *et al.*, 2021). As such, there are many advantages in using zebrafish to assess myelination in the CNS.

However, there are also limitations of using zebrafish to model mammalian myelin. Firstly, while zebrafish myelin contains many orthologous proteins to those seen in mammals, there are a number of zebrafish-specific proteins that are yet to be identified in humans or mice (Morris *et al.*, 2004; Möbius *et al.*, 2008; Schaefer and Brosamle, 2008). It has been proposed that these proteins may serve an additional function in the zebrafish, which – as cold-blooded animals – are unable to regulate their own body temperature, and therefore require additional proteins to ensure consistent membrane fluidity (Möbius *et al.*, 2008; Ackerman and Monk, 2016). As such, it is possible myelin composition is adapted to serve slightly different roles across species.

In addition, there is one fundamental factor which may limit the utility of zebrafish in modelling disorders of myelin – their vast ability for regeneration. Even in the CNS, zebrafish axons can be remyelinated after a variety of types of injury, whereas the capacity for remyelination in rodents is much more limited (Becker and Becker, 2008; März *et al.*, 2011; Vajn *et al.*, 2013). Accordingly, it is possible that zebrafish mutants may show a lesser degree of myelin pathology than might be expected, due to their ability to remyelinate and regenerate – or even, withstand initial insult. Although the extent of species-specific compensation remains unclear, there remain a variety of zebrafish models of myelination which have reported robust hypomyelination – suggesting this system is still susceptible to white matter abnormalities at a gross and cellular level (Madden *et al.*, 2021; Neely *et al.*, 2022). As

such, the zebrafish remains a simple, vertebrate model in which to study potential changes in myelination in the leukodystrophies.

1.4.3.4 Overview of zebrafish models of leukodystrophy

In alignment with their strength as an animal model of both neurodevelopmental- and white matter disorders, the zebrafish is emerging as a powerful – and popular – model of leukodystrophy biology (Shih, Raas and Bonkowsky, 2024). In the last decade, over twenty zebrafish models have been published across fifteen different leukodystrophies (summarised in Table 1.6). These studies have informed our understanding of leukodystrophy at a genetic, cellular and behavioural level. At a genetic level, the tractability of zebrafish has not only allowed the field to generate models of known leukodystrophies, but also investigate the functional consequences of variants of unknown significance identified in patients – leading to the characterisation of new ultra-rare disorders (Derksen *et al.*, 2021; Berdowski *et al.*, 2022; Yan *et al.*, 2022; Raas *et al.*, 2024). The use of cellular reporters has revealed changes in the density of microglia and oligodendrocytes, and extent of myelination, in a variety of models (Strachan *et al.*, 2017; Oosterhof *et al.*, 2018; Keefe *et al.*, 2020; Derksen *et al.*, 2021; Lee *et al.*, 2021; Berdowski *et al.*, 2022; Fleming *et al.*, 2022; Yan *et al.*, 2022). The ease of automated behavioural assessments in larvae has demonstrated that variety of zebrafish leukodystrophy models develop motor dysfunction, as is seen in patients (Strachan *et al.*, 2017; Pant, Boespflug-Tanguy and Pujol, 2019; Derksen *et al.*, 2021; Takashima *et al.*, 2021; Berdowski *et al.*, 2022; Shih, Raas and Bonkowsky, 2024). In combination with the rapid development and high fecundity of zebrafish larvae, the ease of behavioural assessment has facilitated high-throughput drug screening assays in a zebrafish model of ALD – where over two thousand compounds were screened to identify drugs that rescue motor behaviour in *abcd1*$^{sa509/sa509}$ larvae, with the top hit validated in patient-derived fibroblasts and a mouse model (Raas *et al.*, 2021). Subsequent transcriptomic analysis suggested that this drug candidate may act by increasing expression of enzymes associated with very long chain fatty acid metabolism (known to be deficient in ALD), which was later confirmed as CRISPR/Cas9-targeting of these genes mimicked ALD phenotypes in larvae – an experiment which was relatively easy to perform thanks to the well-characterised genetics and ease of tractability of the zebrafish model. Live imaging also revealed this compound rescued the number of oligodendrocytes and expression of myelin transcripts in the spinal cord – elegantly demonstrating how the unique advantages of the zebrafish model can not only lead to candidate identification but elucidate the mechanisms by which these drugs may act, relatively quickly and easily. As such, there is a growing precedent for the use of zebrafish in leukodystrophy research, with this model making valuable contributions to the field.

Table 1.6. Zebrafish models of leukodystrophy.

Disease	Zebrafish model	Phenotype	Reference
Aicardi Goutières Syndrome (AGS)	*adar*$^{-/-}$	Elevation of interferon-stimulated gene expression	(Niescierowicz *et al.*, 2022)
	samhd1 knockdown	Cerebral haemorrhage; upregulation of innate immune response	(Kasher *et al.*, 2015)
	samhd1$^{\Delta 23/\Delta 23}$	Elevation of interferon gene signature; microcephaly; increased number of uncleared apoptotic cells; impaired motor function; cerebral haemorrhage	(Withers *et al.*, 2023)
Adult-onset leukoencephalopathy with axonal spheroids and pigmented glia (ALSP)	*csf1ra*$^{-/-}$/*csf1rb*$^{+/-}$	Lifelong reductions in number of microglia; no change in myelin amount or structure	(Oosterhof *et al.*, 2018)
	csf1ra$^{Val614Met/+}$; *csf1rb*$^{-/-}$ (missense mutations observed in patients)	Reduced number of microglia; reduced number of oligodendrocytes without reductions in myelinated area	(Berdowski *et al.*, 2022)
CSF1R-deficient paediatric-onset leukodystrophy	*csf1ra*$^{-/-}$/*csf1rb*$^{-/-}$	Near complete absence in number of microglia; reduced expression of neuronal markers	(Oosterhof *et al.*, 2019)
	csf1ra$^{Val614Met/Val614Met}$; *csf1rb*$^{-/-}$ (homozygous missense mutation)	Reduced number of microglia; reduced number of oligodendrocytes and reductions in myelinated area; impaired motor function	(Berdowski *et al.*, 2022)
DEGS1-related leukodystrophy	*degs1* knockdown	Reduced myelination; impaired motor function	(Pant, Boespflug-Tanguy and Pujol, 2019)
Krabbe Disease	*galca/galcb* knockdown	Disorganised expression of neural markers	(Zizioli *et al.*, 2014)
LSM7-related leukodystrophy	*lsm7*$^{-/-}$	Reduced eye size; reduced oligodendrocytes; motor impairment	(Derksen *et al.*, 2021)
Metachromatic leukodystrophy (MLD)	*arsa*$^{-/-}$	Accumulation of sulfatides; normal motor function and survival	(Shih, Raas and Bonkowsky, 2024)
Mitchell Disease	*hACOX1*^{N237S}	Impaired locomotion; activation of integrated stress response; no change in oligodendrocyte number	(Raas *et al.*, 2024)
Multiple sulfatase deficiency	*sumf1*$^{-/-}$	Increased numbers of microglia at 3dpf, which do not persist to 5–7dpf	(Fleming *et al.*, 2022)
SUPV3L1-related leukodystrophy	*supv3l1* crispant	Impaired survival; mitochondrial dysfunction; activated microglia; upregulation of interferon signalling	(Green *et al.*, 2024)

TMEM163-related leukodystrophy	*tmem163* knockdown	Impaired locomotion; reduced myelin and oligodendrocyte; increased apoptotic cells	(Yan *et al.*, 2022)
Vanishing white matter disease (VWM)	*eif2b5*$^{zc102/zc102}$ + *eif2b5*$^{zc103/zc103}$	Mild increase in number of microglia undergoing cell division; activation of integrated stress response	(Keefe *et al.*, 2020)
	eif2b3$^{-/-}$	Decrease in overall microglia number, hypomyelination and reduced eye size; activation of integrated stress response	(Lee *et al.*, 2021)
X-linked adrenoleukodystrophy (X-ALD)	*abcd1*$^{sa509/sa509}$	Hypomyelination of spinal cord; reduced number of oligodendrocytes; impaired motor function; reduced survival	(Strachan *et al.*, 2017)
Zellweger Spectrum Disorders (ZSD)	*pex2*$^{-/-}$	Accumulation of very long chain fatty acids; reduced survival; impaired locomotion	(Takashima *et al.*, 2021)
4H-leukodystrophy	*polr3b*	Reduction in Purkinje cell progenitors, mirroring cerebellar atrophy	(Yang *et al.*, 2023)

1.4.3.5 Zebrafish models of RNASET2-deficient leukodystrophy

Just as within the broader leukodystrophy field, the zebrafish is emerging as a powerful model of RNASET2-deficient leukodystrophy. To date, three zebrafish models of this disorder have been published, with largely similar phenotypes. The first zebrafish model to be published was the *rnaset2*^{AO127} mutant, which was generated by N-ethyl-N-nitrosourea (ENU)-mutagenesis (Haud *et al.*, 2011b). This model contains a mutation in the open reading frame of the zebrafish *rnaset2* gene, introducing a premature stop codon and truncating the resulting protein between the first and second catalytic site. The second published zebrafish model is the *rnaset2*^{sh532} line, which was generated by CRISPR/Cas9 targeting of the same exon altered in *rnaset2*^{AO127} mutants, after the original line was lost (Hamilton *et al.*, 2020a). The *rnaset2*^{sh532} mutant allele contains an 8 base pair deletion which, like its predecessor, induces a premature stop codon ahead of the second catalytic domain – resulting in truncation of the rnaset2 protein and loss of key catalytic sites. The most recent zebrafish model of RNASET2-deficient leukodystrophy – the *sa138* strain – was generated by ENU-mutagenesis as part of an ambitious project to systematically identify and characterise mutations in every zebrafish protein-coding gene (Kettleborough *et al.*, 2013; Weber *et al.*, 2020). The *sa138* allele also induces a premature stop codon, this time within the second catalytic domain (rather than prior to it) which also results in a truncated, catalytically inactive protein. The relevance of all three of these models to the human condition has been assessed.

As previously discussed, white matter pathology is central to leukodystrophy – with RNASET2-deficient patients presenting with white matter lesions and cysts (Henneke *et al.*, 2009b). Strikingly – despite the failure of rodent models to develop white matter pathology – such changes have now been observed in two zebrafish models of leukodystrophy: the *rnaset2*^{sh532} mutant and its predecessor (*rnaset2*^{AO127}) (Haud *et al.*, 2011b; Hamilton *et al.*, 2020a). These models develop white matter lesions around the ventricles which can be visualised both with MRI and immunohistochemistry (Haud *et al.*, 2011b). Although macroscopic white matter abnormalities of the *sa138* zebrafish have not been assessed, the use of transgenic reporters have suggested that there is no change in the number or distribution of oligodendrocyte precursor cells in larval mutants relative to wild type animals at 3- to 5dpf (Weber *et al.*, 2020). However, this timepoint represents a relatively early stage in myelination – whereas robust myelinated tracts do not arise until around 7–8dpf – making it difficult to establish the true myelination phenotype of the *sa138* model (Brösamle and Halpern, 2002). As such, the *rnaset2*^{sh532} and *rnaset2*^{AO127} lines remain the models with the greatest face validity when recapitulating white matter lesions observed in human patients.

In addition to white matter phenotypes, all three zebrafish models develop evidence of prominent neuroinflammation, consistent with patient phenotypes. Immunohistochemistry has revealed enhanced staining histological markers of neuroinflammation, including astrocyte reactivity, around sites of white matter lesions in *rnaset2*^{AO127} mutants (Haud *et al.*, 2011b). Additionally, across both the *sa138* and *rnaset2*^{sh532} zebrafish, widespread microgliosis has emerged as one of the earliest signs of neuropathology (Hamilton *et al.*, 2020a; Weber *et al.*, 2020). In *rnaset2*^{sh532} mutant brains, upregulation of the antiviral response is also evident during both embryonic and adult stages – recapitulating the interferon response seen in patients (Hamilton *et al.*, 2020a). As such, together these zebrafish models demonstrate a role for neuroinflammation throughout pathogenesis, similar to that seen in patients.

Finally, the *rnaset2*^{sh532} mutant remains the only zebrafish model for which robust motor abnormalities – mirroring those seen in patients – have been published (summarized in Table 1.5) (Hamilton *et al.*, 2020a). These mutants show a hypoactive phenotype which emerges in development (observed at 5dpf) – suggesting impaired motor development. Interestingly, *rnaset2* mutants do not continue to show this reduced locomotor phenotype into adulthood – instead, they show an abnormal, repetitive, stereotyped movement pattern and tilted swimming behaviour, indicative of abnormal vestibular righting reflex or movement deficit (Kalueff *et al.*, 2013). While it remains unclear why the overall speed and distance travelled by *rnaset2*^{sh532} mutants somehow rectifies with age in adult animals, these potential vestibular abnormalities may be indicative of impaired inner ear development – mirroring the sensorineural hearing difficulties reported in patients (Whitfield, 2002; Henneke *et al.*, 2009b; Hamilton *et al.*, 2020a). These findings are in contrast to mammalian models – whereby the *RNASET2*$^{-/-}$ mouse and *RNaseT2*$^{-/-}$ rat show normal motor functioning, with impaired learning and memory. Memory phenotypes have not yet been investigated in any of the *rnaset2* mutant zebrafish: nonetheless, to date, the *rnaset2*^{sh532} line remains the only model to develop robust motor phenotypes consistent with those that might be expected in patients.

As such, zebrafish models – and specifically the *rnaset2*^{sh532} fish – remain the only system in which to assess the effects of potential therapies on both white matter lesions and behavioural abnormalities and can provide a powerful tool with which to investigate the pathogenesis of these disease hallmarks.

1.4.3.6 Limitations of zebrafish as a model RNASET2-deficient leukodystrophy

Although the *rnaset2* mutant zebrafish provides a useful tool with which to further our understanding of leukodystrophy, there are several limitations which must be considered when using this model.

Firstly, as a teleost, the zebrafish are highly evolutionarily divergent from humans and other mammalian models – adding a degree of complexity at the genetic level. Zebrafish possess a higher number of species-specific genes relative to humans, mice and other species (Howe et al., 2013). Additionally, following divergence from a common ancestor, teleosts underwent a whole-genome duplication – meaning there are duplicate orthologues of many human genes which may have adopted distinct functions. Such examples include the zebrafish MBP orthologues, *mbpa* and *mbpb*, which have distinct spatiotemporal expression patterns (discussed in section 1.4.3.3) (Torvund-Jensen *et al.,* 2018). Finally, approximately 30% of human genes have no identified genetic homolog, including genes with prominent roles in inflammation (Howe et al., 2013). As such, while much of the zebrafish genome is now annotated, there remain clear gaps in our understanding of teleost genetics and how this many impact the function of myelin-, inflammation- and other leukodystrophy-associated transcripts.

Additionally, as a non-mammalian model, there are also clear differences in neuroanatomy which make modelling human disease challenging. Brain atlases for zebrafish are lacking, with relatively few regions mapped to mammalian equivalents (Burgess and Burton, 2023). While transgenic reporters have allowed us to begin unpicking circuitry at a cell-by-cell level, a degree of variability within the zebrafish as a species continues to challenge direct comparison with human neuroanatomy. This issue is further complicated when attempting to compare developmental stages between zebrafish and humans. By just 24 hours post-fertilisation, zebrafish embryos exhibit simple sensorimotor reflexes, progressing to more complex behaviours such as navigation and hunting from 4dpf (Filippi, Mueller and Driever, 2014). This rate of development is significantly faster than that seen in mammals, making it difficult to relate specific developmental stages across species. Finally, the zebrafish's tremendous capacity for repair and regeneration may also limit comparisons with human disease. The zebrafish brain grows continuously throughout life, supported by constitutive neurogenesis and multiple stem cell niches in the adult brain (Burgess and Burton, 2023). As such, these factors pose important considerations for modelling disorders at the intersection of neurodevelopmental and neurodegenerative disease, like the leukodystrophies.

Finally, there are also specific limitations of the *rnaset2* mutant zebrafish in its ability to recapitulate the human condition. Firstly, there are aspects of neuropathology which remain to be understood in *rnaset2* mutants. While previous publications have reported the presence of white matter lesions visible on MRI in adult animals, no characterisation of other radiological features – such as the presence of cysts or intracranial calcification – has been reported (Hamilton et al., 2020; Haud et al., 2011). Calcification, in particular, is a core finding in patients with RNASET2-deficient leukodystrophy,

and the presence of calcium deposits with the brain could be assessed through calcein staining in zebrafish larvae; however, no such characterisation has been performed to date (Zhao et al., 2022). As such, the extent to which *rnaset2* mutant zebrafish recapitulate the broader neuropathological findings seen in patients is unclear. Furthermore, previous reports have suggested that *rnaset2* mutant zebrafish present with a progressive phenotype – with mutants showing increasingly impaired survival into adulthood (Hamilton et al., 2020). This contrasts the non-progressive clinical presentations of patients – whereby many patients experience psychomotor developmental delay with lifelong speech and intellectual disabilities in the absence of severe clinical worsening (Kameli et al., 2019). Indeed, to our knowledge, no case reports have identified patients with reduced survival, although many patients were still in early adulthood at follow-up (Kameli et al., 2019). As such, it remains unclear how the progressive pathology of the *rnaset2* mutant zebrafish relates to human disease. Nonetheless, the presence of white matter lesions, neuroinflammation and locomotor dysfunction in *rnaset2* mutant zebrafish suggests that this still provides a useful tool with which to study potential drives of pathogenesis in this disorder.

1.4.4 Microglia in RNASET2-deficient leukodystrophy

In alignment with the growing body of research implicating microglia in leukodystrophy pathogenesis more broadly, research using animal models of RNASET2-deficient leukodystrophy have suggested that microglia may be the cellular drivers of pathology in this order.

Neuroinflammation – and particularly antiviral response – has emerged as a core feature of mammalian and zebrafish models, as well as in patients. As previously discussed, individuals with RNASET2-deficient leukodystrophy present with an upregulated antiviral response, with elevation of interferon-stimulated genes (Tonduti *et al.*, 2016b). Similarly, antiviral transcripts are increased in the brains of both zebrafish and mouse models of disease, relative to wild type controls (Hamilton *et al.*, 2020a; Kettwig *et al.*, 2021). Single cell RNA sequencing from the brains of *Rnaset2*$^{-/-}$ mice has revealed that upregulation of immune response- type I interferon signalling- associated transcripts is particularly enriched in microglia, with other cell types contributing to a much lesser extent. Furthermore, *Rnaset2*$^{-/-}$ microglia showed downregulation of genes associated with microglial homeostasis, and upregulation of markers of activation. As such, it seems that microglia may be the mediators of this aberrant antiviral response in these models.

Moreover, one of the most striking phenotypes seen in several *rnaset2* mutant zebrafish models is the increased number of morphologically abnormal microglia in mutant brains – displaying a bloated, highly circular morphology with many vacuoles – suggesting increased recruitment of peripheral

macrophages into the brain (Figure 1.1 a–d) (Hamilton *et al.*, 2020b). Subsequent characterisation has revealed *rnaset2*^{sh532} mutant microglia and macrophages are not only morphologically abnormal, but functionally impaired. One of the principal triggers of infiltration of peripheral macrophages into the brain is a process known as developmental apoptosis, whereby cells in the developing brain apoptose in an effort to balance cell proliferation (Casano, Albert and Peri, 2016b; Voss and Strasser, 2020). Notably, the number of apoptotic cells in mutant brains was significantly greater compared to their wild type counterparts – suggesting this increased recruitment of peripheral cells may be triggered by an excess of apoptotic neurons (Figure 1.1 e, h) (Hamilton *et al.*, 2020b). Curiously, depletion of the microglia by targeting expression of *irf8* – a transcription factor critical for the differentiation of macrophages and microglia – did not lead to a change in the number of apoptotic cells in mutant brains, while in microglia depletion in wild type animals lead to a three-fold increase in apoptotic cell number (Figure 1.1 g, h). This suggests mutant microglia fail to clear developmental apoptosis, rather than an intrinsic increase in the rate of apoptosis in *rnaset2*^{sh532} mutant brains.

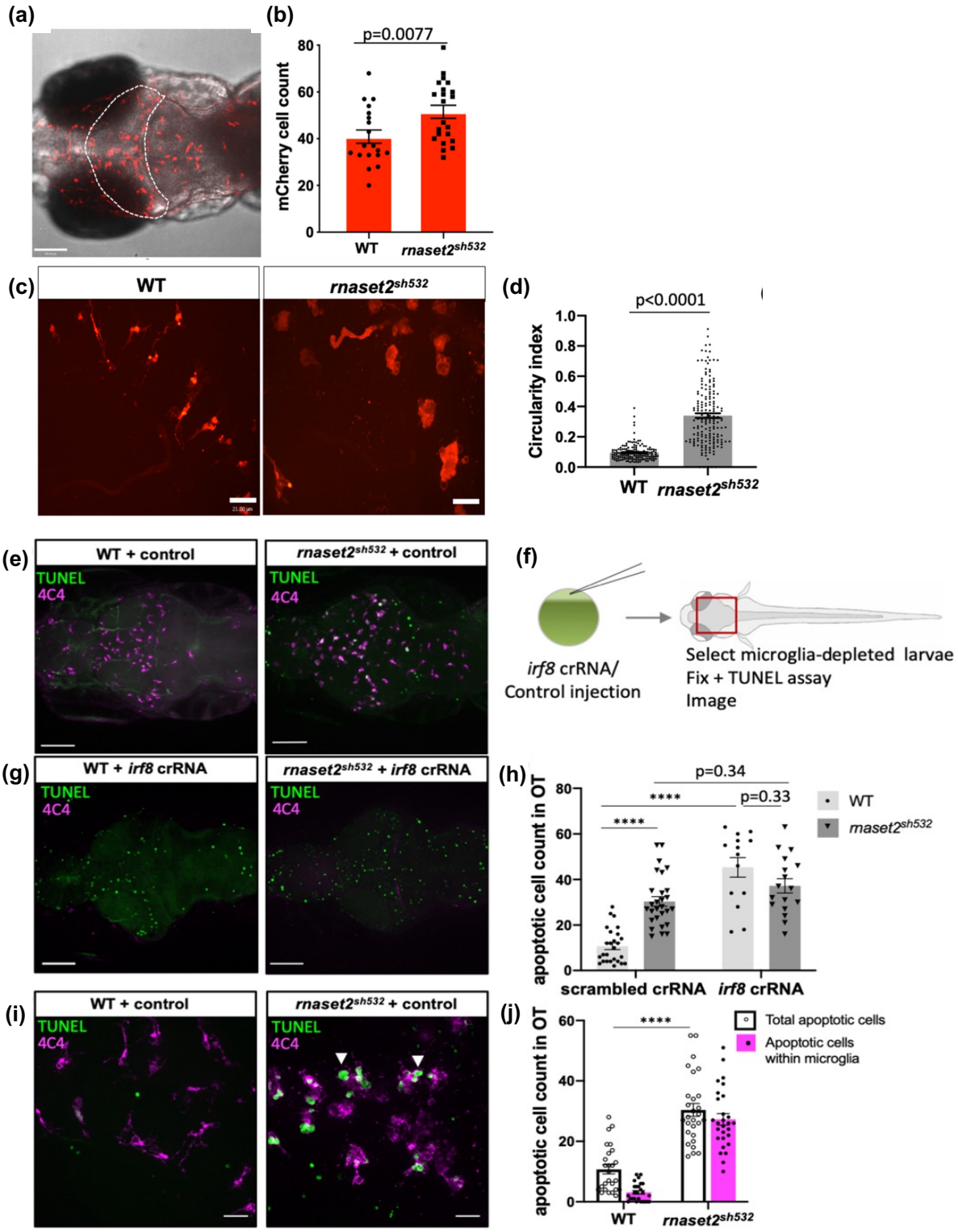

Figure 1.1. The failure of microglia to digest developmental apoptotic cells contributes to the pathology of *rnaset2* mutants. Adapted from Hamilton *et al.,* 2020.

(a, b) Microglia/macrophage count in the optic tectum of 5dpf wild type siblings and *rnaset2*^{sh532} larvae. Representative images of the whole head with optic tectum outlined (dotted white line) **(a)** and quantification of mCherry positive cells from the *Tg(mpeg1:mCherryCAAX)sh378* reporter line labeling both microglia and macrophages **(b).** n = 19–22 larvae from three independent experiments, two-tailed Mann–Whitney U test. Scale bar represents 50µm. **(c)** Representative images of microglia morphology using the 40× objective. Scale bar 21 µm. **(d)** Quantification of microglia circularity using the circularity index analysis from Fiji. n = 48–50 larvae from three independent experiments, two-

tailed Mann–Whitney U test. **(e–h)** Higher number of apoptotic cells in mutant is due to defective microglia and not excessive neuronal cell death. Representative images of apoptotic cells (as visualized by TUNEL staining) in brains of 5dpf *rnaset2*^{sh532} mutants and wild type siblings in scrambled crRNA injected control **(e)** and following injection of *irf8* crRNA **(g).** Scale bar 70 µm. **(f)** Diagram of experimental flow. Injection of *irf8* crRNA or scrambled crRNA control was performed into one-cell stage embryos, which were raised until 5dpf and microglia-depleted larvae were selected in irf8 crRNA injected animals. Control and depleted larvae were fixed and stained for apoptotic cells using TUNEL assay and microglia using 4C4 antibody. **(h)** Quantification of apoptotic cells in the optic tectum. n=15–28 from three independent experiments, using multiple two-tailed U test with Bonferroni's multiple comparisons test (****p < .0001). **(i, j)** Undigested apoptotic cells are contained within microglia. **(i)** High resolution images of apoptotic cells (fluorescein TUNEL staining) and microglia (4C4 magenta) in brains of 5dpf *rnaset2*^{sh532} mutants and wild type siblings with apoptotic cells mainly appearing within microglia (white arrowheads). Scale bar 20 µm. **(j)** Quantification of total number of apoptotic cells and number of apoptotic cells contained within microglia. n = 26–28 from three independent experiments, using multiple two-tailed U test with Bonferroni's multiple comparisons test (****p < .0001).

Almost all apoptotic cells in *rnaset2*^{sh532} mutant brains were contained within microglia – suggesting mutant microglia are able to phagocytose but not digest dying cells (Figure 1.1 i, j) (Hamilton *et al.*, 2020b). Electron microscopy revealed the presence of large, electron dense inclusions alongside intact apoptotic cells within the microglial-cell body – further confirming a defect in digestion which aligns with the role of RNASET2 as a lysosomal hydrolase and strengthening the hypothesis that deficient microglia may be a possible driver of pathology in these animals.

Finally, perhaps the most convincing evidence for microglia as the drivers of RNASET2-deficient leukodystrophy was the finding that induced macrophage/microglia-specific expression of functioning *rnaset2* was sufficient to rescue the phenotype of *rnaset2*^{sh532} mutants - both in terms of microglial morphology and apoptotic cell count (Hamilton *et al.*, 2020a).

Thus, there is convincing evidence that *rnaset2* mutant zebrafish pathology may be driven by a deficiency of microglia in clearing developmental apoptosis. Despite retaining their ability to detect and phagocytose dying cells, mutant microglia are unable to digest apoptotic debris – suggesting a defect in their housekeeping, rather than sentinel roles (Hickman *et al.*, 2018b; Hamilton *et al.*, 2020b). This abnormal phenotype emerges long before the development of white matter lesions or altered survival, and at a similar type to the emergence of behavioural abnormalities. Hence, in combination with data from other animal models, these findings suggest abnormal microglia may be among the initial triggers of neuropathology in RNASET2-deficient leukodystrophy, and that these cells may provide a valuable target for therapeutic interventions.

1.5 Hypothesis and aims

Characterisation of animal models of RNASET2-deficient leukodystrophy has revealed that microglial abnormalities throughout development contribute to neuropathology in these animals. Accompanied by widespread neuroinflammation, RNASET2-deficient microglia display altered morphology and number across a range of animal models and, critically, fail to digest apoptotic cells during early development in *rnaset2*^{sh532} mutant zebrafish (Sinkevicius *et al.*, 2018; Hamilton *et al.*, 2020a; Weber *et al.*, 2020; Kettwig *et al.*, 2021). As such, I hypothesise that microglia are the cellular drivers of RNASET2-deficient leukodystrophy, and that replacing these dysfunctional cells will have therapeutic benefits in this disease. Accordingly, the aims of my project are as follows:

1. **Further evaluate the contribution of microglia to RNASET2 pathology in *rnaset2*^{sh532} animals (hereafter referred to as *rnaset2* mutants).** Published work has demonstrated that a failure of microglia to clear developmental apoptosis may contribute to the neuroinflammatory

phenotype of *rnaset2* mutants. However, the broader impact of this microglial dysfunction on myelin pathology, neuroinflammation and motor function – all key hallmarks of RNASET2-deficient pathology – remain unclear. Thus, I will investigate whether microglial dysfunction during early development is the sufficient trigger for downstream pathology in *rnaset2* mutant larvae.

2. **Develop a strategy for the replacement of microglia in zebrafish.** If microglia are truly the principal drivers of pathology in RNASET2-deficient leukodystrophy, replacing these diseased microglia with healthy cells should improve pathology. As such, I will develop a strategy to functionally replace microglia in wild type zebrafish embryos, by exploiting the ability of peripheral macrophages to infiltrate the CNS to contribute to the zebrafish microglial population (Ferrero *et al.*, 2018, 2021). As such, I will investigate the ability of transplant-derived cells to engraft and persist within the brain in order to replace microglia.
3. **Assess the impact of microglia replacement in *rnaset2* mutant zebrafish**. Finally, I will assess whether microglial replacement in *rnaset2* mutants is sufficient to rescue markers of pathology in this model, including neuroinflammation, myelin abnormalities and behavioural dysfunction. Together, the findings of these studies will demonstrate whether microglial dysfunction is central to RNASET2-deficient leukodystrophy pathology and establish the potential therapeutic impact of targeting the microglia in this disease.

Chapter 2. Materials and Methods

2.1 Materials

2.1.1 Ethics statement

All procedures and maintenance of fish followed the Animal [Scientific Procedures] Act 1986 under the Home Office Project Licence (PPL P254848FD). Where fish were raised over 5dpf, procedures were performed by personal licence holders (Noémie Hamilton and Holly Rutherford) in accordance with licence guidelines.

2.1.2 Zebrafish husbandry

All adult animals were raised and maintained in the Bateson Centre Zebrafish facility under careful monitoring at 28°C under a 14/10-hour light/dark regimen. Zebrafish embryos were maintained in petri dishes of approximately 60 embryos in E3 media in light cycling incubators at 28°C until 5 days post-fertilisation (dpf).

rnaset2^{sh532} mutant fish were previously generated using CRISPR/Cas9 genome editing technology in *Tg(mpeg1:mCherryCAAX)sh378* embryos with founders identified and bred to produce a stable line (Hamilton *et al.*, 2020a). Wild type and homozygous adults were identified using fin clip genotyping and isolated for breeding. *csf1ra*$^{-/-}$*;csf1rb*$^{+/-}$ mutants were in-crossed to generate double-mutant offspring and were genotyped as described in section 2.2.3.4 (Parichy *et al.*, 2000; Oosterhof *et al.*, 2018). For isolation of GFP-positive macrophages, *Tg(fms:GFP)sh377* animals were used (Dee *et al.*, 2016). For assessment of oligodendrocyte numbers, *rnaset2*^{sh532} homozygous adults were crossed with *Tg(mbpa:GFP)* animals to product offspring heterozygous for both the *rnaset2* mutant allele and the *mbpa:GFP* transgene (Almeida *et al.*, 2011). These animals were then in-crossed and the offspring genotyped to identify wild type and homozygous adults for breeding.

2.1.3 Microscopy and imaging

For micro-injection, transplantation and adult kidney dissection, Leica S6D light microscopes were used. For screening of microglia depletion or transplantation efficiency, a ZEISS Axio Scope was used to quantify endogenous microglia or transplant-derived cells using mCherry and GFP channels, respectively. For high resolution of live embryos using a transgenic reporter, or fixed embryos following immunohistochemistry, the Nikon W1 Spinning Disk was used. For brightfield imaging of embryos following *in situ* hybridisation, Nikon SMZ Extended Focus Stereomicroscope was used.

2.1.4 Injection equipment

Micro-injection needles were pulled from glass capillaries using the P-1000 Next Generation Micropipette Puller (Sutter Instrument) and stored in sterile, RNase-free petri dish prior to injection. To facilitate precise control of injection volume, loaded needles were inserted into an injection rig attached to a PV820 Pneumatic Picopump (World Precision Instruments).

2.1.5 Behavioural analysis

Behavioural analysis was performed using the previously published Zebrabox tracking system and Zebralab software (ViewPoint Life Science, France) (Moravec *et al.*, 2015; Faught and Vijayan, 2018; Gauthier and Vijayan, 2018; Ibhazehiebo *et al.*, 2018; Li *et al.*, 2019).

2.1.6 RT-PCR

RT-PCR reactions were performed using the BioRad C1000 Touch or T1000 thermocycler, using the primers listed in

Table 2.1. These machines were also utilised for gDNA extraction and cDNA synthesis.

2.1.7 qRT-PCR

qRT-PCR reactions were performed using the CFX96 Bio-Rad machine using the primers shown in

Table 2.1.

Table 2.1 RT-PCR and qRT-PCR primers used in this study

Gene	Primer name	Sequence
cd68	cd68_fwd_1	GGCTGACTTTGCAATTGGGA
cd68	cd68_fwd_2	ATGTGCAGCTTGTGGAAGTT
cd68	cd68_fwd_3	CAGCTCTCAGACGGTGTACA
cd68	cd68_rev_1	TTCCGAACATCCTCCACTGG
cd68	cd68_rev_2	GACCAGGAACAGAAGCAAACA
cd68	cd68_rev_3	GTTGATCAGCCTTGCACACA
cmpk2	cmpk2_fwd_1	GGCTCCTTTCAGACAACG
cmpk2	cmpk2_fwd_2	GGAGGAGTCAGTGAAGCAGT
cmpk2	cmpk2_fwd_3	TACGTTTGGCCAGAAGACCT
cmpk2	cmpk2_rev_1	TTCAACCCTACCACCAAC
cmpk2	cmpk2_rev_2	CAGGGATAATGTCAGCGCAC
cmpk2	cmpk2_rev_3	TCAGTGGTCTTGTCCTGTCC
csf1rb	csf1rb_geno_fwd	CTTGCTGACAAATCCAGCAG
csf1rb	csf1rb_geno_rev	AAACTAAATGCGGCCATACG
ef1α	ef1a_qPCR_fwd	CAGCTGATCGTTGGAGTCAA
ef1α	ef1a_qPCR_rev	TGTATGCGCTGACTTCCTTG
ifnΦ1	IFNphi1sec_qPCR_fwd	TGAGAACTCAAATGTGGACCT
ifnΦ1	IFNphi1sec_qPCR_rev	GTCCTCCACCTTTGACTTGT
il1β	il1beta_fwd	GAACAGAATGAAGCACATCAAACC
il1β	il1beta_rev	ACGGCACTGAATCCACCAC
isg15	isg15_qPCR_fwd	AACTCGGTGACGATGCAGC
isg15	isg15_qPCR_rev	TGGGCACGTTGAAGTACTGA
mbpa	mbpa qPCR 1_fwd	GTTCTTCGGAGGAGACAAGAAGAG
mbpa	mbpa qPCR 1_rev	GTCTCTGTGGAGAGGAGGATAGATGA
mbpa	mbpa qPCR 2_fwd	GCAAGCACCTCTGGACAAAA
mbpa	mbpa qPCR 2_rev	TGTCTCCTCCGAAGAACCTG
mbpb	mbpb qPCR 1_fwd	TTCGCAGTCAACATTCAGGC
mbpb	mbpb qPCR 1_rev	CCCCTCCAAAGAACTTTCCG
mbpb	mbpb qPCR 2_fwd	CAGTCAACATTCAGGCTGGG
mbpb	mbpb qPCR 2_rev	CCCCTTCTTCTTCTTCTCCCC
mpz	mpz qPCR 1_fwd	CTGTGATGCCAAGAACCCAC
mpz	mpz qPCR 1_rev	ACCAGGAAGCGCATCAGATA
mpz	mpz qPCR 2_fwd	GGGCTAAGGACGCAATCTCA
mpz	mpz qPCR 2_rev	GTGGGTTCTTGGCATCACAG
mxa	mxa_qPCR_fwd	GACCGTCTCTGATGTGGTTA
mxa	mxa_qPCR_rev	GCATGCTTTAGACTCTGGCT
plp1a	plp1a qPCR 1_fwd	GGTGTTCTCCCTCTCTGCAT
plp1a	plp1a qPCR 1_rev	ACCGTACTGTCTGGCATCAA
plp1a	plp1a qPCR 2_fwd	TGTAGTCTGGTTGCTGGTGT
plp1a	plp1a qPCR 2_rev	AGCTTTTCCGGGAATTGCAG

zferv1a_pol	ZFERV pol-1S	GCTAGGACATCCCATTGTGT
zferv1a_pol	ZFERV pol-2A	GGGAATGTGTTCTGGTGTCT
zferv1a_env	ZFERV env1a_fwd	CTACCACCACGCTTCCGAA
zferv1a_env	ZFERV env1a_rev	TTGGATGCTGTCTGCCTTGG
zferv1a_gag	ZFERV gag1a_fwd	GGAAGAAGGGAGCAGCAAAC
zferv1a_gag	ZFERV gag1a_rev	GAGTCCCTTTGATCTGCCCA
ZfPV	ZfPV_F2	CCGCCCTCATCTACCGAAAA
ZfPV	ZfPV_R2	ACGCAGAGGGGTCAAATTGT

2.1.8 In situ hybridisation

Sense and antisense probes were generated by Noémie Hamilton according to the methodology outlined in Rutherford *et al.,* 2021. PreHyb solution contained final concentrations of 50% formamide, 5xSSC, 0.1% Tween20, 50µg/ml heparin, 500µg/ml tRNA and citric acid to pH6, in diethyl pyrocarbonate (DEPC)-treated water. ProbeHyb contained a 1:1000 dilution of synthesised probe (diluted 1:200 in formamide) in PreHyb. WashHyb contained final concentrations of 50% formamide, 5xSSC, 0.1% Tween20 and citric acid to pH6, in DEPC-treated water. Staining wash contained final concentrations of 100mM Tris-HCl pH9.5, 50mM $MgCl_2$, 100mM 1aCl, 0.01% Tween20 in H_2O. Staining solution was made up of 100mg/ml NBT and 50mg/ml BCIP in staining buffer. Finally, 1mM EDTA pH8 in PBS was used as stop buffer.

2.1.9 Tissue clearing reagent preparation

CUBIC reagents were prepared according to published protocols (Susaki *et al.*, 2015). CUBIC-1 was made by mixing 25% (by weight) urea, 25% Quadrol and dH_2O on a hot stirrer, before cooling and adding 15% Triton X-100. This solution was diluted with the same quantity of dH_2O to make 50:50 CUBIC-1:dH_2O. To make CUBIC-2, 25% (by weight) urea and 50% sucrose were mixed on a hot stirrer with dH_2O, before adding 10% triethanolamine once cooled to room temperature. This solution was diluted with phosphate-buffered saline (PBS) to make 50:50 CUBIC-2:PBS. Reagents were made in small volumes and refreshed regularly to minimise degradation.

2.1.10 Flow cytometry

For zebrafish-to-zebrafish transplants, whole kidney marrow (WKM) was isolated from *Tg(fms:GFP)sh377* adults and GFP-positive macrophages were sorted using the BD FACSMelody™ (BD Biosciences), using TO-PRO^{TM}3 (ThermoFisher, R37170) to identify and exclude dead cells.

2.1.11 7.4.C4 hybridoma culturing

7.4.C4 mouse hybridoma cells were cultured in the Clinical Medicine core cell culture facility. Establishing cell culture was performed with the help of Kay Hopkinson and Jonathon Kilby. Routine cell maintenance was performed by Kay Hopkinson and Jonathon Kilby.

After amplification, 7.4.C4 cells and supernatant were sterile filtered using the Stericup Quick Release-GP Sterile Vacuum Filtration System (Sigma Aldrich, S2GPU05RE) into sterile containers. For long-term preservation, either sodium azide (to final concentration of 0.02%) or 1 M Tris pH 7.5 (to final concentration of 3%) was added, before aliquoting for storage.

The presence of 4C4 antibody was confirmed using immunoprecipitation using Dynabeads (Protein G) and visualisation on polyacrylamide gel with Expedeon Instant Blue Coomassie. Preparation and running of the gel was performed with the help of Dr Heba Ismail.

2.1.12 Key reagents

	SOURCE	IDENTIFIER
General use reagents		
Tricaine	Sigma-Aldrich	E10521
Phosphate Buffered Saline Tablets (PBS)	Thermo-Fisher Scientific	10209252
TWEEN® 20	Merck	P1379
Low Melting Point Agarose	Sigma	A9414
Agarose	SLS	BI041025
7.4.C4 hybridoma culturing, antibody purification and preservation		
7.4.C4 mouse hybridoma cells	Sigma	92092321-1VL
High Glucose DMEM (-Glut/-Pyr)	Thermo Fisher	11960044
L-Glutamine (200 mM)	Thermo Fisher	25030149
HT supplement (100X)	Thermo Fisher	11067030
Foetal bovine serum	Sigma	F7524-100ml
Hybridoma-Serum Free Medium	Life Tech	12045084
Trypan Blue stain 0.4%	Life Tech	T10282
DMSO	Sigma-Aldrich	276855
Dynabeads, Protein G	Invitrogen	10003D
1M Tris pH7.5	Invitrogen	10123722
Sodium azide	Merck	S2002
Immunohistochemistry		
4C4 hybridoma line 7.4.C4	Developmental Studies Hybridoma Bank	92092321
Chicken polyclonal GFP antibody	GeneTex	GTX13970
Alexa Fluor™ 647 goat anti-mouse	Thermo-Fisher Scientific	A-21235
Alexa Fluor™ 488 goat anti-chicken	Thermo-Fisher Scientific	A-11039
DAPI (4',6-diamidino-2-phenylindole, dihydrochloride)	Thermo-Fisher Scientific	62247
Myelin basic protein polyclonal antibody	Proteintech	10458-1-AP
Zebrafish myelin basic protein antibody	*gifted from Appel lab	-
Proteinase K	Thermo Fisher	4333793
Trisodium citrate	Merck	1.37042
CUBIC tissue clearing		
N,N,N',N'-Tetrakis(2-hydroxypropyl)ethylenediamine (Quadrol)	Sigma	122262-1L
2,2',2"-Nitrilotriethanol (triethanolamine)	Sigma	90278-100ML
Urea	Sigma	15604-1KG
Polyethylene glycol (PEG) mono-p-isooctylphenyl ether (Triton X-100)	Sigma	X100-500ML
Sucrose	Fisher	10386100
***irf8* knockdown**		
irf8 CRISPR RNA (crRNA) guides	Sigma	-
transactivating RNAs (tracrRNA)	Merck	-
Cas9 nuclease	New England Biolabs	MO386M
Zebrafish-to-zebrafish transplantation		
L15 media	Gibco	21083-027
Foetal bovine serum (20%)	Sigma-Aldrich	ES009-M

EDTA (5mM)	PanReac AppliChem	A4892,0500
CellTrace™ CFSE cell proliferation kit	Invitrogen	C34554
RNA extraction		
TRIzol	Invitrogen	Invitrogen
Chloroform	Fisher scientific	C/4920/08
Isopropanol	Thermo-Fisher Scientific	42385000
Ethanol	Thermo-Fisher Scientific	E/0665DF/17
Nuclease-free water	Qiagen	129114
RNeasy MinElute Cleanup Kit	Qiagen	74204
cDNA synthesis, RT-PCR, restriction digest and qRT-PCR		
Superscript II RT kit	Invitrogen	18064022
RNaseOUT	Invitrogen	10777019
5x FIREPol DNA Polymerase Master Mix	Solis BioDyne	04-12-00125
SYBR Safe DNA gel stain	Invitrogen	S33102
MspI (restriction enzyme)	New England Biolabs	R0106L
2x SYBR Green Master Mix	Applied Biosystems	4309155

2.2 Methods

2.2.1 General methods (used across multiple chapters)

2.2.1.1 Zebrafish brain dissection

Brain dissection was performed on either fresh (recently culled) or fixed tissue, according to experimental purpose. Both methods are regulated K procedures and were performed by a personal licence holder in accordance with the regulated killer register.

For fresh tissue dissection, animals were placed in concentrated tricaine observed until non-responsive to touch stimuli. Fish were then removed from the tricaine and placed on a clean petri dish, before a sharp razor was used to make a single cut across the gills and head to decapitate the animal. Samples were then placed into a petri dish of autoclaved PBS placed on ice and dissected under a light microscope. Briefly, sharp sterile tweezers were used to remove the soft tissue, gills and jaw from the ventral surface of the head, and to sever the cranial nerves projecting from the skull. The base of the skull was then gently peeled from the ventral surface of the brain, before peeling away the remainder around the sides and dorsal surface whilst being mindful not to disturb tissue integrity while ensuring dissection. Tweezers were then used to remove any remaining skull fragments, connective tissue, and the ears. The sample was then transferred to a clean Eppendorf for further processing as required per experiment.

For fixed tissue dissection, animals were culled by decapitation (as above). Rather than immediate dissection, each head was placed into 2ml 4% paraformaldehyde (PFA) and gently inverted to ensure the entire tissue was fully submerged, before leaving at 4°C overnight to ensure fixation of the tissue.

The following morning, samples were rinsed in autoclaved PBS three times, one hour each. Samples were then placed into a petri dish of autoclaved PBS and dissected as described above. For fixed tissue, samples were then transferred to a clean Eppendorf containing fresh PBS, and gradually dehydrated using sequential 30-minute washes in methanol (MeOH): 25% MeOH: 75% PBS; 50% MeOH: 50% PBS; 75% MeOH: 25% PBS; 100% MeOH). For long-term storage, samples were placed in fresh methanol and stored at –20°C.

2.2.1.2 Trizol RNA extraction

Prior to RNA extraction, animals were culled as appropriate to their developmental stage. For larval samples (5–8dpf), embryos were culled by terminal anaesthesia in concentrated tricaine, before being transferred to Eppendorf tubes and the addition of 500µl Trizol reagent. For adult samples, animals

were culled by regulated K procedures and their brain dissected as described in section 2.2.1.1. Tissue dissected from freshly culled animals was used for RNA extraction, with dissected brains placed directly into 500µl Trizol.

Once in the Trizol reagent, culled embryos or freshly dissected brains homogenized using a handheld homogenizer (T 10 basic ULTRA-TURRAX, IKA Dispersers, product no. 0003737002). Following complete homogenisation, 100µl chloroform was added and the sample was mixed vigorously. After 2–3 minutes at room temperature, samples were centrifuged at 12,000g for 30 minutes at 4°C. The upper aqueous phase was removed (200µl) and transferred to a clean Eppendorf with 200µl isopropanol, before leaving overnight at –20°C. The following morning, samples were again centrifuged at 12,000g for 30 minutes at 4°C before the supernatant was removed and pellet washed with 1000µl ethanol. Samples were centrifuged at 12,000g for 15 minutes at 4°C (repeated as needed) until all supernatant could be removed and pellet left to air-dry for 10 minutes. Finally, the resultant pellet was dissolved in 20µl nuclease-free water to be used for cDNA synthesis.

2.2.1.3 cDNA synthesis

cDNA was synthesised utilising Superscript II according to manufacturer's instructions. Briefly, 2µg RNA was transferred to a microcentrifuge tube with 1µl oligo(dT), 1µl dNTP mix and nuclease-free water to 10µl before incubating at 65°C for 5 minutes. Samples were briefly chilled on ice, before the addition of 4µl 5x First Strand Buffer, 2µl DTT, 1µl RNase-OUT RNase inhibitor and 1µl Superscript II reverse transcriptase. The mixture was incubated to 42°C for 50 minutes before inactivation at 70°C for 15 minutes. The resultant cDNA was diluted 1:20 for qPCR and RT-PCR.

2.2.1.4 RT-PCR

Standard RT-PCR reactions included 2µl 5x FIREPol DNA Polymerase master mix, 0.5µl forward and reverse primer (10µM), 2µl template (gDNA/cDNA) and 5µl nuclease free water (10µl total volume) unless otherwise stated. RT-PCR was performed using the BioRad C1000 Touch or T1000thermocycler as follows: Step 1: 98°C for 5 minutes, Step 2: 95°C for 30 seconds, Step 3: chosen annealing temperature for 30 seconds, Step 4: 72°C for 20 seconds, Step 5: 72°C for 5 minutes with steps 2–4 repeated 34–40 times. For specific annealing temperatures and cycle numbers, please see the relevant section.

2.2.1.5 *Gel electrophoresis*

Following RT-PCR, samples were run on an agarose gel made up in tris-acetate-EDTA (TAE) buffer, and imaged using the Syngene U:Genius gel dock. SYBR Safe DNA Gel Stain was added to allow visualisation of DNA. For gel percentages, please see the relevant section.

2.2.1.6 *Optimisation of primers for qRT-PCR*

Where not previously published by our lab group, primers were designed and optimised by qPCR as follows. Primers were designed using Primer 3 (https://primer3.ut.ee/), such that the selected primer pairs had a GC content of 50–60% and a T_m of 50–65°C, were 18–23 base pairs in length and produced a product of 100–200 base pairs. In order to perform an initial assessment of primer efficiency, each primer pair was tested with RT-PCR using a standard cDNA stock to confirm whether each reaction gave a single fragment at the expected size, with no off-target amplification. For each primer pair, reactions were performed as described in section 2.2.1.4. A reference gene (*ef1α*) was used as a positive control. The resulting products were run on a 2% agarose gel and visualised using SYBR safe to establish whether primers amplified a fragment of the expected size.

In order to assess primer efficiency in amplifying transcripts in an exponential manner, each primer pair was subjected to qRT-PCR using sequential cDNA dilutions as follows: 1:20, 1:40, 1:80, 1:200, 1:500, 1:1000 and 1:5000. Each reaction was run in triplicate, with the following reaction mix in each well: 5µl SYBR green, 2µl milli Q water, 2µl cDNA, 0.5µl forward primer and 0.5µl reverse primer. The qRT-PCR reaction was run on a CFX96 Bio-Rad machine as follows: Step 1: 95°C for 2 minutes, Step 2: 95°C for 10 seconds, Step 3: 57°C for 30 seconds, Step 4: 72°C for 25 seconds, Step 5: 95°C for 30 seconds, Step 6: 65°C for 10 seconds, Step 7: 95°C for 20 seconds with Steps 2–4 repeated 39 times and increment of 0.2°C every 10 seconds between Steps 6 and 7. In order to calculate primer efficiency, the mean Cq value for dilution was plotted against the logarithmic of that dilution, to produce a scatter graph with a linear trendline Efficiency was calculated according to the following equation:

$$Efficiency = 10^{\left(\frac{-1}{trendline\ gradient} - 1\right)} \times 100\%$$

2.2.1.7 *qRT-PCR*

Following RNA extraction and cDNA synthesis as described in sections 2.2.1.1 and 2.2.1.3, qRT-PCR was performed to assess relative gene expression. Reaction mixtures were as follows: 5µl SYBR green, 2µl milli Q water, 2µl cDNA, 0.5µl forward primer and 0.5µl reverse primer (unless otherwise stated). The qRT-PCR reaction was run on a CFX96 Bio-Rad machine as follows: Step 1: 95°C for 2 minutes, Step 2: 95°C for 10 seconds, Step 3: 57°C for 30 seconds, Step 4: 72°C for 25 seconds, Step 5: 95°C for

30 seconds, Step 6: 65°C for 10 seconds, Step 7: 95°C for 20 seconds with Steps 2–4 repeated 39 times and increment of 0.2°C every 10 seconds between Steps 6 and 7. As previously published, *ef1α* was used as a reference gene for each sample (Hamilton *et al.*, 2020a). Each reaction was run in triplicate, with the mean Cq value for each reaction used to determine relative expression as below:

$$Relative\ expression = 2^{(-\Delta Cq)}$$

where $\Delta Cq = mean\ Cq\ of\ gene\ of\ interest - mean\ Cq\ of\ reference\ gene$.

2.2.1.8 Immerse fixation

To preserve tissue for immunohistochemistry and terminal deoxynucleotidyl transferase dUTP nick end labeling (TUNEL staining), larvae were first terminally sedated in concentrated tricaine and fixed with 4% PFA overnight at 4ºC. For 8dpf samples, fixation was performed by personal license holder under approved individual study plan. Following fixing, samples were rinsed with PBST and dehydrated with increasing concentrations of methanol (25% MeOH:75% PBS; 50% MeOH:50% PBS; 75% MeOH:25% PBS; 100% MeOH) and stored at –20ºC until the TUNEL assay and/or immunohistochemistry was performed.

2.2.1.9 Whole mount immunohistochemistry of zebrafish embryos

Following storage at –20ºC, embryos were rehydrated in decreasing concentrations of methanol (75% MeOH:25% PBS; 50% MeOH:50% PBS; 25% MeOH:75% PBS) and then washed in PBST. In order to permeabilise the tissue, embryos were then incubated with proteinase K (20µg/ml) for 2 hours at room temperature for 5dpf embryos, and 37ºC for 8dpf embryos. Embryos were then washed and fixed for a further 20 minutes in 4% PFA at room temperature. To further promote antigen availability, embryos were washed with deionised water before being placed in acetone at –20°C for twenty minutes, before incubation in blocking buffer (10% sheep or goat serum, 0.8% Triton X-100, 1% bovine serum albumin in PBT) for 3 hours at room temperature. Primary antibodies were then added, diluted in blocking buffer at the concentrations described in the relevant sections. Embryos were incubated in primary antibody solution for 48 hours at 4ºC, before being thoroughly washed with PBS at room temperature. Samples were then incubated in the relevant secondary antibodies (anti-mouse far red, anti-chicken GFP and anti-rabbit RFP, all used at 1:500 dilution throughout) for 24 hours at 4ºC, before rinsing again and mounting in low melting point agarose for imaging.

2.2.1.10 Behavioural analysis

2.2.1.10.1 Larval free swim analysis

In order to assess larval free-swimming behaviour, embryos were raised to 8dpf under approved individual study plan. Briefly, animals were raised in petri dishes – 12 embryos per dish – containing E3 media which was refreshed daily by the personal licence holder. Embryos were fed daily, using a Pasteur pipette to ensure uniform distribution of food between plates. On the morning of the experiment, embryos were transferred to 24 well plates (one embryo per well) without anaesthetising, with 500µl clear E3 per well. Plate layout was alternated between experimental groups to ensure no location-specific effects – and allowed to habituate for at least 4 hours. Swimming distance was recorded across a 20–60-minute period, with alternating light-dark cycles of 10 minutes. Outliers were manually excluded based upon movement analysis trace automatically generated by the Zebralab software, as illustrated in Figure 2.1.

2.2.1.10.2 Larval startle response analysis

To assess swimming behaviour in response to a loud sound stimulus (known as the startle reflex), embryos were raised to 8dpf under an individual study plan as in section 2.2.1.10.1. On the evening prior to analysis, 7dpf larvae were transferred into six-well plates (ten embryos per well, 3ml E3 media) and allowed to habituate overnight. As in the free-swimming analysis, mutant and wild-type siblings were placed in alternating wells in order to account for proximity to sound source or any location specific effects Figure 2.2. On the day of recording, each plate was transferred to the Zebrabox platform and allowed to habituate for 30 minutes, after which time recording began. Embryos were presented with 10 sound stimuli at a frequency of 1000Hz and a duration of 3ms, at intervals of 10 seconds, as described in previously published protocols (Madden *et al.*, 2021). Their responses were recorded using the Fast Camera add-on to allow observation with millisecond resolution. The resulting data was then compiled into a single spreadsheet using Microsoft Excel, with the relevant data points extracted and analysed using GraphPad Prism.

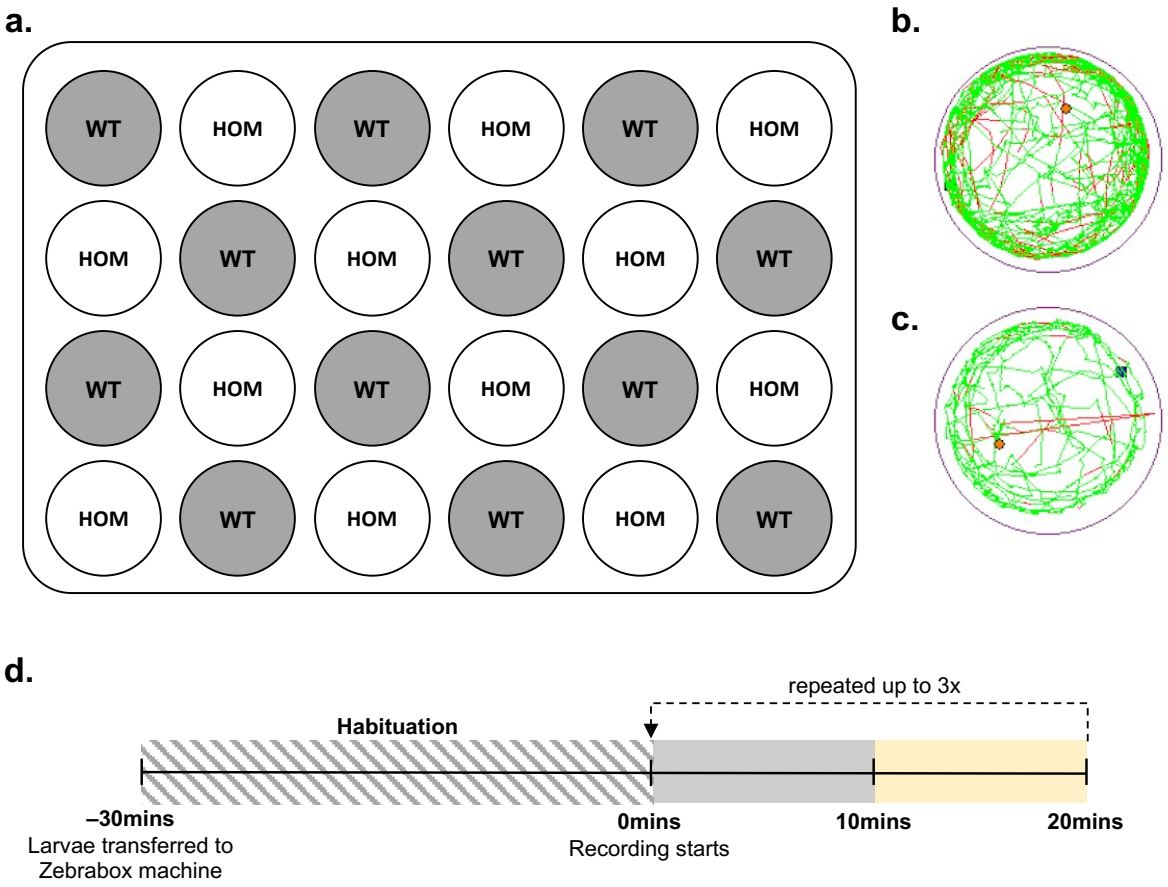

Figure 2.1. Larvae free-swimming analysis methodology.
Example plate layout for wild type (WT) and *rnaset2* mutant (HOM) free-swimming analysis. 8dpf embryos were placed into 24 well (1 embryo per well) using an alternating layout for each experimental group (a). Following data acquisition, any recordings which failed to accurately track larval movement were manually excluded – representative traces of an accurately-tracked and excluded larvae are shown in (b) and (c) respectively. Following habituation, larvae were subjected to periods of light and dark alternating at 10-minute intervals for 20–60 minutes total duration (d).

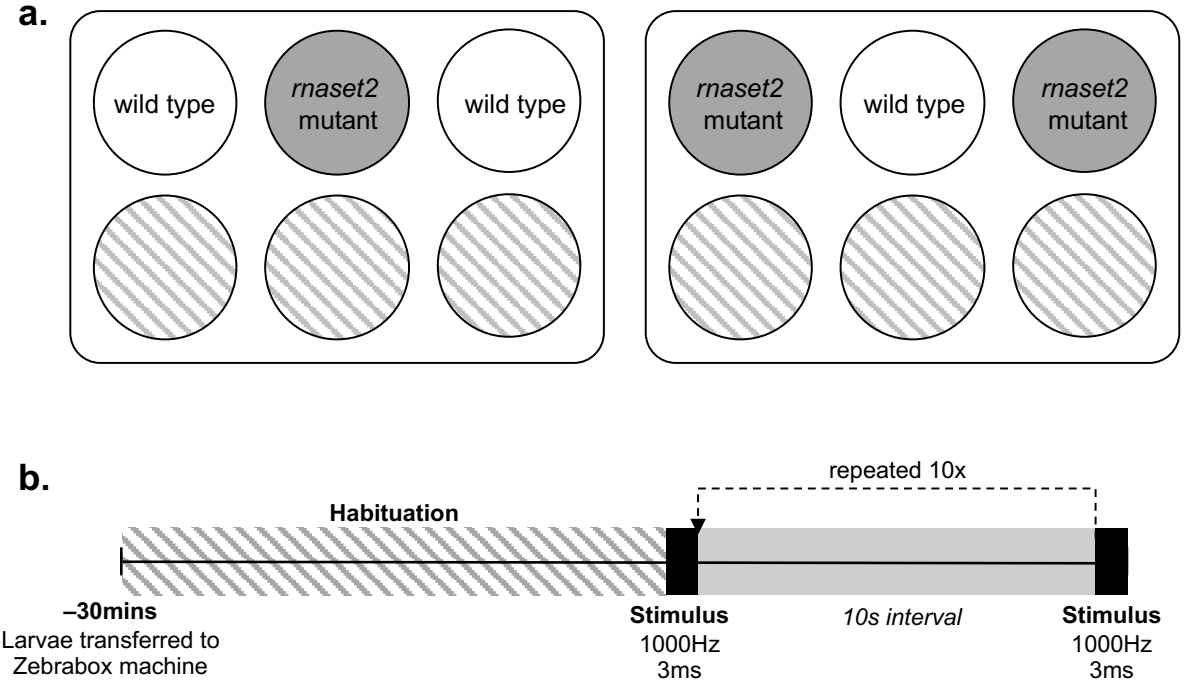

Figure 2.2. Larval startle response analysis methodology

Example plate layout for larval startle response analysis. Ten 8dpf embryos were placed into the top wells of a six-well plate, using an alternating layout to minimise sound location effects (a). Dashed wells indicate those out of the view of the camera (no fish were placed in these wells). On the day of recording, larvae were allowed to habituate in the Zebrabox recording machine for 30 minutes, before presentation with ten sound stimuli (1000Hz, 3ms duration) at intervals of 10 seconds (b).

2.2.1.10.3 Adult free swim analysis

For adult swimming behaviour analysis, fish were raised as normal to juvenile/adult stages. On the morning of recording, food was withheld from behavioural subjects to minimise the impact of defaecation on swimming behaviour. Animals were transferred to the behavioural facility on the morning of recording and allowed an initial 30-minute habituation period to recover from any stress when transferring between rooms. For recording, each adult was placed in an individual 0.7L tank (Tecniplast) containing 200ml aquarium water. The walls of each tank were covered with white paper to ensure the animals were unable to interact or be distracted by their surroundings.

After transfer to the behavioural tanks, fish were given a further 10 minutes to habituate to their environment, before recording for a period of 10 minutes. The movement thresholds for recording were set to allow identification of multiple speeds according to wild type animal swimming: small/large threshold = 6.0cm/sec, inactive/small = 3.0cm/sec. The resulting data was then analysed by GraphPad Prism.

Following recording, animals were either culled by schedule 1 or by decapitation (regulated K) if their brains were required for further experiments (as described in section 2.2.1.1). Animal length was recorded to minimise any size-linked effects. At the 4wpf timepoint, animal sex could not be determined due to their small size and early development.

2.2.1.11 Survival analysis of adult animals

To assess survival of animals beyond 4wpf, healthy embryos of the required genotype with inflated swim bladders were selected for raising, using consistent animal numbers across groups.

Adult survival was assessed at 1 month after raising, and every two weeks thereafter, by taking two images of each tank from above and quantifying the number of surviving fish at each time point. Quantification at two weeks from the point of raising was attempted, but a reliable count could not be obtained due to the small size of the animals at this time. Fish were routinely monitored and any animals displaying sickness phenotypes (including spiral swimming) were humanely culled, with this taken as the death outcome.

2.2.1.12 Statistical analyses

Unless otherwise stated, statistical analysis was performed with GraphPad Prism v10.1.0 throughout. For experiments with two groups only, data were entered into a column table (two samples, one

variable) and analysed by Mann-Whitney test. For comparisons of three or more groups, data were analysed by Kruskal-Wallis test with Dunn's multiple comparisons. For survival analysis, death outcome was recorded when an animal met the threshold for routine culling. Statistical differences in survival were assessed using log rank Mantel-Cox test, with Bonferroni's multiple comparison correction for pair-wise comparisons between groups. Non-parametric tests were used throughout as visualisation of data by histogram failed to identify a normal distribution for all groups for any given experiment; therefore, the most stringent statistical tests were performed. Individual p values are displayed throughout, and details of statistical tests are provided in figure legends. Where suitable, sample size calculations were performed using G*Power v3.1, where power (1–β) was set at 80% (0.8) and significance threshold (α) was set at 0.05. Assumptions estimated effect sizes and required sample sizes are detailed in results section for each experiment.

2.2.2 Chapter 3 methods

2.2.2.1 Quantification of myelin and oligodendrocytes

2.2.2.1.1 Primer design

Primers were designed to perform qRT-PCR for all four myelin-associated transcripts known in the zebrafish: *myelin basic protein a (mbpa), myelin basic protein b (mbpb), myelin protein zero (mpz)* and *proteolipid protein 1a (plp1a)*. Each of these genes has multiple isoforms – to ensure all coding transcripts were quantified by qRT-PCR, all transcripts for each of these genes were aligned using SNAP gene with the MUSCLE tool to identify a common region to target. For *mbpb*, only isoforms 201 and 203 were aligned, as alternative transcripts 202 and 205 encode an unrelated protein (Golli) which has a distinct function to Mbpb (Fulton *et al.*, 2010; Torvund-Jensen *et al.*, 2018). Two pairs of primers were ordered for each gene, including previously published primers for *mbpa* (Preston *et al.*, 2019).

2.2.2.1.2 Optimisation of primers for qRT-PCR

After design, primers were optimised as per section 2.2.1.6, beginning with RT-PCR and visualisation on a 2% agarose gel. All primer pairs except *mbpb* pair 2 and *plp1a* pair 2 gave single bands of the expected size as predicted by Primer 3 and were taken forward for efficiency analysis by qRT-PCR (Figure 2.3a).

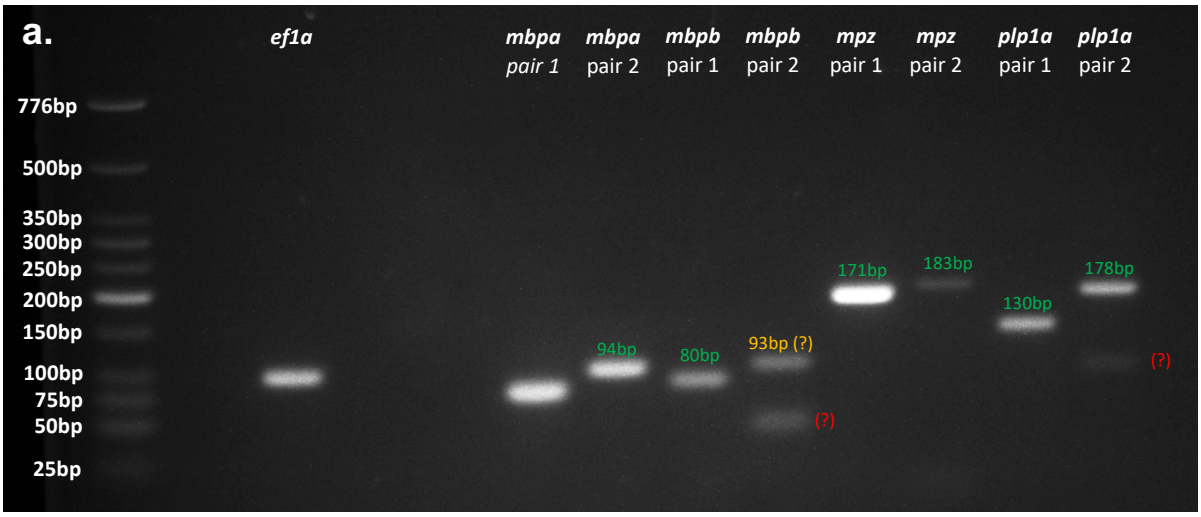

b.

mbpa pair 1

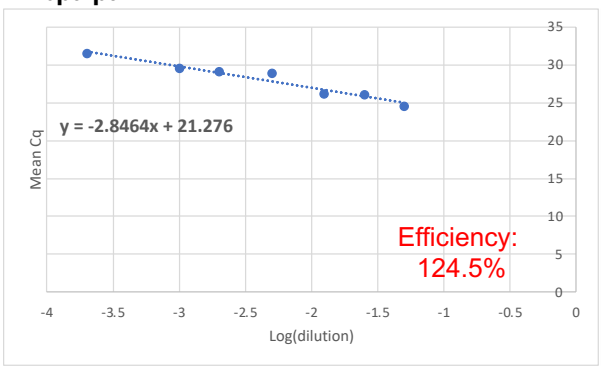

mbpa pair 2

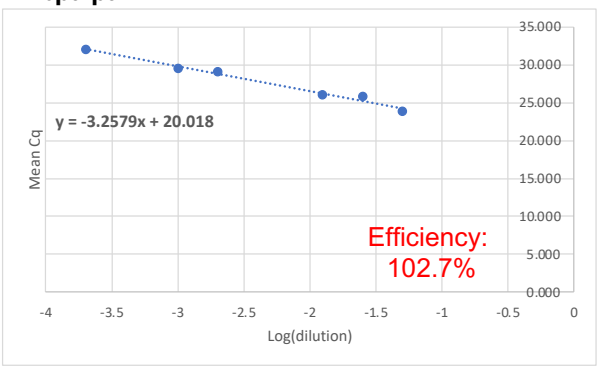

mbpb pair 1

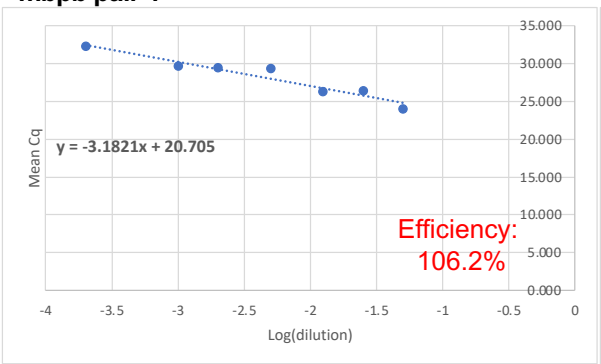

plp1a pair 1

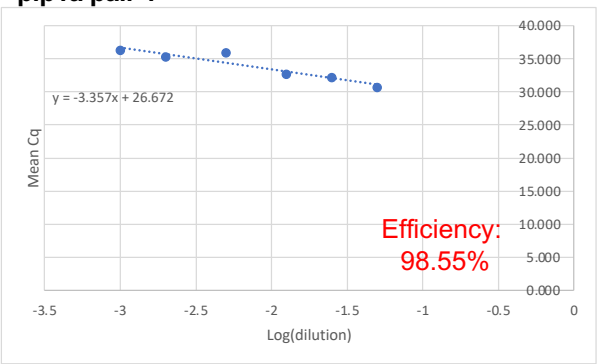

mpz pair 1

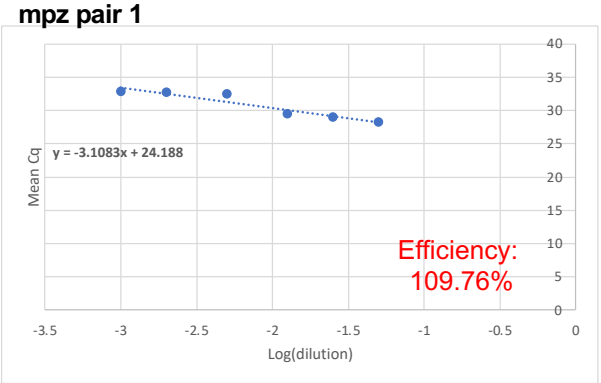

mpz pair 2

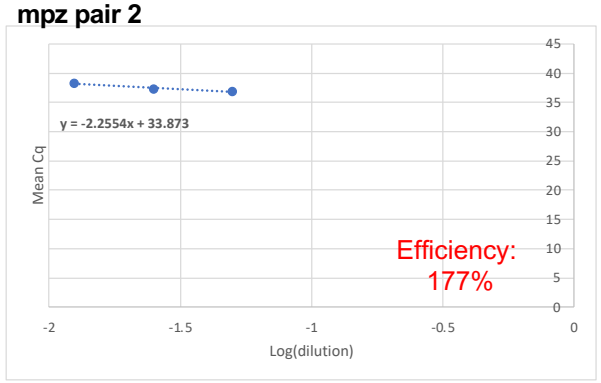

Figure 2.3. Optimization of primers for qRT-PCR or myelin transcripts.
(a) RT-PCR of two primer pairs for each myelin-associated transcript (*mbpa, mbpb, mpz* and *plp1a*) was performed to confirm whether each primer pair yielded a single product of the expected size, with no off-target amplification. Previously published primers for ef1α were used as a positive control. Expected product sizes (where known) are annotated above each band, where green labels indicate bands of the expected size, and orange/red labels indicate unclear product sizes. Single products were identified for *mbpa* primer pairs 1 and 2, *mbpb* pair 1, *mpz* pair 1 and 2, and *plp1a* pair 1. (b) qRT-PCR was used to confirm efficiency of each primer pair in amplifying serial cDNA dilutions in an exponential manner. The resulting scatter graphs and trendlines are shown, plotting mean Cq for each cDNA dilution against the logarithmic of that dilution. Trendline gradients were used to calculate efficiency, shown in red.

qRT-PCR was performed using serial dilutions of cDNA and efficiency calculated as described in section 2.2.1.6. The resulting scatter graphs and efficiency quantifications are shown in Figure 2.3b. Primer pairs with efficiencies of 90–110% were selected for future experiments: *mbpa* pair 2 (efficiency: 102.7%), *mbpb* pair 1 (efficiency: 106.2%), *plp1a* pair 1 (efficiency: 98.55%) and *mpz* pair 1 (efficiency: 109.76%).

2.2.2.1.3 qPCR of myelin-associated transcripts

qRT-PCR was performed with the primer pairs optimised in sections 2.2.2.1.1 and 2.2.2.1.2. RNA was obtained from 8dpf whole embryos as in section 2.2.1.1, and transcribed into cDNA as per section 2.2.1.3. To obtain RNA from 3mpf and 7.5mpf brains, adult fish were culled by regulated K procedures (overdose in anaesthetic, then decapitation) and brains were dissected out of the skull (performed by PIL holder). RNA extraction and cDNA synthesis was then performed as per sections 2.2.1.1 and 2.2.1.3. To assess relative expression, qRT-PCR was performed as described in section 2.1.7.

2.2.2.1.4 Live imaging of oligodendrocytes

To allow quantification of oligodendrocyte cell number, *rnaset2*^{sh532} and wild type larvae (each in the *Tg(mbpa:GFP)* background) were imaged at 5- and 8dpf. Larvae were screened at 5dpf to ensure the presence of the transgene, before either selecting healthy embryos to be raised for imaging at 8dpf or mounting for imaging at 5dpf. Notably, embryos were sedated with tricaine only once (just before imaging on day 5), as tricaine may have potential effects on myelination: as a blocker of voltage-gated sodium channels, tricaine blocks action potential generation (Attili and Hughes, 2014). As neural activity is known to influence myelination and oligodendrocyte development, it is possible that the use of tricaine may alter oligodendrocyte dynamics – hence, larvae were sedated for minimal durations just before the point of legal protection to minimise these potential impacts (Gibson *et al.*, 2014; Hughes *et al.*, 2018; Mitew *et al.*, 2018; Swire *et al.*, 2019).

Following sedation and screening, embryos were mounted in 0.1% low melting point agarose with 100mg/L tricaine to maintain anaesthetic throughout imaging. Embryos were either mounted dorsally (to allow imaging of the brain) or laterally (to allow imaging of the spinal cord). Larval brains were imaged using 20x magnification, using a 100µm Z-stack for 5dpf embryos and 140µm for 8dpf embryos, with 2µm per slice. For spinal cord imaging, 100µm Z-stacks were taken for both age groups, again with 2µm per slice. Following imaging, 8dpf embryos were culled by schedule 1.

2.2.2.1.5 Image analysis and oligodendrocyte count

Oligodendrocyte counting was performed by semi-automated analysis in ImageJ, allowing comparison of manual and automated counts. Briefly, a composite maximum intensity projection was created to allow quantification. A region of interest was manually identified using the brightfield to exclude any potential noise from particularly auto fluorescent structures (i.e. the eye or gut). Manual counts were used to allow assessment of true cell number, as the *Tg(mbpa:GFP)* line labels not only oligodendrocyte cell bodies but also sheath projections towards myelin – as such, cells can be identified by their bright, rounded morphology. To quantify the overall extent of mbpa expression (including any sheaths projected by the oligodendrocytes), each image was subjected to auto-thresholding using default parameters in ImageJ to allow assessment of overall fluorescence intensity across the region of interest.

2.2.2.1.6 Optimisation of mbpa antibodies

In other to visualise mbpa by immunohistochemistry, two antibodies were trialled on whole mount larval samples. The first was a polyclonal antibody generated against e coli-derived MBP fusion protein with known reactivity against multiple species (rat, mouse and human). UniProt Align (https://www.uniprot.org/align) was used to investigate alignment of this MBP fusion protein with zebrafish mbpa and mbpb. The second antibody was synthesised and kindly shared by Bruce Appel (Kucenas *et al.*, 2009). Immunohistochemistry was performed as per 2.2.1.9, with the addition of antigen retrieval steps: following proteinase K treatment, samples were incubated for 5 minutes at room temperature then 15 minutes at 70°C with either 150mM TrisHCl pH9 or 1M citrate buffer 1M pH6 (2.9% trisodium citrate in dH_2O). Samples were then returned to room temperature, rinsed 3 x 5 minutes with PBST, then immunohistochemistry was performed as per routine protocol.

2.2.2.2 Impact of viral exposure on rnaset2 pathology

2.2.2.2.1 Experimental modulation of viral exposure

In order to manipulate the level of viral exposure, zebrafish embryos (*rnaset2* homozygous mutants and wild-type controls) were randomly assigned to one of four experimental conditions: conventional rearing, sterile rearing (hereafter called “bleached”), sterile rearing with the addition of adult gut extract (“bleached with gut”) and conventional rearing with the addition of adult gut extract (“conventional with gut”) (summarized in Figure 2.4).

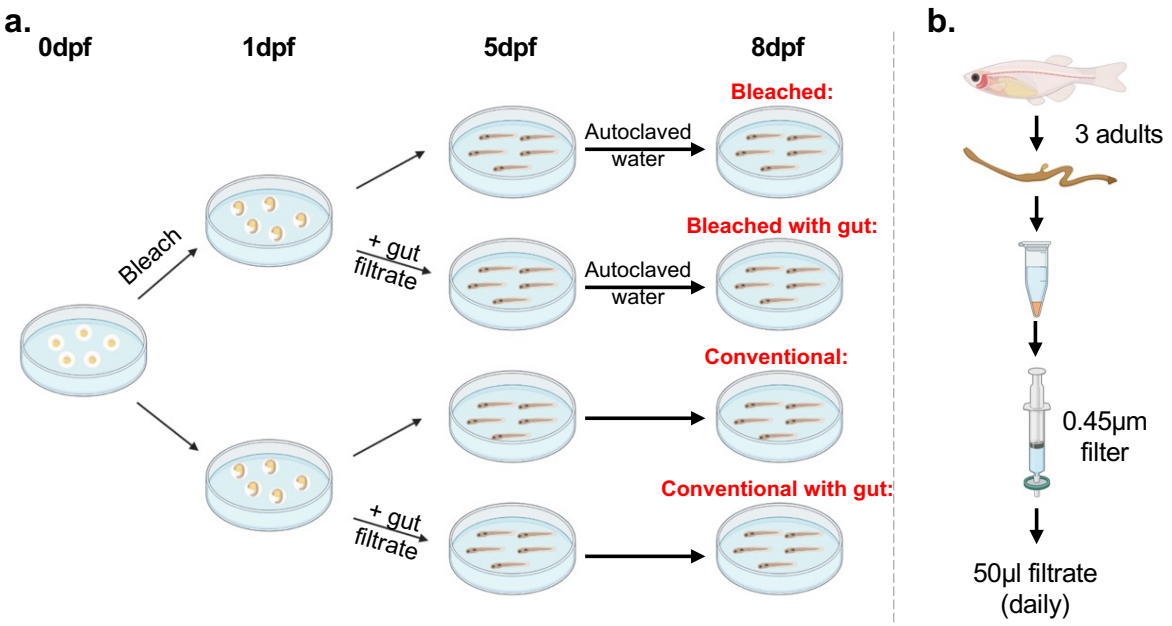

Figure 2.4. Schematic depicting experimental modulation of environmental viral exposure of wild type and *rnaset2* larvae.
(a) Treatment of larvae from 0–8dpf. Selected groups were bleached at 1dpf, with gut extract added where required at 5dpf and daily thereafter. **(b)** Gut extract purification was performed by dissecting out the intestines of adult animals and homogenizing in clear E3. Samples were centrifuged to remove large debris before filtering through 0.45µm to isolate potential viral particles.

To minimise viral exposure, 24hpf embryos were bleached in a solution of 400µl/L sodium hypochlorite and raised thereafter in autoclaved clear E3 media until 5dpf. Briefly, embryos were placed in a fine-mesh sieve and bathed in the following solutions: 5 minutes bleach; 5 minutes in distilled water; 5 minutes bleach; 5 minutes in distilled water; 5 minutes E3 unloading bath. As bleaching embryos can harden the chorion, bleached groups were manually dechorionated at 3dpf using sharp tweezers (if unable to do so independently). At 5dpf, bleached embryos were transferred into autoclaved aquarium water and fed daily with sterile food (kept isolated from general food supplies). Conventional groups were reared in clear E3 media until 5dpf and then transferred to non-autoclaved aquarium water thereafter.

To increase viral load, "bleached with gut" and "conventional with gut" groups were treated with purified gut extract from adult fish. Gut extract was obtained from 3 randomly selected adult fish housed in the same zebrafish facility as the *rnaset2* mutant line. Adult fish were euthanised and the intestines removed by dissection. First, a small incision was created between the pelvic and anal fins, followed by a shallow incision the ventral midline, around gills and over the abdomen to reveal the insides of the abdominal cavity. The gastrointestinal system was detached from the animal, with the liver, spleen and gall bladder removed. Isolated intestines were placed into 2mL clear E3 and homogenised using electronic homogeniser to break up the tissue. The gut sample was then centrifuged at 4°C, 3000g for 5 minutes and finally the supernatant was filtered through a sterile 0.45µm membrane. Samples were treated with 50µl filtrate each day from 5–8dpf.

RNA was then extracted from embryos at 8dpf to allow quantification of ZfPV burden and antiviral gene expression. Pools of 25 embryos were briefly transferred to fresh autoclaved aquarium water to remove any faecal debris, before euthanasia with by overdose of tricaine (confirmed by cessation of circulation). Following culling, RNA was extracted using the Trizol RNA extraction method described in section 2.2.1.1.

2.2.2.2.2 Optimisation of ZfPV primers

To assess viral burden in our embryos, we used the recently characterised zebrafish picornavirus (ZfPV) known to be present in zebrafish aquaria as a proxy for overall viral load. To quantify ZfPV, we utilised previously published primers targeting the 2C helicase domain of the ZfPV genome. RT-PCR was used to establish the optimal annealing temperature and cDNA concentration for these primers: briefly, cDNA (2µl, 4µl or 7µl) was mixed with 2µl 5x FirePol, 0.5µl each forward and reverse primers and milliQ water to a total volume of 10µl. RT-PCR reactions were performed using annealing temperatures of

56°C, 56.6°C, 57.6°C, 59.1°C and 60.9°C and the resultant products ran on 2.5% agarose gel (alongside a control sample of *ef1α* ran at 57.6°C). RT-PCR reaction was run as described in section 2.2.1.4. UV imaging revealed the band with the greatest intensity was achieved with a 56.6°C annealing temperature and 4µl cDNA template, indicating the addition of any further starting material may have an inhibitory effect on reverse transcriptase function.

These parameters were trialled with qRT-PCR using the ZfPV primers and samples of interest. Briefly, 4µl cDNA (synthesised with Superscript II in section 2.2.1.3) was added to 0.5ul each forward and reverse primers, alongside 5µl SYBR green. The qPCR reaction was run on a CFX96 Bio-Rad machine as described in section 2.1.7. Unfortunately, this reaction did not yield any CT values for ZfPV samples. The above reaction was re-run using cDNA synthesised using gene specific primers (Superscript II gene-specific primer protocol, using 3' ZfPV primer) and random hexamers (qScript) – these too did not yield CT values. As such, RT-PCR and automated band intensity quantification was used to quantify ZfPV burden hereafter.

2.2.2.2.3 Quantification of ZfPV burden

As above, ZfPV burden was quantified using RT-PCR and automated band intensity quantification. For the ZfPV RT-PCR, 4µl cDNA, 2µl 5x FirePol, 3µl milliQ water and 0.5µl each forward and reverse primers were added to microcentrifuge tubes and subjected to the reaction described in section 2.2.1.4, using an annealing temperature of 57°C and 40 cycles. To provide a baseline, quantification of a reference gene (*ef1α*) was performed using RT-PCR with 2µl cDNA, 2µl 5x FirePol, 5µl milliQ water and 0.5µl each forward and reverse primers – the reaction was performed as above, but with 20 cycles. For quantification, all reactions were performed in triplicate. RT-PCR products were run on 2.5% agarose gel containing SYBR safe and imaged using Syngene U:Genius gel dock.

Images were processed using Fiji ImageJ. Image colour was inverted to facilitate analysis. The "Analyse > Gels" function was utilised to identify individual lanes in each gel and generate a profile plot. Once plotted, the line tool was used to enclose the peak of the profile plot and area under the curve was quantified and used as a proxy for band intensity. To allow normalisation across samples, ZfPV burden was quantified as: $\frac{ZfPV\ band\ intensity}{ef1a\ band\ intensity}$.

2.2.2.2.4 qPCR of antiviral markers

qPCR of the antiviral marker *isg15* was performed using the protocol listed in section 2.2.1.7, using primers listed in

Table 2.1.

2.2.2.3 Investigation of endogenous retroviruses in zebrafish larvae

2.2.2.3.1 ZfERV in situ hybridisation

Two fully functional endogenous retroviruses have been identified in the zebrafish genome: *zferv1a* and *zferv1b*. In order to establish expression patterns of each of these retroviruses, probes were created against the envelope proteins of *zferv1a* and *zferv1b* (hereafter referred to as *env1a* and *env1b* respectively) and the reverse transcriptase gene of *zferv1a* (hereafter referred to as *pol1a*) (performed by Noémie Hamilton, as described in Rutherford *et al.,* 2021).

In order to assess expression of these ZfERV transcripts in zebrafish embryos, wild type embryos were fixed in 4% PFA at 4°C overnight, before being rinsed in PBS with 0.1% Tween (PBST) and dehydrated in sequential dilutions of methanol at room temperature: 10 minutes in 25% MeOH in PBST; 10 minutes in 50% MeOH in PBST; 10 minutes in 75% MeOH in PBST; 10 minutes in 100% MeOH. Samples were then transferred to a –20°C freezer for long term storage.

At the time of staining, embryos were rehydrated and washed in PBST, before being digested in 20µg/ml proteinase K in PBST for 1 hour at room temperature. Embryos were then re-fixed in 4% PFA for 20 minutes at room temperature, before being washed in PBST. Embryos were then incubated in pre-heated PreHyb for 3 hours at 70°C, before incubation in ProbeHyb overnight (again, at 70°C). The following morning, the ProbeHyb was removed and washed in serial WashHyb:SSC dilutions at 70°C for 15 minutes per wash as follows: 100% WashHyb; 75% WashHyb:25% 2xSSC; 50% WashHyb:50% 2xSSC; 25% WashHyb:75% 2xSSC; 100% 2xSSC. Samples were then washed in 0.2xSSC for 30 minutes at room temperature, and then for 10 minutes in sequential dilutions of 75% 0.2xSSC:25% PBST, 50% 0.2xSSC:50% PBST and 25% 0.2xSSC:75% PBST. After one further wash in PBST, samples were blocked in blocking solution for 3 hours at room temperature, before incubation in 1:5000 dilution in α-DIG-AP antibody at 4°C overnight.

The following morning, samples were washed six times in PBST (15 minutes per wash) and transferred to a 6-well plate for staining. Samples were then washed three times in staining wash for 5 minutes per wash, before incubation in the staining solution for 2 hours at room temperature for 5dpf samples, or overnight at 4°C for 3dpf samples. The following morning, samples were washed in stop solution at room temperature, and fixed again in 4% PFA before clearing with methanol overnight. Finally, fish

were rehydrated and cleared in glycerol, before being transferred to 100% glycerol for imaging and storage.

Embryos were imaged in glycerol using the Nikon SMZ Extended Focus Stereomicroscope from a lateral view of the whole body, or a dorsal view of the head.

2.2.2.3.2 qPCR of ZfERV transcripts

To quantify *zferv1a* transcripts in *rnaset2* mutant larvae, cDNA was synthesised from the heads of 8dpf embryos as per section 2.2.1.3. Primer sequences targeting the envelope (*env*), polyprotein (*gag*) or reverse transcriptase (*pol*) genes of *zferv1a* were taken from previously publications (Rutherford et al., 2020). qRT-PCT was performed as per section 2.2.1.7.

2.2.2.4 Microglia depletion by knockdown of irf8

To deplete microglia from embryonic brains, CRISPR/Cas9 genome editing was utilised to target interferon regulatory factor-8 (*irf8*) – a transcription factor essential for the development of macrophages and microglia (Li et al., 2011a). To achieve maximum depletion, pairs of guides targeting *irf8* expression were injected at a final concentration of 50µM each by creating an injection mix of 0.5µl of each guide at 100µM, 1µl of 50µM tracer and 1µl Cas9 stock (Figure 2.5, Table 2.2). As a control, scrambled crRNA was used at 50µM in the place of *irf8*-targetting guides (Table 2.2).

To facilitate injection at the single cell stage, adult fish were placed in pairing tanks the evening before microinjection with dividers pulled approximately twenty minutes before egg collection. Glass needles were loaded with injection mix immediately prior to the collection of fresh eggs and inserted into the injection rig. Needles were clipped using sharpened forceps to allow a volume of 0.5µl or 1µl to be injected with a single press of the attached pedal. Injection volume was measured using a graticule coated with mineral oil.

Embryos were lined up in the lid of a petri dish alongside a glass-slide and injected directly into the yolk sac with the 2µl of injection mix and placed thereafter in fresh E3 media, approximately 60 embryos per dish. Fish were screened for survival using light microscopy each day following injection, with unhealthy or dead embryos removed. To assess microglia depletion, the number of *mpeg:mCherry* cells in the brain were quantified at 5dpf using ZEISS Axio Scope. Microglia depletion efficiency was defined as the percentage of screened fish with no visible microglia upon screening.

Guide A

irf8

```
>chromosome:GRCz11:18:30567748:30568370:1
30567748 AGTGGATGAACCTGTAAAGTCCCCTTCCCCTCTTTTCCTTTCAGACAGATTTCTTGTAAA 30567807
30567808 TGCCTCCGTTTCGTGTAATCTCATTTACATATTCATGGTACGGCAACATAAGGCGTAGAG 30567867
30567868 ATTGGACGCCTTGGAGTTGCGCAAGCCAATCCGTTCTCACTACACTCTCCGTTCCCTTGC 30567927
30567928 GCGGGTGTCTTTTAGATTATAAATAAAGCTGCTTGGATGCCGTGAGTATGTACTTTATAA 30567987
30567988 TCCTCAGCTGCTGTTTGTAACGGCATACTAGTGAAGTAAAGGTCTACAAGATGAACTCGG 30568047
30568048 GCGGTCGCAGACTGAAACAGTGGCTTATAGAACAGATAAACAGTAACATCTATAATGGAC 30568107
30568108 TGCAGTGGGAGGATGAGGACCGCACTATGTTTCGAATCCCCTGGAAACATGCGGGAAAAC 30568167
30568168 AAGATTACAATCAAGAGGTGGATGCGTCCATTTTCAAAGTAAGCGAAACATTATAGTAAT 30568227
30568228 AATAATAGTAGATTTAACAGTAACAATATGATTAAAAATAATGCAGCATTGCTATATTAT 30568287
30568288 TATTATTATTATTATTATTATTAATATTAATATTAATAATAAAAATAATAATAATATTAA 30568347
30568348 TAATAATATTATGGTTGTTATTG                                     30568370
```

CABZ01044048.1

```
>chromosome:GRCz11:15:46608620:46609236:1
46608620 GGGCATCCGCTGCGTAAAAACTTGCTTGATAAGTTGGTGGTTCATTCCACTGTGGCGACC 46608679
46608680 CTGGATTAATAAAGGGATCAAGCCGACAAGAAAATGAATGAATGAATGTATGAGTGTGTG 46608739
46608740 TGTGGATGTTTCCCAGAGATGAGTTGCAGCTGGAAGGGCATCAGCTGCGTAAAAACGTGC 46608799
46608800 TTGATAAGTAGGTGGTTCATTCCACTGTGGCGAGCCCTGATTAATAAAGGGACTAAGCCG 46608859
46608860 AAAAGAAAATGAATGAATGAACCTTTGAGCTATTTGGGAGTCACAGGCATTTTTATTTTA 46608919
46608920 GCGGTCGCAGACTGAAATGTTTGGCAACCCCTGGTCTCCAGTGACAAACCACTGTTATAT 46608979
46608980 AATGACTTGCCTAATTACCCTAACTCTACCCTAATTAACCTAGTGAAGCCTTTAAATGTC 46609039
46609040 ACTTTAAGCTGTATAGAAGTGTCTTGAAGAATATCTAGTCTAATATTATTTACTGTCATC 46609099
46609100 ATGGCAAAGAGAAAATAAATCAGTTATTAGTGATGAGTTATTAACACTATTATGATTAGA 46609159
46609160 AACGGCTGAATAAATCTAATAATTCTGACTGTATAGTTCCCTCCTGAAGAGTGTGTTGCT 46609219
46609220 GTTGTTCAGTGTTTCTG                                           46609236
```

Guide B

irf8

```
>chromosome:GRCz11:18:30567729:30568348:1
30567729 AAATTGAGCTTAGGTATAAAGTGGATGAACCTGTAAAGTCCCCTTCCCCTCTTTTCCTTT 30567788
30567789 CAGACAGATTTCTTGTAAATGCCTCCGTTTCGTGTAATCTCATTTACATATTCATGGTAC 30567848
30567849 GGCAACATAAGGCGTAGAGATTGGACGCCTTGGAGTTGCGCAAGCCAATCCGTTCTCACT 30567908
30567909 ACACTCTCCGTTCCCTTGCGCGGGTGTCTTTTAGATTATAAATAAAGCTGCTTGGATGCC 30567968
30567969 GTGAGTATGTACTTTATAATCCTCAGCTGCTGTTTGTAACGGCATACTAGTGAAGTAAAG 30568028
30568029 GTCTACAAGATGAACTCGGGCGGTCGCAGACTGAAACAGTGGCTTATAGAACAGATAAAC 30568088
30568089 AGTAACATCTATAATGGACTGCAGTGGGAGGATGAGGACCGCACTATGTTTCGAATCCCC 30568148
30568149 TGGAAACATGCGGGAAAACAAGATTACAATCAAGAGGTGGATGCGTCCATTTTCAAAGTA 30568208
30568209 AGCGAAACATTATAGTAATAATAATAGTAGATTTAACAGTAACAATATGATTAAAAATAA 30568268
30568269 TGCAGCATTGCTATATTATTATTATTATTATTATTATTATTAATATTAATATTAATAATA 30568328
30568329 AAAATAATAATAATATTAAT                                        30568348
```

Guide C

irf8

```
>chromosome:GRCz11:18:30567829:30568448:1
30567829 CATTTACATATTCATGGTACGGCAACATAAGGCGTAGAGATTGGACGCCTTGGAGTTGCG 30567888
30567889 CAAGCCAATCCGTTCTCACTACACTCTCCGTTCCCTTGCGCGGGTGTCTTTTAGATTATA 30567948
30567949 AATAAAGCTGCTTGGATGCCGTGAGTATGTACTTTATAATCCTCAGCTGCTGTTTGTAAC 30568008
30568009 GGCATACTAGTGAAGTAAAGGTCTACAAGATGAACTCGGGCGGTCGCAGACTGAAACAGT 30568068
30568069 GGCTTATAGAACAGATAAACAGTAACATCTATAATGGACTGCAGTGGGAGGATGAGGACC 30568128
30568129 GCACTATGTTTCGAATCCCCTGGAAACATGCGGGAAAACAAGATTACAATCAAGAGGTGG 30568188
30568189 ATGCGTCCATTTTCAAAGTAAGCGAAACATTATAGTAATAATAATAGTAGATTTAACAGT 30568248
30568249 AACAATATGATTAAAAATAATGCAGCATTGCTATATTATTATTATTATTATTATTATTAT 30568308
30568309 TAATATTAATATTAATAATAAAAATAATAATAATATTAATAATAATATTATGGTTGTTAT 30568368
30568369 TGGAAAAAGTCAGATTTTTTCAGACTGTTATTAGATCATAGATCCCTGTGTACATGCAAT 30568428
30568429 TTGTCACAATCATAACATTT                                        30568448
```

Figure 2.5. *irf8* crRNA guides target non-overlapping regions of *irf8* exon sequence.
Searching with Ensembl genome browser reveals the target sequences of guides A–C lie within the same exon of the irf8 gene without overlapping (guide A: bases 30568048–70; guide B: 30568029–48; guide C: 30568129–148). Guide A target shares partial homology with intronic region of the coagulation factor IX-like gene (CABZ01044048.1). Orange highlight indicates exon, red text indicates target sequence.

Table 2.2. CRISPR guides used in this study.

Gene	Guide name	Target Sequence: 5'-3' (does not include PAM)
irf8	**irf8_crRNA_A**	**GCGGTCGCAGACTGAAACAG**
irf8	**irf8_crRNA_B**	**GTCTACAAGATGAACTCGGG**
irf8	**irf8_crRNA_C**	**GCACTATGTTTCGAATCCCC**
n/a	**Scrambled_crRNA**	**GACCTGAGGGAGCAAGATCC**

2.2.2.5 Production of 4C4 antibody from 7.4.C4 mouse hybridoma cells

7.4.C4 cell culture and antibody production protocol was kindly shared by Katy Reid (formerly of the Sieger lab, University of Edinburgh).

2.2.2.5.1 7.4.C4 cell culture

At the time of culturing, 7.4.C4 cells were thawed at 37°C for 2 minutes, before resuspension in hybridoma base medium with 20% foetal bovine serum (FBS) and seeding at a density of $6x10^5$ cells/ml in a T25 flask (Greiner Bio-One). Cells were maintained at at 37°C and 8% CO_2. Cell number and viability was monitored daily using a haemocytometer and Trypan Blue staining until cells reached a density of $8–9x10^5$ cells/ml, at which point subculture was performed and cells were transferred to T75 flasks (Greiner Bio-One) at a live cell density of $3x10^5$ cells/ml. After the culture was established, cells were sequentially adjusted to 15% then 10% FBS in hybridoma base medium after three subculture routines, respectively.

In order to ensure pure antibody production, the hybridoma cells were then adapted to serum-free media, as the presence of bovine IgGs from the FBS in the final supernatant could mask the presence of the antibody heavy- and light chains upon visualisation. Serial dilutions of serum supplemented medium (hybridoma base medium with 10% FBS) (SSM) in serum free media (SFM) were prepared. Cells were subcultured using 25%:75% SSM:SFM and monitored daily until density reached $8–9x10^5$ cells/ml, at which point serum concentration was reduced to 50%:50%, 75%:25% and finally 90%:10% SSM:SFM, before cells were resuspended in 100% SFM + 1% HT supplement.

To increase antibody yield, cells were subcultured in 100% SFM + 1% HT, maintaining a density of 3–9 10^5 cells/ml in increasing size flasks, until a final total of twenty T125 flasks (Greiner Bio-One) (each containing 50ml cells and media) were obtained. At this time, cells were starved for 14 days in order to stress the hydridomas and increase antibody production.

2.2.2.5.2 Harvesting and preserving 4C4 antibody from cell supernatant

After 14 days of starvation, the contents of each T125 flask were transferred into a 50ml falcon and centrifuged at 4000rpm for 10 minutes at 4°C to pellet the cells. The supernatant was then transferred to a fresh 50ml falcon and centrifuged again at 4000rpm for 10 minutes at 4°C to pellet any remaining debris. The remaining supernatant was then filtered through the Stericup Quick Release-GP Sterile Vacuum Filtration System and collected in sterile containers. At this stage, 5ml of filtered supernatant was placed on ice for later immunoprecipitation.

In order to preserve the antibody within the supernatant for long-term storage, two approaches were used. To 500ml supernatant, 1000ul of 10% sodium azide stock was added in a fume hood, to a final concentration of 0.02% - this stock will be used for immunohistochemistry on fixed samples. To the remaining 100ml, 3mls of 1M Tris pH7.5 was added to preserve the antibody for live cell-labelling (such as for flow cytometry). Both stocks were then aliquoted into 15ml falcons and stored at -80°C for future use.

2.2.2.5.3 Confirming the presence of 4C4 antibody in the cell supernatant

To confirm that the purified supernatant contained 4C4 antibody, raw filtered supernatant was used (without addition of sodium azide or Tris) using serum-free media as a control. The Thermo Scientific Nanodrop 2000 was used to measure protein concentration of the supernatant, using SFM as a blank, revealing a concentration of 2.6mg/ml.

To purify the antibody, Dynabeads protein G were utilised according to manufacturer's instructions. Briefly, Dynabeads were resuspended by vortexing for 30 seconds, before transferring 125µl to two 5ml culture tubes. The tubes were then placed within a Dynamag™ magnet to allow removal of the bead buffer. Beads were washed with 1000µl, before the supernatant and SFM were added to each tube respectively. The samples and Dynabeads were then rotated end-over-end for 1 hour at room temperature to allow the protein to bind, before the tubes were placed back into the magnet and beads washed three times with 2000µl PBS – each wash supernatant was kept on ice to be later run on the gel. Following the final wash, beads were transferred into a 1.5ml Eppendorf and resuspended in 50µl 2x SDS loading buffer.

In order to visualise protein content, the sodium dodecyl sulfate-polyacrylamide gel electrophoresis (SDS-PAGE) system was used with the following samples: raw filtered supernatant and SFM, each of the three washes from each sample and beads bound to either supernatant or SFM in 2x loading buffer (as above). For each of the liquid samples, 2x loading buffer was added in a 1:1 ratio. All samples were then boiled at 95°C for 5 minutes, before being pulse centrifuged, vortexed then pulse centrifuged for a final time. Finally, the samples containing beads were returned to the magnet and the bound fraction removed.

Samples were then loaded into an 8% acrylamide gel, and ran at 140V for 50 minutes, before the gel was removed from the casing and wells detached. The gel was then stained with Expedeon Instant

Blue Coomassie for 1 hour at room temperature following manufacturer's instructions. Following staining, the gel was rinsed three times with milliQ water and then destained in milliQ overnight.

The gel was imaged the following morning, revealing the presence of the IgG heavy chain (~50kDa) and IgG light chain (~25kDa) both in the raw supernatant (input) and bound fraction (elute) (Figure 2.6) – demonstrating presence of antibody at a satisfactory concentration to be trialled with immuno histochemistry.

2.2.2.5.4 Confirmation with immunohistochemistry

In order to confirm that the antibody found within the 7.4.C4 cell supernatant was in fact specific to microglia, immunohistochemistry was performed on a known macrophage reporter line – the *Tg(fms:GFP)sh377* line, in which macrophages and microglia are labelled with GFP. 4dpf embryos were fixed as per section 2.2.1.8 and subjected to immunohistochemistry as detailed in section 2.2.1.9. The previously validated anti-GFP primary antibody and old 4C4 antibody stocks were used at a concentration of 1:500 and 1:100 respectively, while the novel 4C4 primary antibody stock was tested at the following doses: 1:50, 1:100, 1:200 and 1:500 (with a no primary control).

Following staining, samples were embedded in low melting point agarose and imaged with the Nikon Spinning Disk (50 slices, 2µm per slice; 100µm total). Imaging revealed robust co-localisation of the fms:GFP and 4C4 signal across all concentrations, with minimal off-target binding (Figure 2.7). A small number of GFP-positive, 4C4-negative cells were observable across multiple dilutions – however, this is to be expected due to the nature of 4C4 as a microglia-specific marker, where recently infiltrating macrophages may not yet express this protein. Indeed, GFP-positive, 4C4-negative cells are also seen with the old, previously published 4C4 stock. Together, these data confirm that the 7.4.C4 supernatant does in fact contain an antibody which specifically binds microglia.

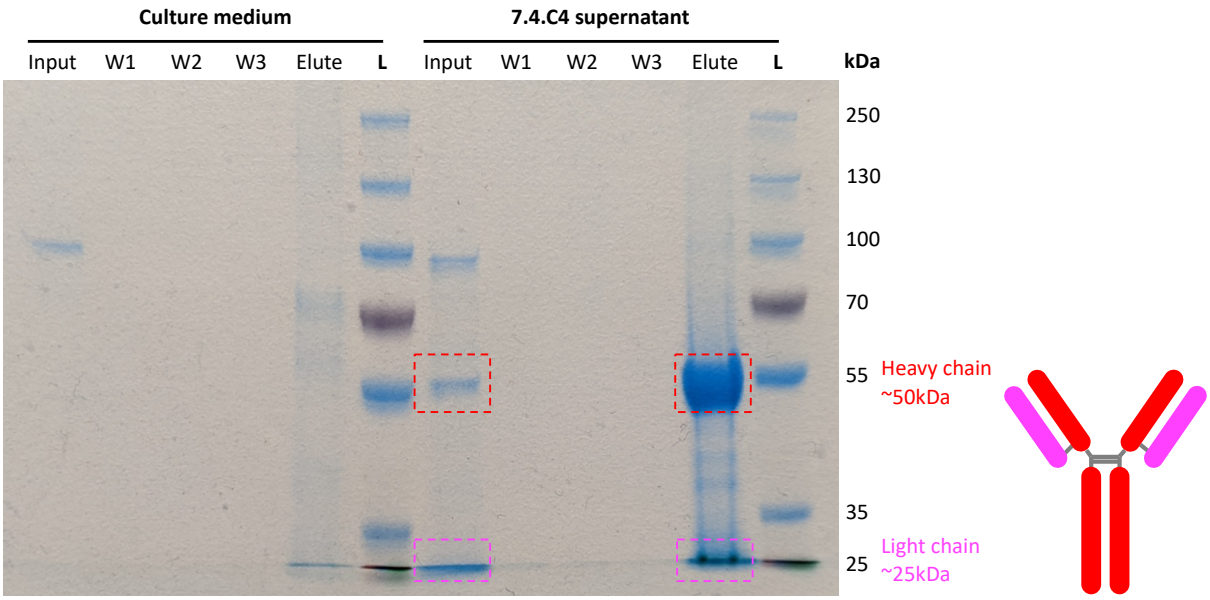

Figure 2.6. SDS-PAGE confirmation of antibody in 7.4.C4 cell supernatant.
8% polyacrylamide gel loaded with raw culture medium or cell supernatant (Input), PBS washes following bead binding from each sample, (W1–3) and bound fraction (Elute). L denotes the ladder lane. Gel shows presence of protein at ~50kDa (red box) and ~25kDa (magenta box), revealing presence of the antibody heavy and light chains (respectively) in raw supernatant and bound fraction, which are absent in culture medium alone. No protein expression is visible in any wash step, suggesting minimal loss of bound antibody during each wash.

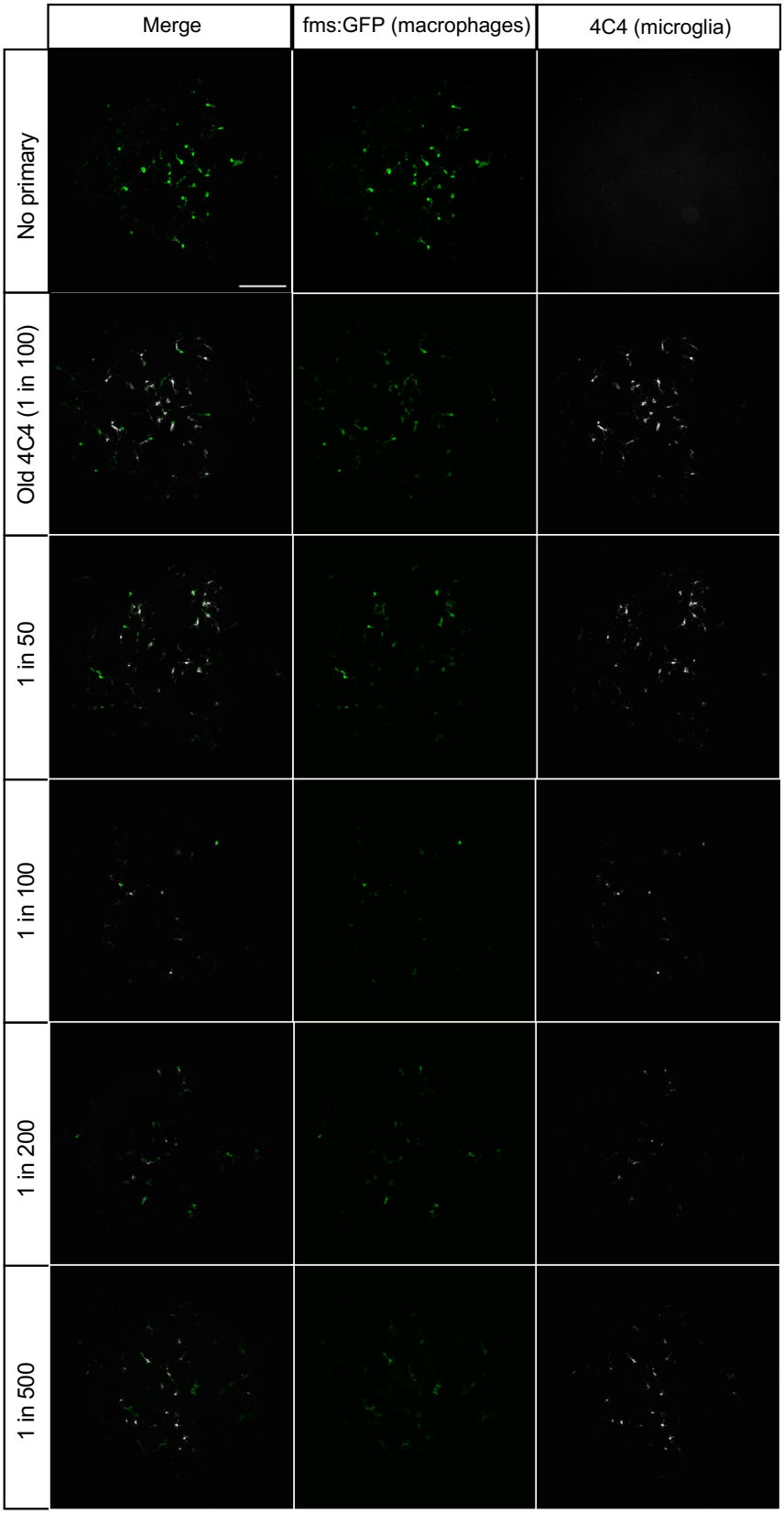

Figure 2.7. New 4C4 stock robustly labels host microglia at a range of concentrations.
20x imaging revealed co-localisation of 4C4 signal with fms:GFP-expressing macrophages in the brains of 4dpf larvae. Staining was comparable across a range of dilutions. Scale represents 100µm.

2.2.3 Chapter 4 methods

2.2.3.1 Zebrafish-to-zebrafish immune cell transplantation

For zebrafish-to-zebrafish transplantation, macrophages were isolated from whole kidney marrow using flow cytometry, before injection into microglia-depleted embryos via the systemic circulation (for summary, see Figure 2.8).

2.2.3.1.1 Graft preparation

To prepare grafts for transplantation, whole kidney marrow was isolated from ten transgenic adult fish with GFP-labelled macrophages (Tg(fms:GFP) and GFP-negative controls (nacre). Animals were culled by schedule 1 methods: first, animals were supplied with terminal anaesthesia in a tricaine bath (1.33g/L in aquarium water) followed by destruction of the brain. Culled animals were then secured on an agarose dissection plate with the abdominal cavity exposed via a deep incision along the ventral midline. To retrieve the kidney, internal organs were removed (including any egg debris) and the exposed kidney was peeled from the dorsal surface using forceps. Each kidney was then placed in 200µl of cold live sorting buffer (L15 media, 20% foetal bovine serum and 5mM EDTA) and mechanically separated using repeated pipetting by P1000 and P200 pipettes, to encourage dissociation of cells from connective tissue. Samples from each fish were kept separate, and on ice, until immediately before flow cytometry to prevent cross-reactivity or immune activation. Finally, samples were filtered through fluorescence-activated cell sorting (FACS) tubes and pooled for sorting.

2.2.3.1.2 Flow cytometry

To isolate GFP-positive cells, samples were loaded into the BD FACSMelody™ cell sorter at 4°C. GFP-negative samples were sorted first to determine thresholds for GFP-fluorescence, and TO-PRO™3 was used to facilitate removal of dead cells. GFP-positive cells were sorted into an Eppendorf tube containing 500µl live sorting buffer and placed on ice before transplantation. Cell yields of approximately 500,000 cells were optimum for transplantation.

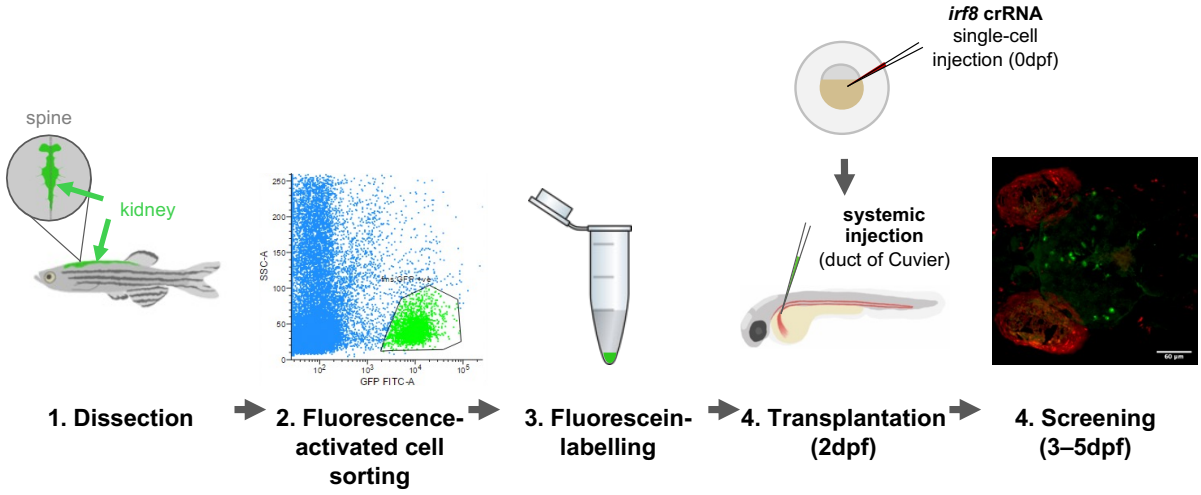

Figure 2.8. Whole kidney marrow transplantation methodology.
To prepare graft for transplantation, kidneys were dissected from transgenic adult fish with GFP-labelled macrophages (*Tg(fms:GFP)*). Fluorescence-activated cell sorting (FACS) was used to isolate the population of GFP-expressing macrophages, which were then transiently stained with fluorescein to allow visualisation after photobleaching by the flow cytometer. The prepared graft was then injected 2dpf embryos into the systemic circulation via the duct of Cuvier. Transplanted fish were screened from 3-5dpf to score the number and location of GFP/fluorescein-positive cells.

2.2.3.1.3 CFSE labelling

After FACS, GFP-labelled cells can become photobleached, making visualisation and quantification of transplanted cells challenging in host embryos for several days post-transplantation. To allow immediate visualisation, sorted cells were labelled with the fluorescent dye carboxyfluorescein succinimidyl ester (CFSE). Sorted cells were centrifuged for 6 minutes (1000rpm) at 4°C to pellet cells and allow removal of serum-containing buffer which may comprise cell staining. Pelleted cells were then rinsed with 500µl PBS to remove any remaining serum, before resuspending in 1:10,000 CFSE dilution in PBS and incubating for 15 minutes at 26°C. After incubation, cells were centrifuged and resuspended in live sorting buffer to stop any further labelling.

2.2.3.1.4 Transplantation into zebrafish embryos

After graft preparation, transplanted cells were centrifuged with excess supernatant removed until graft contents could be transferred to microcentrifuge tube. Cells were suspended in 1% polyvinylpyrrolidone (PVP) in live sorting buffer, before final centrifugation and resuspending at a concentration of approximately 20–30 cells per nanolitre.

Cells were then loaded into glass needles using loading pipette tips and inserted into the injection rig. Each needle was clipped using forceps such that 1nl was injected with a single press of the attached pedal. The approximate number of fluorescent cells per nl was quantified using the Zeiss AXIO scope before transplantation.

Transplants were performed on 2dpf embryos with their endogenous microglia and macrophages labelled with mCherry (*Tg(mpeg1:mCherry CAAX)*). As we have previously established that transplantation efficiency is maximised in microglia-depleted animals, host embryos were injected with *irf8* crRNA guides A and B as in section 2.2.2.4. On the day of transplantation, hosts were dechorionated, anaesthetised with 4.2% tricaine and lined up on a moist 28°C agarose plate for injection. Sorted cells were injected into the systemic circulation via the duct of Cuvier. Hosts were then rescued from anaesthesia in fresh E3 and returned to the incubator for recovery.

As a negative control, approximately 60 embryos received a sham transplant containing only 1% PVP in live sorting buffer, without any cells present.

For longitudinal quantification of transplanted cells, embryos were sedated with 4.2% and screened using a Zeiss Axioscope. Positive embryos were isolated in individual wells of 48-well plates for

longitudinal follow-up. The number and location of green-fluorescing cells were manually counted for each fish from 1–3 dpt.

2.2.3.2 Immunohistochemistry on adult brain sections

Selected adult fish were fixed by placing first into a tricaine bath for anaesthesia, then into 4% paraformaldehyde. Fixed fish were then embedded in paraffin and sectioned in 5µm increments along the sagittal plane until the approximate midline of the fish. At the time of staining, tissue sections were deparaffinised and hydrated by bathing in the following solutions, each for five minutes: Xylene (x2), 100% ethanol (x2), 90% ethanol, 75% ethanol, distilled water (x2). Sections were then placed in a bath of 0.01M citrate buffer, heated until boiling and allowed to simmer for approximately 10 minutes for antigen retrieval. After cooling, sections were permeabilised with 0.5% Triton X-100 in PBS at room temperature. Tissue sections were then blocked in a solution of 3% bovine serum albumin, 5% goat serum and 0.3% Tween-20 in PBS for 1 hour at room temperature. Excess blocking solution was removed from the samples, before adding primary antibodies diluted in fresh blocking solution. Anti-4C4 mouse polyclonal antibodies (1:50 dilution) were used to label endogenous microglia, while anti-GFP chicken polyclonal antibodies (varying dilutions, see below) were used to label any cells of transplant origin. Samples were incubated in primary antibody overnight at 4°C in a humid incubating chamber. After incubation, excess primary antibody was removed and tissue sections were rinsed three times with 0.1% Tween-20 in PBS, each wash 10 minutes. Relevant secondary antibodies were diluted 1 in 500 in fresh blocking solution and added to the sample for 1 hour incubation at room temperature in humid incubating chamber. Excess secondary antibodies were removed, and sections were washed three times in 0.1% Tween-20 in PBS, 10 minutes per wash. After washing, coverslips were mounted onto samples using Vectashield Vibrance hard-set mounting medium and sealed with a small amount of nail polish in preparation for imaging with the Spinning Disk confocal microscope.

Initial imaging of paraffin sections of adult brains in the GFP channel revealed substantial background noise – likely due to the high degree of autofluorescence in the brain, and in cerebral blood vessels in particular. Thus, in order to optimise staining of GFP-positive cells, trial sections from *Tg(fms:GFP)* adult brains were treated with increased concentrations of primary or secondary antibodies. As before, sections were imaged using the UltraVIEW VoX Spinning Disk Confocal Microscope with exposure and gain set at the lowest settings required for cell visualization. Increasing both the primary and secondary antibody concentrations resulted in improved signal-to-noise ratio, with slides treated with primary antibodies of 1:200 allowing most reliable visualization of cells in the absence of visible autofluorescence (see Figure 2.9). As such, further work on paraffin sections utilised an anti-GFP primary antibody concentration of 1:200.

2.2.3.3 Tissue clearing adult brains

2.2.3.3.1 Sample preparation

Dissected brains were obtained as described in section 2.2.1.1. For tissue clearing and immunohistochemistry, dissections were performed on fixed tissue to allow for careful extraction of the brain with minimal disruption to the structure, as this could impact resulting imaging. Following dissection and dehydration in methanol series, samples were stored at –20°C in 100% methanol to ensure preservation of tissue and quenching of fluorescent signal to minimise interference with subsequent staining.

2.2.3.3.2 Tissue clearing and immunohistochemistry

Tissue clearing and immunohistochemistry methodology was adapted from Susaki *et al.,* 2015 and Ferrero *et al.,* 2018. The overall workflow is summarised in Figure 2.10a.

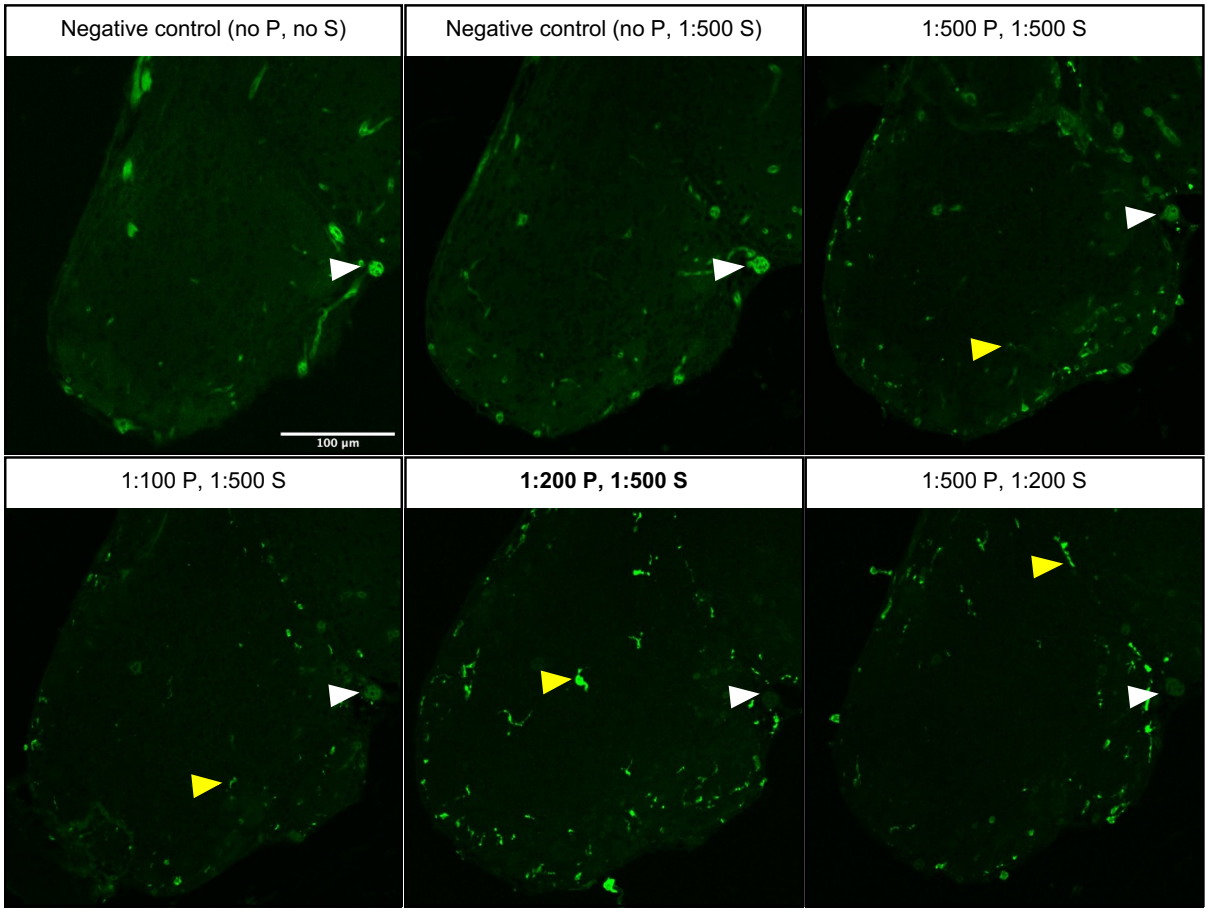

Figure 2.9. Optimisation of immunohistochemistry for transplanted cells in adult brains.
Sagittal sections of adult olfactory bulb were immuno-labelled with varying concentrations of anti-GFP primary (P) and GFP-tagged secondary (S) antibody and imaged using UltraVIEW VoX Spinning Disk Confocal Microscope (20x magnification). Optimal signal-to-noise obtained using 1:200 P, 1:500 S staining. Background autofluorescence is indicated by white arrows, GFP-tagged microglia are indicated by yellow arrows. Imaging parameters were optimised for each slide, with negative control slides imaged according to settings for 1:500 P; 1:500 S sample.

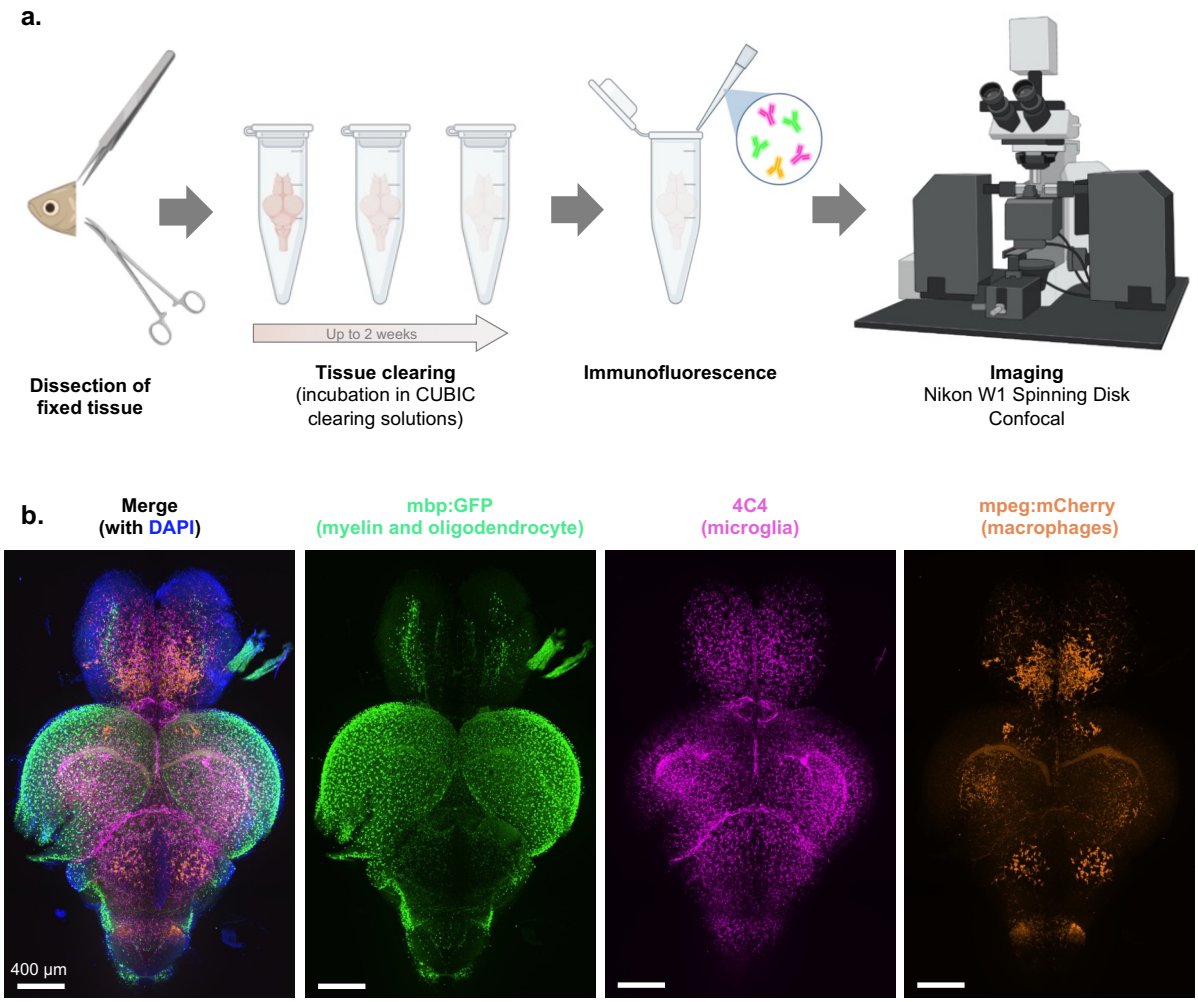

Figure 2.10. Tissue clearing workflow.
(a) At the appropriate age for a given experiment, adult animals were sacrificed, and their brain dissected. Brains were then incubated in CUBIC tissue clearing solutions for up to two weeks before whole mount immunohistochemistry. Stained samples there then imaged using the Nikon W1 Spinning Disk Confocal microscope. (b) An example of a cleared, stained brain from a *Tg(mbpa:GFP;mpeg1.1:mCherry CAAX)sh378* animal, demonstrating the ability of this technique to image multiple cell types across multiple channels. Scale bar represents 400µm.

At the time of clearing, samples were rehydrated from 100% methanol using serial MeOH dilutions in dH_2O, as PBS is known to interfere with clearing via CUBIC-1. Samples were washed for 30 minutes in 75% MeOH: 25% dH_2O, 50% MeOH: 50% dH_2O, and 25% MeOH: 75% dH_2O, before three five-minute PBS washes. At this stage, samples <14dpf were taken forward for immunohistochemistry without any additional clearing, due to their small size and transparency. For samples 28dpf and older, brains were then submerged in 1ml 50:50 CUBIC-1:dH_2O for up to six hours. Following full equilibration of the sample (confirmed by checking that the sample has sunk to bottom of the tube), 50:50 CUBIC-1:dH_2O was removed and 1ml CUBIC-1 was added. Samples were then left to incubate at room temperature for 3 days.

After CUBIC-1 clearance, samples were washed three times with PBS, before being immersed in 1ml 50:50 CUBIC-2:PBS and incubated for up to 24 hours. 50:50 CUBIC-2:PBS was then replaced with CUBIC-2, and samples left to incubate for 3 days for 28dpf animals, and 6 days for 42dpf and older.

After clearance, samples were ready for immunohistochemistry. CUBIC-2 was removed and washed four times with PBS. Samples were then digested in 1:500 proteinase K for 2 hours at room temperature, before three five-minute washes with PBS. Samples were then blocked in blocking buffer (10% sheep serum, 0.8% Triton X-100, 1% bovine serum albumin in PBT), before incubation in primary antibody solution for 48 hours at 4°C. Anti-GFP chicken was used at a 1:500 dilution to label transplant-derived cells, anti-mCherry rabbit was used at 1:500 dilution to label endogenous macrophages and microglia and anti-4C4 mouse was utilised at a 1:50 dilution to label microglia (endogenous or transplant-derived). Following primary antibody incubation, samples were washed thoroughly with PBS at room temperature, before incubating in secondary antibody overnight at 4°C. All secondary antibodies (anti-chicken 488, anti-rabbit 568 and anti-mouse 647) were used at 1:500 dilution. The following morning, samples were incubated in 1:5000 4',6-diamidino-2-phenylindole (DAPI) solution (in PBS) for 60–90 minutes at room temperature, followed by thorough washes. Once staining was complete, the samples were re-cleared with CUBIC (overnight incubation with 50:50 CUBIC-2:PBS and 3–6 days in CUBIC-2) to ensure full transparency for imaging.

2.2.3.3.3 Imaging of cleared brains

Samples were mounted in CUBIC-2 and aligned so that the dorsal surface of the brain was flush against the coverslip, before imaging with the Nikon W1 spinning disk confocal microscope. For each sample, a 500µm Z-stack was taken with 10x or 20x lens, using the Z-spacing recommended by NIS Elements (0.9µm for 20x images, 2.5µm for 10x images). Large images were taken using the tiling function (3x2

grid) within NIS elements. Samples from each timepoint were imaged on the same day to ensure fair comparison between groups.

To trial parameters for imaging, brains from *Tg(mbpa:GFP;mpeg1.1:mCherry CAAX)* adults were stained for anti-GFP (myelin and oligodendrocytes), anti-mCherry (macrophages), 4C4 (microglia) and DAPI (nuclei). Imaging of these brains confirmed that each of these cell types could be clearly visualised, and that clearing was compatible with imaging in all four channels (Figure 2.10b).

2.2.3.3.4 Analysis

For analysis of such large imaging data, a semi-automated approach was required. Initial segmentation was trialled with Imaris, which allows visualisation and processing of large three-dimensional datasets. To begin processing, the raw ND2 file from the Spinning Disk was converted into an Imaris compatible IMS file. The optic tectum was manually identified as a region of interest from each whole brain image, as processing the whole image was beyond the capabilities of the analysis computers available in the Light Microscope facility. The optic tectum was chosen as a region of interest to allow alignment with the embryonic data sets from other transplant assays (TUNEL etc.), and because this area remained robustly intact after dissection, immunohistochemistry and clearing while other more peripheral regions (such as the olfactory bulb or hindbrain and spinal cord) were frequently damaged.

Following selection of a region of interest, the surface model creation wizard was utilised to detect objects of strong fluorescent intensity (pipeline summarised in Figure 2.11). This tool allows automated identification of cells, based on several parameters which are adjusted by the user to promote best fit of the surface model with actual signal. For the current surface model, the detail level was set at 1µm – ensuring a high level of surface detail was preserved by the model, resulting in more accurate capturing of microglia morphology. Thresholding was then applied using the background subtraction tool, which utilises local cut-off values for intensity and is particularly useful where objects of interest are not uniformly stained. To inform this thresholding, the diameter of the largest sphere which could fit into any given cell was set at 4.13µm, based on manual measurements of the smallest regions of real cells visible in this dataset. Finally, the resulting identified surfaces were filtered by volume, to exclude any objects greater than 9000μm^3. This value was estimated by measuring the diameter of some of the largest cells visible in the raw image (~25µm) and calculating the volume of a sphere of this radius. This gives a value that is likely much larger than any real cell but should ensure only the largest objects (those that include multiple cells merged with each other, or with auto-fluorescent blood vessels) are excluded. The resulting data was then exported to an Excel sheet.

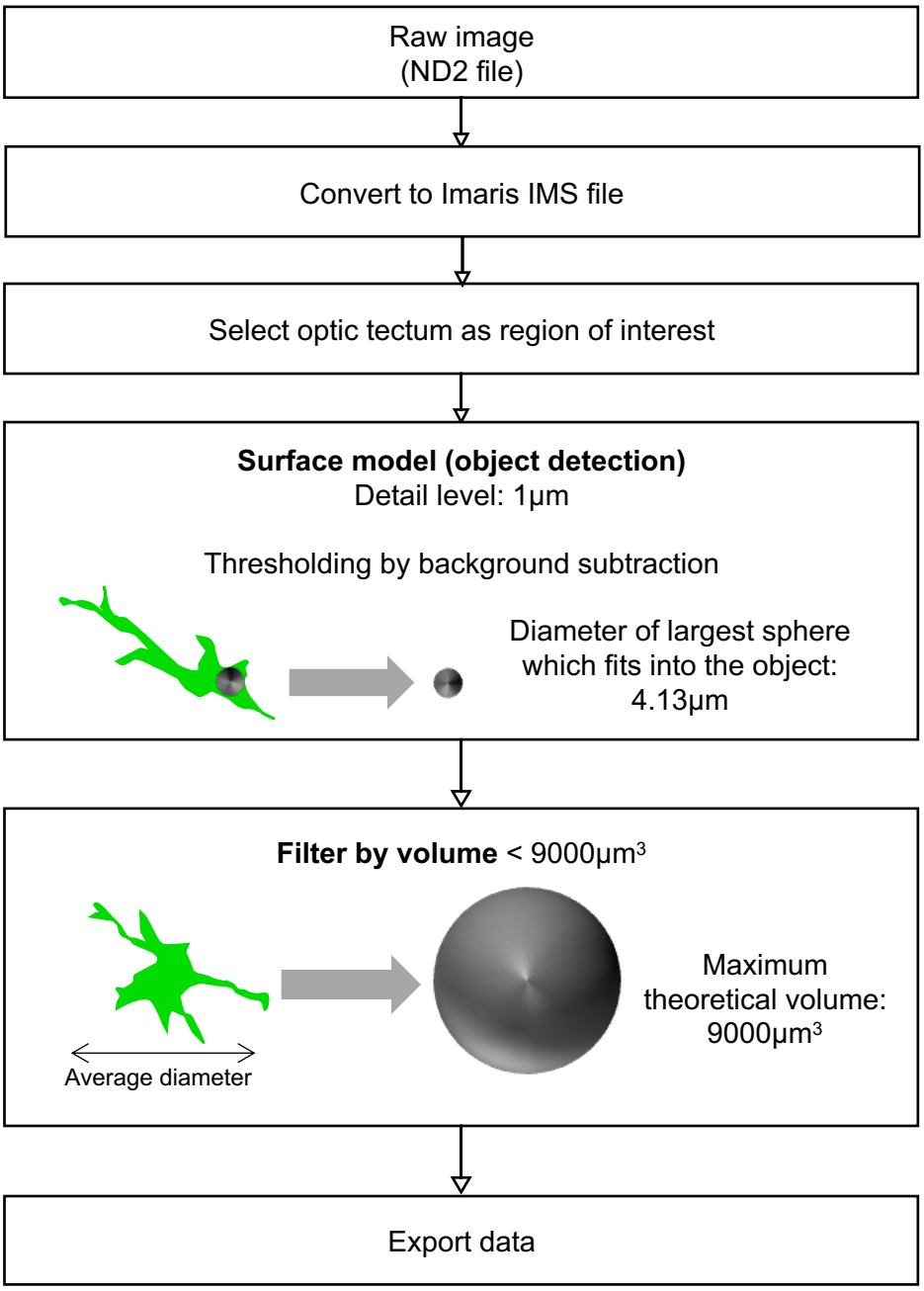

Figure 2.11. Summary of Imaris tissue clearing image processing pipeline.

This strategy mapped well to datasets of smaller brains (e.g. at 4wpf), but had minimal accuracy when mapping larger samples (from 6wpf onwards). Similarly, the local thresholding tool – while accurate in identifying cells in well repopulated samples – resulted in many false negatives in samples where cells where lacking, as the algorithm identified small regions of increased brightness as objects in the absence of the bright fluorescence of real cells to perform auto-thresholding. However, the alternative thresholding strategy (absolute intensity) was also not suitable for this image, as this was unable to account for the increased brightness cells at the tissue surface and dimmer cells within. As such, automated quantification with Imaris was abandoned in favour of software that facilitated more complex segmentation.

After the difficulties described above with Imaris, an automated pipeline was established using Arivis Vision 4D, which allows more sophisticated segmentation of complex datasets (summarised in Figure 2.12). As above, this pipeline also began by converting the ND2 file from the Spinning Disk into an Arivis compatible SIS file. The image was then manually cropped to focus on the optic tectum, for the reasons described above.

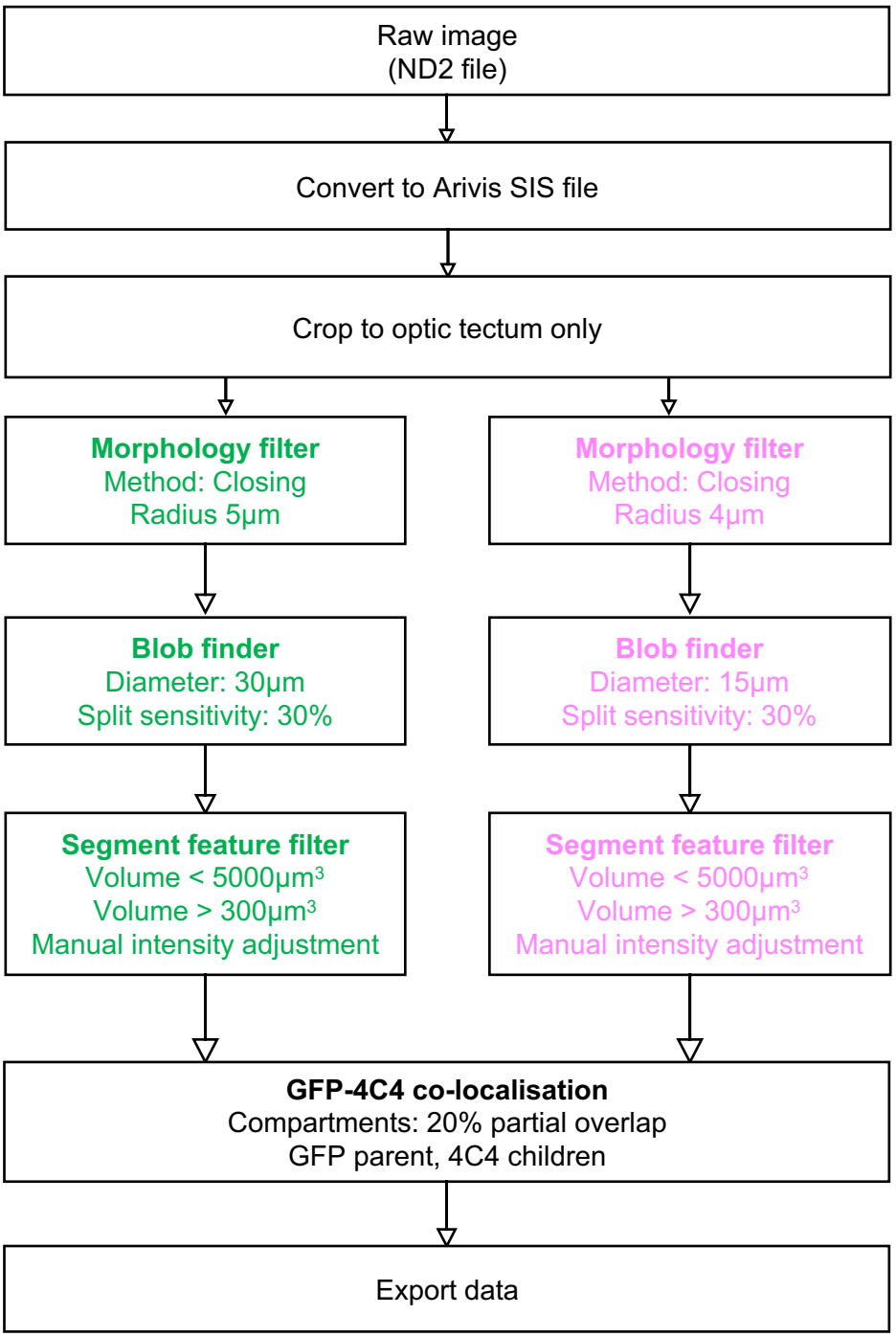

Figure 2.12 Summary of Arivis tissue clearing image processing pipeline.

Following cropping, the pipeline first applied a closing morphology filter, which smooths the appearance of otherwise highly ramified and irregular microglia to create a more uniform structure that can be better identified by subsequent segmentation tools – essentially, closing the gaps between the furthest points of each cell. The pipeline then performed the 'blob finder' segmentation tool – an analysis tool suited to finding irregular, rounded objects. The parameters of this blob finder segmentation were adjusted to most accurately capture the relevant cell population, using an average diameter of 30µm for objects in the GFP channel, and 15µm for 4C4-positive cells. Diameters were established by using manual measurement of cells in the raw image as a starting point, then adjusting the value until the segmentation most accurately mapped visible cells. The differing diameters set for each channel – despite labelling the same cell type – are attributed to the different cellular localisation of the marker proteins: fms:GFP being a cytoplasmic marker distributed throughout the cell, while the 4C4 antigen may be more discrete. Using these parameters, the blob finder segmentation identifies cells in three dimensions, as shown in Figure 2.13.

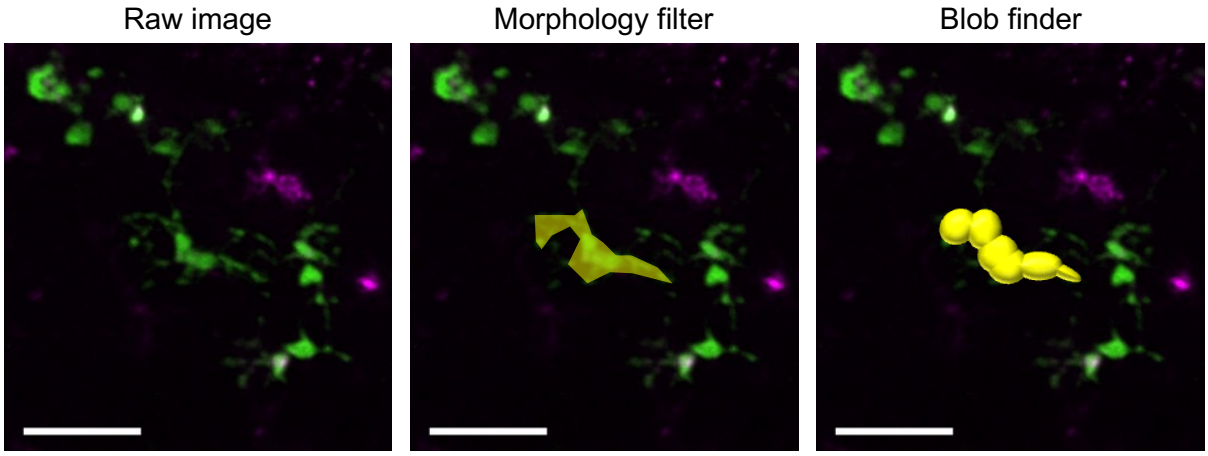

Figure 2.13 Filtering and segmentation of raw images. Note – schematic only.

To remove any analysis artefacts, the resulting segments were filtered to exclude any objects with a volume larger than 5000µm^3 or less than 300µm^3. These values differ to those used for the Imaris segmentation – however, this is because Imaris requires spherical estimations of volume to provide a threshold, while Arivis is better able to calculate the volume of irregular objects and filter accordingly. At the final stage, objects were manually filtered by intensity to account for differing staining efficiencies between timepoints to ensure the final object count best reflected the true number of cells.

To establish the co-localisation of 4C4 and GFP signal, a parent-child analysis was performed to quantify the number of GFP-positive objects that contained a 4C4-positive object, with a minimum overlap of 20%. Data was then exported into an Excel spreadsheet and visualised with GraphPad Prism.

2.2.3.3.5 Transplant engraftment time-course

For long-term assessment of transplant engraftment, successfully transplanted animals were raised according to standard zebrafish husbandry. Fish were checked weekly to observe any potential side effects of transplantation, and to maintain fish health. At the desired timepoint, fish were culled, and their tissue processed via pipeline described in section 2.2.3.3. Samples were collected until a timepoint at which cells were no longer visible in host brains, and any remaining animals culled by schedule 1 thereafter.

2.2.3.4 csf1rb genotyping

In order to investigate the engraftment of transplanted WKM-derived macrophages in the absence of endogenous microglia, *csf1ra*$^{-/-}$*; csf1rb*$^{-/-}$ double mutant zebrafish (hereafter referred to as *csf1r*^{DM}) were selected as hosts. This line exhibits an almost complete lack of microglia throughout embryonic and adult stages (Oosterhof *et al.*, 2018). Double mutants contain both an ENU-induced point mutation in the tyrosine kinase domain of *csf1ra* (known as the panther mutation), and a transcription activator-like effector nucleases (TALEN)-mediated deletion inducing an early stop codon in exon 3 of *csf1rb* (Parichy *et al.*, 2000; Oosterhof *et al.*, 2018).

To obtain this line, *csf1ra*$^{-/-}$*; csf1rb*$^{+/-}$ animals were in crossed at the University of Edinburgh, and resulting embryos kindly shipped to us by Dirk Sieger and Julie Mazzolini. Upon arrival, embryos were bleached according to standard practice (described in section 2.2.2.2.1) and raised in the Bateson Centre Aquaria quarantine facility.

Once of breeding age, these fish were genotyped by offspring for the *csf1rb* allele. Genotyping was performed by diagnostic digest – exploiting the fact that the mutant *csf1rb* allele lacks an *MspI* restriction site due to the TALEN-induced 4bp deletion. As such, genotyping was performed by PCR amplification of a 363 base pair region of the *csf1rb* gene (in exon 3, from 3328bp to 3690bp), and digested with the *MspI* restriction enzyme. Following incubation with *MspI,* the wild type allele yielded fragments of 203, 132 and 28 bp as the restriction enzyme was able to cut at both *MspI* restriction sites present in the PCR fragment (see Figure 2.14). In contrast, the mutant allele contained only one restriction site and as such was digested into fragments of 331 and 28bp. Heterozygous mutants

showed bands corresponding to both the wild type and mutant fragment sizes, with one allele containing both *MspI* sites and the other with just one.

The stock of *csf1ra*$^{-/-}$*; csf1rb*$^{+/-}$ animals maintained in quarantine were genotyped by breeding with wild type animals and genotyping of the resulting embryos. The genotype of each parent could then be inferred from the ratio of wild type, homozygous and heterozygous embryos in the resulting clutch. This method of genotyping was selected rather than conventional fin clipping to minimise the risk of infection for these immune-compromised animals after an injury, particularly whilst held in quarantine. Briefly, 24 embryos were selected from each pair for genomic DNA (gDNA) extraction and placed into individual microcentrifuge tubes containing 45µl of sodium hydroxide (50mM). Samples were then heated to 95°C for 25 minutes, before the addition of 5µl Tris HCl (1M, pH 8).

Following extraction of gDNA, RT-PCR was performed as per the reaction described in section 2.2.1.4 with 34 cycles, using the primers described in Table 2.1 (csf1rb_geno_fwd and csf1rb_geno_rev, kindly shared by the Sieger lab). To first establish the most appropriate annealing temperature for these primers, an RT-PCR primer gradient was performed at the temperatures of 64°C, 63.5°C, 62.5°C. 61°C, 59.2°C, 57.9°C, 56.8°C and 56°C. The resulting products were run on a 2% gel as shown in Figure 2.15. All trialed temperatures resulted in a clear band at the expected size of 381 base pairs, but lower temperatures permitted more off-target expression. As such, subsequent RT-PCRs were performed at 64°C.

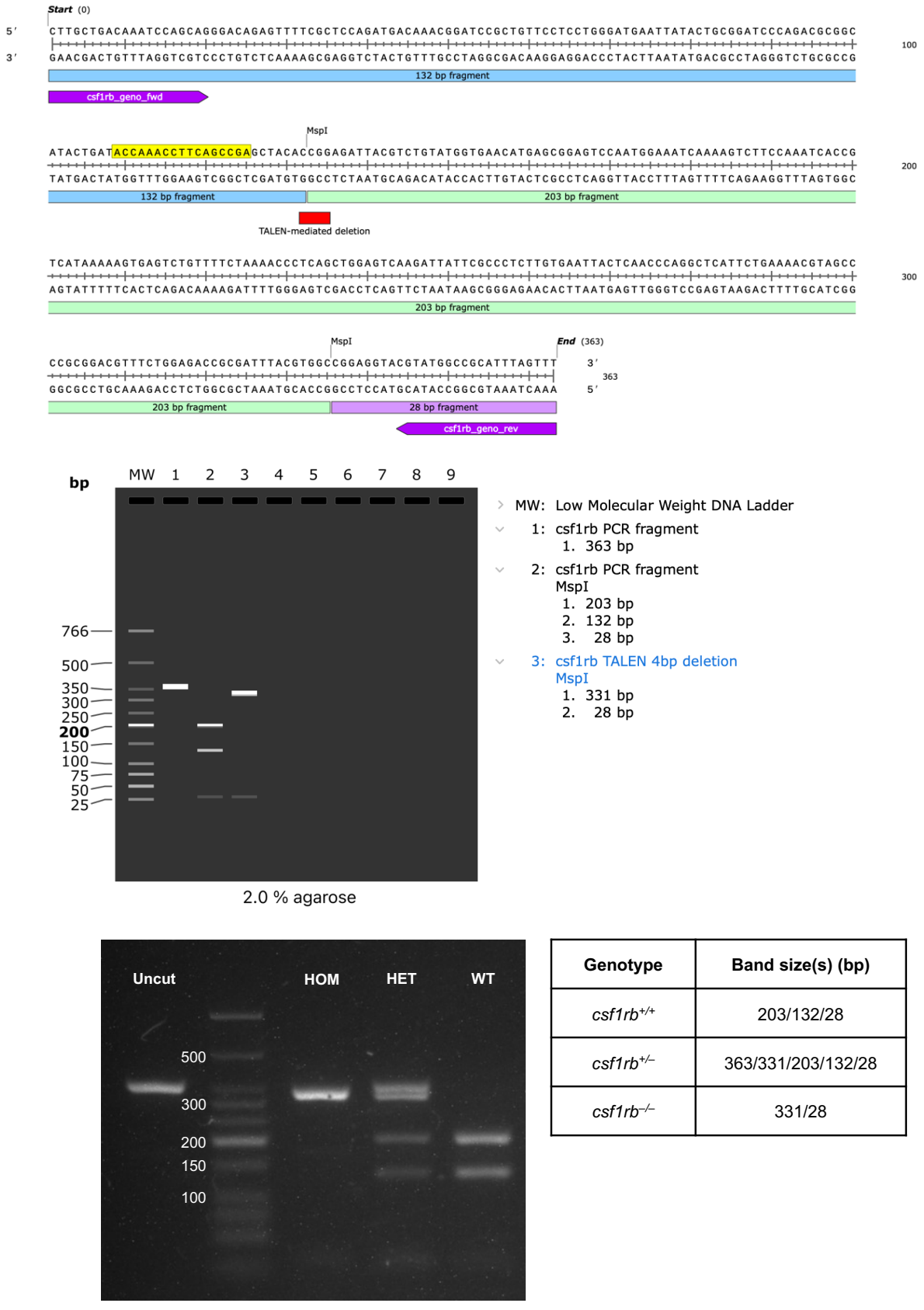

Genotype	Band size(s) (bp)
csf1rb$^{+/+}$	203/132/28
csf1rb$^{+/-}$	363/331/203/132/28
csf1rb$^{-/-}$	331/28

Figure 2.14. *csf1rb* diagnostic digest strategy.

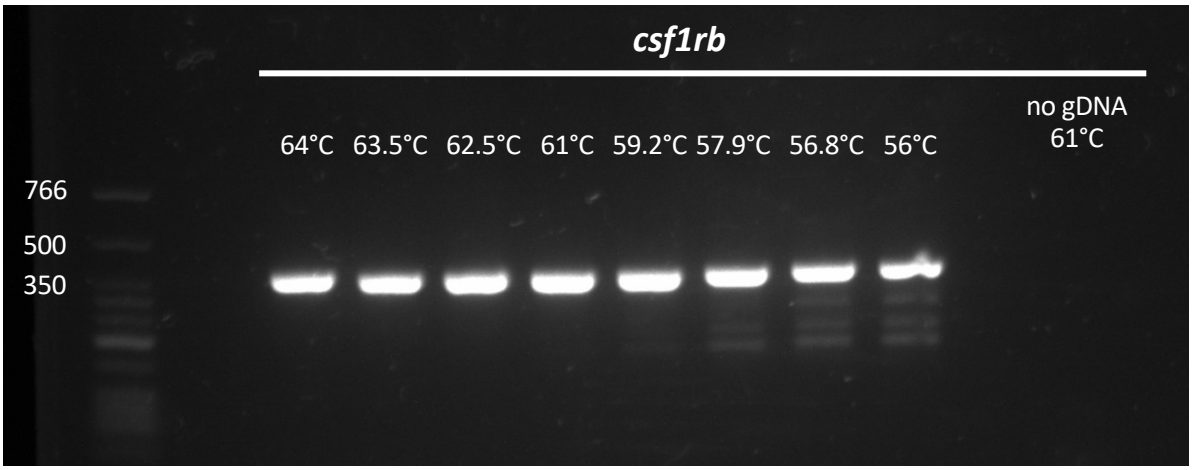

Figure 2.15. *csf1rb* primer gradient.

Following PCR amplification, 0.5µl of *MspI* was added to 4µl of PCR product and incubated for 1–2 hours at 37°C. The resulting digest was run on a 3% agarose TAE gel at 100V for 1 hour to allow identification.

Genotyping in this manner revealed 12 wild type, 15 heterozygous and 2 homozygous adults for *csf1rb*. It should be noted that several animals were culled prior to genotyping due to spine abnormalities, difficulty swimming or other sickness phenotypes, while others failed to produce viable offspring – all of which have been previously reported in *csf1r*^{DM} fish. Hence, the ratios of identified parents suggest many of these culled animals are likely to have been double mutants. Unfortunately, the homozygous adults identified by these crosses were also too sick to breed and were culled. Therefore, transplant experiments were performed on the offspring of *csf1rb*$^{+/-}$ parents, which were bleached before leaving quarantine (as described above) and raised in the standard Bateson Centre aquaria thereafter.

To investigate the engraftment of transplanted cells in animals of various *csf1rb* genotypes, transplantation was performed as described in section 2.2.3. Successfully transplanted larvae were raised and culled to obtain brain tissue for clearing at relevant intervals, as described in section 2.2.3.3. At the time of culling, a fin clip was taken to allow genotyping of each individual (workflow summarised in Figure 2.16). Briefly, a sharp razor was used to remove a small section of the caudal fin after terminal anaesthesia of the fish and placed into 90µl sodium hydroxide (50mM). As with embryonic samples, fin tissue was then heated to 95°C for 25 minutes, before the addition of 10µl Tris HCl (1M, pH 8). This gDNA was then subjected to PCR and digest, as described above.

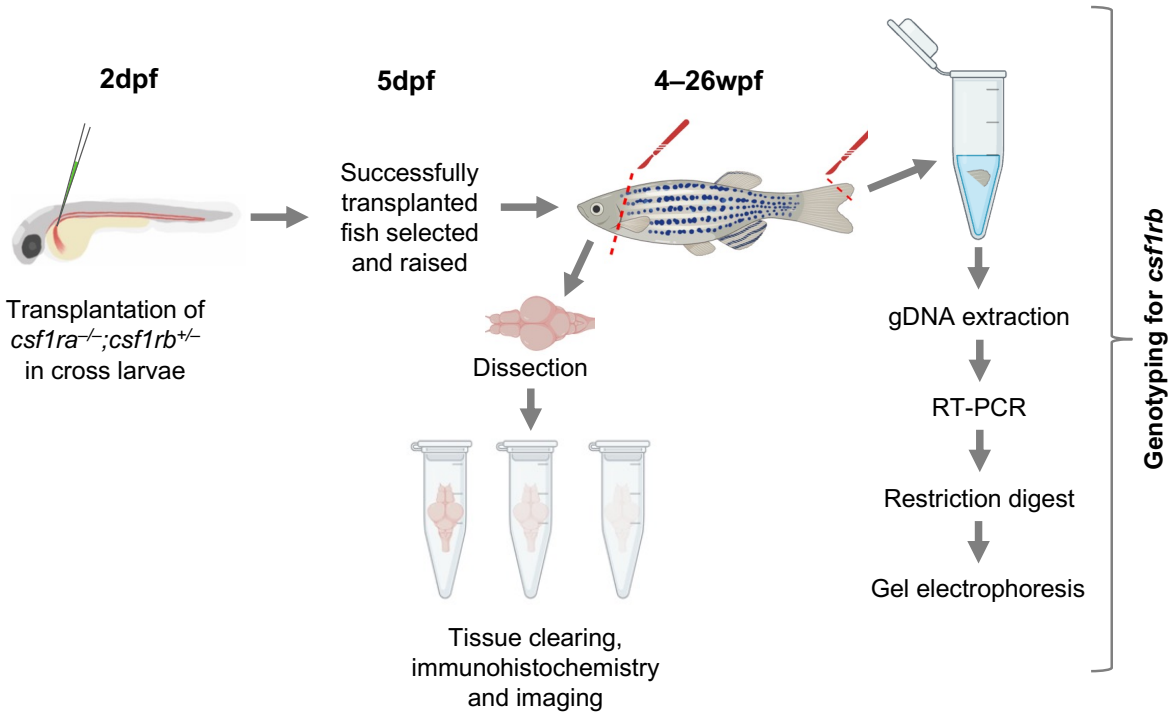

Figure 2.16. *csf1r*^{DM} transplantation and genotyping workflow

2.2.4 Chapter 5 methods

2.2.4.1 Assessment of transplanted cell engraftment in rnaset2^{sh532} mutants

To assess whether transplanted cell engraftment was affected by microglia-depletion in *rnaset2^{sh532}* embryos, 2dpf mutants and wild-type siblings – either *irf8* or scrambled crRNA-injected – were transplanted as per section 2.2.2.4.

Due to the small diameter of the microinjection needle and the tendency of cells to clump while sitting in the needle holder, the number of cells injected with each nanolitre can vary throughout the course of transplantation – with particularly high numbers of cells transplanted at the start and end of the needle. Thus, in order to ensure each group collectively received a comparable number of cells, 10 embryos from each condition were transplanted and transferred into one well of a 6-well plate, before moving onto the other groups sequentially (see Figure 2.17). This alternating order was repeated throughout the course of transplantation, until no cells remained in the needle. For each transplant, a different group was chosen to be the first to be transplanted, to account for any overall order effects. As such, this alternating approach should minimise the effects of any periods of time where the needle was delivering an unusually high or low number of cells.

Following transplantation, animals were raised into 5dpf in 6-well plates, at which point embryos were sedated in 4.2% tricaine, and the number of GFP-expressing cells within the brain was manually quantified using the Zeiss Axioscope.

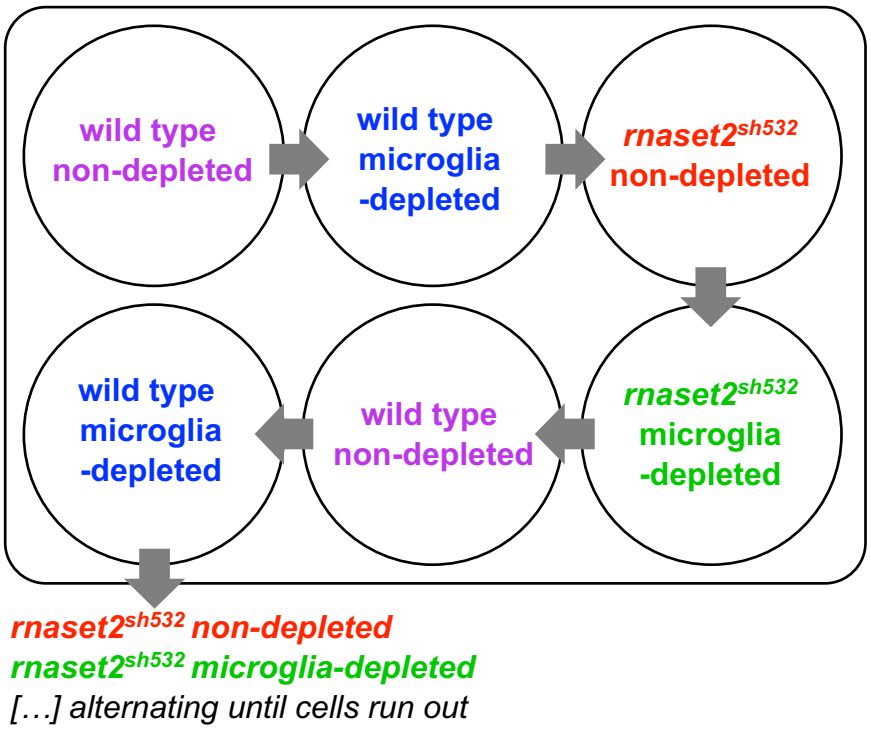

Figure 2.17. Assessment of transplanted cell engraftment efficiency.
To assess efficiency of engraftment while minimising the effect of cell clumping within the needle, ten embryos from each experimental group were injected at a time. Embryos were placed into a 6-well plate, and experimental group alternated until no cells remained in the needle.

2.2.4.2 Raising successfully transplanted embryos

Following transplantation, embryos were screened at 5dpf to confirm robust engraftment of transplant-derived cells. Animals with ten or more GFP-positive cells in the brain were then selected for immediate sample collection by immerse fixation (see section 2.2.1.8) or raised for further experiments, along with the appropriate experimental controls (wild type sham injection, *rnaset2* sham injection with and without microglia depletion).

Before raising, embryos were checked to ensure fully inflated swim bladders, and complete recovery from anaesthesia and screening. Animals to be raised into adulthood were then transferred to the aquarium nursery and cared for according to usual zebrafish husbandry (see section 2.1.2). Larvae selected for raising until 8dpf were transferred to fresh petri dishes containing E3 media and kept in a light cycling incubator. Media was changed daily, along with the addition of fresh food and removal of any unhealthy larvae for culling by schedule 1.

At 8dpf, larvae were then either taken forward for behavioural experiments (section 2.2.1.9) and/or culled by immerse fixation (section 2.2.1.8) or decapitation for RNA extraction (section 2.2.4.3).

2.2.4.3 RNA extraction of 8dpf transplanted larvae

To assess gene expression, larvae were selected for RNA extraction, cDNA synthesis and qPCR. In order to investigate the impact of transplantation on the brain, with minimal interference from gene expression elsewhere in the body, transplanted larvae were decapitated prior to RNA extraction. Due to the small size of the larvae and amount of tissue required to extract sufficient RNA, dissecting out the brains from each animal was deemed to be too impractical – the time required to perform such miniscule dissections on sufficient animal numbers would likely lead to substantial RNA degradation and/or contamination. As such, separation of the heads from the rest of the body was chosen as the most suitable alternative, with the caveat that these samples will include some gills, skin and skull in addition to brain tissue.

To perform the decapitations, 15 larvae per experimental group were terminally anaesthetised in concentrated tricaine, before removal of the head using a sharp razor. Incisions were performed just anterior to the swim bladder to ensure consistency in sample collection. The heads and rest of the body of each group was then collected in an RNAse-free Eppendorf tube. Trizol RNA extraction was then performed as described in section 2.2.1.1.

2.2.4.4 Whole mount TUNEL and immunohistochemistry

In order to assess the functionality of transplanted cells in *rnaset2* mutant embryos at 5dpf and 8dpf, TUNEL staining (to visualise uncleared apoptotic debris) and immunohistochemistry (to visualise expression of microglia-specific markers) were performed in parallel on the same samples.

Following screening to ensure transplanted cell engraftment and effective microglia depletion (where necessary), 5dpf and 8dpf embryos were immerse fixed as described in section 2.2.1.8.

To quantify apoptosis, we utilised the TUNEL assay – a standard protocol in the assessment of controlled cell death – using the commercially available ApopTag® Red In Situ Apoptosis Detection Kit (Sigma, S7165). Briefly, embryos were incubated with proteinase K (20µg/ml) for 2 hours at room temperature for 5dpf embryos, and 37ºC for 8dpf embryos, in order to permeabilise the tissue. Embryos were then fixed for a further 20 minutes in 4% PFA at room temperature before being placed at -20°C in 1:2 acetone:ethanol for 7 minutes. Following incubation at 37°C with 50µl equilibration buffer for 1 hour, the reaction solution (16µl TdT enzyme and 30µl reaction buffer; Apoptag Kit) was added to the embryos—again, incubating at 37°C for 90 minutes. Embryos were then placed in 200µl stop buffer (Apoptag kit) for 2 hours at 37°C, before placing in antibody and blocking solution (62µl anti-Dig Rhodamine or Fluorescein [depending on sample] and 68µl blocking solution) overnight at 4°C. The following morning, embryos were again fixed in PFA for 30 minutes at room temperature. All liquid was removed and embryos thoroughly rinsed PBST between each stage (5 minute washes at room temperature, repeated three to four times as needed).

Following completion of the TUNEL, immunohistochemistry was performed as described in section 2.2.1.9, with the exception of the proteinase K digestion and PFA fixation steps, as these were already performed within the TUNEL protocol. For GFP/4C4 co-localisation experiments, primary antibodies were used at following concentrations: anti-4C4 mouse antibodies at 1:100 (produced as per section 2.2.2.5), and anti-GFP chicken antibodies at 1:500.

Following staining, embryos were embedded in low melting point agarose for imaging. Samples were imaged with the Perkin Elmer Spinning Disk at 10x magnification (100µm Z-stack, 50 slices), or the Nikon W1 Spinning Disk at 20x magnification (100µm Z-stack, 50 slices).

2.2.4.5 Zebrafish-to-zebrafish immune cell transplantation

Immune cell transplantation was performed as optimised in section 2.2.3.

2.2.4.6 qRT-PCR of antiviral markers

qPCR of antiviral markers was performed using the protocol listed in section 0, using primers for *isg15*, *mxa*, *il1β*, and *ifnΦ1* listed in

Table 2.1.

2.2.4.7 Tissue clearing and immunohistochemistry

Tissue clearing and immunohistochemistry of juvenile and adult brains was performed as optimised in section 2.2.3.3.

2.2.4.8 Quantification of myelin

Quantification of myelin transcripts was performed by qPCR as detailed in 2.2.2.1.

2.2.4.9 RNA sequencing

2.2.4.9.1 Sample collection, RNA extraction and clean-up

For RNA sequencing, 4wpf transplanted *rnaset2* mutants and sham controls were culled and brains dissected as described in section 2.2.1.1. Dissected brains were placed immediately into liquid nitrogen to snap freeze the tissue and preserve RNA integrity for extraction at a later timepoint. RNA was then extracted using Trizol as described in section 2.2.1.2, except for the final step in which the resulting RNA pellet was dissolved in 100µl nuclease-free water (rather than 10µl) to aid column purification.

The RNeasy MinElute Cleanup Kit was used to purify RNA for sequencing. According to manufacturer's instructions, the dissolved RNA was mixed with 350µl buffer RLT (from kit) before the addition of 250µl 100% ethanol to promote binding of the RNA to a silica membrane. This mixture was then transferred to a RNeasy MinElute spin column (from kit) and centrifuged for 30 seconds at 10,000 rpm. The membrane was then washed with 350µl buffer RW1 to remove contaminants and span again 30 seconds at 10,000 rpm. On recommendation by our sequencing provider, we then added 10µl DNaseI mixed with 70µl RDD buffer to each column and incubated at room temperature for 15 minutes to remove any gDNA contamination. Following DNaseI treatment, samples were washed again in buffer RW1, then again with 500µl of buffer RPE and finally with 500µl 80% ethanol. After drying, 14µl nuclease-free water was then added to the centre of the silica membrane to elute the RNA, which was then stored at –80°C until quality control.

2.2.4.9.2 Quality control

Quality control was performed by The Genomics Laboratory at the University of York, using the Agilent BioAnalyzer 2100. Samples were first assessed for quality using the RNA Integrity Number (RIN) given by the BioAnalyzer, which measures the ratio of each ribosomal subunit along with potential degradation products to give a measure of RNA quality. Samples were also assessed by visual

inspection of the resulting electrophoretic trace, looking for two clear peaks representing the 18S- and 28S-fragments respectively – examples of accepted and rejected traces are show in

Figure 2.18. Samples with a RIN exceeding 7.0 were taken forward, and RNA concentration measured. Sample RINs and concentrations can be seen in Table 2.3.

Figure 2.18. Example RNA integrity numbers for quality control.
Electrophoretic traces from Agilent BioAnalyzer 2100 showing examples of good quality RNA **(a)**, partially degraded RNA **(b)** and poor-quality RNA **(c)**.

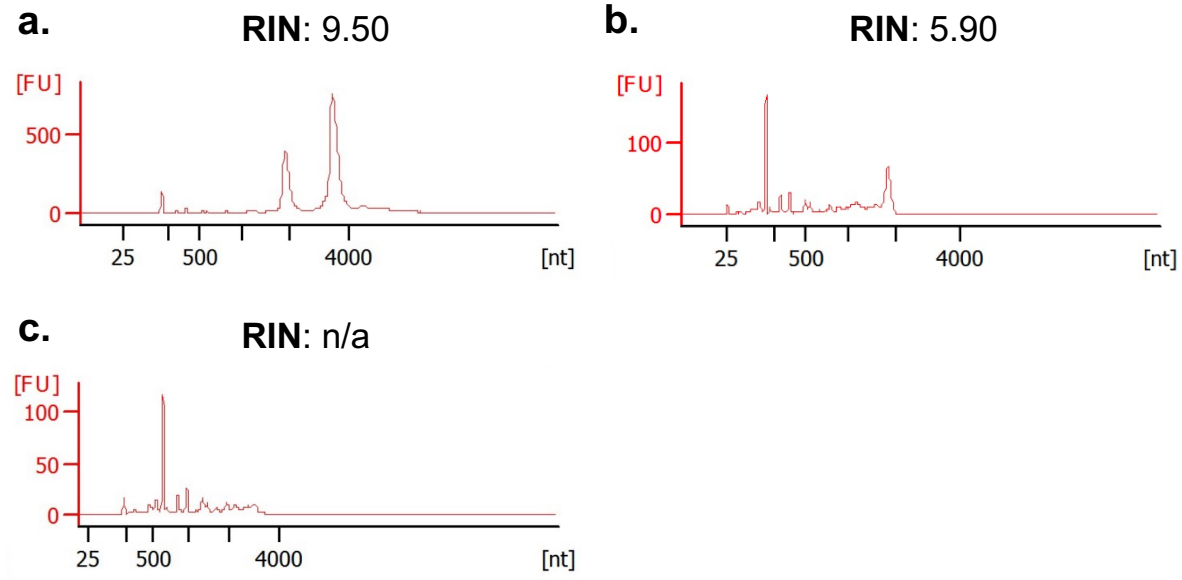

Table 2.3. Quality control report from University of York Genomics Laboratory.
Table of RNA integrity numbers (RINs) and concentrations for samples sent to the University of York for analysis. Samples highlighted in green indicate those which were taken forward for sequencing.

sample	RIN	concentration (ng/µl)
wild type non-depleted sham		
A1	9.5	93
A2	9.2	50
A3	5.9	
A4	9.8	65
A5	n/a	
A6	2.5	
A7	2.2	
A8	n/a	
A9	7.5	97
wild type microglia-depleted sham		
B1	n/a	
B2	8	78
B3	9.7	89
B4	9.6	53
B5	2.5	
B6	9.5	103
B7	2.2	
B8	2.1	
B9	2.1	
B10	n/a	
***rnaset2* non-depleted sham**		
C1	2	
C2	9.2	85
C3	9.4	85
C4	9.4	18
C5	9.4	68
rnaset2 microglia-depleted sham		
D1	n/a	
D2	8.5	81
D3	6.8	
D4	8.7	22
D5	7.8	70
D6	8.5	108
D7	7.9	160
D8	n/a	

sample	RIN	concentration (ng/µl)
***rnaset2* non-depleted transplanted (visible cells)**		
E1	2.6	
E2	n/a	
E3	9.5	44
E4	9.4	57
E5	9.3	80
***rnaset2* non-depleted transplanted** (no visible cells)		
F1	9.5	69
F2	9.7	57
F3	9.7	90
F4	8.4	90
F5	7.1	81
***rnaset2* microglia-depleted transplanted** (visible cells)		
G1	9.2	14
G2	2.6	
G3	n/a	
G4	9.3	23
G5	9.1	65
G6	n/a	
G7	2.1	
G8	9.6	75
G9	2.6	
G10	n/a	
G11	n/a	
***rnaset2* microglia-depleted transplanted** (no visible cells)		
H1	2.5	
H2	n/a	
H3	9.2	
H4	8.7	
H5	2.7	
H6	1.9	
H7	2.2	
H8	n/a	

2.2.4.9.3 Sequencing

Library preparation was performed by The Genomics Laboratory at the University of York, using the NEBNext Ultra II Directional Library prep kit for Illumina in conjunction with the NEBNext® Poly(A) mRNA Magnetic Isolation Module and unique dual indices (New England Biolabs), according to the manufacturer's instructions. Libraries were pooled at equimolar ratios and sent for paired-end 150 base sequencing at Azenta Life Sciences on an Illumina NovaSeq 6000 instrument.

2.2.4.9.4 Bioinformatics analysis

Reads (data accession number PRJNA1047321) were trimmed using Cutadapt v3.4 (Martin, 2011), then mapped to the GRCz11 genome using Spliced Transcripts Alignment to a Reference (STAR) v2.7.10b (Dobin *et al.*, 2013). Counts were generated for each gene using htseq-count v2.0 (Putri *et al.*, 2022). Differential expression analysis was performed using DESeq2 (Love, Huber and Anders, 2014) using three-way comparisons between wild type sham, *rnaset2* sham and *rnaset2* transplanted samples (with separate analyses for microglia-depleted and non-depleted groups). Pathway analysis was performed using g:Profiler (https://biit.cs.ut.ee/gprofiler/gost) (Kolberg *et al.*, 2023). For GSEA, genes were ranked according to their Wald statistic results from the differential expression analysis. The ranked list of genes was then used for a Gene Set Enrichment Analysis using the package *fgsea* v1.28.0 and the results were plotted using the package *ggplot2* v3.4.4. in R v4.3.2. Significance testing was performed using Wald tests with Benjamini-Hochberg p value correction, as previously described (Love, Huber and Anders, 2014).

2.2.4.9.5 Validation of RNA sequencing hits by qPCR

To select candidates for validation from the RNA sequencing dataset, Venny 2.1.0 (https://bioinfogp.cnb.csic.es/tools/venny/) was used to identify genes which were differentially regulated in both *rnaset2* sham relative to wild type sham samples and in *rnaset2* transplanted relative *rnaset2* sham samples. From this list, candidates involved in antiviral signalling (*isg15* and *cmpk2*) and macrophage function (*cd68*) were taken forward to qPCR, along with *rnaset2* as a biological control. Primers for *isg15* and *rnaset2* have been previously validated and published by our group (Hamilton *et al.*, 2020a). Published primers are available for *cmpk2* (Liu *et al.*, 2019); these were ordered along with two new primer pairs designed as per section 2.2.1.6. For *cd68*, primers were designed to span exon junctions from exons 2–4 as these exons are common across all three protein-coding transcripts for this gene.

After design, primers were optimised as per section 2.2.1.6, beginning with RT-PCR and visualisation on a 2% agarose gel. All primer pairs except *mbpb* pair 2 and *plp1a* pair 2 gave single bands of the expected size as predicted by Primer 3 and were taken forward for efficiency analysis. qRT-PCR was performed using serial dilutions of cDNA and efficiency calculated as described in section 2.2.1.6. The resulting scatter graphs and efficiency quantifications are shown in Figure 2.19. Primer pairs with efficiencies of 85–115% were selected for future experiments: *cd68* pair 1 (efficiency: 110.6%) and *cmpk2* pair 2 (efficiency: 114.2%).

To validate RNA sequencing hits, qRT-PCR was performed as per section 2.2.17 using the primers described above and cDNA synthesised by University of York Genomics Laboratory using NEBNext® Single Cell/Low Input cDNA Synthesis & Amplification Module (NEB) as per manufacturer instructions.

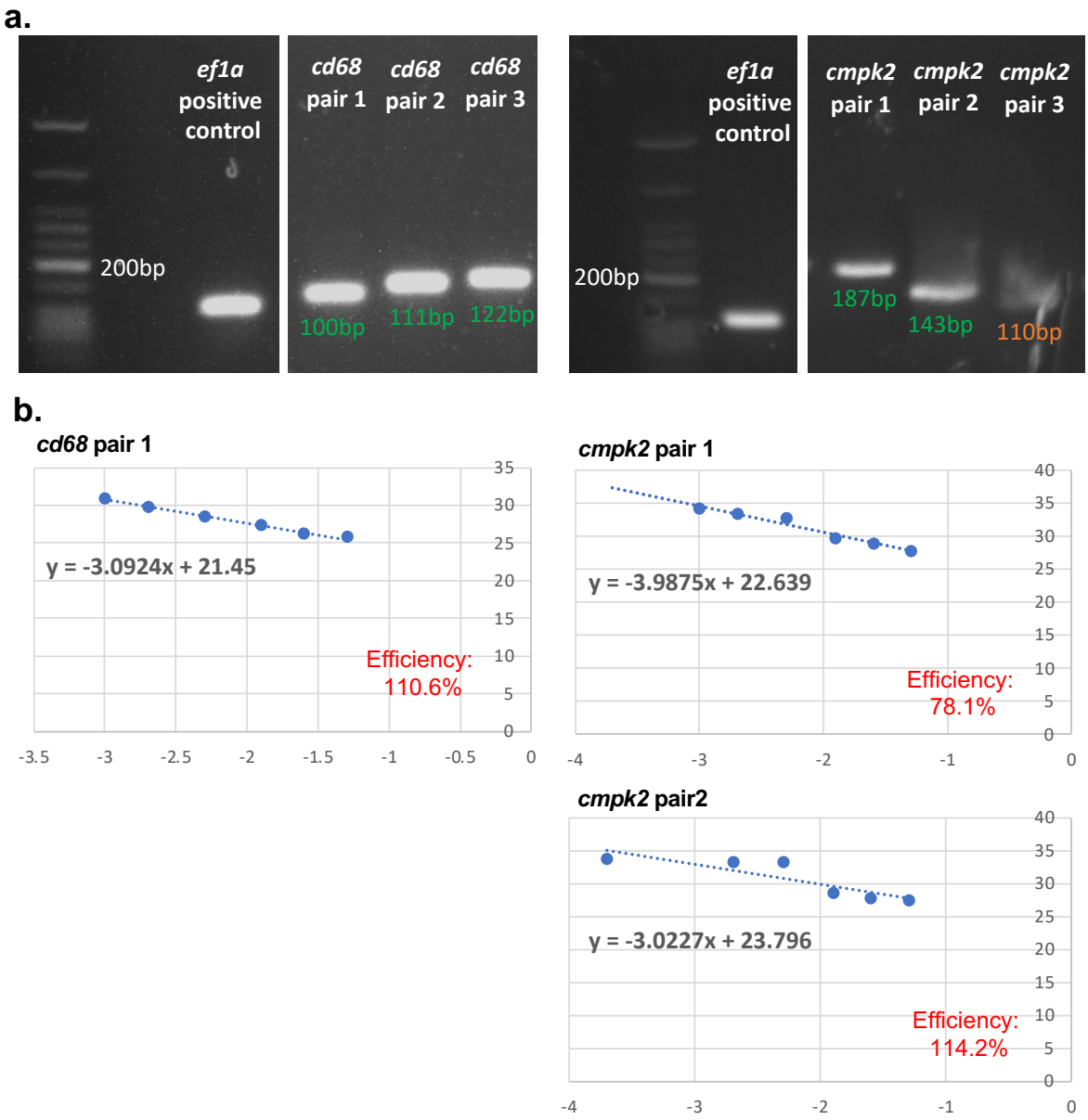

Figure 2.19. Optimization of primers for qRT-PCR validation of RNA sequencing.
(a) RT-PCR of three primer pairs for each candidate gene (*cd68* and *cmpk2*) was performed to confirm whether each primer pair yielded a single product of the expected size, with no off-target amplification. Previously published primers for *ef1α* were used as a positive control. Expected product sizes (where known) are annotated above each band, where green labels indicate bands of the expected size, and orange labels indicate unclear product sizes. Single products were identified for all three *cd68* primer pairs, and *cmpk2* pairs 1 and 2. (b) qRT-PCR was used to confirm efficiency of each primer pair in amplifying serial cDNA dilutions in an exponential manner. The resulting scatter graphs and trendlines are shown, plotting mean Cq for each cDNA dilution against the logarithmic of that dilution. Trendline gradients were used to calculate efficiency, shown in red.

Chapter 3. Broadening our understanding of *rnaset2* mutant zebrafish pathology

3.1 Introduction

As both an interferonopathy and a leukodystrophy, the presence of prominent neuroinflammation and white matter lesions is central to the pathology of RNASET2-deficient leukodystrophy (Henneke et al., 2009b; Haud et al., 2011b; Kameli et al., 2019). In addition to myelin abnormalities, patients with RNASET2-deficient leukodystrophy present with an upregulated antiviral response and particular enrichment of interferon-stimulated genes (Tonduti et al., 2016b). Research using animal models of RNASET2-deficient leukodystrophy has suggested that this elevated brain-wide immune response is among the first pathogenic changes to be observed in this disease, beginning during embryonic stages (Hamilton et al., 2020a; Kettwig et al., 2021). However, it is unclear how, if at all, this elevated interferon response interacts with the white matter pathology and behavioural symptoms seen in patients, or indeed when white matter changes first occur. A deeper understanding of the contribution of each of these factors to pathogenesis may identify potential targets for therapeutic intervention in RNASET2-deficient leukodystrophy, which are currently lacking.

3.1.1 RNASET2-linked white matter pathology

As the name suggests, patients with RNASET2-deficient leukodystrophy develop multifocal white matter lesions, alongside the presence of subcortical cysts and intracranial calcifications which can be visualised with MRI (Henneke et al., 2009b; Kameli et al., 2019; Medline Plus, 2024). However, it is unclear at which stage in pathogenesis myelin abnormalities begin to emerge, particularly in relation to the early emergence of broader neuroinflammatory phenotypes (Haud et al., 2011b; Hamilton et al., 2020a; Kettwig et al., 2021).

Due to the rarity of RNASET2-deficient leukodystrophy, no longitudinal studies have been carried out which may inform our understanding of changes in myelin lesions over time. As such, animal models are an essential tool to study white matter abnormalities as they develop – both at a macroscopic level (i.e. lesion formation) and a cellular level. As previously discussed in section 1.4.3, the *rnaset2* mutant zebrafish remains the only animal model to develop white matter lesions – with rodent models showing some changes in brain structure without observable changes to white matter integrity (Haud et al., 2011b; Sinkevicius et al., 2018; Weber et al., 2020; Kettwig et al., 2021). Alongside the broader strengths of the zebrafish as a model of neurodevelopment and myelination (discussed in section 1.4.3.3), this makes the *rnaset2* mutant zebrafish an invaluable tool to investigate the development of

myelin abnormalities in RNASET2-disorders, and whether these emerge concomitant to other disease-associated phenotypes such as the elevated antiviral response.

3.1.2 Viral triggers of RNASET2-deficient leukodystrophy

Unlike white matter pathology, neuroinflammation is a common feature across all published models of RNASET2-deficient leukodystrophy and affected patients (Haud et al., 2011b; Sinkevicius et al., 2018; Weber et al., 2020; Kettwig et al., 2021). Previous studies have demonstrated that *RNaseT2*$^{-/-}$ rats show elevated numbers of reactive astrocytes in the hippocampus, while *RNASET2*$^{-/-}$ mice present with widespread monocyte infiltration and microglia activation (Sinkevicius *et al.*, 2018; Kettwig *et al.*, 2021). Multiple published zebrafish models of RNASET2-deficient leukodystrophy also have highly abnormal microglia during early development – with a highly bloated, vacuolar morphology which may indicate an activated state (Hamilton et al., 2020a; Weber et al., 2020). Finally, both the *RNASET2*$^{-/-}$ mouse and *rnaset2*^{sh532} and *rnaset2*^{AO127} zebrafish models show significant upregulation of interferon-stimulated genes, suggesting an abnormal antiviral response may be a core feature of RNASET2-deficient pathology (Hamilton et al., 2020a; Kettwig et al., 2021).

The antiviral signature seen in RNASET2-deficient patients is so apparent that the clinical presentation of this disorder (Kameli *et al.*, 2019)mimics that of congenital cytomegalovirus (CMV) infection – a widespread, typically low-virulence herpesvirus, which can cause severe neurological morbidity in up to 25% of infected infants (Pesch *et al.*, 2021). A negative PCR analysis for cytomegalovirus (alongside a confirmed mutation in RNASET2) is therefore required to differentiate RNASET2-deficient leukodystrophy from cCMV infection (Kameli *et al.*, 2019; Pesch *et al.*, 2021). As such, the trigger of the antiviral response remains unknown in this disorder – particularly, whether this interferon response results from an external, environmental stimulus or an autoinflammatory source (Rutherford, Kasher and Hamilton, 2021).

3.1.2.1 Environmental virus exposure

Humans are continuously exposed to a barrage of low-virulence viruses throughout their life, with exposure even beginning *in utero* (Wenstrom *et al.*, 1998; Baschat *et al.*, 2003; Virgin, 2014; Xu *et al.*, 2015). A growing body of literature suggests that such viruses – which may cause an otherwise asymptomatic infection – could serve as a trigger for neuropathology that develops months or even years after viral exposure (van den Pol, 2009). This phenomenon is well-characterised in multiple sclerosis (MS), where infection with the widespread herpesvirus Epstein-Bar virus (EBV) is thought to increase risk of developing MS (Bjornevik *et al.*, 2022). Across a population of over 10 million adults,

EBV infection increased MS risk over 30-fold, despite the widespread and otherwise mild nature of EBV infection. Strikingly, markers of neuroaxonal degeneration began to increase shortly after EBV infection, suggesting a potential trigger for the onset of MS pathology years before symptom presentation. As such, these findings suggest that mild or even asymptomatic infection with high prevalence pathogens is sufficient to trigger pathogenesis in this neurological disorder.

While active CMV infection must be ruled out before a diagnosis of RNASET2-deficient leukodystrophy can be made, testing for previous CMV exposure by measuring CMV immunoglobulin G (IgG) is not routinely performed (Henneke et al., 2009b; Kameli et al., 2019; Pesch et al., 2021). Similarly, assessment of previous infection with other viruses is rarely explored in patients with *RNASET2* mutations. As such, emerging literature has suggested that exposure to commonplace, low-virulence viruses may serve as a risk factor—or even a trigger—for activation of the interferon response in patients that are already genetically predisposed to interferonopathies (Rutherford, Kasher and Hamilton, 2021).

While the clinical relevance of this hypothesis to leukodystrophies remains unclear at this time, careful consideration of viral exposure may be particularly relevant to animal models of interferonopathy – particularly when considering differences between zebrafish and murine models. It has been suggested that differences in viral exposure from the laboratory environment may account – at least in part – for the discrepancy in phenotypes between mouse and zebrafish models of the same gene (Rutherford, Kasher and Hamilton, 2021). Laboratory mice live in highly sterile environments whereby water, bedding and food is delivered with minimal – if any – pathogenic exposure. In contrast, by nature of their aquatic environment, zebrafish may frequently be exposed to low level pathogens throughout their life, much like humans. Multiple RNA sequencing datasets have identified the presence of low-virulence pathogens in several zebrafish facilities across the world, capable of inducing spontaneous interferon response in otherwise asymptomatic animals (Balla *et al.*, 2020). As such, it is possible that low virulence viral exposure in humans and zebrafish alike may serve as a trigger for interferonopathy that is absent in murine models – accounting for the discrepancy in neuroinflammatory phenotypes (Rutherford, Kasher and Hamilton, 2021). Therefore, modulation of viral exposure in zebrafish models of RNASET2-deficient leukodystrophy may elucidate the role of environmental pathogens in disease progression.

3.1.2.2 Endogenous viral triggers of RNASET2-deficient leukodystrophy

In addition to environmental triggers of the antiviral cascade, endogenous stimuli can also trigger an interferon response in an autoinflammatory manner. Each of the neuroinflammatory

interferonopathies (including RNASET2-deficient leukodystrophy and Aicardi-Goutières syndrome) are caused by mutations in genes involved in restricting reverse transcription through the detection or metabolism of nucleic acids (summarised in Figure 3.1) (Henneke et al., 2009b; Crow, Shetty and Livingston, 2020; Rutherford, Kasher and Hamilton, 2021). As such, it has been hypothesised that the type I interferon response seen in these patients is driven, not by the presence of foreign viral transcripts, but by accumulation of self-derived nucleotides (Benitez-Guijarro *et al.*, 2018).

A growing body of literature has hypothesised that the source of these self-derived nucleotides which can trigger an antiviral response are endogenous retroviruses (ERVs) – relics of integrated retroviruses which have been incorporated into vertebrate genomes and are able to act as transposable elements (Lander *et al.*, 2001; Volkman and Stetson, 2014; Bourque *et al.*, 2018; Rutherford *et al.*, 2022). A minority of incorporated ERVs have retained their ability to replicate within our genomes but remain highly suppressed in healthy individuals (Maksakova, Mager and Reiss, 2008; Rowe *et al.*, 2010; Turelli *et al.*, 2014). However, when not properly suppressed, ERVs are thought to play a role in a variety of diseases – from cancers to neurodegenerative diseases (Johnston *et al.*, 2001; Mameli *et al.*, 2007; Li *et al.*, 2015; Bermejo *et al.*, 2020).

The interferonopathies are one such group of diseases where aberrant expression of ERVs has been hypothesised to act as a potential trigger of pathology, with several reverse transcriptase inhibitors being trialled in Aicardi Goutières Syndrome (Stetson *et al.*, 2008; Beck-Engeser, Eilat and Wabl, 2011; Achleitner *et al.*, 2017; Benitez-Guijarro *et al.*, 2018; Rice *et al.*, 2018; Crow, Shetty and Livingston, 2020). However, the role of ERVs in RNASET2-deficient leukodystrophy remains unclear.

As such, further research is needed to investigate the possible triggers of aberrant antiviral response in RNASET2-deficient leukodystrophy – environmental or self-derived.

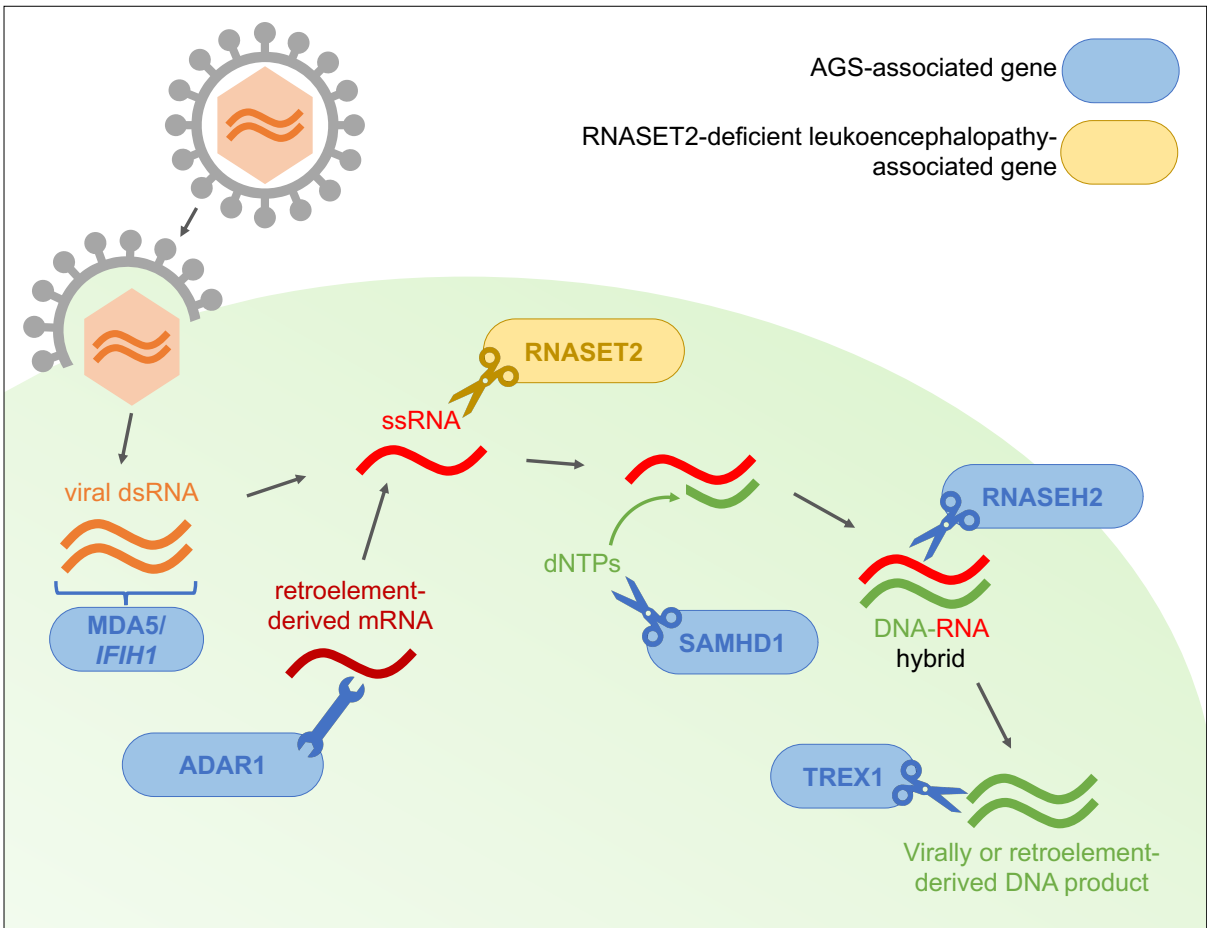

Figure 3.1. Type I interferonopathy-associated genes are involved in the sensing and metabolism of viral RNA.

Genes linked to Aicardi-Goutières Syndrome (AGS) and RNASET2-deficient leukoencephalopathy are thought to encode proteins involved in the restriction of reverse transcription of both viral- and endogenous retroelement-derived DNA. The IFIH1 gene product, MDA5, is involved in the antiviral response through the recognition of dsRNA and subsequent production of type I interferon. With interferon- inducible expression, ADAR1 acts as a suppressor of type I IFN signalling through its RNA editing activity. RNASET2 is a lysosomal hydrolase involved in RNA metabolism. SAMHD1 limits reverse transcription though degradation of deoxynucleotides necessary for complementary DNA strand formation. Among other roles in DNA synthesis and repair, RNASEH2 is thought to degrade the RNA component of DNA-RNA hybrids formed during reverse transcription. Finally, TREX1 is involved in the regulation of the interferon-stimulatory DNA response after viral infection through metabolism of virally derived nucleotides. In the absence of functioning AGS or RNASET2 proteins, accumulation of immunostimulatory deoxyribo- and ribonucleotides may trigger upregulation of type I interferon pathway. Figure published in Rutherford *et al., Front Immunol.* 2020

3.1.3 Microglia – toxic loss- or gain-of-function?

Regardless of the trigger, as the principle immune cells of the brain, the microglia play an essential role in mediating the antiviral response in the CNS – acting both as first responders to pathogenic stimuli and key orchestrators of the antiviral response of brain-resident and infiltrating immune cells (Hickman et al., 2018a; Hatton and Duncan, 2019b; O'Brien, Bennett and Bennett, 2022). In many instances, microglia have been shown to be protective in CNS viral infection – with depletion of microglia leading to higher viral burdens and more severe CNS damage (Seitz, Clarke and Tyler, 2018; Wheeler *et al.*, 2018; Sanchez *et al.*, 2019). However, just as microglia are well positioned to protect from disease, their responder role means microglia may also exacerbate – or even drive – pathology (Hickman et al., 2018a)(Hickman et al., 2018a). Microglia have been shown to drive neuronal injury in multiple neurodegenerative diseases through the production of pro-inflammatory cytokines and reactive oxygen species, as well as seeding protein aggregate formation (Coraci et al., 2002; Gold and El Khoury, 2015; Venegas et al., 2017; Hickman et al., 2018a)(Coraci et al., 2002; Gold and El Khoury, 2015; Venegas et al., 2017; Hickman et al., 2018a). In this regard, microglia are considered to adopt a disease-associated microglia (DAM) phenotype, in which they lose their protective function and serve to exacerbate pathology (Keren-Shaul et al., 2017)(Keren-Shaul et al., 2017). As such, microglia may be either protective or detrimental in instances of neuroinflammation and degeneration.

Our group have previously demonstrated that microglia are dysfunctional in RNASET2-deficient leukodystrophy – with *rnaset2* mutant microglia failing to clear developmental apoptosis and instead adopting a bloated, debris-filled morphology in a zebrafish model (see section 1.4.4) (Hamilton et al., 2020a)(Hamilton et al., 2020a). It is possible that these highly abnormal microglia could then adopt a DAM-phenotype, and further drive pathology in this model. As such, further work is needed to understand the broader impact of this bottleneck of apoptotic cell clearance in microglia.

3.2 Hypothesis and aims

Previous characterisation of *rnaset2* mutant zebrafish has revealed a variety of disease-associated phenotypes, including microglial dysfunction during embryogenesis, white matter lesions in adult animals, and upregulation of the antiviral response and behavioural impairments at multiple ages (Haud et al., 2011b; Hamilton et al., 2020a)(Haud et al., 2011b; Hamilton et al., 2020a). However, several key questions remain unanswered regarding the development of *rnaset2* mutant neuropathology. Firstly, it is unclear when myelin abnormalities begin to emerge in *rnaset2* mutants, and whether these are reflected in changes in the number of myelin-producing cells or myelin-dependent behaviours. Secondly, the principal triggers of the antiviral response – whether

environmental or endogenous – remain to be identified. Finally, it is unclear whether a failure of microglia to clear neurodevelopmental apoptotic debris reflects a loss of a key homeostatic function of these cells, or whether these cells go on to adopt a neurotoxic phenotype. Addressing these unanswered questions is not only essential to increase our understanding of *rnaset2* pathogenesis, but also to identify areas for therapeutic development and establish assays which can measure the efficacy of such interventions.

As such, the overarching aim of this chapter is to broaden our understanding of *rnaset2* mutant pathology, with a view to identifying targets for novel therapies and assays which may be used to assess efficacy of these potential therapeutics. Within this, I aim to:

1. **Determine the spatiotemporal abnormalities of myelination in *rnaset2* mutants.** Previous publications have revealed the presence of macroscopic white matter lesions in the brains of adult *rnaset2* mutants, visible with MRI (Haud et al., 2011b)(Haud et al., 2011b). However, research has not yet determined when these white matter abnormalities emerge in this zebrafish model, nor the cellular or transcriptomic changes which may contribute to this pathology. Given the neurodevelopmental nature of RNASET2-deficient leukodystrophy, I hypothesise that myelin abnormalities emerge in *rnaset2* mutants during embryonic stages. As such, I aim to characterise the expression of myelin-associated genes, quantify the number of myelin-producing cells and assess myelination-dependent behaviours in *rnaset2* mutants to address this hypothesis.
2. **Confirm the aberrant antiviral response in *rnaset2* mutant larvae and test potential triggers.** Published characterisation of the *rnaset2* mutant embryos has shown upregulation of genes associated with neuroinflammation from 5dpf, with particular enrichment in antiviral pathways (Hamilton et al., 2020a)(Hamilton et al., 2020a). Emerging literature has suggested that this antiviral response may be driven by aberrant response to low-virulence viral infection, and/or accumulation of self-derived nucleotides emerging from uncontrolled ERV replication in *rnaset2* mutants (Rutherford, Kasher and Hamilton, 2021)(Rutherford, Kasher and Hamilton, 2021). As such, within this aim, I will test two hypotheses: firstly, that *rnaset2* mutant antiviral response may be modulated by manipulation of pathogen exposure, and secondly, that ERV transcripts will be upregulated in *rnaset2* mutants relative to wild type animals. Establishing the potential triggers of the antiviral cascade may facilitate identification of new disease-modifying interventions.
3. **Test the role of microglia depletion on *rnaset2* mutant pathology.** Multiple publications have demonstrated that microglial abnormalities are among the most prominent pathogenic

changes observed in animal models of leukodystrophy (Haud et al., 2011b; Hamilton et al., 2020a; Weber et al., 2020; Kettwig et al., 2021)(Haud et al., 2011b; Hamilton et al., 2020a; Weber et al., 2020; Kettwig et al., 2021). However, it is still not known whether these diseased microglia drive pathogenesis by adopting a neurotoxic phenotype, or whether it is the failure of these cells to clear apoptotic debris that triggers pathology. I hypothesise that *rnaset2* pathology is driven by a loss of homeostatic function in microglia, rather than toxic gain-of-function, and therefore depletion of microglia will not be sufficient to rescue pathogenesis. To assess this hypothesis, I will test the impact of microglia depletion on the survival deficits observed in *rnaset2* mutants into adult stages. These findings may inform future directions for potential microglia-targeted interventions in this disorder.

3.3 Results

3.3.1 rnaset2 mutants show myelin abnormalities during early development

Previous literature has demonstrated the formation of white matter lesions in adult *rnaset2* zebrafish – recapitulating this key component of human neuropathology (Haud et al., 2011b)(Haud et al., 2011b). However, it is unclear when myelin abnormalities begin in this model, and how oligodendrocytes – the myelin-producing cells of the CNS – are affected in the *rnaset2* mutant. As such, I sought to investigate potential changes in the quantity and composition of myelin in *rnaset2* mutants, both in development and adulthood.

3.3.1.1 rnaset2 mutants show reduced expression of myelin-associated transcripts at 8dpf, but not during adulthood

Many proteins required for myelin composition are conserved between humans and zebrafish, including the three most abundant proteins: myelin basic protein (encoded by two zebrafish orthologues, *mbpa* and *mbpb*), myelin protein zero (encoded by *mpz*) and proteolipid protein 1a (encoded by *plp1a*) (Preston and Macklin, 2015; Siems et al., 2021)(Preston and Macklin, 2015; Siems et al., 2021). As such, I sought to investigate the expression of these genes in the *rnaset2* mutants both during development and in adulthood.

Quantification of these myelin-associated transcripts by qRT-PCR from whole body lysates at both 5- and 8dpf revealed a significant reduction of *mbpa* expression in *rnaset2* mutants. Expression of *mpz* was also significantly reduced in *rnaset2* mutants compared with wild type at 5- but not 8dpf, with a non-significant trend for reduced expression of *mbpb,* and *plp1a* across both ages (Figure 3.2).

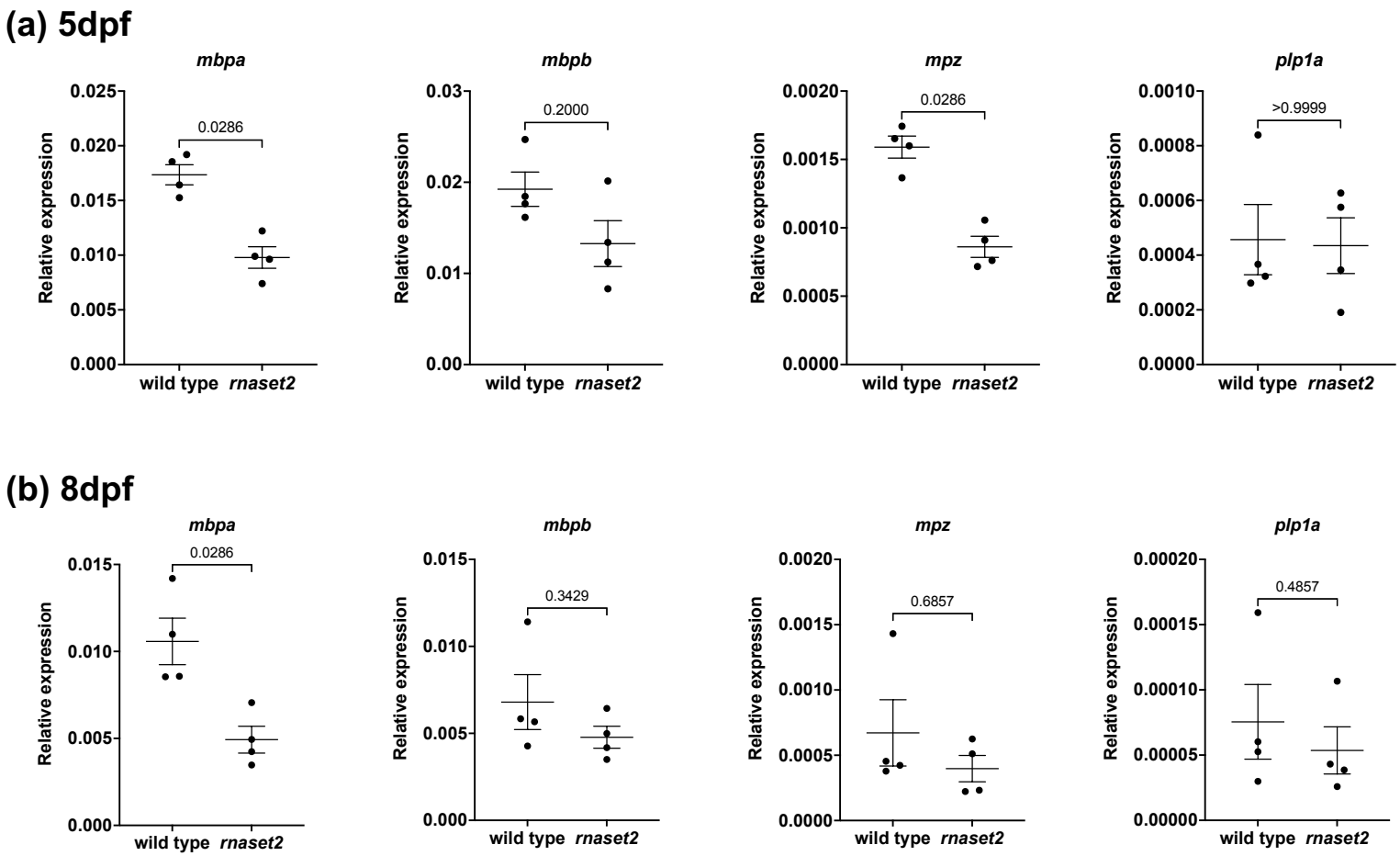

Figure 3.2. *rnaset2* mutant larvae show reduced expression of myelin-associated transcripts.
qRT-PCR reveals that *rnaset2* mutants show significantly reduced expression of *myelin basic protein a (mbpa)* at 5- **(a)** and 8dpf **(b)**, with a non-significant trend towards reduced expression of other myelin-associated genes (*myelin basic protein b [mbpb], myelin protein zero [mpz]* and *proteolipid protein 1a [plp1a]*). Mann Whitney U-test, four biological repeats, 3 technical replicates.

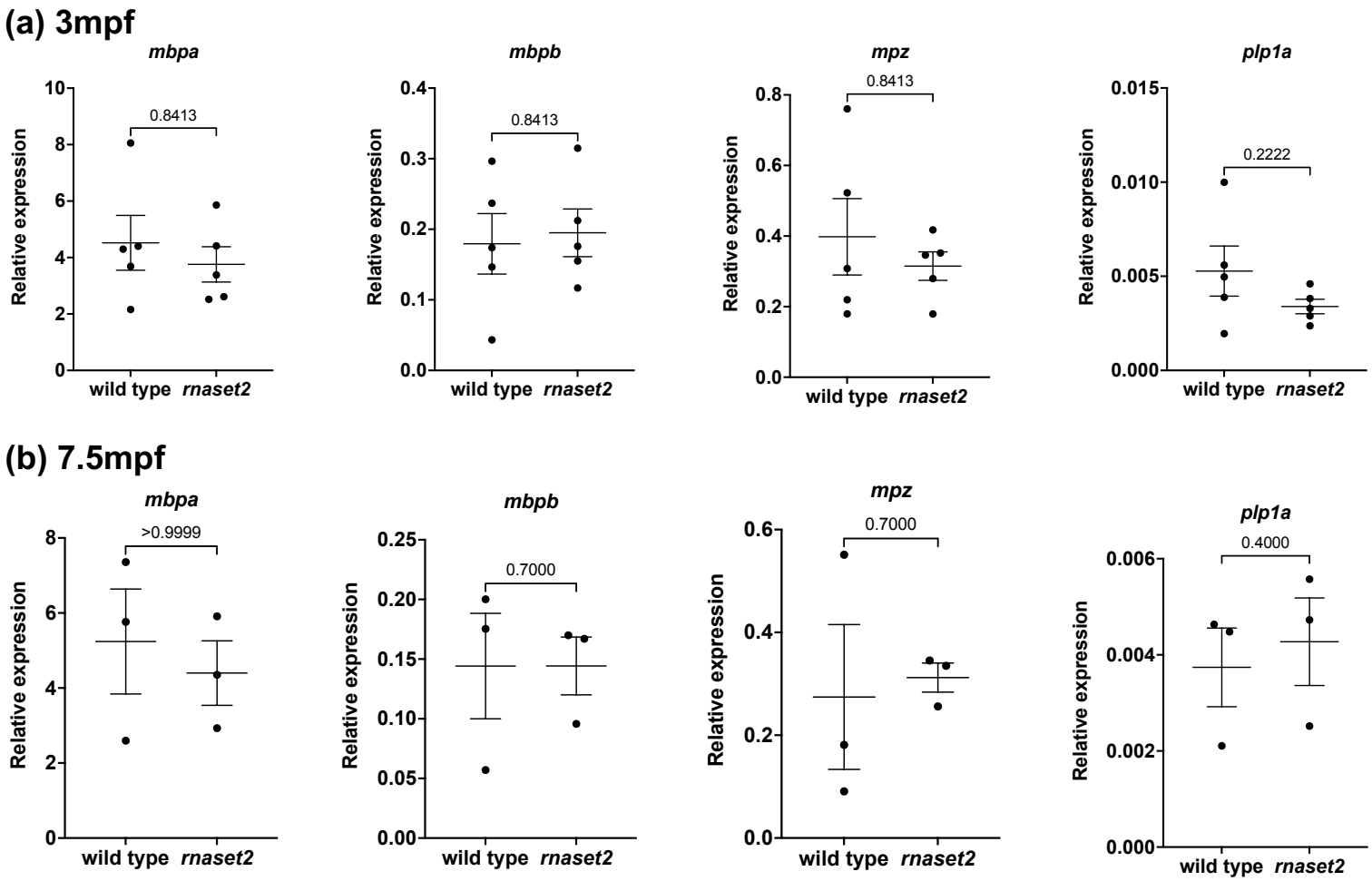

Figure 3.3. Expression of myelin-associated transcripts is unchanged in the brains of *rnaset2* mutants at 3– and 7.5 months post-fertilisation.
qRT-PCR reveals that expression of myelin-associated genes – *myelin basic protein a (mbpa) myelin basic protein b (mbpb), myelin protein zero (mpz)* and *proteolipid protein 1a (plp1a*) are not significantly different in *rnaset2* mutants at 3 months post-fertilization **(a)** or 7.5 months post-fertilization **(b)**, compared to their wild-type siblings. Mann Whitney U-test, three biological repeats, three technical replicates.

However, analysis of transcript level in adult brains revealed no significant differences in myelin-associated gene expression between *rnaset2* mutants and wild type controls at 3– or 7.5mpf (Figure 3.3) – suggesting this reduction in gene expression may be specific to larval stages.

3.3.1.2 Immunohistochemistry against myelin basic protein

In order to investigate whether this reduction in myelin-associated transcript expression in *rnaset2* larvae is accompanied by changes at a protein level, I sought to optimise an antibody against myelin basic protein to allow visualisation of myelin structures by immunohistochemistry.

No commercially available antibodies for MBP have been validated against the zebrafish proteins *mbpa* and *mbpb*. As such, I trialled a polyclonal antibody generated against e coli-derived MBP fusion protein with known reactivity against multiple species (rat, mouse and human) on zebrafish samples to investigate co-localisation with GFP signal in *Tg(mbpa:GFP)* embryos, a transgenic reporter line which drives GFP expression in myelinating oligodendrocytes expressing *mbpa* (Almeida et al., 2011)(Almeida et al., 2011). Confocal imaging revealed some weak labelling of myelin-associated structures in the brain of *Tg(mbpa:GFP)* embryos at 8dpf, with some co-localisation of mbpa:GFP positive cells in the spinal cord (Figure 3.4). However, this signal was weak and required high laser exposure, resulting in significant background noise. Additionally, not all mbpa:GFP positive cells were labelled. Together, this suggests that this antibody is unlikely to be a robust correlate of myelin structure in zebrafish larvae.

It should be noted, however, that zebrafish myelin basic protein shares little homology with mammalian orthologues. Protein alignment revealed that mbpa shares just 36.64% homology with the MBP fusion protein used to generate this antibody, while mbpb has 0% shared sequence (Figure 3.5). As such, antibodies against mammalian proteins are unlikely to show substantial cross-reactivity against zebrafish mbpa/mbpb. As such, I sought to optimise a zebrafish-specific antibody for myelin staining.

While not commercially available, zebrafish-specific antibodies have been generated by other groups and published (Kucenas et al., 2009)(Kucenas et al., 2009). However, these have been used on tissue sections and not whole mount samples. Immunohistochemistry with a previously published zebrafish-specific anti-mbpa antibody revealed no co-localisation with *Tg(mbpa:GFP)* signal in either the tail or brain (Figure 3.6).

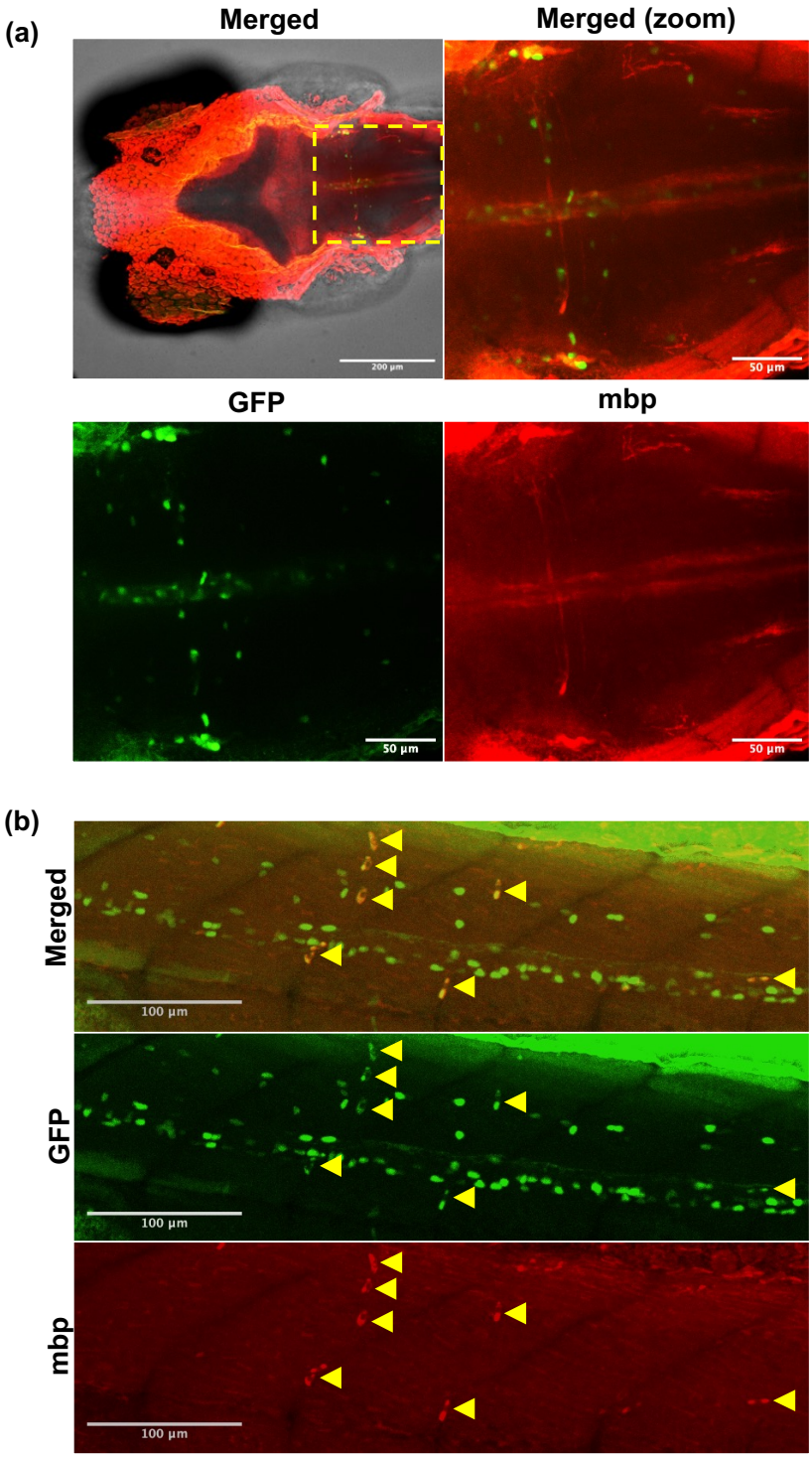

Figure 3.4. Rabbit anti-human MBP antibodies weakly label zebrafish myelin.
Imaging of 5dpf *Tg(mbpa:GFP)* embryos labelled with anti-GFP and anti-MBP antibodies revealed weak labelling of zebrafish myelin in the brain (a) and spinal cord (b). Images taken with 20x magnification. Yellow dashed line indicates region of interest. Arrow heads highlight potential cellular co-localization.

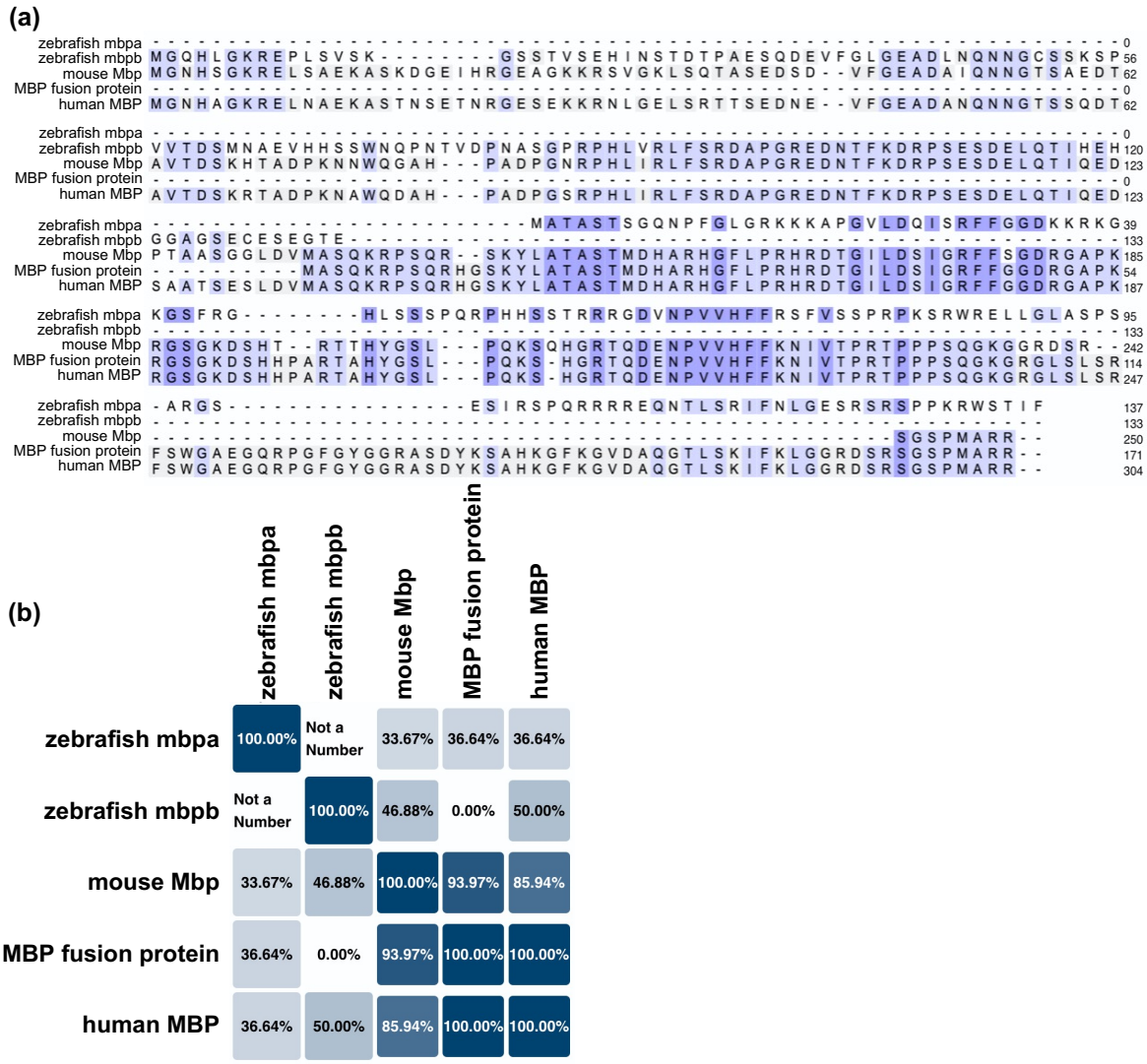

Figure 3.5. Protein alignment of myelin basic protein orthologues across species.
(a) UniProt alignment of myelin basic protein sequences across zebrafish, mouse, human and fusion protein orthologues. **(b)** Percentage identify matrix showing similarity between protein sequences across species. “Not a number” result indicates no overlap of mbpa and mbpb in the current alignment.

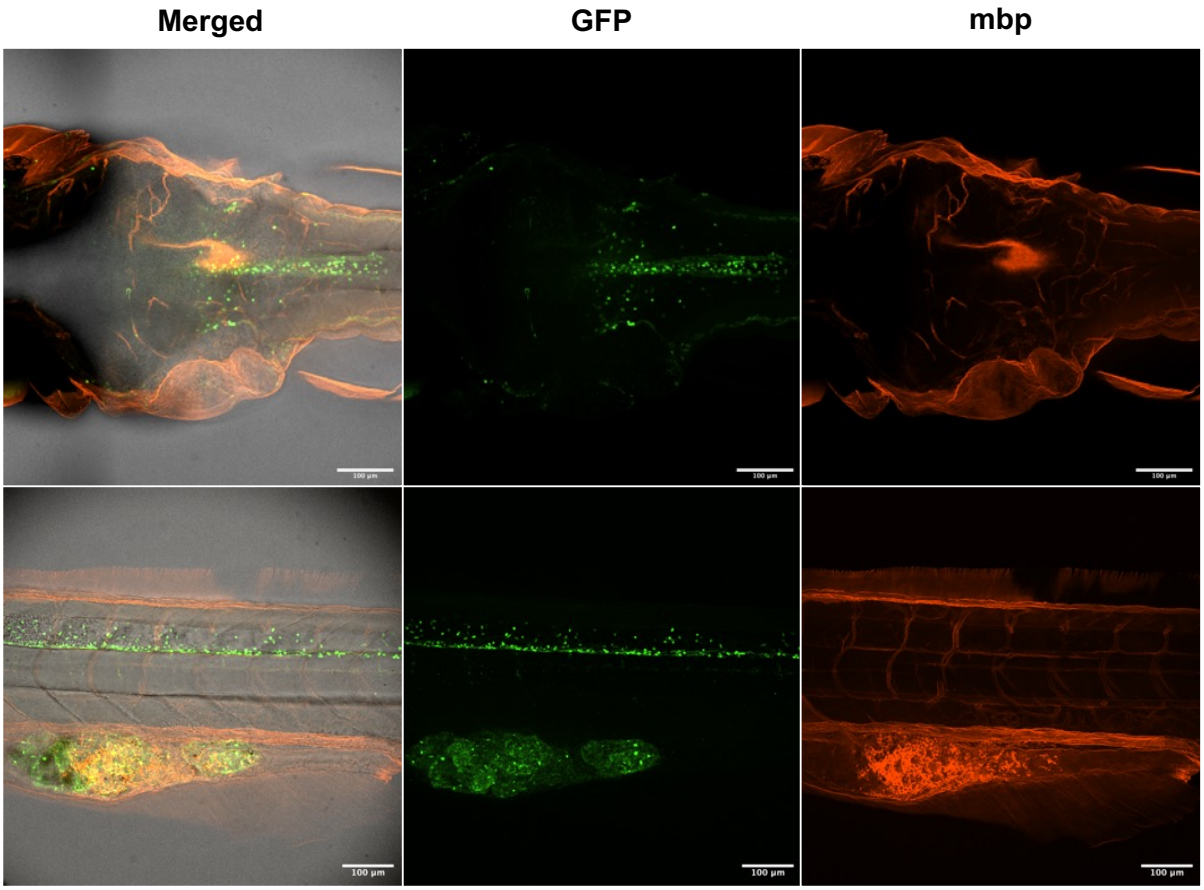

Figure 3.6. Rabbit anti-zebrafish mbpa antibodies do not label myelin in whole mount immunohistochemistry.
Imaging of 8dpf *Tg(mbpa:GFP)* embryos labelled with anti-GFP and anti-mbpa antibodies revealed no labelling of zebrafish myelin in the brain **(a)** and spinal cord **(b)**. Images taken with 20x magnification.

Imaging did not yield labelling of either oligodendrocytes or diffuse myelin structures. Immunohistochemistry was also repeated using multiple antigen retrieval techniques, including boiling in citrate buffer and Tris HCl, but this did not yield improved staining and drastically decreased tissue viability such that positive control antibodies could not be visualised (data not shown as tissue could not be imaged). As such, this antibody also does not reliably label myelin in whole mount zebrafish samples and is unlikely to be useful in assessing myelin structure of *rnaset2* embryos.

3.3.1.3 Oligodendrocyte number is altered in rnaset2 larvae

In lieu of an antibody to detect levels of myelin basic protein, I sought to investigate whether the reduction in myelin-associated transcript expression in *rnaset2* larvae (described in section 3.2.1.1) is accompanied by cellular changes by quantifying the number of oligodendrocytes using the transgenic reporter line Tg(*mbpa:GFP)* (Almeida et al., 2011)(Almeida et al., 2011).

Interestingly, at 5dpf, manual counts of oligodendrocytes in transgenic *rnaset2* embryos were higher than wild type controls in the brain and ventral spinal cord (although, notably, not in the dorsal spinal cord) (Figure 3.7). This change did not persist to 8dpf, where *rnaset2* mutants showed fewer oligodendrocytes in the dorsal spinal cord than age-matched wild type controls, with no difference in oligodendrocyte count in the brain or ventral spinal cord (Figure 3.7). Although the number of oligodendrocytes in the brain and dorsal spinal cord significantly increased in wild type embryos from 5- to 8dpf, oligodendrocyte counts in these regions remained constant in *rnaset2* mutants. Together, these data suggest that oligodendrocyte numbers are abnormal in *rnaset2* mutants throughout these embryonic stages, but that this is not a simple, consistent reduction in cell number at both 5- to 8dpf, as the expression of myelin-associated transcripts may suggest.

3.3.2 rnaset2 mutants show altered locomotion behaviour during larval and juvenile ages

After finding abnormal levels of myelin transcripts, alongside changes in oligodendrocyte number, in *rnaset2* mutants, I sought to investigate the functional consequences of altered myelin – alongside prominent neuroinflammation – on behavioural output. As the primary function of myelin is to increase the speed and efficiency of action potential conduction, a lack of ordered myelin can lead to sensorimotor impairments (Waxman, 1980)(Waxman, 1980). Motor impairments have already been observed in *rnaset2* mutant zebrafish – both in adulthood and to a small but significant extent in larval stages (Hamilton et al., 2020a)(Hamilton et al., 2020a). As such, we first sought to investigate behavioural indicators of simple sensorimotor function in the larval *rnaset2* mutants.

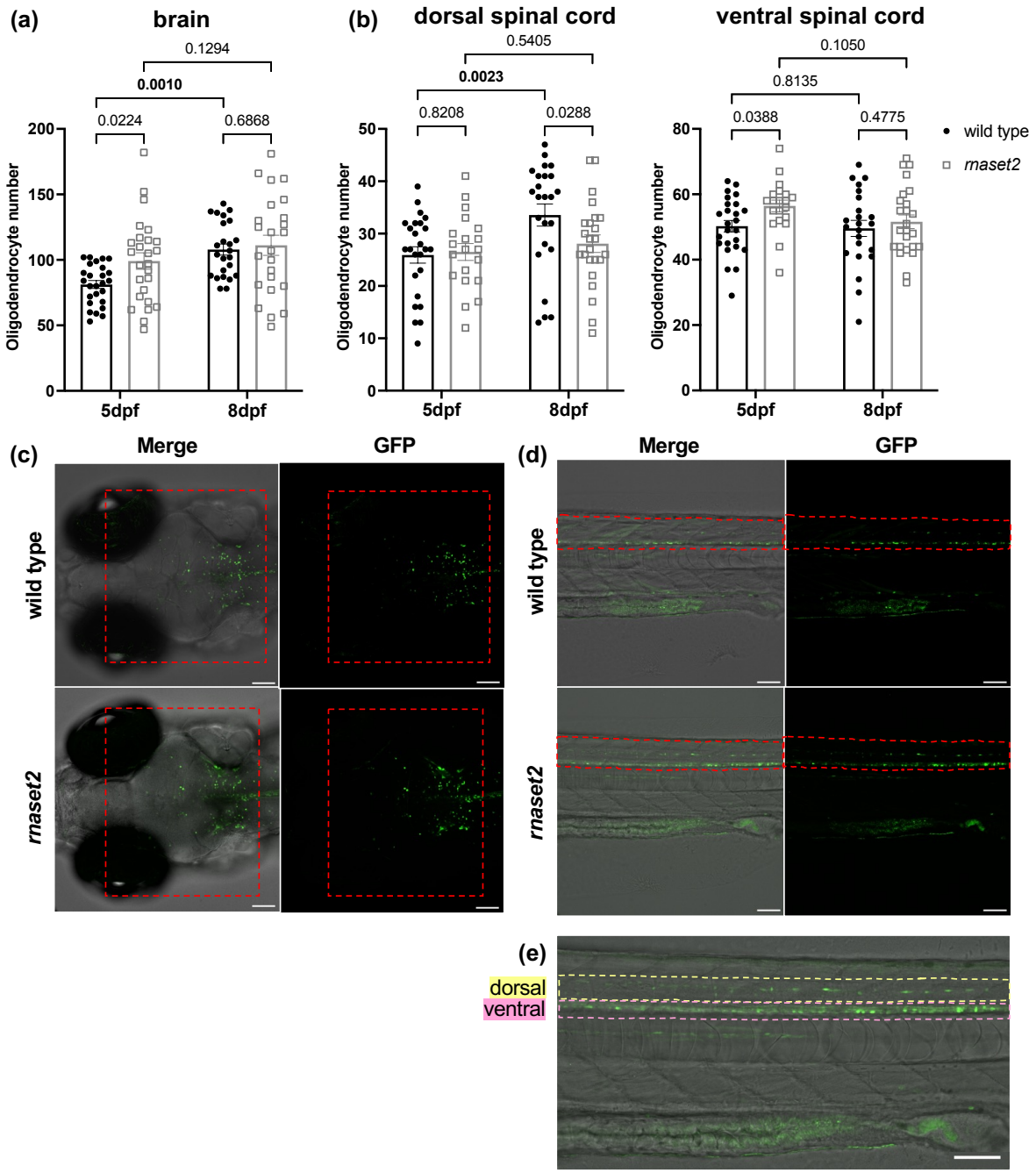

Figure 3.7. Oligodendrocyte count is abnormal in *rnaset2* mutants at 5- and 8dpf.
a, b. Manual quantification of GFP-positive cells in the brains (a) and spinal cord (b) of *Tg(mbpa:GFP)* wild type and *rnaset2* larvae at 5- and 8dpf. Two-way ANOVA with Fisher's LSD test. Bold p values indicate those below significance threshold of 0.0125. **c, d.** Representative images of the brains (c) and spinal cord (d) of *Tg(mbpa:GFP)* wild type and *rnaset2* siblings. Red dotted line indicates region of interest. **e.** Schematic depicting regions identified as dorsal or ventral spinal cord. Scale bar represents 100µm. Three biological replicates, n=24–26 per group. Quantification was performed by SSC student Toby Thomas, under the supervision of Holly Rutherford. Imaging was performed by Holly Rutherford.

3.3.2.1 rnaset2 mutants display reduced free-swimming, but normal exploratory, behaviour

To further understand the reduced locomotive phenotype seen in *rnaset2* mutant larvae at 5dpf, the same assay was repeated on 8dpf embryos, after the emergence of heavily myelinated axon bundles around 7–8dpf (Brösamle and Halpern, 2002)(Brösamle and Halpern, 2002). As previously published, we found that *rnaset2* mutants were hypoactive relative to wild type controls at 8dpf, swimming reduced distances over an hour of recording (Figure 3.8a, b) (Hamilton et al., 2020a)(Hamilton et al., 2020a). This data suggests that, therefore, swimming deficits in *rnaset2* mutants are maintained until at least 8dpf.

Previous work has demonstrated that adult *rnaset2* mutants display a complex behavioural phenotype, whereby they show no gross motor impairments – swimming the same distance as wild type controls – but with prominent abnormalities in exploratory behaviour (Hamilton et al., 2020a)(Hamilton et al., 2020a). Specifically, when swimming around the rectangular tanks, adult *rnaset2* mutants show repetitive stereotyped swimming patterns restricted to a single corner, while wild type animals explore the whole area freely. In contrast, embryonic assays are typically performed in circular multi-well plates – potentially masking any corner-dwelling behaviour. As such, I repeated the free-swimming assay above using a custom square multi-well plate. Larval movements were tracked throughout the whole well, as well as within the centre-most area, to provide a readout for exploratory versus corner-dwelling behaviour. However, *rnaset2* mutant larval swimming behaviour appeared unchanged relative to wild type controls, with mutants swimming similar distances both throughout the whole well and in the innermost area (Figure 3.8 e–f). As such, the stereotyped behaviours reported in *rnaset2* mutant adults do not seem to be present in larvae at this young age.

3.3.2.2 rnaset2 mutants show abnormal startle response at 8dpf

Aside from free swimming, zebrafish embryos show a complex behavioural repertoire that can provide further insights into neurological function. One such behaviour is the acoustic-startle response whereby a sudden acoustic stimulus stimulates a high velocity movement away from the stimuli, known as a “c-bend”, followed by a burst of swimming activity which can be recorded via high-speed camera (Kimmel, Patterson and Kimmel, 1974; Zottoli et al., 1995)(Kimmel, Patterson and Kimmel, 1974; Zottoli et al., 1995). This behaviour is co-ordinated by a well-characterised pair of myelinated neurons – and so can be used as one potential readout of myelin functionality (Madden et al., 2021)(Madden et al., 2021).

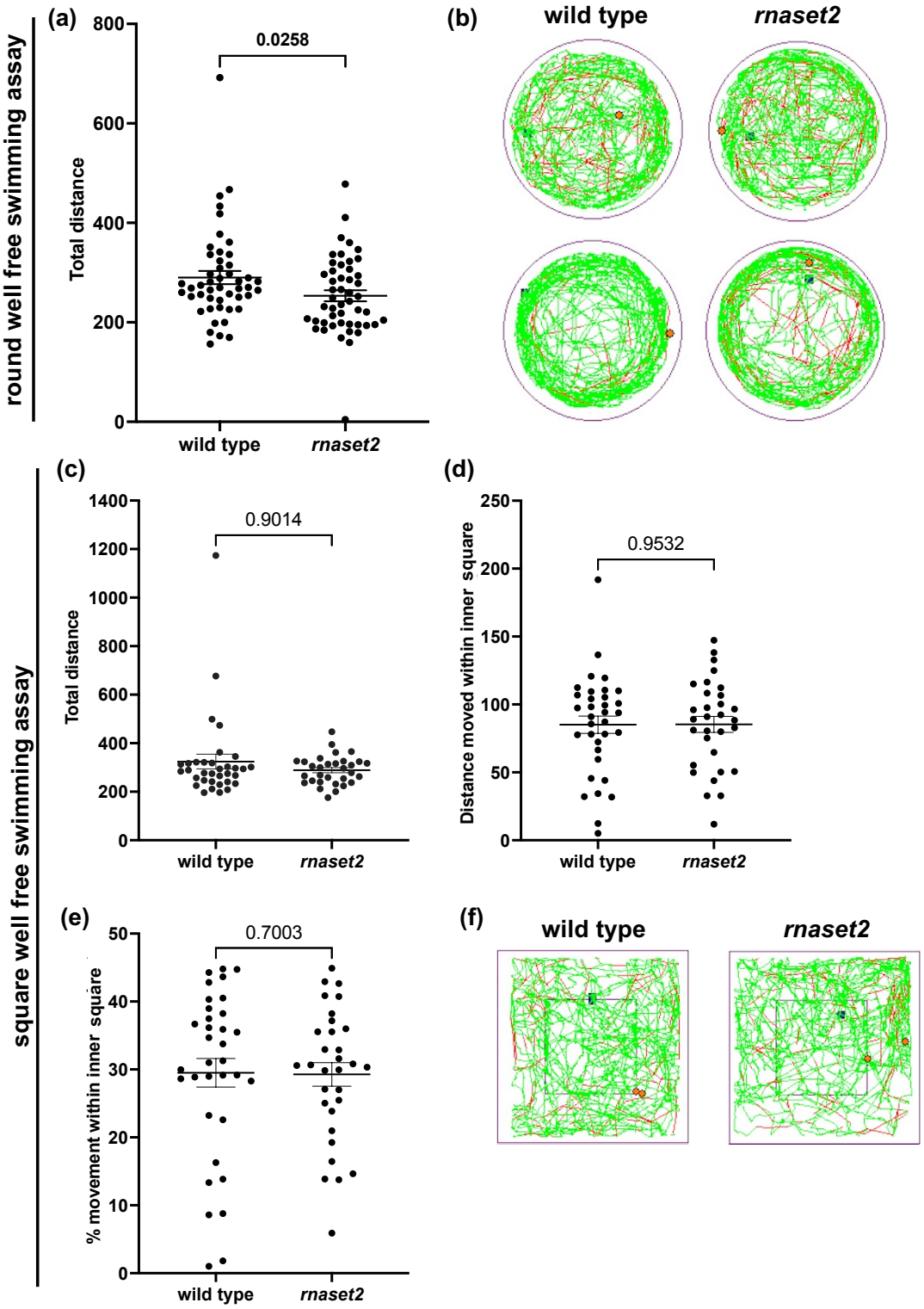

Figure 3.8. Free swimming behaviour is impaired in *rnaset2* embryos at 8dpf.
Zebrabox analysis reveals that 8dpf *rnaset2* are hypoactive relative to wild type siblings in the round well free-swimming assay **(a, b).** Four biological repeats, n=48–49. One tailed Mann Whitney U test. Swimming behaviour is unchanged in 8dpf *rnaset2* mutants in the square well swimming assays **(c–f).** Exploratory behaviour is unchanged in *rnaset2* mutants, as shown by percentage time spent in the inner square of the well (**d, e**). Three biological repeats, n=31–34. Mann Whitney U test. Representative traces of zebrafish swimming behaviour (**b, f**).

Despite the changes in myelination reported in section 3.3.1, 8dpf *rnaset2* mutants did not show a delayed startle response relative to wild type controls, as shown by no significant change in response latency after stimulation with a 1000Hz tone (Figure 3.9a,b). Interestingly, however, *rnaset2* mutants did show a significantly shorter response duration (Figure 3.9c,d). This was accompanied by an increased swimming distance (Figure 3.9 e, f) and displacement (Figure 3.9g,h). Together, these data suggest that *rnaset2* larvae have an excessive, but not delayed, startle response.

An excessive startle response across all ten trials may be indicative of reduced habituation to the sound stimulus. Zebrafish have been reported to show habituation of the startle reflex – whereby larvae show a gradual reduction in behavioural response following repeated exposure to this sensory stimulus (Rankin et al., 2009)(Rankin et al., 2009). This led me to hypothesise that impaired habituation may contribute to the increased displacement of *rnaset2* larvae across multiple trials. As such, larval displacement was re-quantified in an exploratory trial-by-trial manner, which revealed differing response dynamics between wild type and *rnaset2* embryos (Figure 3.10 a, b). While wild type animals showed a steady reduction in startle displacement from the initial trial, *rnaset2* mutants do not begin to show reduced displacement until later trials. Exploratory comparison of displacement across the first, middle (fifth) and final (tenth) trials revealed that wild type – but not *rnaset2* – larvae showed a significant reduction in displacement between trials 1 and 5. In contrast, *rnaset2* larvae showed significantly reduced displacement between trials 5 and 10, which was not seen in wild types, suggesting *rnaset2* habituation may be delayed (Figure 3.10 c). As such, it seems that the habituation dynamics of *rnaset2* mutants may be altered relative to controls during larval stages.

3.3.2.3 rnaset2 juveniles are hypoactive relative to wild type controls

Despite the present findings that *rnaset2* mutants are hypoactive in larval stages, we have previously demonstrated that *rnaset2*-deficient animals swim comparable distances to wild type controls during adulthood, instead showing an abnormal pattern of stereotyped, repetitive swimming (Hamilton et al., 2020a). However, it is unclear at which age this hypoactivity is no longer detectable in mutants.

In order to investigate this, I recorded free swimming behaviour at 4- and 14wpf. As the behavioural phenotypes of *rnaset2* mutants are unknown during juvenile ages, I performed a pilot study with five 4wpf animals per group. This revealed a reduction in the duration and distance moved in *rnaset2* juveniles, relative to wild type (Figure 3.11a, b). In order to perform full analysis, this pilot data was used to calculate the sample size required using G*Power (Figure 3.11c). To assess the difference between the two genotypes, a two-tailed t-test (or equivalent non-parametric test) was selected as

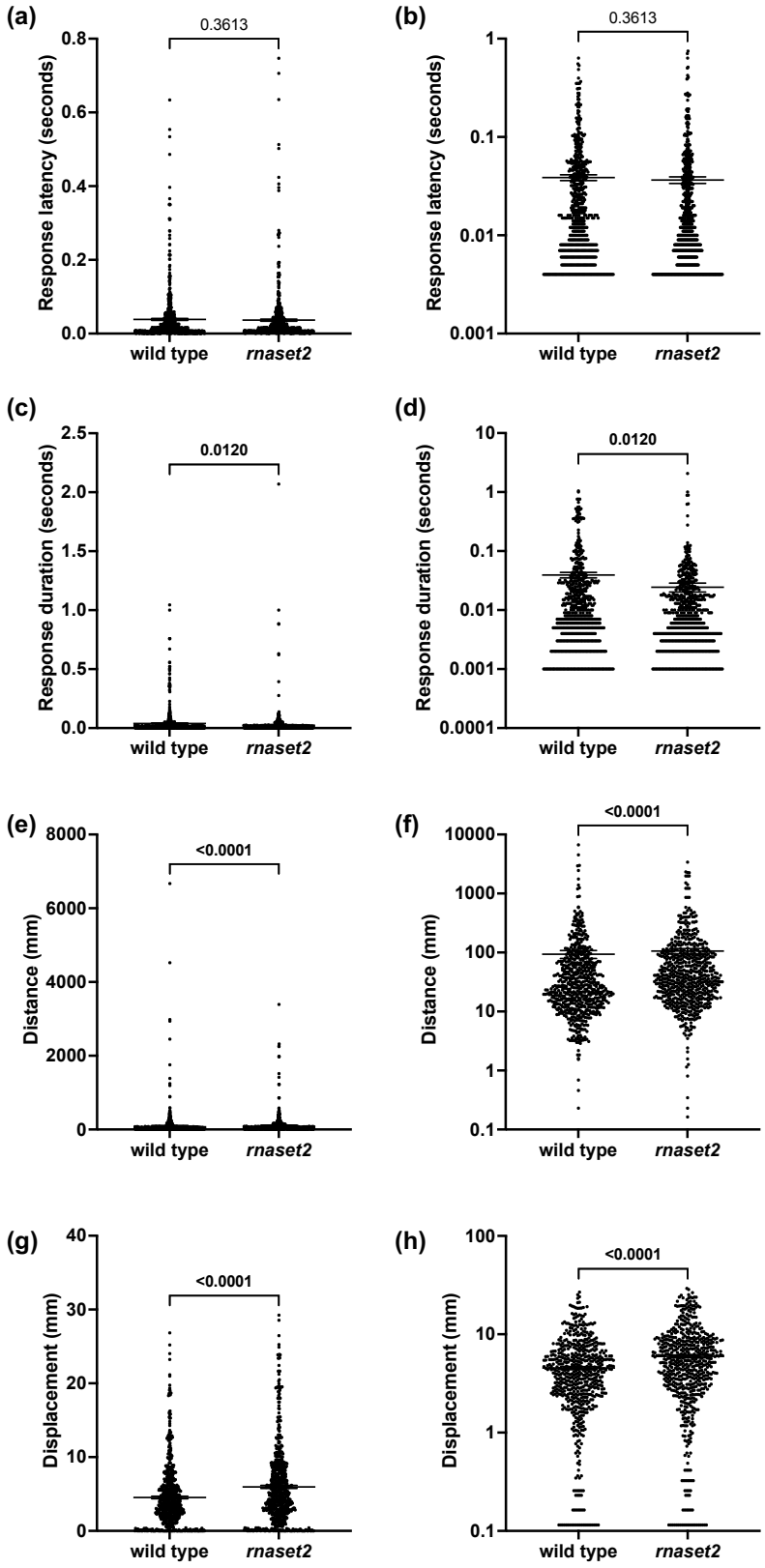

Figure 3.9. *rnaset2* mutants have abnormal startle response at 8dpf.
Fast-cam analysis reveals no significant change in *rnaset2* response latency relative to wild type at 8dpf **(a, b).** Response duration is reduced in *rnaset2* mutant embryos **(c, d),** while both distance **(e, f)** and displacement **(g, h)** are increased relative to wild type controls. Data are shown with a linear **(a, c, e, g)** and logarithmic scale **(b, d, f, h)** for clarity. Three biological repeats, n=70 per group. Each data point reflects the movements of each fish in a single trial. Mann Whitney U test.

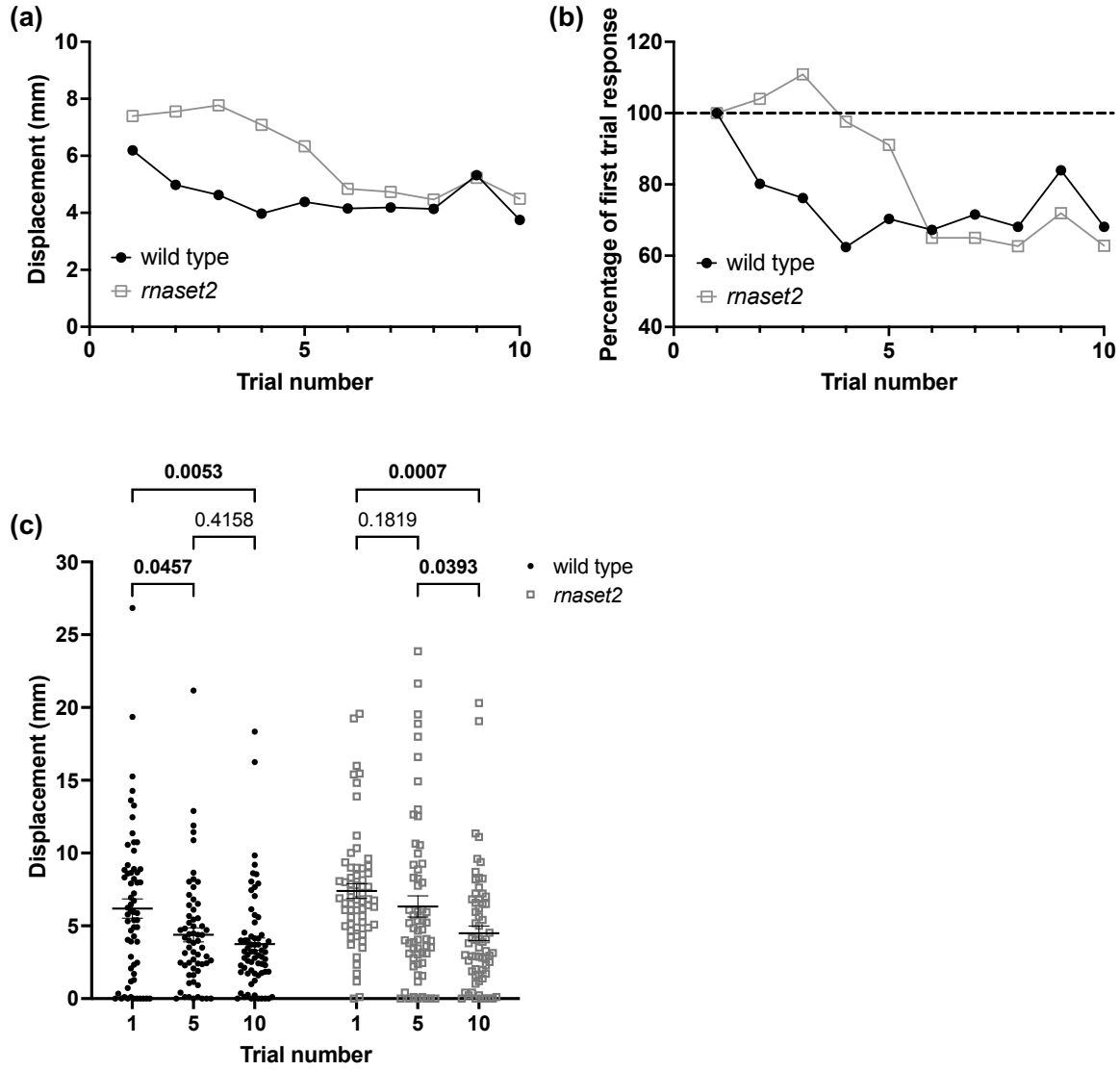

Figure 3.10. Trial-by-trial comparison of wild type and *rnaset2* 8dpf startle displacement.
a, b. Startle response of 8dpf embryos as total displacement **(a)** and percentage of first trial response **(b)** across all ten trials. Dashed line indicates 100% of first trial response **(b)**. **c**. Comparison of startle displacement across the first, fifth and final (tenth) trials trials for *rnaset2* and wild type 8dpf embryos. Two-way ANOVA with Holm-Šídák multiple comparisons. Bold values indicate p values below 0.05. Three biological repeats, n=70 per group.

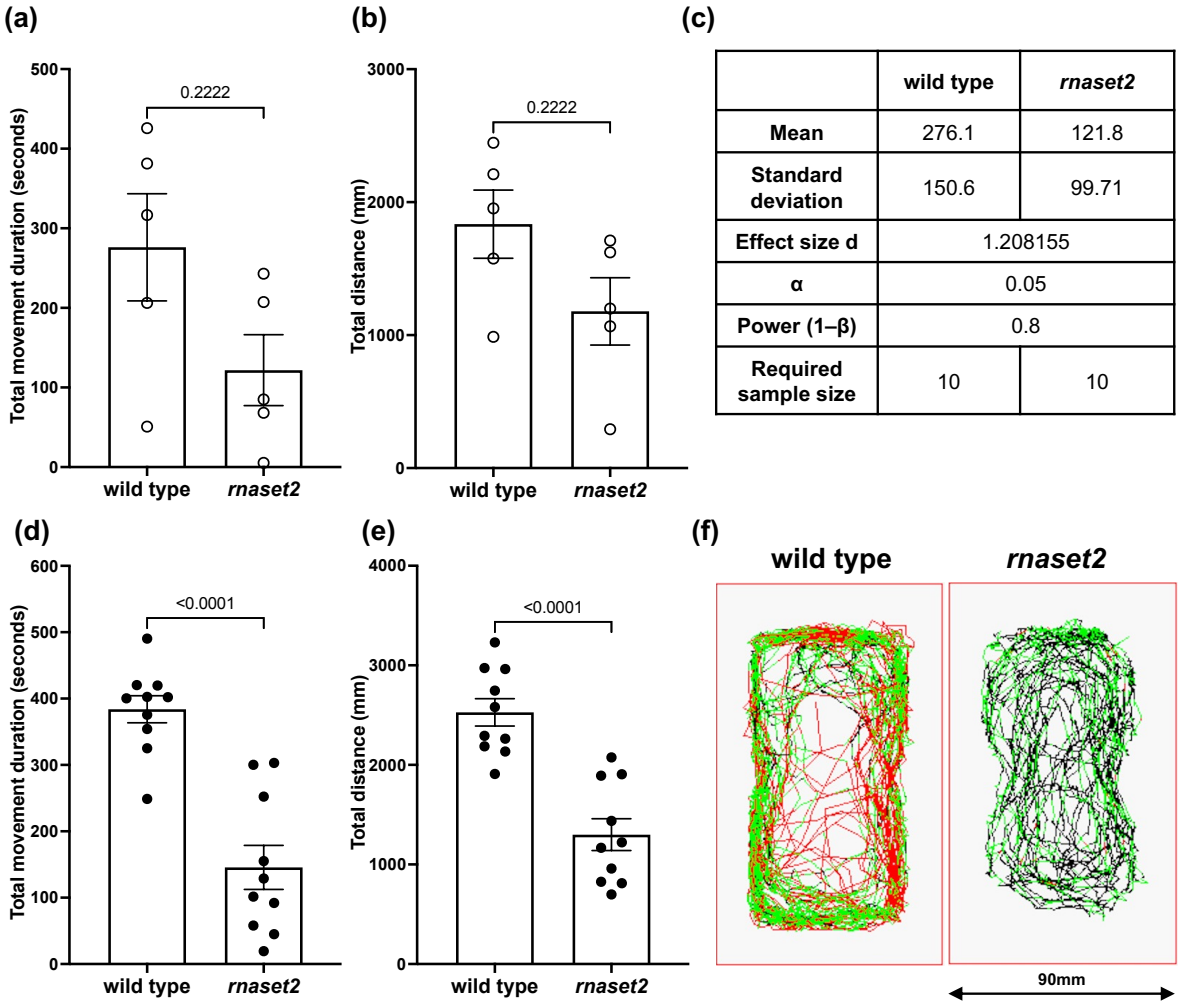

	wild type	*rnaset2*
Mean	276.1	121.8
Standard deviation	150.6	99.71
Effect size d	1.208155	
α	0.05	
Power (1–β)	0.8	
Required sample size	10	10

Figure 3.11. *rnaset2* mutant swimming activity at 4wpf.
a, b. Pilot study recording free swimming duration **(a)** and distance **(b)** of 4wpf wild type and *rnaset2* mutants. **c.** Power calculation reveals a sample size of 10 animals per group is required to detect the effect size shown in (a). **d, e.** Experimental assessment of free-swimming duration **(d)** and distance **(e)** of wild type and *rnaset2* mutants using sample sizes calculated in (c). Mann Whitney U test, 10 animals per group. **(f)** Representative images of swim trace. Scale bar represents 90mm.

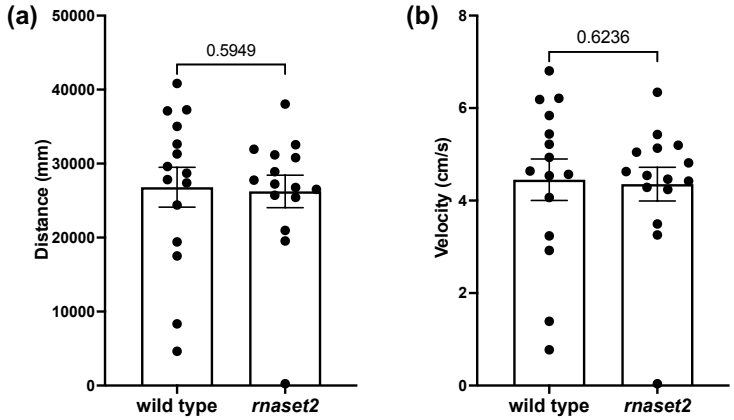

Figure 3.12. *rnaset2* mutant swimming activity at 14wpf.
Experimental assessment of free-swimming distance **(a)** and velocity **(b)** of wild type and *rnaset2* mutants. Mann Whitney U test, 15 animals per group.

the appropriate statistical test. Using the pilot data for movement duration, the anticipated effect size for this analysis was 1.21 (Cohen's d), giving a required sample size of 10 animals per group to detect this effect size (α=0.05, 1–β=0.80). As such, free swimming analysis was repeated using 10 juveniles, which confirmed a robust, significant reduction in the movement duration and distance in *rnaset2* mutants (Figure 3.11d–f), suggesting mutants remain hypoactive until at least 4wpf.

In contrast, when this assay was repeated at 14wpf, no difference in swimming behaviour was observed between wild type and *rnaset2* mutants in terms of distance or velocity (Figure 3.12).

As such, *rnaset2* mutant show a complex behavioural repertoire, including prominent hypoactivity in larval and juvenile stages. Response latency indicates these behaviours are unlikely to be driven by reduced myelination alone – suggesting other circuit-level, brain-wide changes may be causing these phenotypes.

3.3.3 Environmental exposure to viruses does not modulate rnaset2 mutant antiviral response

Upregulation of the antiviral response – and particularly the type I interferon pathway – is one of the most prominent phenotypes displayed by both patients with RNASET2-deficient leukodystrophy and *rnaset2* zebrafish mutants (Henneke et al., 2009b; Hamilton et al., 2020a; Rutherford, Kasher and Hamilton, 2021). A growing body of literature has suggested that asymptomatic infection with low virulence pathogens may act as the principal driver for this antiviral response, due to the increased susceptibility of individuals with mutations in *RNASET2* and other inferonopathy-linked genes to this aberrant upregulation of interferon pathways (Wenstrom *et al.*, 1998; Baschat *et al.*, 2003; van den Pol, 2009; Virgin, 2014; Xu *et al.*, 2015; Balla *et al.*, 2020). As such, I sought to utilise the unique features of the zebrafish laboratory environment – namely, exposure to low levels of circulating pathogens in the aquarium water – to investigate the effect of low-virulence pathogen exposure on *rnaset2* antiviral response using a zebrafish-specific picornavirus-like pathogen known to be present in University of Sheffield aquaria – ZfPV – as a proxy for viral exposure (IDEXX BioAnalytics Health Report, unpublished).

3.3.3.1 Modulating larval environment may alter viral burden

Previous literature has demonstrated that ZfPV burden can be modulated experimentally – whereby bleaching of embryos at 1dpf and raising in sterile environments minimises viral load, while adding purified adult gut extract is able to increase viral burden (Balla *et al.*, 2020). Indeed, in our experimental set-up, sterile raising of both wild type and *rnaset2* larvae following bleaching seemed

to minimise viral burden – with no detectable levels of viral transcript in samples from these conditions (Figure 3.13). In contrast, detectable levels of ZfPV transcripts were observed sporadically in conventionally raised animals, suggesting ZfPV infection can be transmitted either from parent fish at the time of laying, or via the aquarium water itself. In order to mimic transmission from parent fish, purified gut samples were obtained by dissection of adult intestines and filtration to isolate viral particles (Balla *et al.*, 2020). The addition of this gut extract led to detectable levels of ZfPV present in previously bleached embryos, although did not seem to increase the viral burden in otherwise conventionally reared animals. Interestingly, the extent of viral burden was highly variable between animals raised in the same condition, even for those that were treated with the same samples of aquarium water and purified gut extract (see the "with gut" samples from n3, Figure 3.13). Accordingly, a two-way ANOVA revealed that microbiome treatment accounted for only 13.34% of total variation (p=0.4981). As such, it seems viral burden may be modulated – particularly by bleaching to remove viral burden – but to a highly variable extent.

3.3.3.2 rnaset2 antiviral response does not correlate with viral burden

In order to assess the impact of environmental viral exposure on antiviral gene expression, *isg15* transcript levels were assessed by qRT-PCR. This revealed a significant effect of genotype on *isg15* expression – where *rnaset2* mutants showed higher levels of *isg15* transcript across all environmental conditions compared with wild type controls (p=0.0047) (Figure 3.14). However, no significant effect of microbiome treatment was observed, with highly variable *isg15* expression between samples of the same condition (p=0.6355).

As both the observable ZfPV transcript and *isg15* expression were highly variable within each group, I hypothesised that varying levels of viral burden within each microbiome treatment may trigger the antiviral response to variable levels. As such, I sought to investigate the correlation between ZfPV burden and *isg15* expression regardless of treatment condition. In wild type samples, a significant positive correlation was observed between ZfPV burden and *isg15* expression (r=0.8969, p=0.0002), suggesting the extent of antiviral burden is dependent on exogenous viral load in wild type animals (Figure 3.14b). However, in the *rnaset2* mutants, no such significant correlation was observed (r=0.2837, p=0.3670) – suggesting the *isg15* expression was not driven solely by ZfPV burden (Figure 3.14c). As such, it seems *rnaset2* antiviral response may be independent of exogenous viral infection, suggesting a potentially endogenous trigger for this inflammatory cascade.

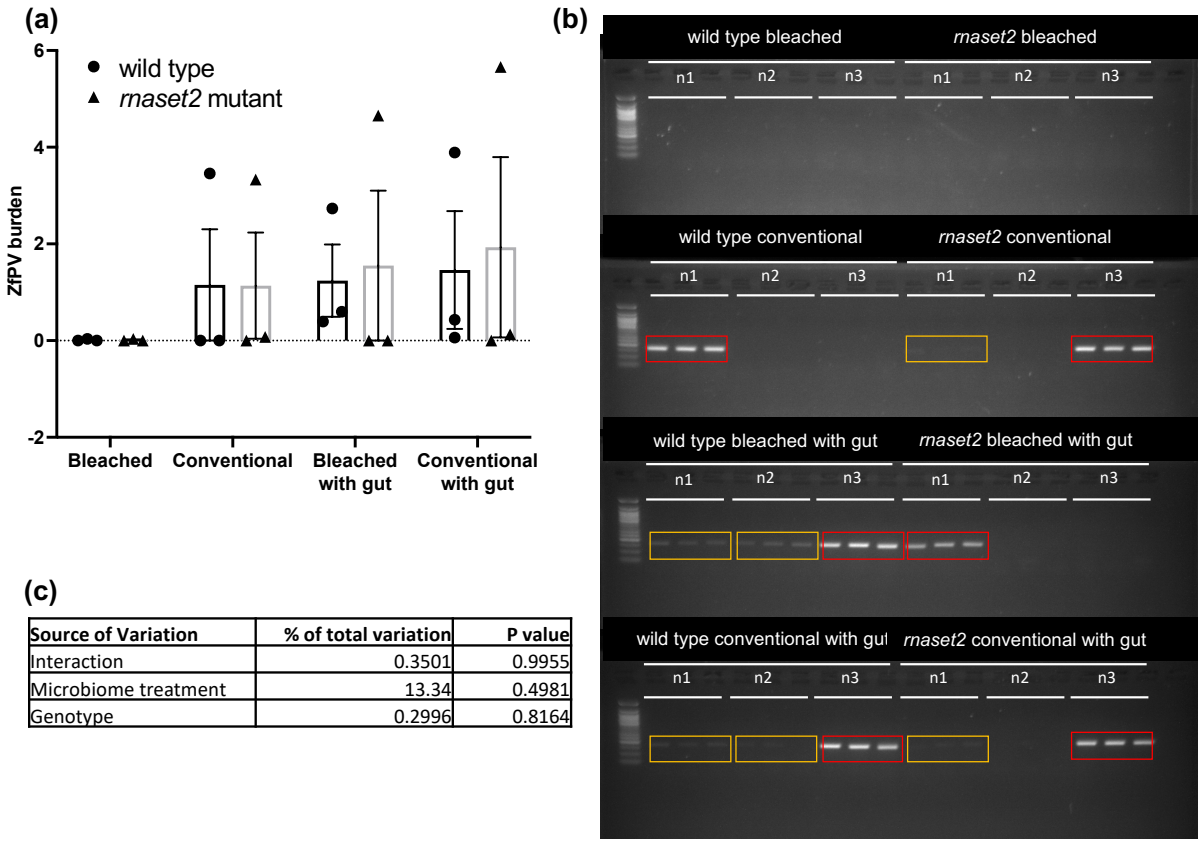

(c)

Source of Variation	% of total variation	P value
Interaction	0.3501	0.9955
Microbiome treatment	13.34	0.4981
Genotype	0.2996	0.8164

Figure 3.13. ZfPV burden may be experimentally modulated, but to a variable extent.
(a) Quantification of ZfPV burden revealed no observable viral transcript in bleached samples across either genotype. Viral transcripts were detected in all other groups, although to variable extents across repeats. ZfPV burden calculated as *ZfPV* band intensity/*ef1α* band intensity. **(b)** Complete agarose gel used to quantify ZfPV burden. Each repeat is shown with each reaction in triplicate. Red boxes indicate strong ZfPV band intensity, orange boxes indicate weak but visible band intensity. **(c)** Summary statistics from two-way ANOVA show no significant effect of microbiome treatment or genotype. 3 biological repeats, 3 technical replicates.

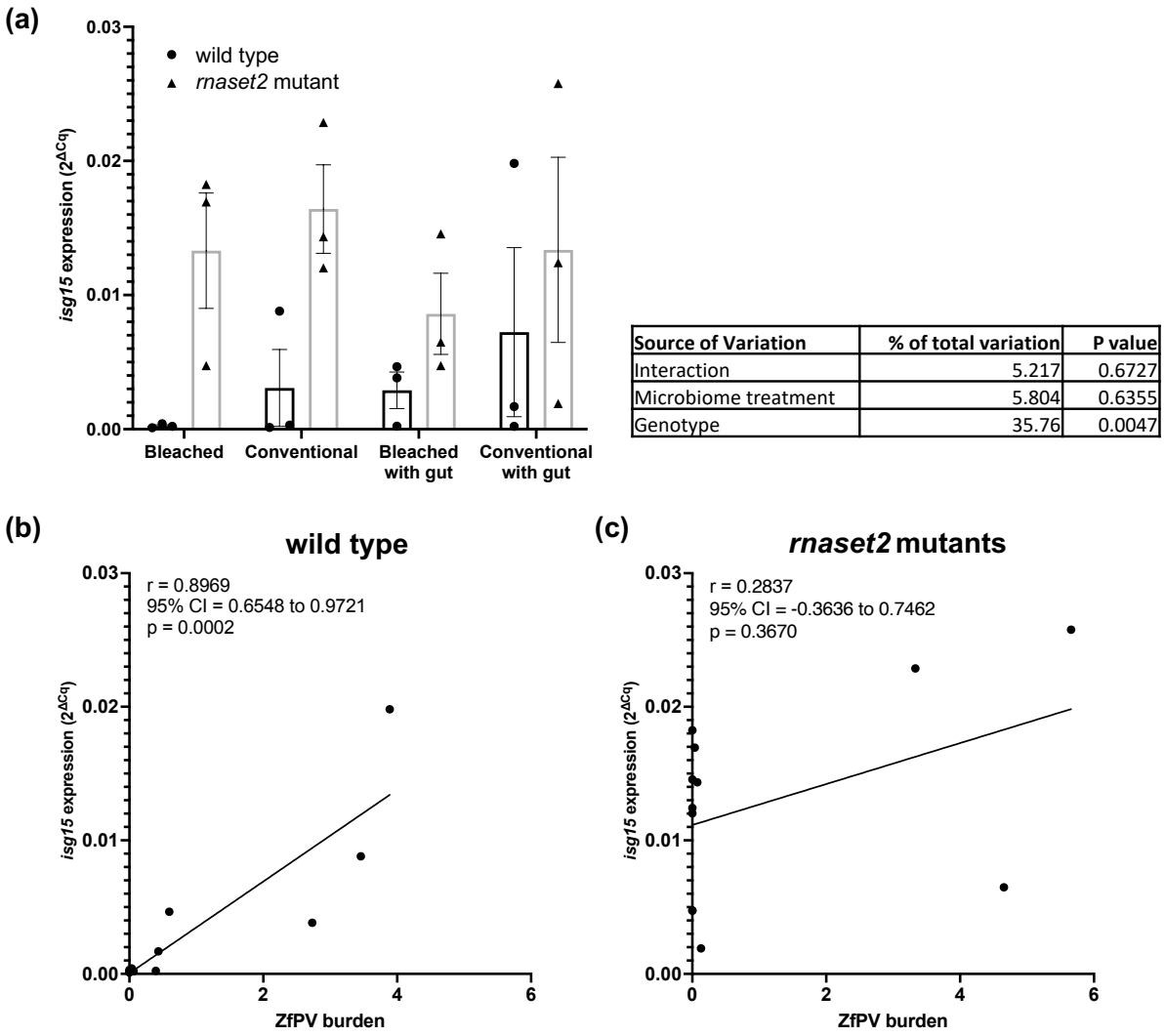

Source of Variation	% of total variation	P value
Interaction	5.217	0.6727
Microbiome treatment	5.804	0.6355
Genotype	35.76	0.0047

Figure 3.14. *rnaset2* antiviral response does not correlate with viral burden.
(a) qRT-PCR revealed a significant effect of genotype on expression of the antiviral gene *isg15* – where *rnaset2* mutants had a higher antiviral gene expression across all conditions – but no significant impact of microbiome treatment condition on *isg15* expression. Summary statistics from two-way ANOVA are displayed in the table. **(c, d)** *isg15* expression is significantly positively correlated with ZfPV burden in wild type animals (r=0.8969, p=0.0002) but not in *rnaset2* mutants (r=0.2837, p=0.3670) – suggesting *rnaset2* antiviral response is not primarily driven by viral ZfPV infection. ZfPV burden calculated as *ZfPV* band intensity/ *ef1α* band intensity. Spearman's r correlation analysis, 3 biological repeats, 3 technical replicates.

3.3.4 Endogenous retroviruses are expressed in zebrafish neurons and immune cells

Beyond exogenous infections, the aberrant expression of endogenous retroviruses (ERVs) has been suggested as one potential driver of pathology in RNASET2-deficient leukodystrophy. However, there remains a lack of validated animal models with which to study ERV function *in vivo*. As such, I sought to characterise the expression pattern of two known fully functioning zebrafish ERVs: *zferv1a* and *zferv1b* (Rutherford *et al.*, 2022).

In situ hybridisation against the envelope sequence of *zferv1a* (hereafter called *env1a*) revealed prominent expression of this transcript in the thymus of larvae at 3- and 5-dpf – suggesting *zferv1a* may be active in this immune organ (Figure 3.15a and Figure 3.16a). Interestingly, *env1a* expression was also observed in the brain, suggesting this ERV is also active in the central nervous system. Almost identical antisense staining was obtained with the *pol1a* probe – labelling the polymerase sequence of the same ERV (*zferv1a*) (Figure 3.15b and Figure 3.16b) – increasing confidence that *zferv1a* is expressed in these locations.

In contrast, a distinct pattern of labelling was observed with the *env1b* probe, which targets the envelope domain of *zferv1b* (Figure 3.15c and Figure 3.16c). *In situ* hybridisation suggests this sequence is expressed in the thymus and, in a more diffuse manner, within the brain, but with no observable signal in the spinal cord at 3- or 5dpf.

Notably, at both 3- and 5dpf, signal was observable in the thymus using the sense probe for *env1a* (Figure 3.15a and Figure 3.16a). This may indicate bidirectional expression of *zferv1a*, which has been reported for some human ERVs (Chiappinelli *et al.*, 2015). Sense labelling was not detected for *pol1a*, nor *env1b*.

Together, this data suggests two ERVs are active in the zebrafish central nervous system in spatially distinct patterns – with *zferv1a* showing particularly robust expression in the brain and spinal cord – suggesting the zebrafish may show utility as an *in vivo* system in which to study ERVs.

3.3.4.1 rnaset2 mutants do not have upregulated zferv1a activity

Given the extensive overactivation of the antiviral immune response observed in *rnaset2* mutants, it has been hypothesised that aberrant *zferv* expression may be a potential driver of pathology in RNASET2-deficient leukodystrophy (Rutherford and Hamilton, 2019a; Hamilton et al., 2020a; Rutherford, Kasher and Hamilton, 2021).

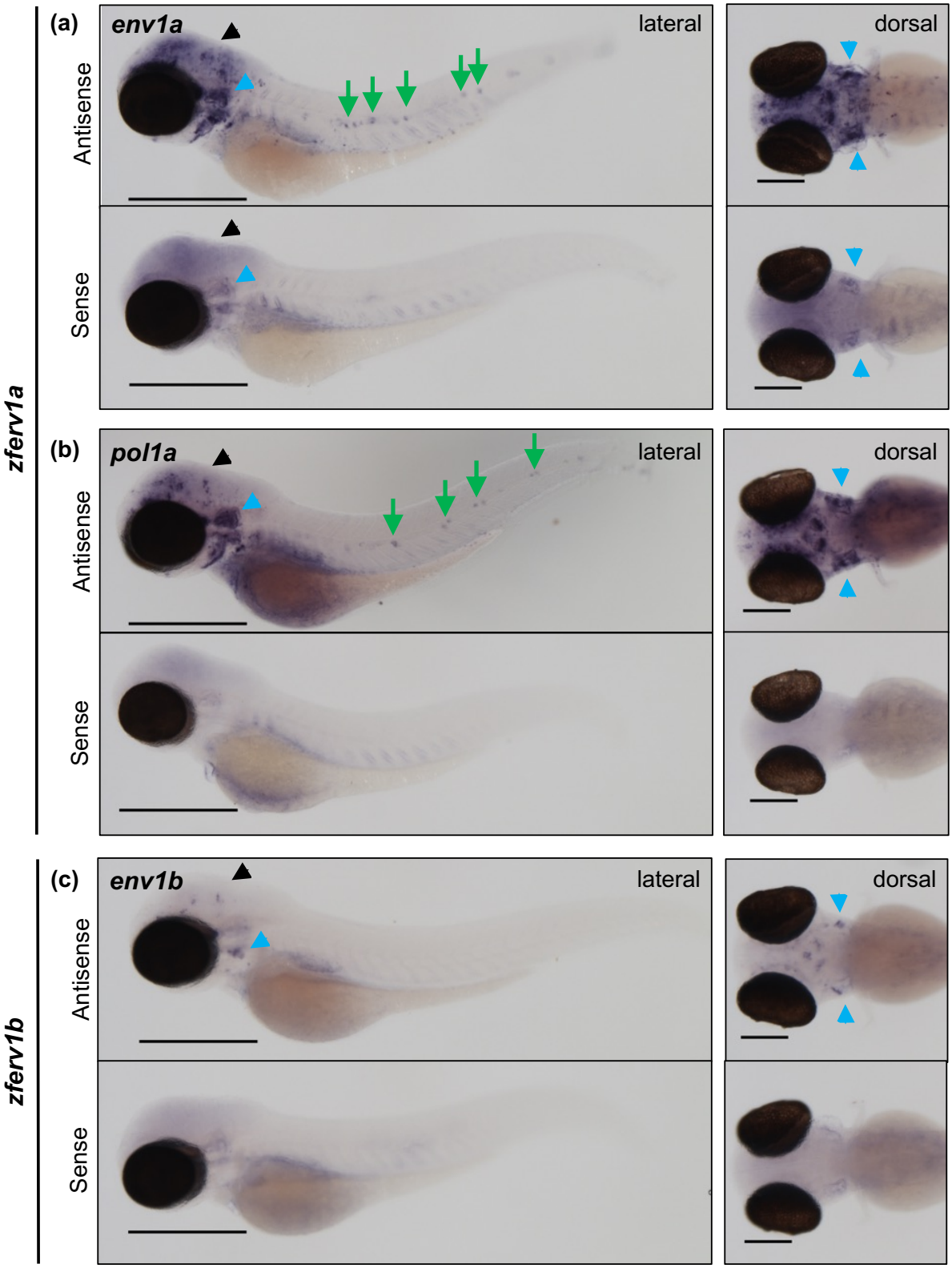

Figure 3.15. *zferv1a* and *zferv1b* are expressed in the brains of 3dpf embryos.
In situ hybridization revealed that the envelope (*env1a*) **(a)** and reverse transcriptase (*pol1a*) **(b)** genes of *zferv1a* are expressed in overlapping patterns in the brain (black arrowhead), trunk (green arrows) and thymus (blue arrowhead). Expression of the env1b gene of *zferv1b* **(c)** is limited to the brain (black arrowhead) and thymus (blue arrowhead). Antisense and sense RNA probes shown throughout. Scale bar for lateral images represents 500µm. Scale bar for dorsal images represents 200µm.

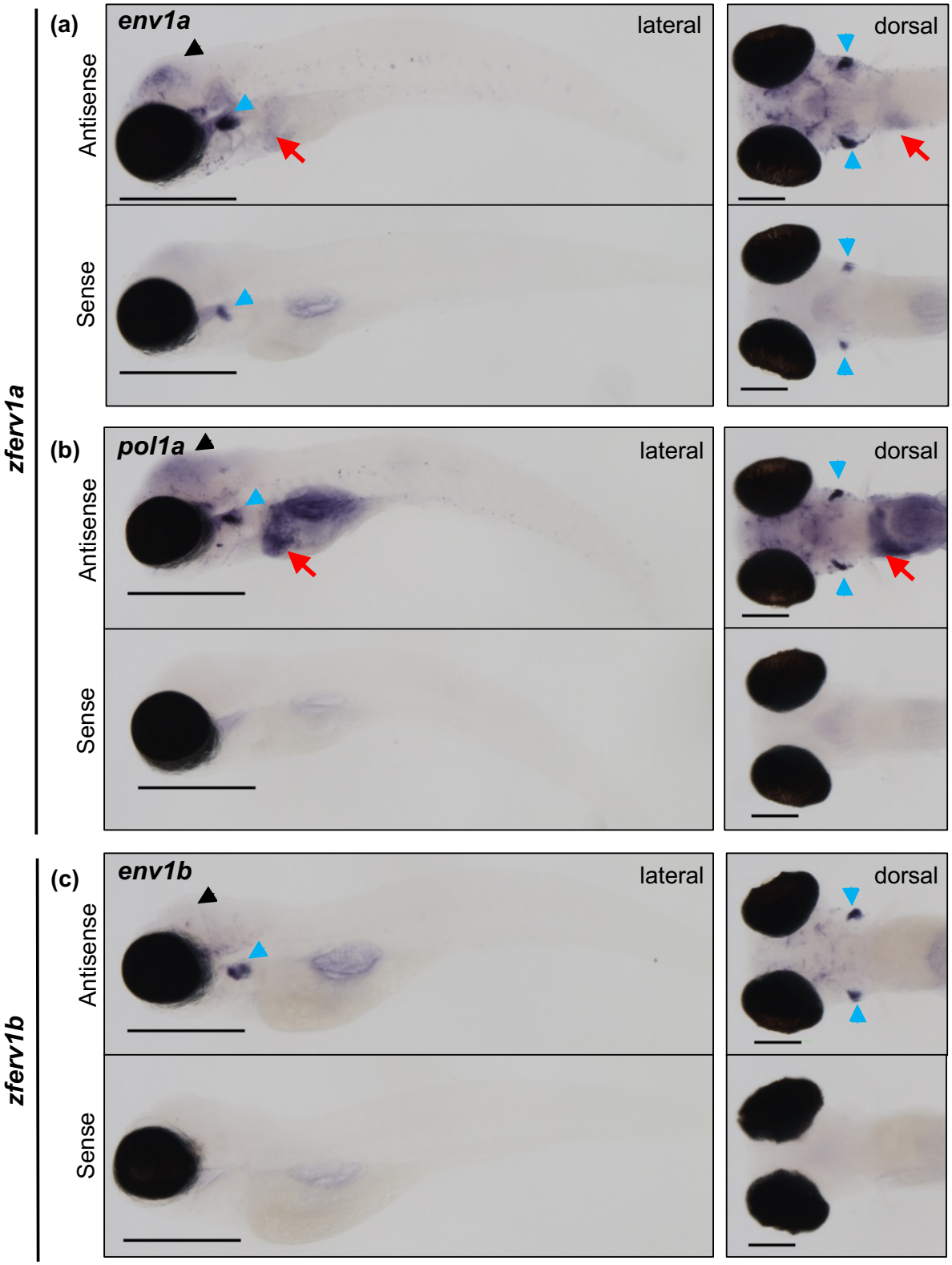

Figure 3.16. *zferv1a* and *zferv1b* are expressed in the brains at 5dpf.
In situ hybridization revealed that the envelope (*env1a*) (a) and reverse transcriptase (*pol1a*) (b) genes of *zferv1a* are expressed in overlapping patterns in the brain (black arrowhead), and thymus (blue arrowhead). Expression is also visible in the liver (red arrow). Expression of the *env1b* gene of *zferv1b* (c) is observable in brain (black arrowhead) and thymus (blue arrowhead), but to a lesser extent than *zferv1a*. Antisense and sense RNA probes shown throughout. Scale bar for lateral images represents 500µm. Scale bar for dorsal images represents 200µm.

As such, I sought to quantify the expression of *zferv* transcripts in *rnaset2* mutants using qPCR. Given the spatial expression pattern of *zferv1a* – with most expression seen in the brain and thymus (Figure 3.15a,b and Figure 3.16a,b) – I utilised cDNA synthesised from the head only to investigate the expression of *zferv1a* genes. Using primers targeting transcripts from the envelope (*env1a*), polyprotein (*gag1a*) or reverse transcriptase (*pol1a*) genes of *zferv1a*, qRT-PCR revealed no significant difference in *zferv1a* expression in *rnaset2* heads at 8dpf – with a non-significant but notable decrease in expression of *zferv1a* transcripts in mutants relative to wild type controls (Figure 3.17). As such, there is no evidence that *zferv1a* activity is upregulated in *rnaset2* mutants during this larval stage.

3.3.5 Depleting endogenous microglia in rnaset2 mutants

As the immune cells of the brain, microglia are essential in defending the CNS against potentially damaging stimuli, including pathogens like viruses (Hickman et al., 2018a; Hatton and Duncan, 2019b)(Hickman et al., 2018a; Hatton and Duncan, 2019b). As such, the overactive antiviral response in *rnaset2* mutants may trigger, or even be contributed to by, an aberrant microglial response. As such, I sought to establish an assay to assess the effect of microglial depletion on the survival of *rnaset2* animals.

3.3.5.1 Injection of paired guides targeting irf8 efficiently depletes embryonic microglia

Previous work has revealed knockdown of interferon regulatory factor 8 (*irf8*) – a transcription factor critical to the development of embryonic microglia and macrophages – by injection of a single crRNA can transiently deplete the microglial niche in zebrafish embryos in the first days of life (Li et al., 2011b; Hamilton et al., 2020a)(Li et al., 2011b; Hamilton et al., 2020a). However, this approach has limited efficiency – resulting in only approximately 50% of embryos with a fully depleted niche. Hence, I sought to develop a strategy with greater microglia depletion efficiency at 5dpf through injection of multiple *irf8*-targeting crRNAs.

To increase depletion efficiency, I combined the previously published guide (hereafter called guide A) with a novel guide (guide B) in equimolar concentrations (50µM each). While the sequence of guides B is specific to *irf8*, it should be noted that the target sequence of guide A also shares homology with an intron region in the coagulation factor IX-like (CABZ01044048.1) gene. However, this previously published crRNA has not been associated with any overt coagulation phenotypes thus far (Hamilton et al., 2020a)(Hamilton et al., 2020a).

This guide pairing led to efficient microglia depletion in *Tg(mpeg1:mCherryCAAX)* – as quantified by live screening of mCherry positive cells in the brain at 5dpf – with 80% of injected embryos in showing a complete absence of visible microglia (Figure 3.18). Additionally, there was no significant difference

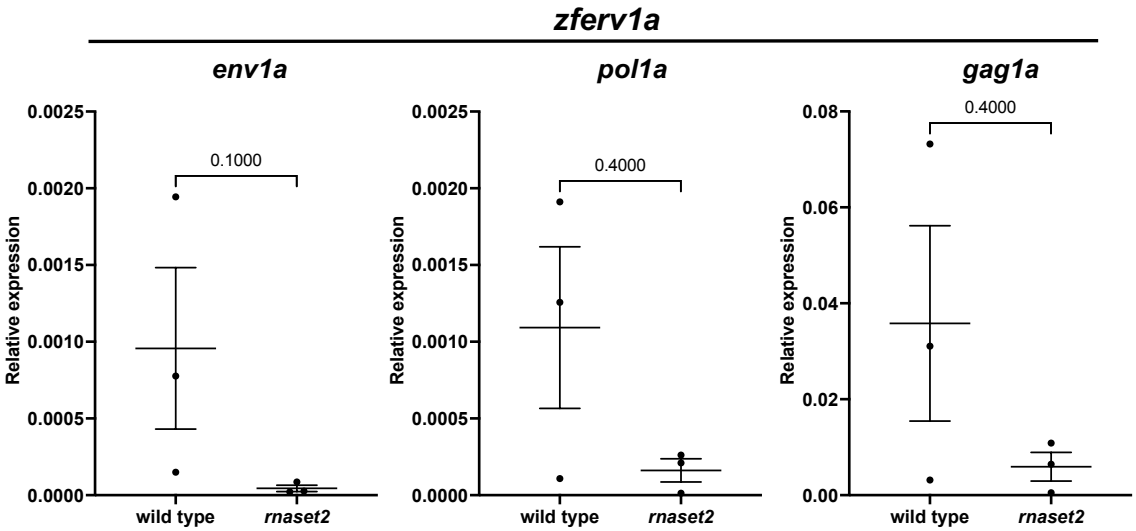

Figure 3.17. *rnaset2* mutants do not have elevated zferv1a transcripts at 8dpf.
qRT-PCR reveals that *rnaset2* mutants show no significant changes in expression of the envelope (*env*), polyprotein (*gag*) or reverse transcriptase (*pol*) genes of *zferv1a*, using cDNA synthesized from RNA extracted from heads only. Mann Whitney U-test, three biological repeats, three technical replicates.

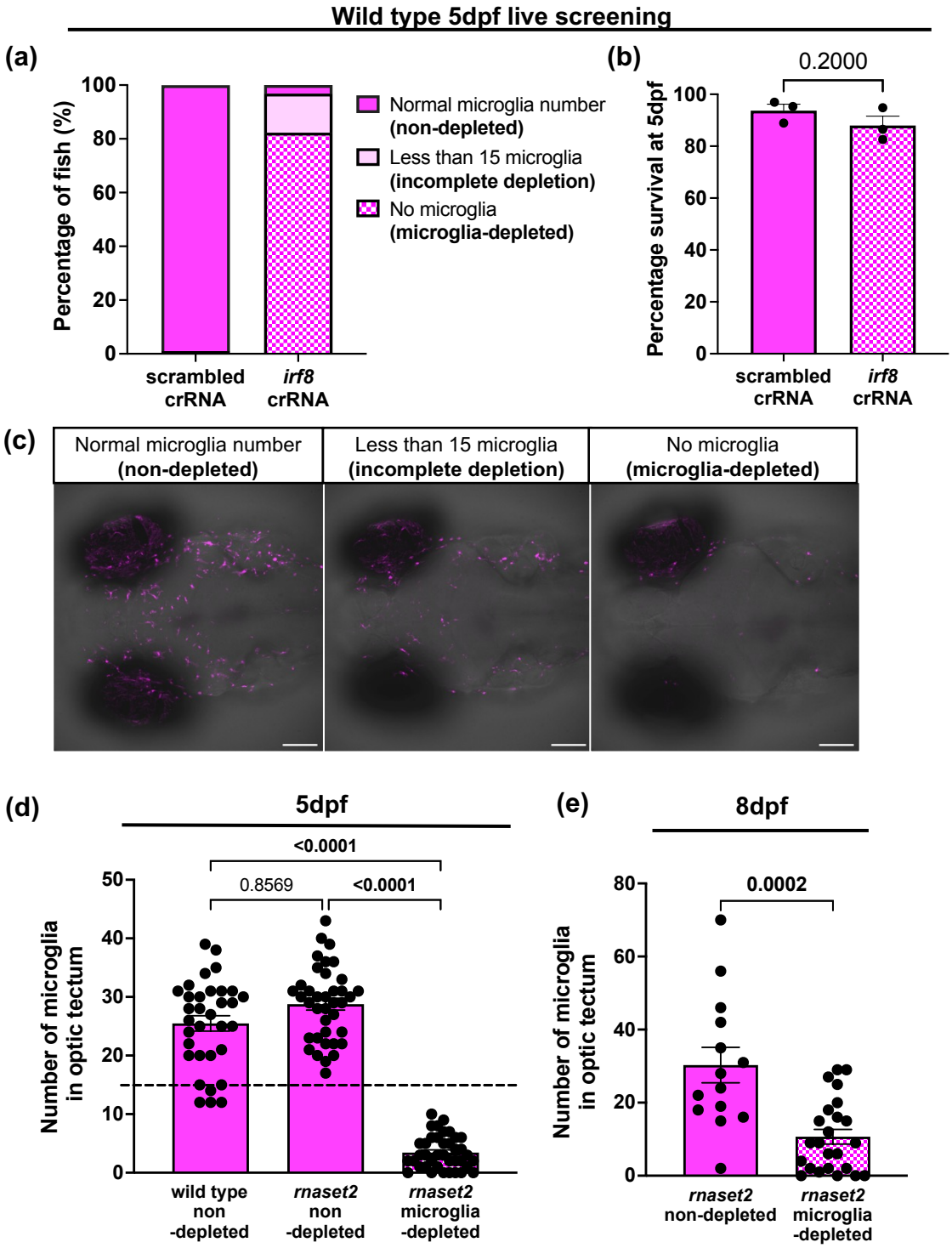

Figure 3.18. Quantification of microglia depletion by CRISPR/Cas9-mediated *irf8* knockout.
a. Live screening of 5dpf *Tg(mpeg:mCherry CAAX)sh378* embryos injected with double *irf8* targeting crRNAs revealed robust depletion of microglia compared with scrambled crRNA-injected controls. **b.** Survival of wild type hosts following microglia depletion. Mann Whitney test, three biological repeats. **c.** Representative images of *Tg(mpeg:mCherry CAAX)sh378* embryos with normal microglia number (non-depleted), less than 15 microglia (incomplete depletion) and no microglia (microglia-depleted). Scale bar represents 100µm. **d, e.** Immunohistochemistry against the microglia marker 4C4 revealed a significant reduction in microglia number in *irf8* crRNA-injected (microglia-depleted) *rnaset2* mutants relative to scrambled crRNA-injected (non-depleted) controls at 5- **(d)** and 8dpf **(e).** Kruskal-Wallis test with Dunn's multiple comparisons. 3 biological repeats, n=14–39.

in mortality between *irf8* crRNA-injected and scrambled injected wild type embryos at 5dpf, suggesting CRISPR-Cas9 targeting of *irf8* does not impact survival in wild type embryos (Figure 3.18b).

To confirm microglia-depletion in *rnaset2* mutant embryos, I performed immunohistochemistry against the microglia-specific marker 4C4 followed by confocal microscopy. Manual quantification of the number of 4C4-positive cells revealed a significant reduction in the number of microglia in *irf8* crRNA-injected embryos at 5- and 8dpf relative to non-depleted controls (Figure 3.18d, e).

Therefore, injection of paired *irf8*-targeting crRNA leads to highly efficient microglia depletion in embryonic stages.

3.3.5.2 Knockdown of irf8 does not robustly affect microglia number or density in 1 year old adult brains, as quantified on tissue sections

In the zebrafish, microglia are derived from two distinct waves of cellular migration and differentiation, whereby embryonic yolk sac-derived microglia are gradually replaced by adult HSC-derived cells (Ferrero et al., 2018)(Ferrero et al., 2018). The transcription factor *irf8* is thought to be essential for maturation of embryonic, but not adult, microglia – suggesting *irf8* may be required only for this first wave of microglia and, as such, depletion of the microglial niche by targeting of *irf8* is likely to be transient through embryogenesis only. Hence, I sought to investigate whether embryonic the effects of *irf8* CRISPR/Cas9-targeting on adult microglial populations.

To assess the long-term impact of *irf8* targeting on microglia, embryos were injected with *irf8* crRNA and transient microglia depletion was confirmed using fluorescent microscopy at 5dpf. Microglia-depleted animals and non-injected controls were then raised into adulthood, before culling and fixing at approximately 1 year of age. To quantify microglia in adult brains, immunohistochemistry with the microglia-specific 4C4 antibody was performed on sagittal brain sections, with microglia density calculated as the number of cells per million pixels.

Microglia were observable in all regions quantified, albeit with some variability between animals of each group (Figure 3.19). There was no observable, robust difference between the number or density of microglia between non-injected or *irf8* crRNA injected animals, either in the whole brain or the regions quantified. However, due to small sample sizes, further repeats may be required to confirm this finding – particularly with regard to the density of microglia in olfactory bulb and medulla of non-

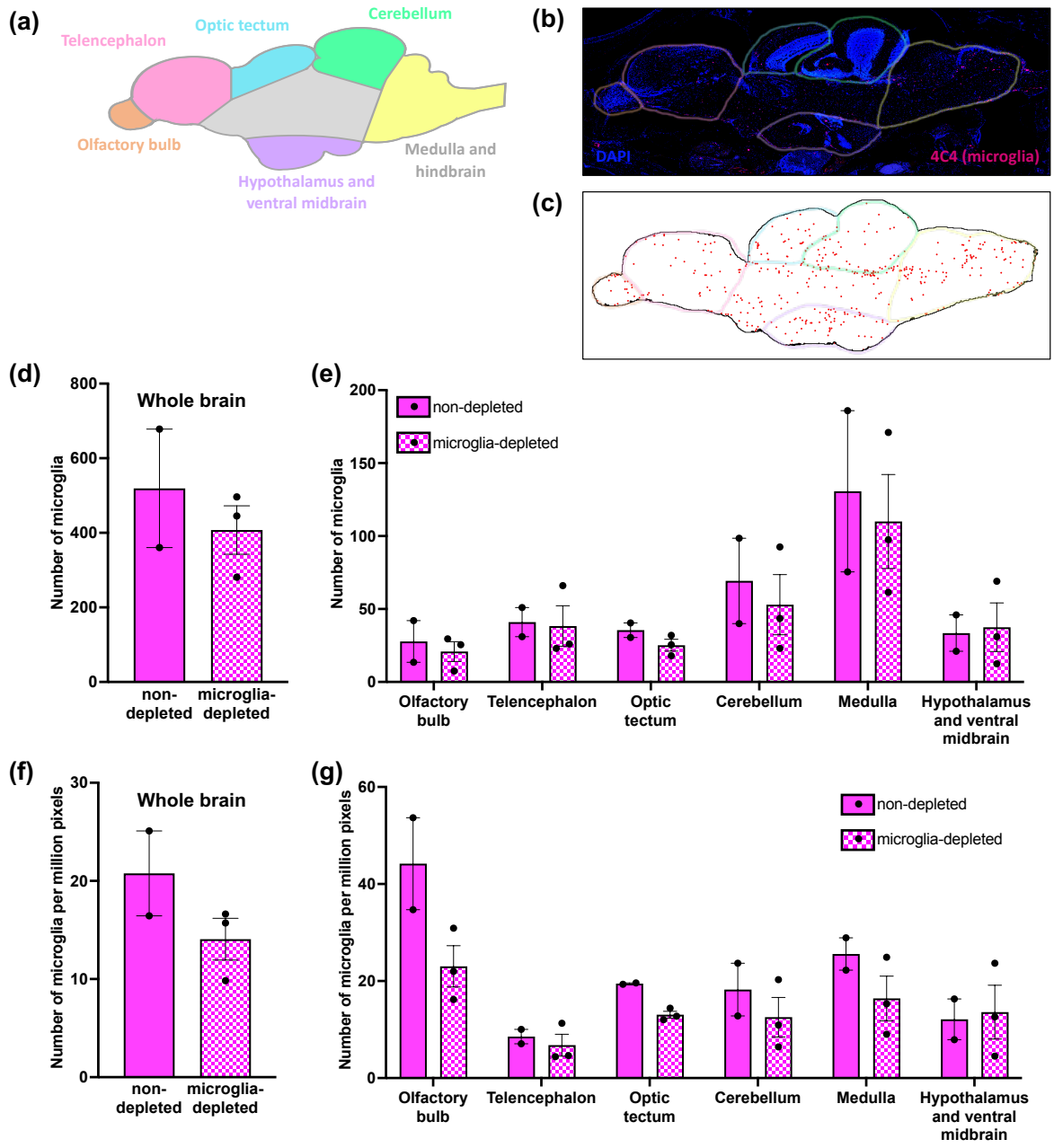

Figure 3.19. Embryonic microglia depletion does not affect microglia number or density in adult brains.

Immunohistochemistry against microglia marker (4C4) on sagittal sections of 1 year-old adult brains. **(a)** Schematic depicting anatomically defined brain regions used for quantification of microglia. **(b, c)** Representative image depicting microglial distribution within pre-defined regions, with the accompanying dot plot. No difference was identified for the number **(d, e)** or density **(f, g)** of microglia in the whole brain, or within each region, between microglia-depleted animals and non-depleted controls. Microglia density defined as the number of microglia counted per region normalized to region area (per million pixels). Each data point reflects average value per fish calculated from two technical replicates. No statistical analysis performed, 2–3 fish per group.

injected or *irf8* crRNA-injected animals. Nonetheless, these findings suggest transient depletion of microglia during embryogenesis does not significantly alter microglia number or distribution into adulthood.

3.3.5.3 Transient microglial depletion may impact survival in wild type and rnaset2 animals

The finding that microglial number and density are unchanged in *irf8* crRNA-injected adults suggests that any effects of *irf8* knockdown on *rnaset2* mutant health are likely to be observed within the first year of life. Previous publications have suggested that *rnaset2* mutants show increased mortality in adulthood, with homozygous animals showing reduced survival from around 4 months post-fertilisation (Hamilton et al., 2020a)(Hamilton et al., 2020a). Thus, I sought to investigate whether transient microglia depletion via *irf8* targeting affected the survival phenotype of mutants both in embryogenesis and early adulthood.

Despite previous quantification suggesting that microglial depletion does not impact mortality of wild type embryos up to 5dpf, analysis of *rnaset2* mutants suggests that transient depletion of the microglia (and macrophages) may cause significantly impaired survival up to 5dpf, relative to injection of a scrambled crRNA control (Figure 3.20). However, these data should be interpreted cautiously, due to poor survival of the non-depleted wild type group. This group should serve as a positive control to ensure fish were generally healthy – suggesting, across this set of experiments, embryo health may be somehow compromised. Nonetheless, it is interesting that microglia-depleted *rnaset2* mutants showed approximately ~15% impairment in survival relative to non-depleted *rnaset2* controls (Figure 3.20).

To assess the effect of transient microglia depletion into adulthood, *irf8* crRNA-injected wild type and *rnaset2* embryos were screened at 5dpf to ensure robust microglia depletion and then raised in the aquarium. Log-rank Mantel Cox analysis revealed a significant difference in survival at a group level (for comparisons between all four experimental groups: wild type and *rnaset2*, with and without microglia depletion) (Figure 3.21a). Direct comparisons between microglia-depleted and non-depleted animals for each genotype did not yield significant differences, although there was a trend for reduced survival in microglia-depleted adults for both genotypes (Figure 3.21b–d). Interestingly, no differences in survival were reported between non-depleted *rnaset2* adults and wild type controls, as previously published (Hamilton et al. Glia 2020). Nonetheless, together these data suggest that depletion of embryonic microglia does not have beneficial effects on survival in *rnaset2* mutants – instead, causing potentially deleterious phenotypes in these animals.

(a)

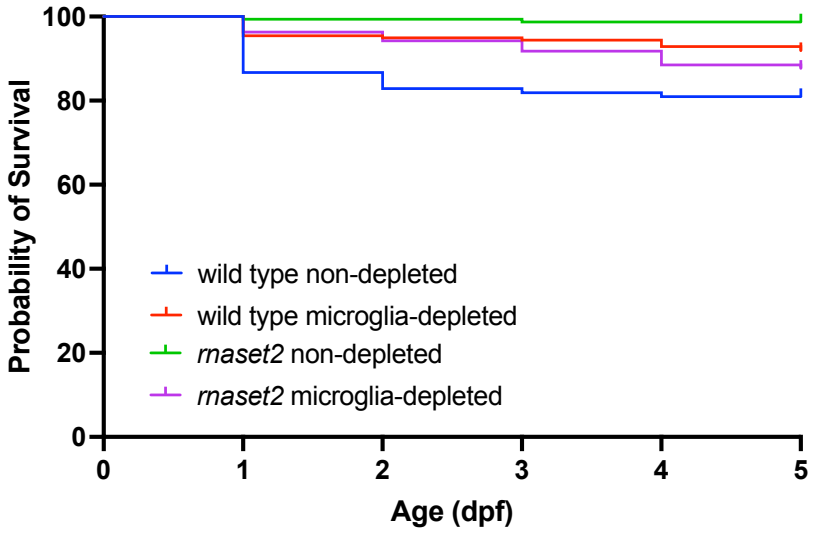

(b)

	wild type microglia-depleted	*rnaset2* non-depleted	*rnaset2* microglia-depleted
wild type non-depleted	**0.0046**	**<0.0001**	0.0774
wild type microglia-depleted		**0.0043**	0.1565
rnaset2 non-depleted			**<0.0001**

Figure 3.20. Transient microglia-depletion affects survival in embryogenesis.
(a) Survival analysis of *rnaset2* embryos and wild-type siblings suggests transient depletion of microglia and macrophages may impair survival during embryogenesis (Log-rank Mantel-Cox test, p<0.0001). **(b)** Table shows p-values for each comparison (Bonferroni-corrected threshold: p<0.00833; family-wise significance threshold: P<0.05). Two biological replicates, n=68 per group.

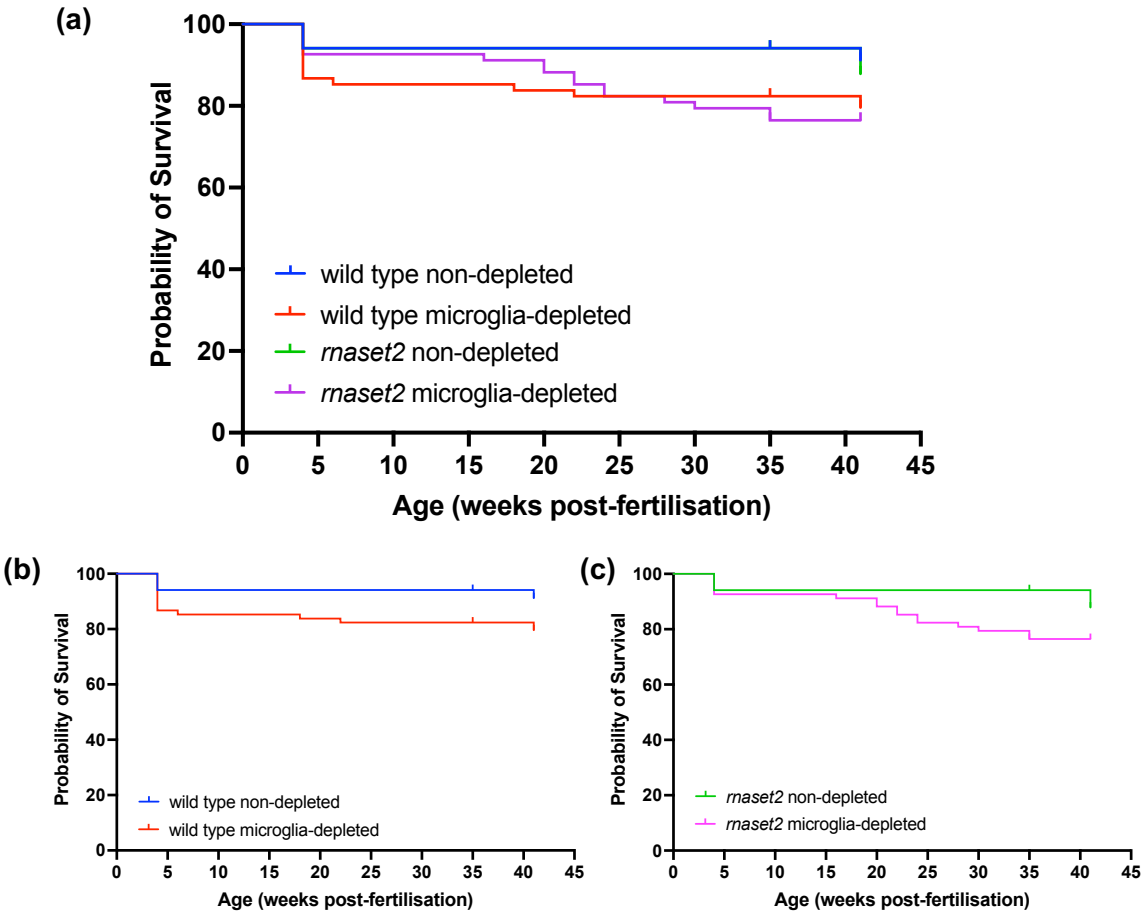

(d)

	wild type microglia-depleted	*rnaset2* non-depleted	*rnaset2* microglia-depleted
wild type non-depleted	0.0451	0.7348	0.0098
wild type microglia-depleted		0.0896	0.5866
rnaset2 non-depleted			0.0200

Figure 3.21. Transient microglia-depletion may affect survival in early adulthood.
(a–c) Longitudinal follow-up of adult *rnaset2* animals and wild-type siblings suggests transient depletion of microglia and macrophages may impair survival during adulthood (Log-rank Mantel-Cox test, **p=0.0183**). For clarity, individual plots are shown for each genotype (b, c). **(d)** Table shows p-values for each comparison (Bonferroni-corrected threshold: p<0.00833; family-wise significance threshold: P<0.05). Two biological replicates, n=68 per group.

3.3.6 Survival analysis of rnaset2 mutants

The data above reports no observable difference in survival in non-depleted *rnaset2* mutants relative to wild type controls in adulthood – in direct contrast to previous publications (Hamilton *et al. Glia* 2020). The present study used a subsequent generation of *rnaset2* mutants, suggesting there may be some genetic compensation in this survival phenotype (El-Brolosy and Stainier, 2017; Buglo et al., 2020; Rouf et al., 2023)(El-Brolosy and Stainier, 2017; Buglo et al., 2020; Rouf et al., 2023). As such, I repeated this survival assay using increased animal numbers to further investigate the survival phenotype of the current generation of *rnaset2* mutants.

In alignment with Figure 3.21, no significant differences in survival were observed in *rnaset2* mutants up to one-year post-fertilisation (Figure 3.22). However, there was a clear trend towards reduced survival, suggesting a more robust survival phenotype may have been observed if these animals had been followed beyond one year. Nonetheless, this data demonstrates a clear difference in the survival phenotype of the current *rnaset2* generation relative to previous generations, of which only 10% survived to 9 months post-fertilisation (Hamilton et al., 2020a)(Hamilton et al., 2020a).

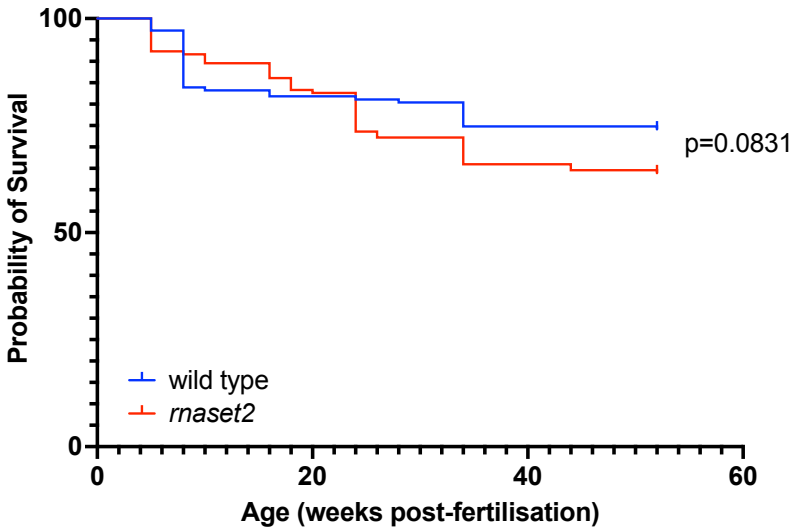

Figure 3.22. Survival of *rnaset2* mutants is not significantly impaired, relative to wild type controls, up to one-year post-fertilization.
Log-rank Mantel-Cox test. Two biological replicates, n=144 per group.

3.4 Discussion

Sitting at the intersection of interferonopathies and leukodystrophies, RNASET2-deficient leukodystrophy is characterised by white matter lesions alongside brain-wide neuroinflammation – exemplified by upregulation of the antiviral response and microglial dysfunction (Henneke et al., 2009b; Haud et al., 2011b; Kameli et al., 2019; Hamilton et al., 2020a; Kettwig et al., 2021). In this chapter, I have demonstrated *rnaset2* mutant zebrafish present with myelin abnormalities during embryonic stages, accompanied by abnormal motor and learning behaviours and the previously characterised antiviral response (Hamilton Glia 2020). Neither environmental virus exposure nor ERV activation can fully account for the upregulation of interferon-stimulated genes in *rnaset2* mutant embryos, suggesting another innate driver of neuroinflammation at these early developmental stages. Despite their complex role in coordinating the neuroimmune response, depletion of the microglia via targeting of *irf8* does not improve survival phenotypes in *rnaset2* mutants – instead causing impaired survival of embryos and adults – suggesting that microglia may be key mediators in limiting phenotype severity in this zebrafish model. Therefore, together these findings demonstrate that a broad spectrum of *rnaset2*-linked pathology emerges during embryonic stages and provide further support for the *rnaset2* mutant zebrafish as a model of this disorder.

Moreover, the work detailed in this chapter highlights several assays can be used to assess the impact of potential treatments in *rnaset2* mutants. In addition to the use of MRI to detect white matter lesions in adult animals, both qPCR of myelin-associated transcripts and imaging of oligodendrocyte reporter lines may be used to quantify the effect of interventions on myelin abnormalities in *rnaset2* mutant embryos. Motor impairments may also provide a robust and high throughput strategy with which to screen potential treatments, during embryonic and juvenile ages. Furthermore, despite the trigger remaining unknown, the confirmation of the antiviral response in *rnaset2* mutants suggests that transcriptomic approaches may be used to understand the impact of therapies on the neuroinflammatory response – in addition to the previously characterised reduction in apoptotic cell clearance in *rnaset2* mutant larvae. Finally, the subtle survival impairments seen *rnaset2* mutants may also provide a readout of therapeutic success in the longer term. As such, this battery of assays – each of which recapitulates phenotypes associated with disease in patients – provides a powerful foundation for the use of this zebrafish model in developing novel therapeutics for RNASET2-deficient leukodystrophy.

3.4.1 rnaset2 myelin abnormalities begin during early development

3.4.1.1 Myelination may be disrupted in rnaset2 mutant larvae

The current study supports the hypothesis that myelin abnormalities emerge during early development in *rnaset2* mutant zebrafish. qPCR revealed a significant reduction in the myelin-associated transcripts *mbpa* and *mpz* during larval stages, with a trend for reduction of *mbpb* and *plp1a*. Intriguingly, this was accompanied by elevated, and then reduced, numbers of oligodendrocytes in *rnaset2* mutants at 5dpf and 8dpf respectively. Unfortunately, a robust antibody for the labelling of zebrafish mbpa protein could not be identified – making it difficult to link these transcriptional and cellular changes and establish how, if at all, myelin structure is altered in *rnaset2* mutants. Nonetheless, these changes in *mbpa* and oligodendrocyte count demonstrate that white matter components are abnormal in this model to some extent.

The apparent change in oligodendrocyte number from 5- to 8dpf, whereby *rnaset2* mutants have increased oligodendrocyte counts relative to wild type at the younger age but reductions in cell number at the latter, is particularly interesting. One potential explanation for this change may be due to apoptosis of *rnaset2* oligodendrocytes between 5- and 8dpf. Oligodendrocyte apoptosis has been reported in multiple sclerosis and vanishing white matter disease (another leukodystrophy) (Lucchinetti *et al.*, 2002; Bugiani *et al.*, 2010; Prineas and Parratt, 2012). Furthermore, several proinflammatory mediators – including those thought to be upregulated in *rnaset2* mutants, such as interferons – have been shown to induce apoptosis of oligodendrocytes *in vitro* and *in vivo* (Buntinx *et al.*, 2004; Lin and Lin, 2010). Indeed, there is a slight – albeit nonsignificant – decrease in *rnaset2* oligodendrocyte counts in the ventral spinal cord from 5- to 8dpf (although these data should be interpreted cautiously, as these are not repeated measurements of individual fish but rather quantification of separate animals from the same clutch). As such, oligodendrocyte cell death may provide some explanation for abnormal *mbpa*-positive cell numbers in *rnaset2* mutants.

Alternatively, the differences in oligodendrocyte number in *rnaset2* mutants relative to age-matched wild types may be due to a difference in the rate, or timing, of oligodendrocyte maturation at these ages. While wild type oligodendrocyte counts increase significantly in the brain and dorsal spinal cord from 5- to 8dpf, the number of *rnaset2* oligodendrocytes seem to remain relatively constant over this time. There are reports that some inflammatory signals – such as IL-1B, also known to be upregulated in *rnaset2* mutants – cause impaired oligodendrocyte maturation, leading to an increase in the number of oligodendrocyte precursor cells (OPCs) alongside a reduction in myelinating oligodendrocytes (Favrais et al., 2011; Hamilton et al., 2020a). As *mbpa* is expressed only in myelinating oligodendrocytes (and Schwann cells of the peripheral nervous system), the dynamics of such

precursor populations remain unclear in our model (Jung *et al.*, 2010; Almeida *et al.*, 2011). Published literature in another *rnaset2* mutant zebrafish model – the *sa138* (*rnaset2*$^{-/-}$) zebrafish – has reported no changes in OPC number at 3–5dpf using the *Tg(olig2:GFP)* reporter (Weber *et al.*, 2020). Therefore, this suggests there is unlikely to be a backlog of undifferentiated OPCs, nor a reduction in OPC proliferation, which could explain reduced oligodendrocyte numbers in our model.

It is also interesting to consider that, at 5dpf, *rnaset2* mutants have a greater number of mbpa:GFP positive cells than wild type at the same age as a reduction in *mbpa* transcripts. The relationship between the number of mbpa:GFP positive cells and tissue-wide quantity of *mbpa* transcripts is not necessarily linear, perhaps explaining why these findings are somewhat in conflict. It should be noted that the quantification of the *mbpa*:GFP transgenic line in this study investigated only the number of cells that express *mbpa*, rather than the amount of transcript present, which could instead be potentially inferred by looking at fluorescence intensity of each given cell. It is possible that each individual oligodendrocyte may express downregulated levels of myelin-associated genes, possibly due to the neuroinflammatory environment of the *rnaset2* mutant brain or cell autonomous effects of loss of functioning rnaset2 in the oligodendrocytes. This is one potential explanation for why a reduction in *mbpa* gene expression was observed in *rnaset2* mutants relative to wild types at 5dpf, alongside increased numbers of oligodendrocytes.

Alternatively, the discrepancy between the level of *mbpa* transcripts and mbpa:GFP positive cell count may be due to RNA degradation. Myelin basic protein is translated at the cell membrane after transport from the nucleus in its mRNA form (Ainger *et al.*, 1993). This mRNA is thought to be packaged into non-membranous ribonucleoprotein complexes (‘granules’) in the cytoplasm following nuclear export, and this then transported to the membrane via microtubules in a kinesin-dependent manner to the membrane where the granules disassemble to facilitate local translation at the axon-glial contact site (Baron and Hoekstra, 2010). Accordingly, dysfunction of any component along this pathway can result in aberrant MBP expression. For example, in the zebrafish, loss-of-function in the kinesin motor protein kif1b is essential for trafficking of *mbpa* transcripts to the membrane, with ectopic myelin-like structures formed within cell bodies of *kif1b* mutants (Lyons *et al.*, 2009). As such, *mbpa* transcripts may be particularly susceptible to degradation, which could also explain the diminished levels of *mbpa* transcript without a reduction in the number of mbpa:GFP positive cells at 5dpf.

Finally, it should be noted that the quantification of *mbpa* transcripts used cDNA synthesised from whole body RNA, while the mbpa:GFP counts were performed in the brain and spinal cord only. In

addition to expression by myelinating oligodendrocytes, *mbpa* is also expressed by Schwann cells of the peripheral nervous system (Jung *et al.*, 2010; Almeida *et al.*, 2011). Myelinating Schwann cells are present in zebrafish larvae at 8dpf, meaning their contribution of *mbpa* transcripts may confound changes in the CNS (Lyons *et al.*, 2005). Accordingly, future work may investigate the expression of myelin-associated transcripts specifically in dissected brains in *rnaset2* larvae, as was performed for adults in this study. Nonetheless, quantification of *mbpa* expression may be used to assess the effect of potential treatments on myelin pathology in *rnaset2* mutant larvae.

3.4.1.2 Myelin associated transcripts are not altered in rnaset2 adults

Despite a downregulation of *mbpa* during larval stages, no significant difference in expression of myelin-associated transcripts was identified between *rnaset2* mutants and wild type controls during juvenile (3mpf) and adult (7.5mpf) ages, despite previous publications demonstrating white matter lesion formation in adults of a similar age (Haud et al., 2011b). This poses an interesting question – how, if at all, are changes in myelin-associated gene expression linked to white matter lesion formation in our model?

Firstly, it must be acknowledged that the level of mRNA is by no means a direct correlate of the overall amount of protein at a specific time (de Sousa Abreu *et al.*, 2009; Maier, Güell and Serrano, 2009; Vogel and Marcotte, 2012). Multiple factors may influence protein levels beyond mRNA, including modulation of translation by regulatory proteins and small RNAs (sRNAs), ribosomal density and protein half-life (which itself can be governed by post-translational modifications, localisation and degradation) (Maier, Güell and Serrano, 2009). Likewise, alternative splicing may confer changes in the amount, structure and function of myelin-associated proteins. For example, human *MBP* transcripts can be alternatively spliced to form several isoforms which can be grouped into two categories – those containing exon 2, which are found in earlier development, and those lacking exon 2, which are thought to predominate in more mature, adult myelin (Barbarese, Carson and Braun, 1978; Gogate *et al.*, 1994). Alternative splicing of *mbpa* has also been reported in the zebrafish, with *mbpa*-transcripts including exon-5 being shown to be exclusive to the peripheral nervous system – however, it is unclear if developmentally-specific isoforms are present in this model (Torvund-Jensen *et al.*, 2018). As such, this assessment of myelin-associated transcripts by qPCR can only infer changes which may or may not be reflected at a protein level.

Similarly, the present study investigated only four of the most abundant myelin-associated proteins, while a further 1000 proteins have been detected in zebrafish myelin (Siems *et al.*, 2021). It is possible that not all of these proteins are altered in all white matter lesions. For example, focal demyelination

lesions in patients with multiple sclerosis, viral encephalitis or stroke have been associated with a loss of myelin-associated glycoprotein in human tissue, while other myelin proteins (including MBP and PLP) are preserved (Aboul-Enein *et al.*, 2003). Therefore, lesion formation may be better assessed with a transcriptomic approach to assess changes in genes not included in this study.

Even if protein levels are affected in sites of lesion formation, myelin abnormalities may not be sufficient to change brain-wide transcript/protein levels. In multiple sclerosis, the percentage of white matter that is classified as a lesion is from ~1–10% and varies significantly by region (Sperling *et al.*, 2001). In Vanishing White Matter disease – a leukodystrophy with particularly striking white matter loss – up to 23.3% of total white matter was considered abnormal in individuals with the earliest-onset and most severe disease, and as low as 2.1% for those with milder clinical courses (Stellingwerff *et al.*, 2021). Therefore, abnormal white matter likely only comprises a small proportion of the CNS and may not be best studied by a whole brain approach.

Instead, future work may seek to investigate lesion-associated changes in a more local manner. Isolation of areas of white matter abnormality may allow for proteomic analysis of any changes in protein composition specific to lesion formation. Any identified candidates could then be validated using immunohistochemistry to visualise protein distribution and amount, alongside other markers of lesion severity such as microglial- and astrocyte- reactivity and amyloid precursor protein as previously validated (Haud et al., 2011b). Alternatively, transgenic reporters, such as the *Tg(mbpa:GFP)* or *Tg(olig2:GFP)* reporters, could be used to investigate changes in oligodendrocyte or OPC numbers and morphology, respectively. As such, much remains to be understood about the changes in adult *rnaset2*-deficient myelin, both leading up to and during lesion formation.

3.4.1.3 More tools are needed to study myelin in rnaset2 mutants

To truly assess the levels of myelin protein, an antibody which reliably detects myelin components is required. Published antibodies are available to label zebrafish mbpa, although none are commercially available (Lyons *et al.*, 2005; Kucenas *et al.*, 2009; Preston *et al.*, 2019). For the present study, one such antibody was kindly gifted to us by the Appel lab (University of Colorado), which had been commercially generated against the peptide sequence CSRSRSPPKRWSTIF. This antibody has been used in whole mount immunohistochemistry assays to assess mbpa localisation from 5dpf with specific, albeit weak labelling (Lyons *et al.*, 2005). Despite this, in the current study, accurate labelling of myelin at 8dpf could not be achieved. This may have been due to insufficient antigen retrieval, particularly considering the highly compact nature of the myelin sheath (Buckley, Goldsmith and Franklin, 2008). However, the antigen retrieval techniques trialled in this study did not improve staining

intensity, and instead compromised tissue integrity. Another potential explanation may be simply due to the age and storage of the antibody, which was synthesised in 2009 and subjected to freeze-thaw before and during international shipping to the UK, which may have damaged the antigen binding site. Nonetheless, this previously published antibody did not yield robust myelin staining in my assays.

I also trialled a commercially available antibody with known reactivity against rat, mouse and human orthologues of MBP. Zebrafish mbpa and mbpb share very little homology with mammalian Mbp, with just 36.64% similarity between mbpa and the Mbp fragment used to generate this antibody. Accordingly, this yielded weak staining of myelin-associates structures in the zebrafish, but with significant background noise due to the high laser power and exposure times need to visualise this signal, making quantification near impossible. As such, this antibody was also not suitable for assessment of myelin structures in zebrafish embryos.

In lieu of a suitable antibody, different transgenic reporter lines may provide a solution, such as the use of fluorescent-tagged fusion proteins. In these reporter lines, expression vectors containing cDNA of a relevant gene sequence fused to the sequence encoding a fluorescent reporter are used to visualise the protein of interest directly tagged by fluorescence (Weber and Köster, 2013). To my knowledge, an mbpa-fusion protein reporter is not yet available in zebrafish, but the tools are widely available. Alternatively, use of a *Tg(mbpa:GFP-CAAX)* transgenic – which labels the membranes rather than cytoplasm of oligodendrocytes – may better allow visualisation of myelin structure, as this labels the large, highly wrapped oligodendrocyte projections, which are only partly captured by the cytoplasmic mbpa:GFP reporter alone (Almeida *et al.*, 2011). As such, future work should seek to cross these transgenic lines with the *rnaset2* mutants to further elucidate the true changes in myelin structure throughout embryonic to adult stages.

One final tool which could be explored to investigate *rnaset2* myelin structure is transmission electron microscopy (TEM). This methodology is widely used to assess myelin structure in zebrafish and has highlighted potential mechanisms of remyelination in a variety of screens (Brösamle and Halpern, 2002; Münzel *et al.*, 2014). TEM can allow visualisation of the percentage of myelinated axons, the thickness of individual sheaths and degree of myelin compaction – a level of detail beyond that which can be observed in the transgenic lines described above.

Therefore, there is a great deal of future work required to understand the relevance of *rnaset2* mutant myelin abnormalities, and the potential relevance of this to the human disease.

3.4.2 rnaset2 mutants display a complex repertoire of behavioural changes

Both neuroinflammation and myelin abnormalities may cause behavioural deficits. The present study demonstrates that *rnaset2* mutants are hypoactive through embryonic and juvenile ages from 8dpf – the age at which myelin-abnormalities and upregulation of the antiviral response emerge in this model (Hamilton et al., 2020a). This is in alignment with previous literature, which has demonstrated a small but significant reduction in *rnaset2* mutant locomotion relative to wild types at 5dpf (Hamilton et al., 2020a). Additionally, *rnaset2* mutants displayed an enhanced startle response to auditory stimuli in larval stages, which may be indicative of abnormal learning or memory in this model. As such, *rnaset2* mutant zebrafish recapitulate many of the behavioural phenotypes reported in human patients, which may be used for the assessment of potential therapies in this model.

3.4.2.1 rnaset2 mutant larvae show increased responsiveness to auditory startle stimuli

One of the principal functions of myelination in the CNS is to increase the speed and efficiency of action potential propagation, essential for co-ordination of sensorineural information and motor output (Waxman, 1980). The assessment of primitive reflex behaviours – particularly, simple motor outputs in response to external stimuli – can therefore be a useful tool to study the functional consequences of myelin disturbances. One such example is the acoustic-startle reflex in the zebrafish, whereby a high-intensity auditory stimulus results in a stereotyped, high velocity "c-bend" response, followed by escape in zebrafish larvae (Kimmel, Patterson and Kimmel, 1974; Zottoli *et al.*, 1995; Madden *et al.*, 2021). This well-characterised behaviour is co-ordinated by the Mauthner cells – a specific set of myelinated reticulospinal neurons originating in the mid- and hindbrain, with projections to the spinal cord which co-ordinate motor output in response to sensory stimuli (Gahtan and O'Malley, 2003; Hale *et al.*, 2016; Madden *et al.*, 2021). These neurons are among the first to be myelinated in zebrafish larvae, around 3dpf (Koudelka *et al.*, 2016). The circuitry underpinning the acoustic-startle behaviour is initiated by action potential conduction along these Mauthner cells throughout the spinal cord (Hale *et al.*, 2016). As such, the latency at which an animal performs the c-startle response can be taken as a proxy for action potential propagation and, accordingly, myelination efficiency – given that myelination is known to speed up conduction velocity along the axon (Waxman, 1980; Madden *et al.*, 2021). Interestingly, the present study did not find any differences in startle latency in *rnaset2* mutants, using an established protocol known to be sensitive to changes in myelination (Madden *et al.*, 2021). As such, it appears that this specific correlate of myelin integrity does not appear to be altered in *rnaset2* mutants – suggesting no functional changes in the myelination of the Mauthner neurons co-ordinating this reflex.

Instead, *rnaset2* mutants showed an increased magnitude of startle response – with significantly increased displacement and distance travelled following a sound stimulus. This finding may indicate more complex changes in the circuitry underpinning the startle reflex, rather than simple changes in action potential propagation along the Mauthner cells. It is notable that, while the Mauthner cells are often considered to be responsible for such escape behaviours, there are multiple reticulospinal neurons which can modulate the response behaviour (O'Malley, Kao and Fetcho, 1996; Liu and Fetcho, 1999). These neurons are thought to be involved particularly in responding to touch stimuli closer to the head, while the Mauthner neuron is essential for responding to tail-directed stimuli (O'Malley, Kao and Fetcho, 1996; Liu and Fetcho, 1999). Together, the combined action of these neurons is responsible for co-ordinating the latency, directionality and velocity of the escape response stimuli (Liu and Fetcho, 1999). In addition, the Mauthner cell circuitry incorporates a series of interneurons – some of which are excitatory and promote Mauthner cell depolarisation, and others which provide inhibitory input to form a negative feedback loop – which themselves modulate the startle response (Hale *et al.*, 2016). Finally, it is possible that the abnormal startle response in *rnaset2* mutants is caused, in part, by sensory neuron dysfunction, as patients with RNASET2-deficient leukodystrophy present with sensorineural deafness which may be attributed to sensory neuron loss (Henneke et al., 2009b; Kameli et al., 2019). As such, it is possible that the increased displacement by the *rnaset2* mutants may be due to subtle alterations in the circuitry between these neurons resulting in an increased response to the auditory stimulus – although the specific neurons affected remain unclear.

Alternatively, the increase in displacement across multiple exposures to loud tones may represent a failure of *rnaset2* mutants to habituate to auditory stimuli. While wild type animals showed a gradual reduction in escape behaviour with each sequential stimuli, *rnaset2* mutants did not begin to show reduced response until later trials, suggesting a delay in habituation (Rankin *et al.*, 2009). Habituation is among the most basic forms of learning – whereby an innate response to a stimulus gradually diminishes following repeated exposure – and has been well characterised in the zebrafish following both acoustic and visual stimuli (Roberts *et al.*, 2011, 2016; López-Schier, 2019). The data presented in this study may suggest an impairment in learning and memory in the *rnaset2* mutant zebrafish. Other models of RNASET2-deficient leukodystrophy have also shown similar changes: both *RNaseT2*$^{-/-}$ rats and *Rnaset2*$^{-/-}$ mice display deficits in episodic learning and memory – with impaired performance in the novel object recognition task during juvenile and adult ages (Sinkevicius *et al.*, 2018; Kettwig *et al.*, 2021). As many patients experience cognitive difficulties, this suggests another aspect of RNASET2-deficient pathology which may be conserved in the zebrafish.

It must be noted that the current study was not designed to assess habituation response, and all analyses here are simply exploratory. Literature has suggested that the optimal auditory stimuli for eliciting habituation have lower frequencies and longer durations than the tones used in this experiment (Beppi, Straumann and Bögli, 2021). Nonetheless, this data suggest that learning and memory phenotypes should be further explored in *rnaset2* mutants.

3.4.2.2 rnaset2 mutants are hypoactive during free swimming

In addition to their abnormal startle response, *rnaset2* mutants showed significantly reduced free swimming activity at 8dpf and 4wpf – consistent with previous observations (Hamilton et al., 2020a).

One potential explanation for this reduced locomotion may be due to developmental delay. Developmental delays have been reported in several zebrafish mutants – modelling disorders from cancer to learning disability – resulting in reduced swimming activity in some instances (Elabd *et al.*, 2019; Jia *et al.*, 2020; Jones, Renshaw and Barry, 2024). Behavioural phenotypes of larval zebrafish are highly dependent on age, with 6dpf larvae swimming up to twice as far as 5dpf animals in the same conditions (Padilla *et al.*, 2011). As such, any delays in the neurodevelopment of *rnaset2* mutants may account for reduced larval swimming. Indeed, some patients with RNASET2-deficient leukodystrophy also experience psychomotor delays (Kameli *et al.*, 2019). However, no overt changes in *rnaset2* mutant development have been reported thus far (including hatching behaviour, length or head size), although these have not been formally characterised. Similarly, the magnitude of the *rnaset2* swimming deficit seems to only increase at 4wpf, whereby *rnaset2* mutants swim only half as far as wild type controls, compared with the relatively modest reduction at 8dpf. As such, future work may be needed to explore potential delays in the neurodevelopment of *rnaset2* mutant larvae.

Alternatively, hypoactivity may reflect general sickness behaviour in *rnaset2* mutants. Sickness behaviour is a subset of behavioural changes associated with lethargy, anxiety and mood, and reduced physiological functioning (such as movement or food intake) which has now been robustly associated with activation of the immune system and, subsequently, inflammation (Lasselin, 2021). Accordingly, immune challenge – particularly viral infection – has been found to induce sickness behaviour-like reductions in swimming activity, alongside reduced exploratory and social behaviours, in zebrafish (Kirsten *et al.*, 2018; Mojzesz *et al.*, 2021; Maleski *et al.*, 2022). This immune-behavioural interaction has been suggested to be mediated by pro-inflammatory cytokines, released either from peripheral immune cells or activated microglia. As such, it is possible that the behavioural deficits demonstrated

in this study are mediated by the aberrant antiviral response in the brain, suggesting targeting of neuroimmune pathways may be beneficial in this model.

3.4.3 Antiviral response in rnaset2 mutants unlikely to be driven by either environmental pathogens or the endogenous retrovirus zferv1a

Elevated antiviral response is one of the most prominent hallmarks of RNASET2-deficient leukodystrophy. The data described in this study align with clinical criteria, in that the onset of interferon response did not correlate with environmental viral infection, and therefore do not support the hypothesis that *rnaset2* mutant antiviral response is modulated by pathogen exposure (Henneke et al., 2009b). Furthermore, despite some clinical success of reverse transcriptase inhibitors in similar interferonopathies, the present study does not support the hypothesis that ERV transcripts are upregulated in *rnaset2* mutants, or that antiviral signalling is triggered by activation of *zferv1a* in this model. As such, the downstream mechanism by which RNASET2 mutations cause activation of the antiviral response requires further investigation in patients and animal models.

3.4.3.1 Limited effect of environment on antiviral response

Unlike rodent models of disease, the environment in which zebrafish are reared may lend itself more to human conditions – where the aquatic environment may result in low level viral exposure throughout the life of the animal, similar to those patients may encounter (Balla *et al.*, 2020; Rutherford, Kasher and Hamilton, 2021). Previous work has highlighted the potential impact of asymptomatic, low virulence viral infection in triggering pathology in genetically susceptible individuals (van den Pol, 2009). As such, this work sought to modulate environmental exposure to viral stimuli present in the aquatic environment – utilising the zebrafish picornavirus-like pathogen ZfPV, known to be present in the aquaria at the University of Sheffield (IDEXX BioAnalytics Health Report, unpublished).

The current study sought to alter viral burden in larvae by sterile rearing (where embryos were bleached and raised in autoclaved E3) or by adding purified gut extract, as had been previously published (Balla *et al.*, 2020). However, this experimental paradigm did not reliably alter levels of detectable viral transcript. Although no viral transcript was detected in any of the bleached groups in this study – suggesting sterile raising may be effective in limiting viral exposure – ZfPV was not consistently detected in conventionally reared animals as might have been expected from previous studies. Similarly, the addition of purified gut extract did not appear to elevate viral load. As such, it has hard to draw conclusions about the mode of ZfPV infection, or its presence in aquarium water or adult faeces.

It is interesting that the extent of viral burden was so highly variable between larvae within each condition. It is notable that the same stock of E3 and aquarium water was used to raise larvae across all three repeats, while the gut samples were obtained from different fish for each repeat (three adult fish per repeat, all selected from the same aquarium). As such, one might expect the wild type and *rnaset2* within each repeat to have comparable levels of viral burden – yet this is not the case. There are several possible explanations for this. The first is a technical explanation: it is possible that the ZfPV primers themselves were unreliable. Indeed, I was unable to establish a protocol for the use of these primers for qRT-PCR (as had been previously published) despite multiple rounds of optimisation. However, for each of the technical repeats per condition, band intensity was highly similar, giving some confidence to the reliability of these primers. Secondly, it is possible that transmission of viral infection itself was highly variable. In the most recent health report from the University of Sheffield, detection of viral infection was highly variable even between adult fish taken from each of the aquariums – suggesting variable transmission of this pathogen is possible. Similarly, analysis of RNA sequencing datasets from around the world found observable ZfPV infection in only 22% of intestinal samples (Balla *et al.*, 2020). Little is known about ZfPV virulence or mode of infection – as such, it is possible that additional factors may affect viral burden that are not yet understood. Therefore, this experimental paradigm was not able to reliably alter viral infection as had been previously published.

Nonetheless, when assessing the impact of viral burden regardless of experimental condition, a significant positive correlation was observed between ZfPV transcript level and *isg15* expression for wild type animals – suggesting that viral burden may trigger a mild antiviral response in healthy larvae. Yet, such a correlation was not observed in the *rnaset2* mutants – suggesting their antiviral response may not be modulated by ZfPV infection.

However, it must be noted that ZfPV is just one virus known to affect the zebrafish: there may well be others which interact to drive antiviral response in a complex manner. There are few known naturally occurring viruses affecting zebrafish (particularly those housed in aquaria) – in fact, two viruses are widely employed by commercial diagnostic tests: ZfPV and infectious spleen and kidney necrosis virus (ISKNV) (IDEXX BioAnalytics health report, unpublished). However, ISKNV is known to cause serious disease phenotypes (including lethargy, loss of appetite, abnormal swimming and even respiratory distress), meaning asymptomatic infection is perhaps unlikely in our model (Bermúdez *et al.*, 2018). Additionally, ISKNV was not detected in any of the aquaria at the University of Sheffield during the most recent health screening (IDEXX BioAnalytics health report, unpublished). Nonetheless, the

possibility remains that viruses yet to be identified may contribute to antiviral response in a manner that could not be observed by the current study.

Finally, it is also notable that *isg15* is just one interferon-stimulated gene, of which several have been reported to be upregulated in *rnaset2* mutants, including *mxa* and *ifnΦ1* (Hamilton et al., 2020a). As such, the current study provides only a snapshot of the immune response to environmental stimuli. Therefore, the full extent of the impact of environmental modulation of the microbiome on antiviral response remains unclear until a panel of interferon-stimulated genes are assessed in this paradigm.

Together, this data provides only limited insights into the impact of environmental viral exposure on *rnaset2* antiviral response and must be interpreted with caution. Nonetheless, these findings may suggest exogenous viral infection is unlikely to be the sole cause of upregulation of *isg15* response, and that exploration of endogenous triggers of pathology warrants further consideration.

3.4.3.2 The contribution of endogenous retroviruses to rnaset2 pathogenesis is unclear

As previously discussed, the *rnaset2* mutant zebrafish has emerged as a leading model of interferonopathy, and so provides a valuable system with which to probe the impact of ERVs in this disorder. Multiple ERVs have now been identified in the zebrafish – named *zferv1–7* – with only two of these sequences appearing to encode functional proteins: *zferv1a* and *zferv1b* (Rutherford *et al.*, 2022).

In situ hybridisation against *zferv1a* and *zferv1b* transcripts revealed expression in the brain, spinal cord and thymus of wild type zebrafish embryos, suggesting that these ERVs are actively transcribed in the central nervous system and immune organs. While it should be noted that there was some observable signal in the thymus of animals labelled with the *env1a* sense strand (albeit not to the same intensity as sense labelling), this signal may arise from bidirectional expression of the *zferv1* sequence, which has previously been reported for human ERVs inducible by chemotherapy (Chiappinelli *et al.*, 2015). Furthermore, this expression pattern has been subsequently validated through the creation of a transgenic reporter line for *zferv1a* – which also showed *zferv1a* expression in the brain, spinal cord and thymus (Rutherford *et al.*, 2022). This transgenic reporter even allowed visualization of *zferv1a* expression in individual neurons in the optic tectum and spinal cord – providing further support that ERVs are active in the zebrafish central nervous system during embryonic stages. Together, these data demonstrate the utility of the zebrafish as a model system for studying ERVs *in vivo*.

However, despite the hypothesis that uncontrolled ERV transcription may trigger the antiviral response in several neurological interferonopathies, this study did not identify any upregulation of *zferv1a* expression in the heads of *rnaset2* mutants (Crow, Shetty and Livingston, 2020; Rutherford, Kasher and Hamilton, 2021). It must be considered that *zferv1a* is not the only ERV to be identified in the zebrafish – a total of eight zferv have been identified in the zebrafish genome, with only *zferv1a* and *zferv1b* known to encode fully functional ERVs without significant frameshifts, deletions or insertions to the genome (Rutherford *et al.*, 2022). The current study focussed on *zferv1a*, as in situ hybridisation revealed the strongest expression of this ERV in the brains of wild type animals at 3- and 5dpf relative to *zferv1b*. However, it is still possible that *zferv1b*, or degenerated fragments of *zferv2–7*, may trigger the antiviral response in *rnaset2* mutants. Similarly, *zferv1–7* were identified based on homology with the original *zferv* transcript and, as such, other entirely distinct ERVs may be active in *rnaset2* mutants. Moreover, the *zferv1–7* sequences were retrieved from the most recent reference genome (GRCz11), which uses the Tübingen strain, while the *rnaset2* mutants in this study had a nacre background. Strain-specific differences in ERVs have been reported and, as such, the ERV profile of *rnaset2* nacre animals may not be fully characterised (Elmer and Ferguson-Smith, 2020). As such, more detailed characterisation of the expression of further ERVs may be necessary to fully conclude that these do not interact with RNASET2-deficient pathology – nonetheless, this study did not find any evidence for their upregulation in *rnaset2* mutants during larval stages.

3.4.3.3 Other potential triggers of rnaset2 antiviral response

If neither environmental pathogenesis, nor endogenous retroelements, act as triggers for the antiviral response in *rnaset2* mutants, this raises the question – what drives aberrant interferon signalling in rnaset2-deficient animals?

RNASET2 is a lysosomal hydrolase, thought to be required for normal lysosomal functions including autophagy and phagocytosis (Campomenosi et al., 2006; Lübke, Lobel and Sleat, 2009; Haud et al., 2011b). Accordingly, functioning RNASET2 has been demonstrated to co-localise with lysosomes in human cell lines, while patient-associated mutations have been shown to be retained within the endoplasmic reticulum (Haud et al., 2011b). In the original *rnaset2*^{AO127} mutant zebrafish, enlarged lysosomes are apparent throughout the brain (but not outside the CNS), each containing ribosomal RNA (rRNA) aggregates (Haud et al., 2011b). Subsequent work has demonstrated a bottleneck of apoptotic cell clearance by microglia in *rnaset2* mutant zebrafish, thereby raising the possibility that these rRNA-filled lysosomes may accumulate with other cell debris in these phagocytic cells and trigger downstream inflammation (Hamilton et al., 2020a).

Most host rRNAs lack the key molecular features needed to trigger antiviral pathways – 28S and 18S rRNAs lack an uncapped 5'-diphosphate, while 5S rRNA contains a heavily methylated 5'-trisphosphate group which is thought to prevent RIG-I activation – and are therefore considered immunologically silent (Ren *et al.*, 2019; Rehwinkel and Gack, 2020). However, emerging evidence has suggested that 5S rRNA can bind to antiviral receptors and trigger interferon response in some circumstances, including the presence of DNA viruses (Chiang *et al.*, 2018). As such, the immunostimulatory effects of rRNA remain unclear in the context of RNASET2-deficient leukodystrophy.

Nonetheless, with their accumulation of undigested substrates and role as orchestrators of the brain's antiviral response current literature points towards a central role for microglia in RNASET2-deficient pathogenesis, independent of the specific antiviral trigger (Hickman et al., 2018a; Hatton and Duncan, 2019b; Hamilton et al., 2020a; O'Brien, Bennett and Bennett, 2022).

3.4.4 Depletion of endogenous microglia impairs survival outcomes in rnaset2 mutants

The current study, along with previous literature, has demonstrated that knockout of interferon regulatory factor-8 *(irf8)* results in transient depletion of endogenous microglia in zebrafish embryos (Hamilton et al., 2020a). This strategy induced robust reductions in microglia number at 5- and 8dpf, with minimal changes in microglia density at 1 year of age. Despite the transient nature of microglia depletion, *irf8* knockdown reduced survival of *rnaset2* mutants relative to non-depleted controls in both embryonic and adult stages. As such, these data support the hypothesis that *rnaset2* pathology is driven by a loss of homeostatic function in microglia, rather than toxic gain-of-function, and suggest that microglia – although dysfunctional – are still protective to an extent in *rnaset2*-deficient pathology (Hamilton et al., 2020a).

3.4.4.1 CRISPR/Cas9 targeting of irf8 depletes embryonic microglia, with unknown impact on the adult population

The transcription factor *irf8* is required for the development of embryonic macrophages and microglia through primitive and transient definitive haematopoiesis but is not required for by the adult microglial population which is derived from adult-phase definitive haematopoiesis (Li *et al.*, 2012; Shiau *et al.*, 2015). Accordingly, we hypothesised that targeting *irf8* expression with CRISPR/Cas9 genome editing would ablate embryonic but not adult microglia.

Previous work has demonstrated that the single-cell injection of a single *irf8*-targeting guide resulted in complete depletion of microglia in 50% of embryos at 5dpf (Hamilton et al., 2020a). In the current study, I demonstrated that injection of paired *irf8*-targeting guides increased the efficiency of this

depletion in wild type animals, with over 80% of embryos having no visible mpeg1:mCherry-positive cells in the brain as validated by live screening of 5dpf embryos. Immunohistochemistry validated this approach in *rnaset2* mutants, which also showed significant reductions in microglia number at 5- and 8dpf when injected with *irf8*-targetting guides.

In adult animals, published literature has demonstrated a complete lack of microglia up to 1–3mpf in stable *irf8*$^{-/-}$ mutants, with a reduction – but not complete absence – of microglia at 4–8mpf (Shiau *et al.*, 2015; Earley, Graves and Shiau, 2018; Rovira *et al.*, 2024). In the current study, immunohistochemistry of sagittal brain sections failed to reveal robust differences in the number or density of microglia in *irf8* crRNA-injected adults or non-injected controls at 1-year post-fertilisation. However, the findings of this experiment must be interpreted cautiously for several reasons. Firstly, small sample sizes prevented statistical analysis of microglia number or density in this study. Secondly, the animals used for this assay were injected with a single *irf8* guide (before the optimisation of the paired guide approach), and so may not reflect the most robust knockdown of *irf8*. Additionally, microglial distribution was assessed only at a single time point when animals were relatively mature adults, which may fail to capture differences in microglial dynamics throughout development. Finally, the section-based immunohistochemistry used for this experiment assesses microglia density in only a very small area of the brain – just 5µm thick. While anatomical landmarks were used to make sure sections were taken from similar brain regions between animals, it is impossible to ensure that identical areas were sampled from each fish, and that this single section reflected the number of cells within the whole brain. This may explain some of the intra-group variability in cell number and density seem in this study. As such, further experiments will be needed to assess microglia number in the whole brain at multiple ages to truly assess the effect of *irf8* knockdown throughout zebrafish development.

3.4.4.2 Embryonic microglia depletion impairs rnaset2 mutant survival in larval and adult animals

A failure of *rnaset2* microglia to clear apoptotic cells during development is thought to be one of the principal triggers of pathology in this model of leukodystrophy (Hamilton et al., 2020a). Depletion of microglia in mutants by knockout of *irf8* does not change the number of apoptotic cells in embryonic brains at 5dpf, suggesting *rnaset2* mutant microglia are entirely deficient in their ability to digest apoptotic cells. However, as mutant microglia become gradually engorged by apoptotic cells, it is possible their homeostasis is impaired, such that they may adopt an ultimately neurotoxic function or DAM-like state. Indeed, toxic gain-of-function has been reported in microglia across several neurodegenerative disorders, including multiple sclerosis and other leukodystrophies (Chitu *et al.*, 2015, 2020; Guerrero and Sicotte, 2020). Depletion of microglia by targeting Irf8 has even shown to

improve survival and delay onset of neurological impairments – albeit only mildly – in a mouse model of the lysosomal storage leukodystrophy, Niemann Pick Type C (Cougnoux *et al.*, 2018). Hence, the current study sought to assess the impact of transient microglia depletion on early survival of *rnaset2* mutants.

Depletion of embryonic microglia led to significant decreases in survival in *rnaset2* mutants during both embryonic and adult stages. This difference is perhaps most striking in adulthood, where both microglia-depleted wild type and *rnaset2* mutants survive more poorly than non-depleted siblings. The effects of microglia-depletion are more difficult to assess in larvae, due to poor survival of the non-depleted wild-type group: nonetheless, microglia-depleted *rnaset2* mutants survived significantly worse than non-depleted controls. As such, this suggests that a lack of embryonic microglia has lifelong effects on the overall health of zebrafish, regardless of genotype, and that the presence of microglia – even in their dysfunctional state – has benefits in *rnaset2* mutants.

There are several potential explanations for the deleterious effects of microglial depletion on long-term survival outcomes in our model. The first could be due to accumulation of uncleared debris following developmental apoptosis in the embryonic brain. We have previously demonstrated that depletion of microglia leads to significant increases in the number of uncleared apoptotic cells in the parenchyma of wild type embryos (Hamilton et al., 2020a). While microglia depletion does not increase the overall number of apoptotic bodies in *rnaset2* embryos, the location of these dying cells is changed after microglia-depletion, with apoptotic debris no longer contained within microglia but instead within the parenchyma (Hamilton et al., 2020a). As such, increased uncontained apoptotic debris in the brain may trigger further neuroinflammation during development in both microglia-depleted wild type and *rnaset2* embryos, which may cause lifelong changes to neurological health. Similarly, increased numbers of apoptotic cells "free" in the parenchyma may drive infiltration of other immune cells at later developmental stages. As previously discussed, increased brain apoptosis is one of the key drivers of immune cell infiltration into the brain (Casano, Albert and Peri, 2016a; Xu et al., 2016; Hamilton et al., 2020a). Studies of microglial depletion in viral infection models have reported increased monocyte/macrophage infiltration into the brain, which coincided with increased viral load, poorer survival outcomes and elevated interferon signalling (Wheeler *et al.*, 2018). Therefore, microglial depletion – and the corresponding increase in apoptotic debris in the brain – may trigger the arrival of peripheral immune cells into the CNS and drive a further inflammatory response, contributing to reduced survival in our model.

Alternatively, the decreased survival of *rnaset2* mutants after microglial depletion may be contributed by the role of these cells in de- and remyelination. In a variety of models, microglial depletion has been shown to increase demyelination and reduce remyelination in adults, alongside reduced numbers of oligodendrocytes, relative to untreated controls (Sariol *et al.*, 2020; McNamara *et al.*, 2023). RNA sequencing of isolated microglia after viral infection suggests these cells upregulate factors linked to remyelination, including upregulation of genes needed for uptake and clearance of myelin debris, and those needed for oligodendrocyte maturation and proliferation (Sariol *et al.*, 2020). Similarly, lack of microglia during development has been shown to result in myelin abnormalities, including out-folding, unravelling and impaired myelin compaction (McNamara *et al.*, 2023). As such, this data may reflect the complexity of interactions between glial cell types and suggests a variety of mechanisms by which microglial depletion – even transiently – could influence survival in our model.

However, it must be noted that *irf8* is essential for the development of both microglia and macrophages, meaning that *irf8* crispants used in this study are not only microglia-depleted, but also have reduced numbers of macrophages (Li et al., 2011b). Depletion of macrophages could have a multitude of effects independent of microglia function, including reduced tissue repair, impaired cardiac development or blunted infection control (Bruton *et al.*, 2022; Speirs *et al.*, 2024; Zhao *et al.*, 2024). As such, future work may also seek to explore the role of peripheral macrophages in *rnaset2* mutant pathology, and whether these may contribute to the survival phenotypes observed in the current study.

3.4.4.3 Survival of the current generation of rnaset2 mutants is not significantly impaired relative to wild type controls

One notable finding from the microglial-depletion survival analysis in this study was the lack of significant difference between survival of non-depleted *rnaset2* mutants relative to wild type controls. This is in direct opposition with previous findings from our lab, which have demonstrated a severe reduction in survival of *rnaset2* mutants, whereby only 10% of mutants survived to 9 months post-fertilisation compared with 100% wild type survival. As such, I sought to repeat the survival analysis of *rnaset2* mutants using the current generation.

Quantification of survival up to 1-year post-fertilisation revealed no significant difference in between the current generation of *rnaset2* mutants and wild type controls. The data may show a trend towards poorer survival of *rnaset2* mutants from ~20wpf; however, this was not a vast nor significant difference. It is possible that the survival phenotype of *rnaset2* mutants is somewhat masked by the poorer-than-expected survival of wild type controls in this study, whereby only ~80% wild type animals

showed event-free survival at just 8wpf, and 74% by 52wpf. This contrasts with the 100% survival of wild type animals previously reported (Hamilton et al., 2020a). This may be explained by a failure of the light cycling software in the Bateson Centre aquarium in which fish were raised, resulting in fish being exposed to constant light for weeks at a time at points throughout this survival analysis. Previous studies have demonstrated that rearing zebrafish in constant white light can lead to reduced length and weight, increased malformations and impaired survival relative to those raised under alternating light-dark cycles (Villamizar *et al.*, 2014). However, if lighting conditions were driving a survival phenotype in wild type animals, one might expect a similar or even greater reduction in survival in *rnaset2* mutants, which was not robustly observed.

Alternatively, it is possible the differences in survival between *rnaset2* mutants used in this study and those used in our 2020 publication are due to genetic compensation in the subsequent generations. There are multiple published examples of zebrafish mutants whereby stable generations lose phenotypes previously observed in the original crispant generation (carrying mosaic mutations induced by CRISPR/Cas9-mediated targeting of a given gene) (El-Brolosy and Stainier, 2017; She *et al.*, 2019; Buglo *et al.*, 2020; Rouf *et al.*, 2023). However, this is less likely to occur in multiple generations of a stable line, as was used in the 2020 publication through to the current study. Similarly, the current generation of *rnaset2* mutants show conservation of other disease-associated phenotypes, such as hypoactivity in larval stages and upregulated antiviral response genes (such as *isg15*). Nonetheless, these data suggest that survival phenotypes are variable in *rnaset2* mutants, and that the only robust impairments in survival observed thus far are those of microglia-depleted animals in both wild type and *rnaset2* mutant backgrounds.

3.4.5 Chapter summary

The data presented in this chapter build upon previously published characterisation of the *rnaset2* mutant zebrafish and further demonstrate the validity of this model for the study of leukodystrophy (Haud et al., 2011b; Hamilton et al., 2020a). Similar to those seen in patients, *rnaset2* mutants present with myelin abnormalities during development, alongside impaired motor function and learning behaviours. Investigation of the antiviral response in this model failed to identify a clear trigger for interferonopathy in zebrafish larvae. However, depletion of microglia – key mediators of the antiviral response in the brain – led to poorer survival outcomes, suggesting an essential role for the neuroimmune response in limiting pathology *rnaset2* mutants. As such, these findings suggest that therapeutic interventions which aim to restore microglial function may have benefits in RNASET2-deficient leukodystrophy and identify numerous assays that could be used to assess the impact of potential treatments in *rnaset2* mutants.

Chapter 4. Macrophage transplantation is an effective strategy for the replacement of microglia

4.1 Introduction

4.1.1 Microglial dysfunction is among the earliest drivers of pathology in rnaset2 zebrafish

Neuroinflammation is the most consistently reported finding across animal models of, and patients with, RNASET2-deficient leukodystrophy. Many patients with RNASET2-deficient leukodystrophy exhibit variable upregulation of the antiviral response– particularly the type 1 interferon response – resulting in clinical manifestations which mimic CMV infection (Henneke et al., 2009a; Tonduti et al., 2016a; Garau et al., 2019). Our group and others have demonstrated that animal models of RNASET2-deficient leukodystrophy are characterised by widespread neuroinflammation, with literature suggesting that impairments of microglial function may emerge as the first signs of pathology (Haud et al., 2011b; Sinkevicius et al., 2018; Hamilton et al., 2020a; Weber et al., 2020; Kettwig et al., 2021).

In the *rnaset2* mutant zebrafish, loss of microglial homeostatic function during development is thought to be a key trigger of pathogenesis (Hamilton *et al.*, 2020a). In *rnaset2* mutants, microglia are unable to clear the apoptotic cells which accumulate during development, instead adopting a highly bloated, ameboid morphology. Strikingly, depletion of microglia by targeting of the transcription factor *irf8* does not affect the number of uncleared apoptotic bodies in the brains of *rnaset2* embryos, phenocopying this aspect of the pathology and suggesting that *rnaset2*-deficient microglia are unable digest apoptotic debris. However, subsequent work (presented here in Chapter 3) has revealed that depletion of microglia by this strategy may impair survival in *rnaset2* mutants throughout embryonic and adult stages. As such, these data suggest that *rnaset2* microglia retain some beneficial effects on neuropathology and are unlikely to adopt a toxic gain-of-function in this model. Therefore, current literature indicates that it is the inability of *rnaset2* mutant microglia to undertake homeostatic functions (including clearance of apoptotic debris) which may contribute to *rnaset2* pathology, and that therapeutic strategies should seek to enhance microglial function, rather than depleting these cells.

4.1.2 Therapeutic strategies to target microglia in leukodystrophies

There is growing evidence for the role of microglia in the pathogenesis of leukodystrophies and, accordingly, there are several therapies in development that target these glial cells (see Table 1.1). While pharmacological approaches are showing some promise in targeting microglia, HSCT remains the most widely employed clinical intervention in the leukodystrophies and is thought to act via the

replacement or supplementation of diseased microglia with competent donor-derived cells (Krivit, 1995; Priller *et al.*, 2001; Asheuer *et al.*, 2004; Yamada *et al.*, 2004; Schönberger *et al.*, 2007; Cronk *et al.*, 2018). However, there remain several limitations of HSCT which are thought to limit its efficacy – most notably, the delay between transplantation and the first signs of any clinical stabilisation (Page *et al.*, 2019). This delay is attributed to the time needed for donor cells to populate the haematopoietic niche, before HSCs give rise to non-proliferative blood monocytes, which can later differentiate into macrophages and, in some conditions, microglia (Sieweke and Allen, 2013; Cronk *et al.*, 2018). Until donor cells arrive in the brain, many patients experience continued degeneration which, in the context of rapidly progressive paediatric disorders such as leukodystrophies, can result in devastating and irreversible disability. Thus, there is a need for an intervention which can effectively and quickly replace microglia to prevent further deterioration of these patients.

Rather than HSCT, transplantation of monocytes or macrophages themselves may represent a more direct means of microglial replacement (Sieweke and Allen, 2013; Cronk *et al.*, 2018). Following transplantation, literature has demonstrated that macrophages are able to infiltrate the CNS, respond to local cues and adopt a microglia-like phenotype (Suzuki *et al.*, 2014; Haideri *et al.*, 2017; Cronk *et al.*, 2018). Accordingly, in one model of a rare childhood-onset leukodystrophy linked to ALSP, transplanted monocytes were able to engraft into the brain parenchyma and express microglial markers in *Csf1r*$^{-/-}$ mice – however, the ability of these cells to rescue pathology was not investigated (Bennett *et al.*, 2018). As such, macrophage transplantation may present a valuable therapeutic intervention in RNASET2-deficient leukodystrophy and warrants investigation in the leading animal model of this disorder: the *rnaset2* mutant zebrafish.

4.1.3 Preliminary data: Macrophage transplantation can replace microglia in wild type zebrafish embryos

Before macrophage transplantation can be explored in zebrafish models of disease, a greater understanding of the ability of transplant-derived cells to give rise to microglia is needed in wild type hosts. As such, preliminary work (collected and assessed during my MSc project, now published in Rutherford *et al.,* 2024) sought to investigate whether macrophage transplantation was a viable approach for microglial transplantation.

Firstly, this preliminary work assessed the ability of transplant-derived macrophages to engraft within host brains, relative to traditional HSCT. This study compared the engraftment of three potential grafts: adult macrophages (isolated from the WKM of *Tg(fms:GFP)* adult donors, which have macrophages labelled with GFP), embryonic macrophages (obtained by dissociation of whole *Tg(fms:GFP)* larvae),

and adult HSCs (isolated from WKM of *Tg(CD41:GFP)* adult donors, with have HSCs labelled with GFP). Live screening of transplant-derived cell engraftment at 5dpf revealed that adult macrophages were more efficient in reaching host brains relative to CD41-positive HSCs (Figure 4.1a–d). This is likely due to the greater time needed for HSCs to engraft in the caudal haematopoietic tissue (CHT), before differentiating into macrophages and ultimately reaching the brain – suggesting macrophage transplantation may be beneficial for rapid brain engraftment. Interestingly, brain engraftment was much poorer following transplantation of embryonic, rather than adult, macrophages (Figure 4.1e,f) – suggesting that WKM-derived adult macrophages may be the optimal graft for immune cell replacement in wild type embryos.

Further characterisation of transplanted WKM-macrophages revealed that these cells can differentiate into microglia in zebrafish larvae. We showed that transplanted macrophages were able to engraft and divide in embryonic brains (Figure 4.2a,b). Following engraftment, transplanted macrophages were able to differentiate into microglia-like cells – adopting a highly branched morphology and expressing microglia-specific markers (Figure 4.2c). Strikingly, up to 80% of transplant-derived cells expressed the microglia marker 4C4, which is similar to the proportion of endogenous leukocytes which have been shown to express microglia-specific genes in other zebrafish models – suggesting robust integration of transplanted cells into the CNS environment (Rovira *et al.*, 2024).

In order to establish the functionality of transplant-derived cells, we assessed the ability of transplanted cells to clear developmental apoptosis in microglia-depleted animals. Similar to *rnaset2* mutants, microglia-depleted (*irf8* knockout) embryos have elevated numbers of apoptotic cells in the brain at 5dpf due to their lack of microglia to clear these dying neurons (Hamilton *et al.*, 2020b). Despite similar whole body engraftment efficiency, we found that recruitment of transplanted cells to the brain was greater in microglia-depleted animals than their non-injected counterparts (Figure 4.1a, b) – suggesting depletion of the microglial niche may recruit transplanted cells to the brain. Following engraftment, transplanted cells were ultimately able to clear these apoptotic cells in a dose-dependent manner – with embryos with 10 or more engrafted cells showing complete rescue of apoptotic cell number, while those with fewer than 10 engrafted cells showed only partial recovery (Figure 4.2d). As

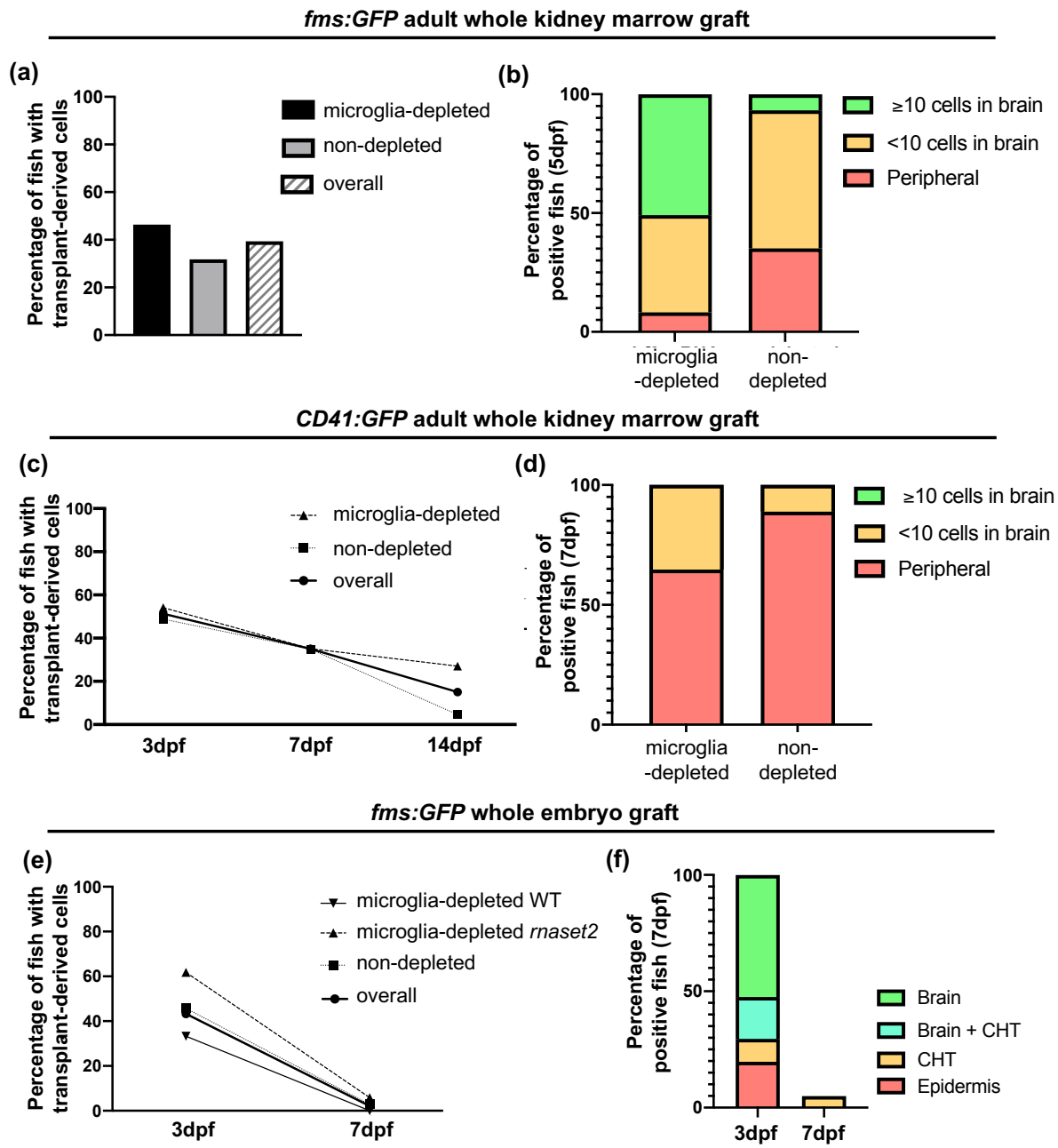

Figure 4.1. Comparison of engraftment efficiency across multiple graft sources.
a, b. Percentage of fish with GFP-positive cells in the body (a) and brain (b) following systemic injection of *fms:GFP* cells from adult whole kidney marrow (*Tg(mpeg:mCherry CAAX)* hosts, 5dpf. 3 biological replicates, n=384–423). **c, d.** Percentage of fish with GFP-positive cells in the body (c) and brain (d) following systemic injection of *CD41:GFP* cells from adult whole kidney marrow (*Tg(mpeg:mCherry CAAX)* hosts, 7dpf. 1 biological replicate, n=37–43). **e, f.** Percentage of fish with GFP-positive cells in the body (e) and brain or CHT (f) following systemic injection of *fms:GFP* cells from whole embryo graft (*rnaset2* mutant and wild type sibling hosts, 7dpf. 1 biological replicates, n=34–72). dpf, days post-fertilization. Preliminary data collected during MSc research project, now published in Rutherford *et al.,* 2024.

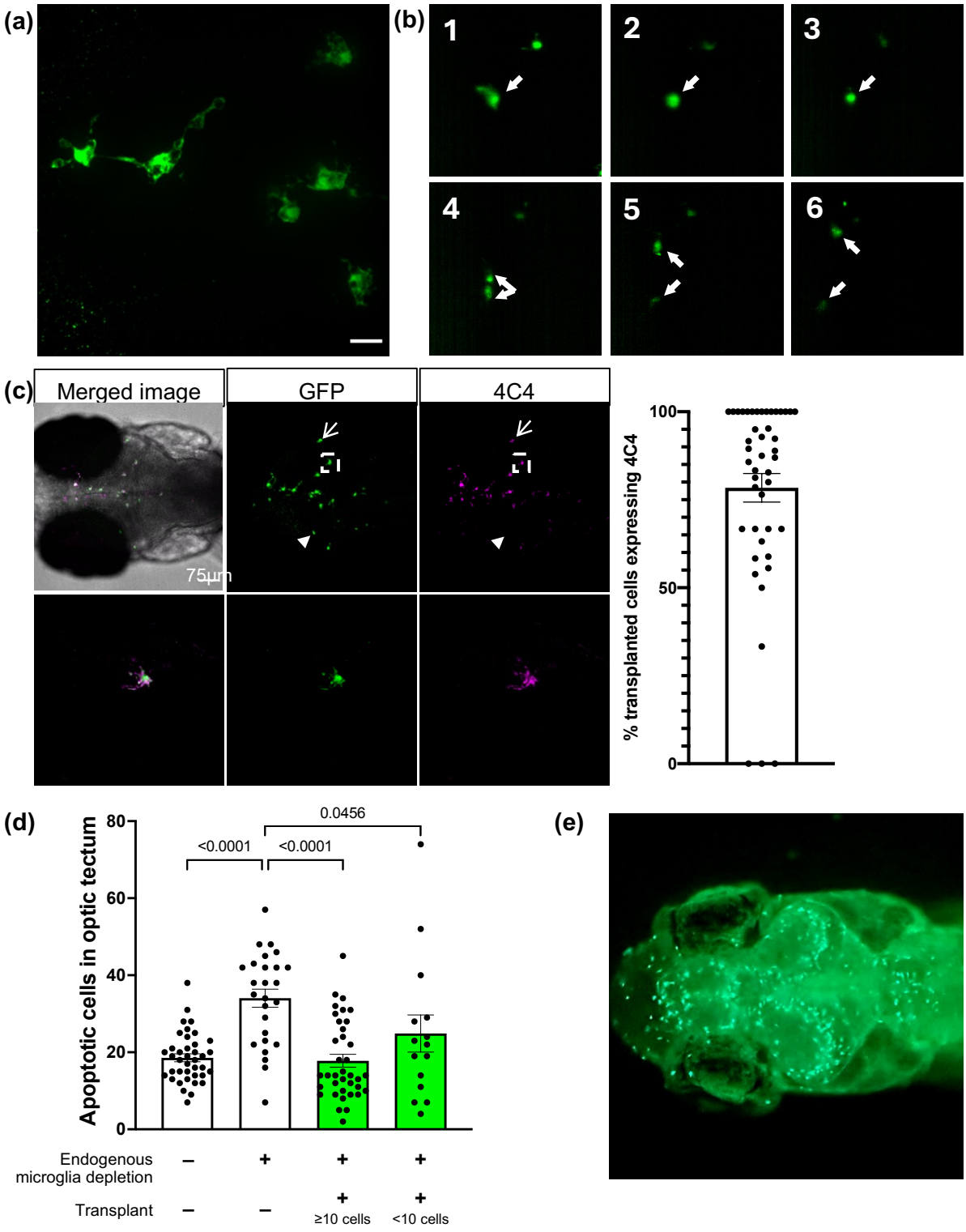

Figure 4.2. Transplanted cells engraft and adopt a microglial phenotype in embryonic brains. **a**. Transplanted cells engraft and adopt a microglia-like morphology in host brains. Scale bar represents 17µm. **b.** Timelapse microscopy reveals that transplanted cells divide within the brain following engraftment (white arrows indicates cell of interest before and after division). **c.** Immunohistochemistry reveals that over 75% of transplanted cells (GFP) express microglia-specific marker 4C4 just three days post-transplant. Pointed arrow indicates cell positive for both GFP and 4C4, closed arrow indicates GFP-positive cell that does not co-localize with 4C4. 40x imaging of the highlighted cell (white box) shows morphology of dual positive cell. 3 biological replicates, n=45. Scale bar represents 75µm. **d.** TUNEL staining reveals that transplantation can rescue the number of

uncleared apoptotic cells in microglia-depleted brains in a dose-dependent manner. Kruskal-Wallis test with Dunn's multiple comparisons. 4 biological replicates, n=15-39. **e.** Transplanted cells persist in the brain until 21dpf. Preliminary data collected during MSc research project, now published in Rutherford *et al.,* 2024.

such, these data suggest transplanted macrophages can functionally replace embryonic microglia up to 5dpf.

Finally, follow-up of hosts revealed that transplanted cells may persist throughout larval stages – with preliminary evidence suggesting the number of transplant-derived cells in the brain increased until at least 21dpf (Figure 4.2e). As such, it is possible that transplant-derived macrophages may replace endogenous microglia throughout development – suggesting it is a worthwhile intervention to explore in *rnaset2* mutant hosts, following further optimisation and characterisation in wild type hosts.

4.2 Hypothesis and aims

Based on the preliminary findings discussed above, I hypothesise that transplantation of WKM-derived macrophages can lead to replacement of endogenous microglia in wild type zebrafish embryos, and that this replacement will persist beyond larval stages. As such, the overarching aim of this chapter is to characterise and quantify repopulation of the microglial population by macrophage transplantation in embryogenesis and adulthood. Within this, I aim to:

1. **Quantify the engraftment dynamics of transplant-derived cells in the days immediately following transplantation.** Preliminary data has demonstrated that transplant-derived cells are present in the brain by 5dpf. However, due to limitations in this preliminary methodology, it is unclear when transplanted cells first infiltrate the brain. Although graft macrophages are GFP-labelled, transient photobleaching during graft preparation (fluorescent-activated cell sorting) prevented visualisation of transplanted cells until approximately 3 days post-transplant (dpt) when GFP-expression is fully restored. As such, although we have observed transplanted cells in the brains of 5dpf embryos, it is not known when these cells first engraft within the brain. Therefore, I aim to further optimise this methodology, and subsequently visualise and quantify transplant-derived cells 1–3 dpt.
2. **Assess the longevity of transplant-derived cells in host brains into adult ages.** Following engraftment in embryonic hosts, it is unclear whether these cells persist in host brains beyond 21dpf and into adulthood. To address this question, there is a need for novel tools to allow the visualisation of transplant-derived cells, and microglia more generally, in adult animals – beyond the age at which zebrafish become opaque. Therefore, I will optimise further methodologies for the imaging of transplant-derived cells and assess the duration of engraftment in host brains at multiple ages.
3. **Further characterise the interactions between transplant-derived and host cells that may influence transplanted cell longevity in the brain.** Preliminary findings have shown that

depletion of embryonic microglia is required to achieve robust engraftment of transplant-derived cells in wild type host brains. However, this depletion approach is thought to be only transient – with embryonic microglia eventually replaced by a distinct wave of adult microglia (Ferrero *et al.*, 2018). Therefore, using the strategies identified in Aim 2, I will characterise the impact of this second wave of host microglia on transplant-derived cell engraftment, and establish whether life-long microglial depletion is necessary for persistent engraftment.

Completion of these objectives will provide a greater understanding of the process by which transplanted cells colonise the brain and allow further assessment of the possible relevance of this protocol to *rnaset2* pathogenesis in subsequent work.

4.3 Results

4.3.1 Transplanted macrophages engraft in host brains within 3 days post-transplantation

Previous work has demonstrated that transplant-derived cells are present in the brain at 5dpf (3dpt). However, assessment of the age at which transplanted cells begin to reach the brain has been limited by transient photobleaching of the GFP-signal by the flow cytometer – whereby the GFP signal of transplanted macrophages is extremely dim after sorting, but gradually recovers in the days following transplant. As such, transient fluorescein-labelling was used to visualise and quantify the number of cells in the days immediately following transplant.

Live imaging revealed that the number of transplant-derived cells per successfully transplanted fish increased almost two-fold from 1 to 3 dpt – suggesting transplanted cells are able to divide within embryonic hosts shortly after transplant (Figure 4.3a). When quantified by region, this increase in the mean number of transplanted cells was greatest in the brain and head (+410.3%), followed by the heart (+117.1%) and CHT (+43.1%) (Figure 4.3b). Notably, the number of cells at the injection site decreased in the days post-transplantation, with no cells visible at the injection site of transplanted animals by 3dpt.

Longitudinal quantification of individual transplanted embryos each day following transplant suggested that fish with more cells engrafted at 1dpt were more likely to have robust engraftment at 3dpt (Figure 4.3c,d). Indeed, correlation analysis confirmed that the number of GFP-positive cells per fish at 1dpt was significantly positively correlated with cell number at 3dpt – both in the whole fish and in the brain ($r=0.6940$ and $r=0.4948$ respectively, Spearman's rank order correlation, $p<0.0001$).

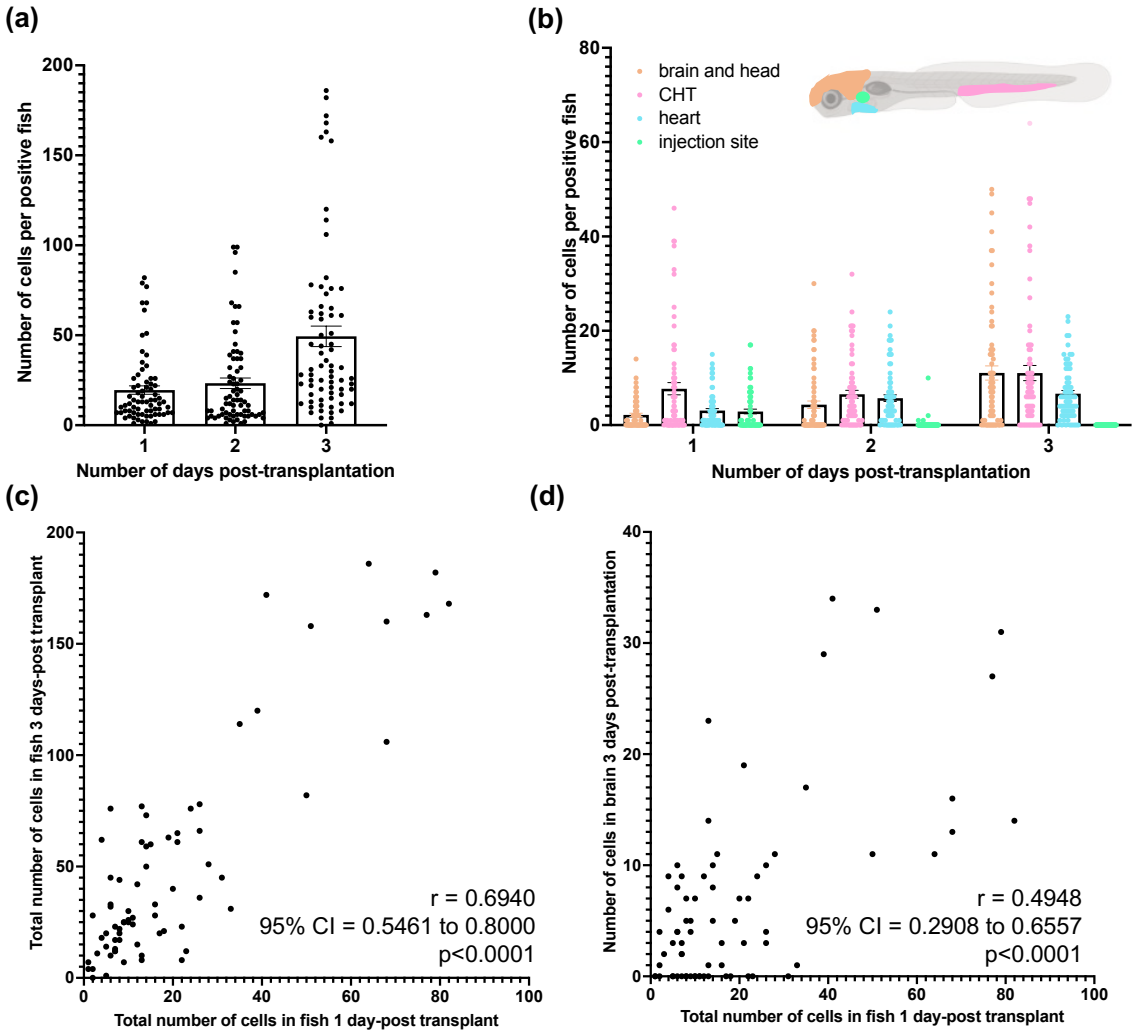

Figure 4.3. Transplanted cells begin to divide and populate the brain within 3 days post-transplantation.

a. Longitudinal imaging of transplanted fish revealed an increase in the total number of transplant-derived cells per positive fish from 1–3 days post-transplantation. **b.** Increases in cell number were observed in the brain and head, CHT and heart, although not at the injection site. **c, d.** The number of positive cells per whole fish at 1 day post-transplant was significantly correlated with number of cells in the whole body (c) and brain (d) at 5dpf. Spearman's rank order correlation, $p<0.0001$. 1 biological replicate, n=72.

This suggests that initial screening just 1dpt could allow selection of well-engrafted animals for raising – providing a useful tool for screening transplanted embryos for future engraftment success.

4.3.2 Transplanted cells do not persist to 1-year post-fertilisation, as quantified on tissue sections

While transplant-derived cells appear to engraft and divide within host brains in embryogenesis, it remains unclear how long these cells may persist within the CNS. Limited imaging evidence of transplanted embryos has revealed that transplant-derived cells are present until a least 21dpf, in numbers greater than those observed at 5dpf – suggesting the initial period of cell division and brain infiltration observed in the first three days following transplantation continues throughout early development. However, quantitative characterisation of transplanted cells has not been performed into adulthood. Hence, I aimed to establish an assay for the screening of transplant-derived cells within adult brains, beginning with a traditional tissue sectioning and immunohistochemistry approach.

4.3.2.1 Establishing an assay for quantification of fms:GFP cells using tissue sectioning and immunohistochemistry

Previous quantification of microglia number in *irf8* crRNA-injected adults and non-injected controls revealed that the olfactory bulb was the most microglia-dense region in both groups – suggesting this region may provide a useful screening area for establishing the presence (or absence) of transplanted microglia (Figure 3.19). Due to its rostral location, the olfactory bulb is easily identified using bright-field imaging – allowing blinded observation of samples – with its small size allowing a section of this whole region to be captured within a single frame at 20x magnification, somewhat minimising sampling bias. As such, the olfactory bulb was selected as the principal region of interest for initial screening to ascertain whether transplant-derived cells are present in the brains of adult hosts.

Next, I sought to optimise an immunohistochemistry protocol for imaging of fms:GFP cells on adult brain sections. The extensive vasculature of the brain results in large amounts of autofluorescence when imaging tissue sections, particularly in the GFP channel. While blood vessels and microglia are morphologically distinct – with microglia displaying a characteristic highly branched morphology, and blood vessels forming circular, chain-like structures – distinguishing true signal is made challenging by colocalization of these structures. Microglia form a crucial part of the neurovascular unit – the functional structure which forms the blood-brain barrier (Neuwelt *et al.*, 2004; Fleming, Diekmann and Goldsmith, 2013; Wang *et al.*, 2014). As such, these cells are likely to cluster around blood vessels, making it hard to distinguish between vessel autofluorescence and true cells without proper signal optimisation.

In order to optimise the signal to noise ratio, two imaging systems were utilised to image the olfactory bulb in sagittal sections of *Tg(fms:GFP)* adult fish – the microglia of which should have a similar phenotype to transplanted *fms:GFP* cells. Previous work from our group has utilised anti-GFP primary antibodies at concentrations of 1:500 for whole mount immunohistochemistry. However, on tissue sections, these concentrations led to a high degree of background noise when imaged with both the UltraVIEW VoX Spinning Disk Confocal Microscope and the EVOS FL Auto Imaging System (Figure 4.4a,b). Even with exposure and gain set at the lowest settings required to visualise cells imaging on the Spinning Disk confocal resulting in an autofluorescent signal of a similar intensity to that of cell staining (Figure 4.4a). Imaging of two control sections (one of which was treated with blocking buffer only, and one which received only secondary antibody) using the same settings resulted in a similar autofluorescent signal without any visible cells – confirming any off-target fluorescence was not due to non-specific binding of either antibody.

In order to boost signal to noise ratio, trial sections were treated with increased concentrations of primary or secondary antibodies. As before, sections were imaged using the UltraVIEW VoX Spinning Disk Confocal Microscope with exposure and gain set at the lowest settings required for cell visualization. Increasing both the primary and secondary antibody concentrations resulted in improved signal-to-noise ratio, with slides treated with primary antibodies of 1:200 allowing most reliable visualization of cells in the absence of visible autofluorescence (Figure 4.4a). Imaging technical duplicates of this section on the EVOS FL Auto Imaging System also led to an improved signal-to-noise ratio in the resulting images, although not to the same extent as the Spinning Disk (Figure 4.4b). Hence, this optimisation experiment suggests sections stained with 1:200 primary antibodies and imaged on the Spinning Disk Confocal microscope led to the optimal quality of imaging for GFP-expressing microglia in our sections.

4.3.2.2 Transplant-derived cells are not visible in the optic tectum of hosts 1-year post-transplantation

Following optimisation of fms:GFP cells with immunohistochemistry, I next sought to investigate whether transplant-derived cells were present in hosts into adulthood. Transplanted animals were raised to approximately 1-year post-fertilisation (13 months post-fertilisation [mpf] and 14.5mpf) before culling and fixing for imaging. Immunohistochemistry with anti-GFP antibodies revealed a complete absence of transplant-derived cells in adult host as determined by blinding screening of the olfactory bulb (n=13) (Figure 4.5). Exploratory visualisation of further brain regions also failed to locate

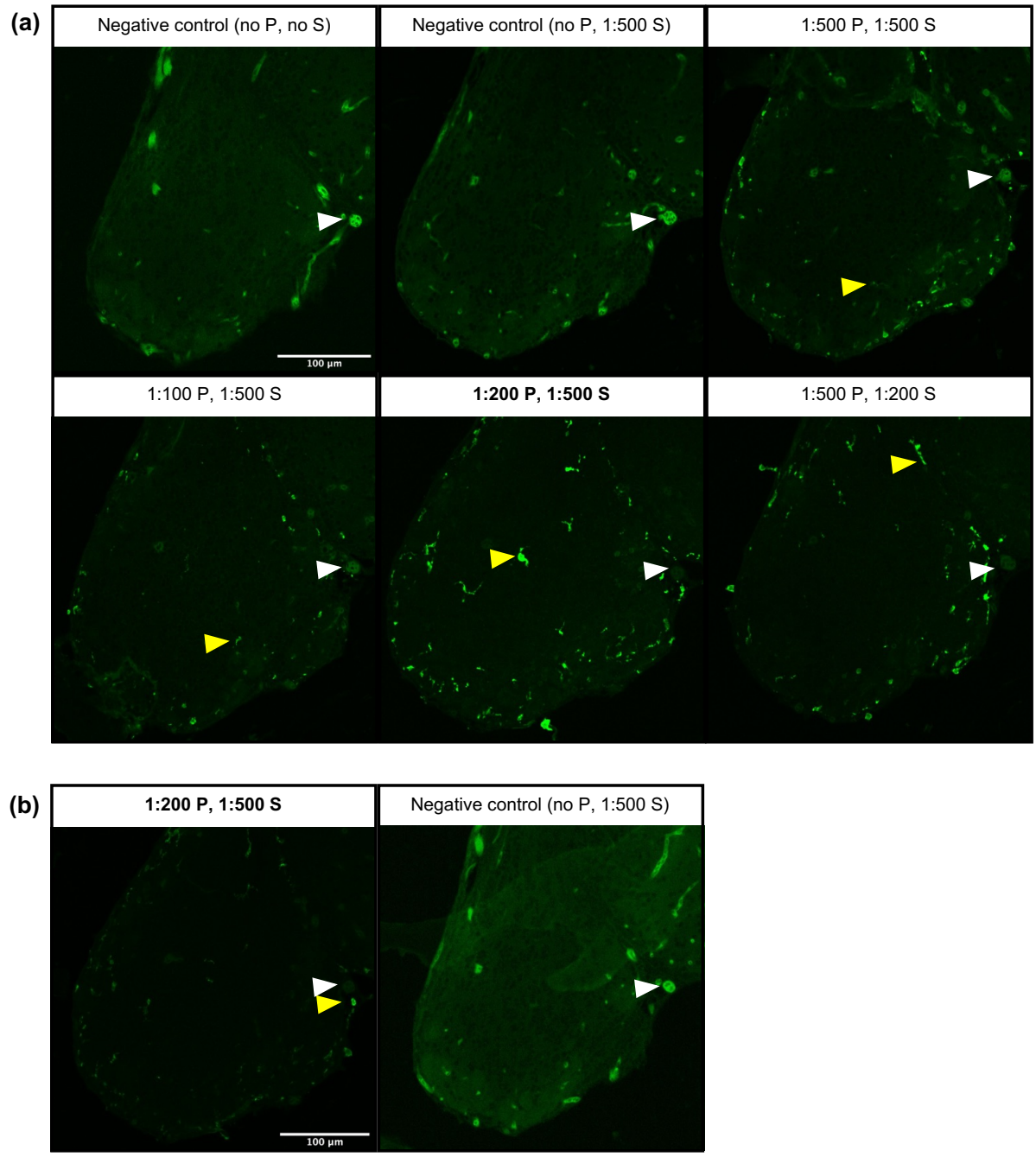

Figure 4.4. Optimisation of immunohistochemistry for transplanted cells in adult brains.
a. Sagittal sections of adult olfactory bulb were immuno-labelled with varying concentrations of anti-GFP primary (P) and GFP-tagged secondary (S) antibody, and imaged using UltraVIEW VoX Spinning Disk Confocal Microscope (20x magnification). Optimal signal-to-noise obtained using 1:200 P, 1:500 S staining. Background autofluorescence is indicated by white arrows, GFP-tagged microglia are indicated by yellow arrows. Imaging parameters were optimised for each slide, with negative control slides imaged according to settings for 1:500 P; 1:500 S sample. **b.** Comparison images of the same sagittal sections stained with 1:200 P and 1:500 S and negative control taken on EVOS FL Auto Imaging System (20x magnification). Negative control imaged according to settings for 1:200 P; 1:500 S.

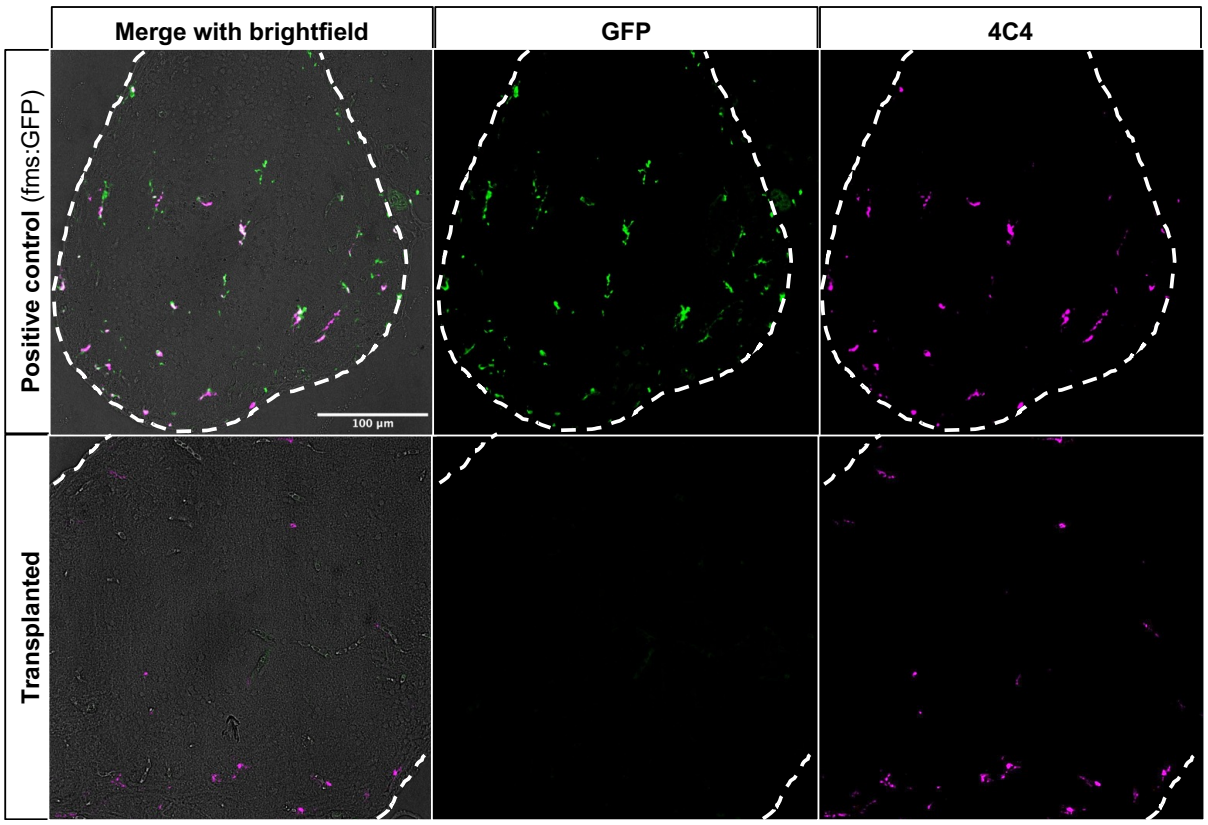

Figure 4.5. Transplanted cells do not persist into adulthood.
Representative images of 1 year old transplanted fish following immunohistochemistry for GFP (labelling transplanted cells) and 4C4 (a microglial marker). No GFP-expressing cells were observed throughout the brains of transplanted fish. Positive control (fms:GFP) included for reference. 20x magnification of olfactory bulb (microglia-dense region).

GFP-expressing cells in transplanted animals (data not shown). Hence, immunohistochemistry suggests transplanted cells do not persist in the brains of transplanted animals up to 1-year post-transplantation.

However, this approach is limited in that only a single section is assessed which may introduce significant sampling bias (even using the microglial-enriched region of the olfactory bulb), whereby transplant-derived cells located around the periphery of the parenchyma could easily be missed. Furthermore, animals were assayed at only one age – failing to identify how transplant-derived cell numbers change throughout development and when, if it all, these cells are truly cleared. Hence, further work required a more structured approach of animal sampling, with visualisation of the whole population of transplant-derived cells throughout the brain.

4.3.3 Transplant-derived cells persist in host brains throughout juvenile, but not adult ages

One of the advantages for using zebrafish for the study of cellular biology is their transparency during development, facilitating live imaging of transgenic reporters and whole mount immunohistochemistry of entire tissues, including the brain. However, this advantage does not persist in adult tissues, which become opaque around 3–4wpf. State-of-the-art advances in tissue clearing – the process of rendering biological samples transparent for imaging – can now circumvent tissue opacity in the brains of zebrafish and other animal models (Ueda *et al.*, 2020; Richardson *et al.*, 2021). One advantage of using this approach in zebrafish is the relatively small size of their brains, relative to mammals – allowing imaging throughout the whole tissue with microscopes of a working distance of 500µm or greater. As such, I sought to optimise a tissue clearing methodology for the assessment of transplanted cell engraftment throughout adult brains.

4.3.3.1 Tissue clearing allows visualisation of fms:GFP- and mpeg:mCherry CAAX-positive cells in adult brains

To confirm that tissue clearing was a viable approach for the imaging of microglia in adult zebrafish brains, I utilised a well-characterised hydrophilic clearing method – known as CUBIC (clear, unobstructed brain imaging cocktails and computational analysis) – to visualise *Tg(fms:GFP)sh377* and *Tg(mpeg1:mCherryCAAX)sh378* brains, stained with anti-GFP and anti-mCherry antibodies respectively. This approach facilitated high quality images in which both fms:GFP- and mpeg1:mCherry-positive macrophages and microglia throughout the thickest part of the brain tissue (the optic tectum) (Figure 4.6). As such, CUBIC clearing provides a useful methodology for the

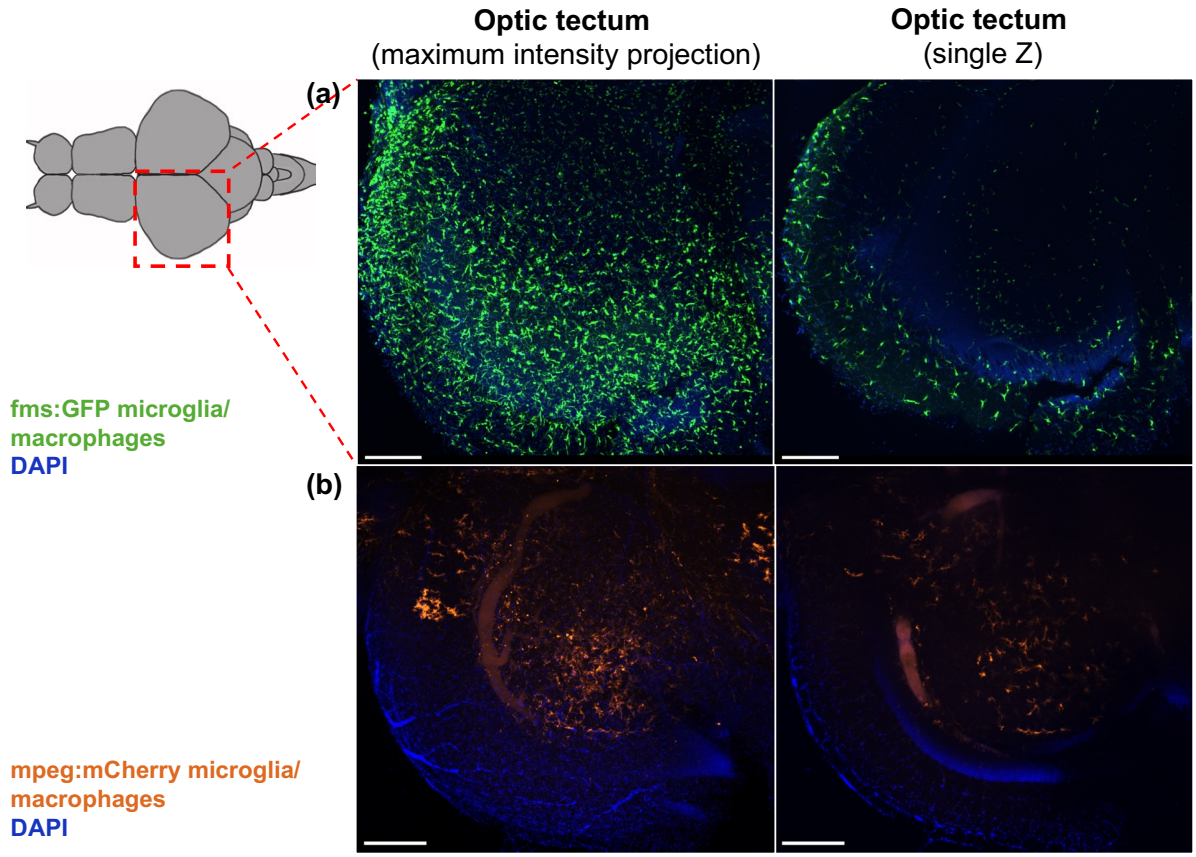

Figure 4.6. Tissue clearing and immunohistochemistry of fms:GFP and mpeg:mCherry brains.
a. GFP-positive cells in the optic tectum of *Tg(fms:GFP)sh377* animals (26wpf) **b.** mCherry-positive cells in the optic tectum of *Tg(mpeg1:mCherryCAAX)sh378* animals (14wpf). Red dashed line indicates area imaged. Scale bar represents 200µm.

visualisation of macrophages and microglia in host brains, including fms:GFP-expressing cells, which should be similar to our transplant graft.

4.3.3.2 Tissue clearing reveals that transplanted cells persist to 10wpf, but not thereafter

To assess whether transplant-derived cells persisted in the brain to provide long lasting therapeutic effects, I used tissue clearing and immunohistochemistry on dissected brains from transplanted, *irf8*-crRNA injected hosts to quantify the number of endogenous microglia versus transplanted cells over time. To establish a full time-course of transplant-derived cell engraftment, 3–4 transplanted animals were culled every two weeks up to 6wpf then every four weeks thereafter. Spinning Disk microscopy was then used obtain high quality images of dissected, cleared brains from juvenile to adult ages (Figure 4.7a). Imaging revealed that transplanted cells were present in the brains of transplanted hosts up to 10wpf, but not thereafter (Figure 4.7a). Quantification of the number of transplant-derived cells versus endogenous microglia revealed a gradual reduction in the percentage of total microglia from transplant origin from 4- to 14wpf (Figure 4.7b). Interestingly, the absolute number of GFP-positive cells peaked at 4wpf – suggesting initial expansion of the transplant-derived population – but subsequently decreased, while the number of endogenous microglia increased from 2–4wpf but remained relatively stable thereafter (Figure 4.7c,d). The reduction in transplanted cell number appeared to be accompanied by a gradual reduction in the percentage of remaining transplant-derived cells which express the microglial-specific marker 4C4 (Figure 4.7e). As such, these data demonstrate that transplant-derived cells persist in the brain and maintain expression of microglial markers beyond embryogenesis through to juvenile ages, but do not provide lifelong repopulation of the microglial niche in *irf8* knockdown hosts where only embryonic microglia are depleted.

4.3.4 Endogenous microglia may outcompete transplant-derived cells and contribute to their clearance

Previous work has demonstrated that depletion of embryonic microglia by CRISPR/Cas9-mediated targeting of *irf8* is required for robust engraftment of transplant-derived cells in host brains (Figure 4.1). However, embryonic microglia depletion via mutation of *irf8* has been shown to ablate embryonic but not adult microglia (Shiau *et al.*, 2015). This second wave of microglia emerge around 20dpf, with cells derived from definitive haematopoietic precursors populating the brain and ultimately replacing all embryonic microglia by approximately 3 months post-fertilisation (Ferrero *et al.*, 2018). Thus, in order to assess whether the arrival of adult, definitive haematopoiesis-derived microglia may drive the clearance of transplant-derived cells in the brain, I repeated the transplant time course in *csf1ra*$^{-/-}$*;*

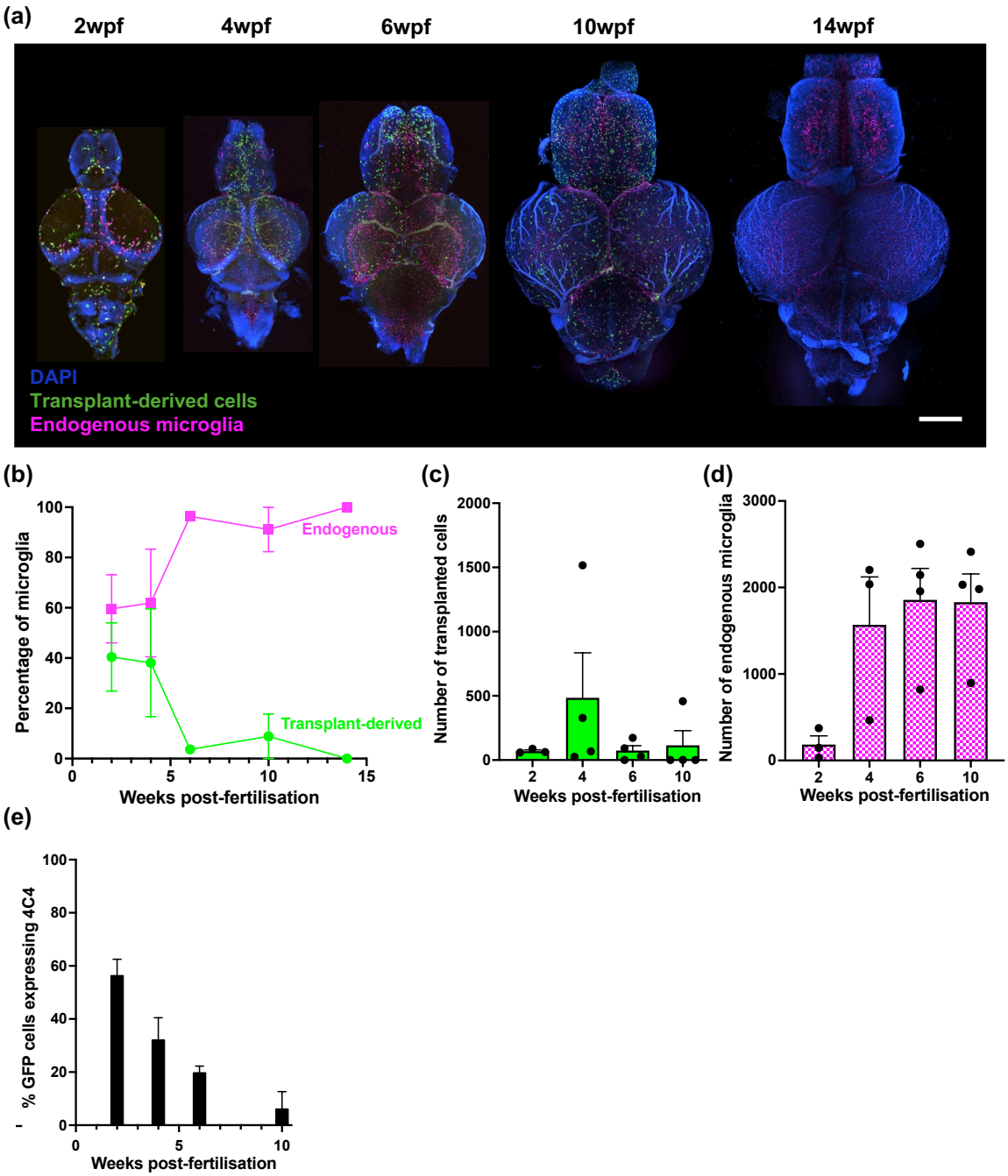

Figure 4.7. Transplanted cells persist in host brains throughout juvenile stages.
a. Tissue clearing and immunohistochemistry reveals that transplant-derived cells persist in host brains until 10wpf but are cleared by 14wpf. Scale bar represents 400µm. **b.** Percentage of microglia from transplant origin gradually decreases in host brains until 14wpf. **c.** The number of transplant-derived cells peaks at 4wpf and rapidly decreases thereafter. **d.** The number of endogenous microglia (4C4 positive, GFP-negative microglia) increases from 2–4wpf. **e.** Percentage of transplant-derived cells expressing microglia marker 4C4 steadily decreases from 2wpf. 3–4 biological replicates per timepoint.

csf1rb$^{-/-}$ (hereafter referent to as *csf1r*^{DM}) hosts, which lack both embryonic and adult endogenous microglia throughout life (Ferrero *et al.*, 2021).

Tissue clearing and immunohistochemistry revealed that transplant-derived cells persist up to 26wpf in *csfr1*^{DM} hosts, beyond the point of clearance in *irf8* crispants (Figure 4.8a). Interestingly, transplant-derived cells were cleared from *csf1ra*$^{-/-}$*; csf1rb*$^{+/+}$ hosts – which lack embryonic, but not adult, microglia – along a similar time course to *irf8* crispants, with clearance of transplant-derived cells around 14wpf (Figure 4.8b,c). Furthermore, *csf1ra*$^{-/-}$*; csf1rb*$^{+/-}$ hosts – which have reduced, but not completely absent adult microglia – showed an intermediate phenotype, where transplant-derived cells were ultimately cleared, but along a slower trajectory to *csf1ra*$^{-/-}$*; csf1rb*$^{+/+}$ hosts. As such, together these data suggest that the presence of endogenous adult microglia contributes to the clearance of transplant-derived cells in host brains and that, in their absence, transplanted cells persist through to adult ages. Nonetheless, transplant-derived cells are present in host brains in robust numbers up to 4wpf regardless of host genotype (*csf1ra*$^{-/-}$*; csf1rb*$^{+/+}$, *csf1ra*$^{-/-}$*; csf1rb*$^{+/-}$, *csf1r*^{DM} or *irf8* crispant) – providing a window in which the potential therapeutic efficacy of this intervention could be assessed.

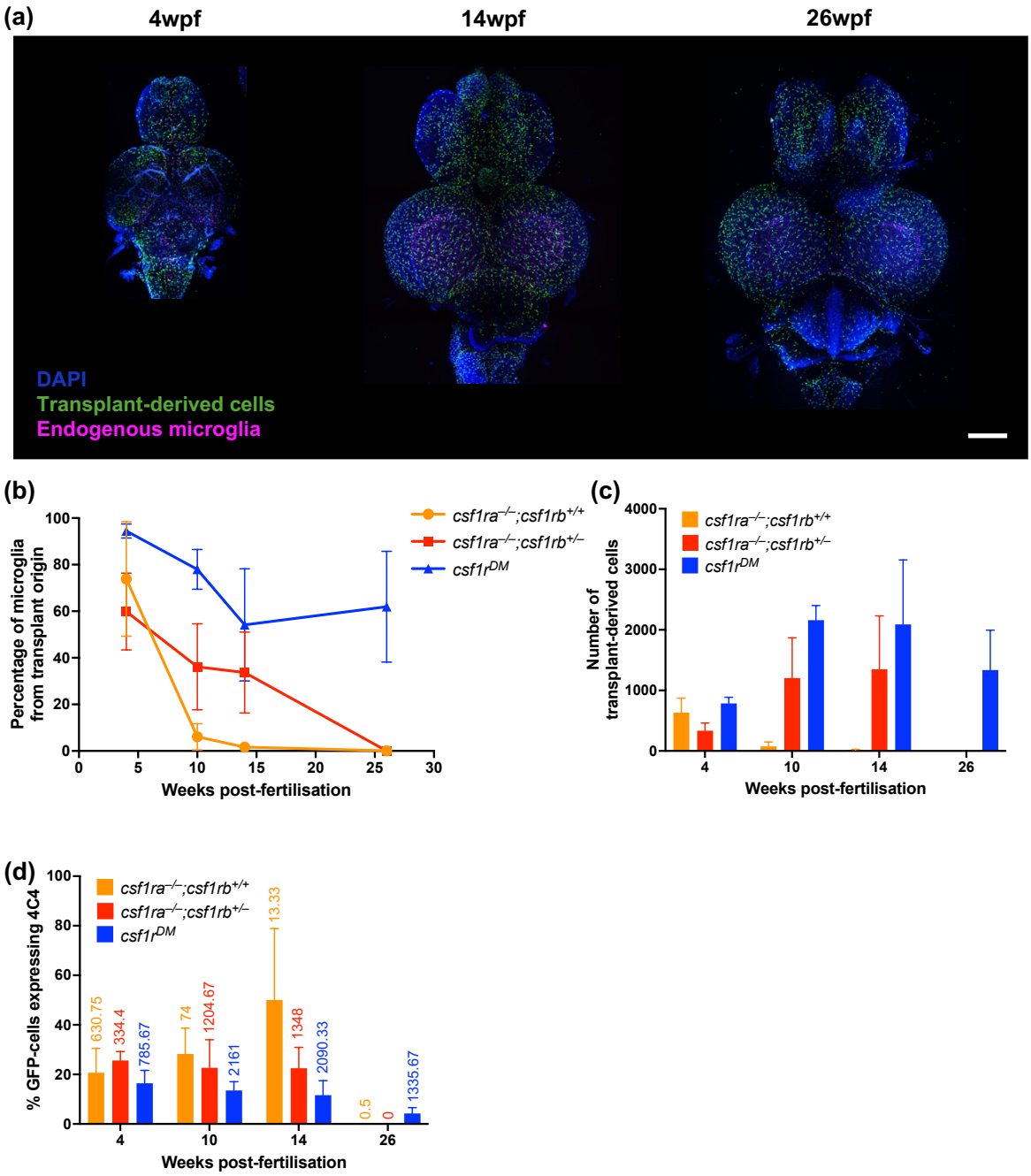

Figure 4.8. Transplanted cells persist beyond 26wpf in *csf1r* double mutants.
a. Tissue clearing and immunohistochemistry reveals that transplant-derived cells persist in microglia-deficient *csf1r*^{DM} host brains until 26wpf. Scale bar represents 400µm. **b, c.** The percentage (b) and number (c) of microglia from transplant origin gradually decreases until transplanted cells are no longer detectable in *csf1ra*$^{-/-}$*;csf1rb*$^{+/+}$ and *csf1ra*$^{-/-}$*;csf1rb*$^{+/-}$ brains over 26 weeks, while transplanted cells remain engrafted at 26wpf in *csf1r*^{DM}. **d.** Only transplant-derived cells in csf1r^{DM} express microglia-specific marker 4C4 by 26wpf. Numbers indicate mean number of transplant-derived cells per group.

4.4 Discussion

Previous work has indicated that transplantation of WKM-derived adult macrophages into zebrafish larvae may lead to replacement of microglia in embryonic hosts. However, until now, it remained unclear to what extent, and along which time course, transplant-derived cells may contribute to the microglial population. In this chapter, I have demonstrated that transplant-derived cells can divide with embryonic hosts and engraft in the brain in increasing numbers in the days following transplantation. Furthermore, both tissue clearing and sectioning methodologies have confirmed that transplant-derived cells can persist in host brains throughout juvenile ages, but not into adulthood. Finally, I have demonstrated that endogenous adult microglia interact with transplant-derived cells and outcompete them for brain engraftment in juvenile and adult stages. Together, these findings demonstrate that macrophage transplantation is a viable strategy for microglial replacement in zebrafish hosts up to 4wpf. Macrophage transplantation therefore provides a powerful tool to study the contribution of microglia to disease pathogenesis and assess the potential therapeutic impact of microglial replacement in larval and juvenile zebrafish models.

4.4.1 Longitudinal assessment of transplanted cells during embryogenesis reveals brain engraftment as early as one day post-transplant

Further to previous findings which established the presence of transplant-derived cells in the brains of zebrafish hosts at 5dpf, the current study revealed a global increase in the number of transplant-derived cells in successfully transplanted embryos from 1–3dpt, suggesting that transplant-derived cells are able to divide in embryonic hosts. Accordingly, the number of GFP-positive cells in the brain, CHT and heart increased in the days post-transplantation. The only region in which an increase in cell number was not observed was the injection site – with the mean number of GFP-expressing cells in this region instead decreasing to zero by 3dpt. This is likely due to migration of these cells to elsewhere in the embryo, or a failure to efficiently engraft leading to cell death. Interestingly, despite the overall increase in the number of fluorescent cells in the CHT from 1–3dpt, a transient decrease in the mean number of cells visible in this region was observed at 2dpt. This may reflect a limitation in our experimental design, rather than a true decrease in cell number. As a transient dye, the fluorescence intensity of CSFE-labelled cells halves with each cell division – limiting the accuracy with which cells can be counted using optical microscopy. While CSFE staining has been reported to track several generations of cells in culture, I noticed a reduction in the fluorescence intensity of green cells throughout the embryo at 2dpt, with cells particularly dim in the CHT. As the site of haematopoiesis in the zebrafish, this likely reflects a reduction in fluorescein intensity due to cell division, before GFP expression is fully restored after photobleaching. As such, transient fluorescein staining may not

entirely bridge the gap between transplantation and restoration of endogenous GFP expression in transplant-derived cells in regions of high cell division. Nonetheless, this methodology was able to identify an embryo-wide increase in the number of transplant-derived cells within each successfully transplanted embryo, demonstrating that transplanted cells are able to divide within microglia-depleted hosts.

The most striking increase in cell number, by far, was observed in the brain and head, with an over four-fold increase in the mean number of cells from 1dpf to 3dpf. This increase could arise from two sources. Firstly, the increased number of GFP-expressing cells in the brain could arise from cell division of macrophages already engrafted within the tissue itself. Time lapse microscopy has previously demonstrated that transplanted cells are able to divide within the brain, suggesting this may contribute at least partially to the expansion of the GFP-expressing population in the brain. In adult animals, microglia are thought to be a slowly self-renewing population – capable of cell division, albeit very slow rates (Ajami et al., 2007b; Mildner et al., 2007b; Réu et al., 2017). Whether the rate of microglia division is greater during development – and specifically in zebrafish embryos – remains unclear. However, with a four-fold increase in the number of transplant-derived cells in the brain, cell division alone is unlikely to contribute to such a drastic expansion of this population. Instead, the growing population of GFP-expressing cells in the brain may also arise from infiltration of cells dividing elsewhere in the body. Indeed, this is a possibility, as an increase in cell number was observed in almost all regions examined, including the CHT – likely site of macrophage cell division. Hence, it is likely a contribution of transplanted cell division and migration that repopulates the microglial niche in *irf8*-depleted animals.

Previous work has demonstrated that recruitment of transplanted cells to the brain is improved in *irf8* knockout animals compared to wild type controls. The current study extends this finding, with the vast increase in the number of cells in the brain compared to all other assessed regions suggesting that transplanted cells may migrate preferentially to the brain even within a single microglia-depleted animal. It is possible that transplanted cells may be selectively recruited to the brain by neuropathology caused by an absence of endogenous microglia. One of the key drivers of initial macrophage colonisation of the brain is developmental apoptosis (Casano, Albert and Peri, 2016b) – a process by which excess neurons are removed from the brain throughout early development. Removal of endogenous microglia results in an increase in the number of apoptotic cells in the brain due to limited clearance of these cells – meaning this brain entry signal may be amplified in microglia-depleted animals. A similar increase in the number of uncleared apoptotic cells has been reported in

rnaset2 mutants compared to wild type siblings, to such an extent that depletion of endogenous microglia by *irf8* knockout leads to no further changes in apoptotic cell number (Hamilton *et al.*, 2020b). Hence, a similar niche for recruitment of transplanted cells to the brain may be created in these mutants – meaning additional depletion of endogenous microglia may not be necessary to drive repopulation of the brain. Future work will therefore explore the dynamics of transplanted cell division and engraftment in *rnaset2* mutants – both with and without *irf8* knockout – to unpick the nature of brain entry signals in zebrafish embryos. Nonetheless, in wild type animals, it seems that transplanted adult macrophages are able to efficiently repopulate the brains of microglia-depleted hosts throughout embryogenesis.

4.4.2 Tissue clearing and immunohistochemistry is a powerful tool for the imaging of microglia in adult brains

While one of the many advantages for the use of zebrafish is their transparency during early development, this does not persist into adult stages – with most tissues becoming opaque around 2–3wpf. As such, additional tools are needed to visualise cells within zebrafish brains beyond these ages.

The current gold-standard for imaging of adult brain tissue – in zebrafish and other animal models alike – is tissue sectioning and immunohistochemistry. In this study, immunohistochemistry of sagittal brain sections revealed relatively robust staining of adult microglia, but is subject to background noise particularly in the GFP-channel – as demonstrated by the high background signal around blood vessels in negative controls (Figure 4.4). Additionally, tissue sectioning is limited in that this approach provides only a snapshot of a single plane of tissue, failing to capture macroscopic connections or patterns of cellular distribution throughout the whole organ. Cell counts from tissue sections may also be skewed by regional heterogeneity when comparing one animal to another – while large, anatomical structures can be used as a reference point to orientate oneself in the brain, it is hard to ensure that exactly the plane is taken from each fish and, as such, regions of differing cell density may be assayed. Finally, tissue sectioning is highly time consuming, may distort or damage tissue, and introduce artefacts (Richardson *et al.*, 2021). As such, there are clear limitations for the use of tissue sectioning to track transplanted cell engraftment over time in adult brains.

In order to circumvent these issues, this study optimised an adapted tissue clearing and imaging strategy to allow three-dimensional, whole brain imaging of adult samples. A variety of tissue clearing methodologies are available and have been well-characterised for clearing and imaging of whole brains (Ueda *et al.*, 2020; Richardson *et al.*, 2021). For this study, I chose to use CUBIC due to its simplicity, compatibility with fluorescent staining, lack of toxicity, relatively short incubation periods

and minimal requirement for specialist equipment (Susaki *et al.*, 2015). CUBIC is a hydrophilic clearing method which renders samples transparent by delipidating and decolourising the tissue, removing the lipids and pigments that scatter light and obscure imaging, respectively (Ueda *et al.*, 2020). Permeation of the tissue with this aqueous clearing agent matches refractive indices across the tissue and minimises light scattering to give sharp images. All reagents used have high biocompatibility and biosafety, meaning tissue integrity is generally maintained (Ueda *et al.*, 2020). It is notable that some tissue expansion has been reported using the CUBIC approach, but this appears to be minor and often resolves following full completion of the protocol (Susaki *et al.*, 2015). As such, CUBIC is a powerful approach, and has been successfully used for the clearing of zebrafish brains (Ferrero *et al.*, 2021).

Trial tissue clearing of two transgenic macrophage-reporters (*Tg(fms:GFP)sh377* and *Tg(mpeg1:mCherryCAAX)sh378*) demonstrated robust labelling of brain macrophages and microglia throughout adult tissue (Figure 4.6). It is interesting to note the differing expression patterns of fms:GFP+ and mpeg1:mCherry+ cells – despite the fact these transgenics are thought to label the same cell populations – whereby fms:GFP+ cells are distributed throughout the optic tectum with uniform fluorescence-intensity, while mpeg1:mCherry+ cells seem to be distributed in clusters with brighter and dimmer populations. Recent work using adult zebrafish has suggested that, while the mpeg1-marker mainly labels macrophages and microglia within the developing brain, the *mpeg1* transgene also labels dendritic cells in adults (Nguyen *et al.*, 2024; Rovira *et al.*, 2024). Interestingly, in these studies, mpeg1-expression was found to be enriched in dendritic cells relative to microglia, with bright mpeg1-positive dendritic cells found in distinct clusters throughout the midbrain and hindbrain in regions, proximal to the ventricles. This bears a striking similarity with the pattern of *mpeg1* expression in tissue cleared brains from the current study – suggesting mpeg does not exclusively label macrophages and microglia in adult brains. Together with this new literature, this imaging data further validates our selection of fms:GFP+ macrophages as our transplantation graft – as *fms* may be a more robust marker of macrophages/microglia in the brain (transplant-derived or endogenous). Crucially, these findings also demonstrate that tissue clearing allows visualisation of distinct cellular populations in adult zebrafish brains (including brain-resident macrophages and microglia) and is a powerful tool for imaging of microglia and transplant-derived cells in adult tissue.

4.4.3 Transplant-derived cells are cleared from host brains when only embryonic endogenous microglia are depleted, but persist in the absence of their adult counterparts

While transplanted WKM-derived macrophages appear to functionally replace microglia during embryogenesis, the duration of transplant-derived cell engraftment in host brains beyond larval stages is essential to facilitate later assessment of the therapeutic potential of this intervention in disease

models. The work detailed in this chapter demonstrates that the contribution of transplant-derived cells to the whole microglial population gradually reduces in *irf8* crispants from 2 to 14wpf, where transplanted cells are completely absent from host brains. This decline in transplant-derived cell number was mirrored in *csf1ra*$^{-/-}$;*csf1rb*$^{+/+}$ mutants – demonstrating an absence of transplanted cells at 14wpf in two models which lack embryonic, but not adult microglia (Ferrero *et al.*, 2021). In contrast, in *csf1r*^{DM} – which are deficient in microglia throughout life – transplant-derived cells persist in host brains, suggesting that a lifelong absence of endogenous microglia may be necessary for long-term engraftment of transplanted cells in the brain. However, the mechanisms by which transplanted cells disappear from host brains are unclear.

One potential explanation may be due to the arrival of host-derived adult microglia into the brain during adult ages, which displace both endogenous embryonic microglia and transplant-derived cells. As previously discussed, fate-mapping analyses have revealed that zebrafish microglia arise from two populations in a temporally distinct manner—with embryonic microglia derived from yolk sac progenitors gradually replaced throughout juvenile stages by a distinct population of adult HSC-derived macrophages (Ferrero *et al.*, 2018). This replacement is thought to be dependent on the arrival of the adult kidney marrow–derived second wave—with embryonic microglia persisting when HSC-derived microglia are genetically depleted (Ferrero *et al.*, 2021). Two lines of evidence point to this explanation: the first is that, in both *irf8* crispants and *csf1ra* mutants which lack embryonic but not adult microglia, the clearance of transplant-derived cells occurs at a similar age to that at which adult microglia are thought to colonise the brain. Secondly, this study found that transplant-derived cells persisted for longer durations in hosts which lacked the HSC-derived adult microglial population (*csf1r*^{DM}). Together, these data suggest that the arrival of endogenous adult macrophages into the brain may be the driver for transplanted cell clearance. This finding is particularly interesting, as the transplant graft used in this study – derived from WKM – is much more similar in ontogeny to the HSC-derived adult microglia than yolk sac embryonic progenitors (Ferrero *et al.*, 2021). As such, it is possible that our transplant-derived cells undergo such extensive reprogramming following engraftment that they are recognised as self, follow the same trajectory as host embryonic microglia and are cleared as the infiltrating adult microglia arrive. Indeed, preliminary data for this project have already shown that transplanted macrophages are quick to express the microglia marker 4C4 within three days of transplantation, suggesting adoption of a microglial phenotype within host brains (Figure 4.2c). Published literature in *csf1r*$^{-/-}$ mice (which also lack endogenous microglia) has also demonstrated that transplanted HSC-derived monocytes cells can adopt a phenotype highly similar to endogenous microglia once engrafted in the CNS, as assessed by single cell RNA sequencing (Bennett *et al.*, 2018).

However, despite their converging phenotypes, HSC-derived cells remain transcriptionally distinct from microglia derived from transplanted yolk sac progenitors (thought to be most similar to endogenous murine microglia) even months after engraftment – suggesting that full reprogramming of transplanted HSC-derived macrophages does not occur this murine model. As such, future work should further investigate the transcriptional similarity of transplanted WKM-derived cells, endogenous embryonic microglia and their adult counterparts using single cell RNA sequencing to truly assess the extent of reprogramming in transplanted brains.

Alternatively, it is possible that the disappearance of transplant-derived cells is simply due to cell-autonomous death. Apoptosis is a vital mechanism by which microglia modulate their own number and prevent overcrowding throughout various brain regions (Askew *et al.*, 2017; Barry-Carroll and Gomez-Nicola, 2024). Although the presence of two discrete waves of microglial colonisation may be specific to zebrafish – with the contribution of HSC-derived cells to the microglial pool being a highly controversial area in mammalian biology – periods of microglial reduction and repopulation have been reported across a multitude of species. In mice, microglia are thought to proliferate extensively throughout embryogenesis, with microglia density peaking in the first few postnatal weeks – similar to the pattern of expansion described for transplanted cells in this study (Barry-Carroll *et al.*, 2023). Following this peak, the microglia population is then refined by apoptosis, which is spatially and temporally coupled with ongoing proliferation (Askew *et al.*, 2017; Barry-Carroll *et al.*, 2023). A similar pattern has been reported in human brain bank tissue – tracked from foetal to adult ages – with multiple waves of microglia proliferation followed by apoptosis observed throughout development (Menassa *et al.*, 2022). Together, these studies emphasise frequent waves of apoptosis as an intrinsic feature of the microglial population. It is possible, therefore, that apoptosis of transplanted cells – alongside endogenous embryonic microglia – may induce proliferation and/or infiltration of adult microglia in our zebrafish hosts. However, the finding that transplant-derived cells survive in the absence of endogenous adult microglia (*csf1r*^{DM}) suggests that clearance of these cells is unlikely to be purely cell autonomous, and that some interaction with host microglia may be necessary to trigger apoptosis. Therefore, it seems the disappearance of transplant-derived cells may reflect the intricately balanced, self-modulating regulation of microglial numbers within the brain, with the role of host- versus graft-derived cells remaining unclear.

Finally, it is possible that transplant-derived cells may simply downregulate GFP expression, and therefore fail to be detected by immunochemistry. However, several lines of evidence suggest that this is unlikely. Firstly, tissue clearing of *Tg(fms:GFP)sh377* and *Tg(mpeg1:mCherryCAAX)sh378*

demonstrates robust and uniform distribution of fms:GFP+ cells throughout the optic tectum, while mpeg1:mCherry+ cells were less widely distributed throughout the tissue with highly variable signal intensity (Figure 4.6). As previously discussed, this suggests that *fms* is expressed in adult microglia, and that it is likely to be a robust marker for transplant-derived cells. Secondly, our finding that transplant-derived cells are detectable in *csf1r*^{DM} hosts until 26wpf – beyond the point of clearance in *irf8* crispants – demonstrates that these cells do not intrinsically downregulate *fms*. Instead, the persistence of transplant-derived cells in entirely microglia-deficient hosts more likely suggests that clearance of transplanted cells is driven by the arrival of adult HSC-derived macrophages into the host brain, rather than changes in fms:GFP expression or other cell autonomous changes.

4.4.4 Macrophage transplantation as a potential therapeutic intervention

The work detailed in this chapter demonstrates the following strengths of microglia replacement by macrophage transplantation as a potential therapeutic intervention in zebrafish models:

1. Transplanted cells reach host brains from one day post-transplant, are able to divide within the CNS and increase in number thereafter.
2. Transplanted macrophages adopt a microglial morphology and express microglia-specific markers in embryonic hosts.
3. Transplanted cells can clear accumulated apoptotic debris in microglia-depleted animals, suggesting functional replacement of microglia.
4. Transplant-derived cells persist in robust numbers and continue to express microglia-specific markers throughout early juvenile stages in hosts with transient microglia-depletion.

Together, these features demonstrate that macrophage transplantation is a compelling strategy for microglia replacement and could be used to investigate the impact of targeting microglia in disease models, including *rnaset2* mutant zebrafish.

However, there are several limitations of macrophage transplantation as a potential therapy which must be considered. Firstly, the full extent to which transplant-derived macrophages adopt a healthy microglial phenotype remains unclear. Previous research has demonstrated that transplanted HSC-derived macrophages can express some key microglial genes following brain engraftment, but also adopt DAM signatures (Bennett *et al.*, 2018). This includes significant enrichment of genes associated with Alzheimer's Disease, Amyotrophic Lateral Sclerosis, inflammation and microglial immaturity – as characterised by elevated expression of *Apoe* and decreased expression of microglia maturation marker *Sall1* (Bennett *et al.*, 2018). However, it must be noted that these cells were transplanted into *Csf1r*$^{-/-}$ mice, which lack all microglia and have severe survival phenotypes (Li *et al.*, 2006). Additionally,

the *CSF1R* gene itself is associated with two leukodystrophies – with heterozygous mutations causing ALSP, while homozygous mutations cause an even more severe paediatric-onset leukoencephalopathy characterised by a congenital absence of microglia (Sundal *et al.*, 2015; Oosterhof *et al.*, 2019). As such, these transplanted cells likely engrafted into a highly diseased brain, and so it is difficult to establish the contribution of the CNS environment versus cell autonomous features. Nonetheless, this literature may raise concerns about introducing dysfunctional microglia into an already pathological environment. As such, the broader impact of the presence of transplant-derived cells – as well as the phenotype of these cells themselves – must be considered when explored as an intervention in disease models.

Secondly, the failure of transplant-derived cells to persist in hosts (without lifelong microglia depletion) may limit the ages at which the therapeutic impact of macrophage transplantation can be assessed, including in *rnaset2* mutants. Several pathological hallmarks of RNASET2-deficient leukodystrophy cannot be measured into adulthood in *rnaset2* mutants. For example, current MRI protocols for the assessment of white matter lesions require fish to reach a minimum size for scanning to be feasible (Hamilton, Allen and Reynolds, 2023). Furthermore, survival impairments may not emerge until over one-year post-fertilisation, long after the clearance of transplant-derived cells in zebrafish hosts (see section 3.3.6). Nonetheless, given the neurodevelopmental nature of leukodystrophy, it is entirely possible that transplantation may delay the onset of pathogenesis and therefore the development of these phenotypes. Additionally, many key markers of pathology develop during larval stages in *rnaset2* mutants, including reductions in myelin-associated transcripts, changes in oligodendrocyte number, behavioural deficits and neuroinflammation (Chapter 5). As such, despite the transient nature of cell engraftment, there remain several viable assays to assess the impact of transplantation on *rnaset2* pathology, forming the immediate next steps for this work.

4.4.5 Chapter summary

In combination with preliminary data (Figure 4.1 and Figure 4.2), the current study lays the foundations for the study of macrophage transplantation as a therapeutic intervention in zebrafish disease models, such as the *rnaset2* mutant zebrafish. This work demonstrates that transplanted macrophages can reach embryonic brains, adopt a microglia-like phenotype, and maintain engraftment for 4–10 weeks post-transplantation. As such, these findings establish proof-of-principle that macrophage transplantation is a viable strategy to replace zebrafish microglia and provides a powerful tool with which to study the role of microglia in *rnaset2* mutant pathology.

Chapter 5. Macrophage transplantation as a potential therapy for *rnaset2* mutants

5.1 Introduction

5.1.1 Neuropathology is triggered by loss of homeostatic microglial functions in rnaset2 mutant zebrafish

Studies of the *rnaset2* mutant zebrafish have demonstrated that microglial abnormalities are among the earliest markers of pathogenesis in this disorder – with the presence of morphologically abnormal cells emerging during development (Hamilton *et al.*, 2020a). Crucially, microglia are functionally impaired, with accumulation of apoptotic debris within these cells suggesting a failure of digestion, but not phagocytosis, of substrates within the brain. In Chapter 3, I demonstrated that depletion of deficient microglia exacerbates disease phenotypes in *rnaset2* mutants, leading to increased mortality during larval and adult stages – suggesting that that *rnaset2* mutant microglia retain some protective functions in mutant brains (Figure 3.20 and Figure 3.21). As such, this growing body of data suggests that it is a loss of microglial function – in particular, their ability to clear apoptotic debris – that perturbs homeostasis in *rnaset2* mutants and may serve as the first trigger for neuropathology.

5.1.2 Macrophage transplantation is a viable strategy for microglial replacement in zebrafish hosts

A variety of strategies are in development with the goal of targeting microglial functions in leukodystrophy (see Table 1.1). Clinically, HSCT shows moderate efficacy across the leukodystrophies – particularly in combination with *ex vivo* gene therapy – which may be dependent on the engraftment of HSCs within the haematopoietic niche and subsequent arrival of donor-derived macrophages and microglia into host brains (Page *et al.*, 2019). However, several studies have demonstrated that transplantation of macrophages themselves, rather than HSCs, may provide a more direct route for microglial replacement (Sieweke and Allen, 2013; Cronk *et al.*, 2018). In mice, transplanted macrophages can engraft within the CNS and adopt microglia-like phenotypes, including in a mouse model of CSF1R-related paediatric leukodystrophy (Suzuki *et al.*, 2014; Haideri *et al.*, 2017; Bennett *et al.*, 2018). Thus, macrophage transplantation may be an attractive alternative to HSCT for microglial replacement.

Indeed, preliminary data presented in Chapter 4 demonstrated that transplantation of macrophages lead to greater engraftment of transplant-derived cells in embryonic brains relative to HSCT, in microglia-depleted wild type hosts. Transplant-derived cells divide in embryonic host brains, express microglia-specific markers and undertake key microglial functions, including phagocytosis of apoptotic

debris. These cells remain engrafted in robust numbers until early juvenile ages, when interactions with host microglia may trigger clearance of transplant-derived cells from the brains of wild type hosts which had undergone depletion of embryonic microglia. As such, macrophage transplantation is a powerful strategy to replace microglia in zebrafish larvae and juveniles and may, therefore, have therapeutic benefits in *rnaset2* mutant hosts.

5.2 Hypothesis and aims

In combination with previous literature, the results presented in Chapters 3 and 4 demonstrate that microglial dysfunction is likely to be the cellular driver of *rnaset2* mutant pathology, and that macrophage transplantation is a viable strategy to replace microglia in zebrafish hosts. I therefore hypothesise that microglial replacement by macrophage transplantation will be sufficient to rescue neuropathology in *rnaset2* mutant zebrafish. As such, the overarching aim of this chapter is to assess the effects of macrophage transplantation on markers of pathology in *rnaset2* mutants, by:

1. **Characterising the ability of transplant-derived cells to engraft and adopt microglial phenotypes in *rnaset2* mutant larvae.** Previous work has demonstrated that transplant-derived cells can engraft within the brain and express microglia-specific markers within 3 days post-transplantation, but that microglial depletion is necessary for robust engraftment in wild type hosts. Given the deficiency of *rnaset2* mutant microglia during early development, it remains unclear whether microglia depletion will be required to promote brain engraftment in mutant hosts. Similarly, it is uncertain how the arrival of transplant-derived cells into a highly inflammatory brain environment of *rnaset2* mutants will affect their engraftment or differentiation state. I will therefore use live imaging and immunohistochemistry to assess the number of transplant-derived cells within host brains, and their ability to express microglial markers.
2. **Assess the effect of transplantation on pathological phenotypes presented during larval stages.** Chapter 3 demonstrated that a multitude disease-associated phenotypes emerge in *rnaset2* mutant larvae by 8dpf, providing a useful age to assess the therapeutic efficacy of potential disease-modifying interventions. Therefore, I will assess the early effects of transplantation in *rnaset2* mutant larvae at 8dpf, including accumulation of apoptotic debris, upregulation of the antiviral response, myelin abnormalities and locomotor dysfunction.
3. **Quantify engraftment of transplant-derived cells into juvenile stages in *rnaset2* mutant hosts.** In wild type, transiently microglia-depleted hosts, transplant-derived cells persist up to 10wpf, but are ultimately cleared (Chapter 4). As previously discussed, it is unclear how the inflammatory environment of *rnaset2* mutant brains or the dysfunction of *rnaset2*-deficient

microglia may affect the duration of transplant-derived cell engraftment. As such, I will perform a tissue clearing and imaging time course – similar to that performed for transplanted wild types – to establish the longevity of transplant-derived cells within *rnaset2* mutant brains.

4. **Perform unbiased transcriptomic analysis of transplanted *rnaset2* mutant brains.** Detailed characterisation of *rnaset2* mutant zebrafish in previous studies and in Chapter 3 have facilitated the development of a battery of assays with which to test the effects of therapeutic interventions in this disease model. However, it is possible that such interventions will have entirely unexpected effects on molecular and cellular signalling in the brain. As such, unbiased transcriptomics analysis – RNA sequencing – will be performed in order to assess the broader effects of transplantation on *rnaset2* mutant pathology.

Together, these findings will provide insights into the role of microglia in the pathogenesis of RNASET2-deficient leukodystrophy, and whether microglia-targeted interventions – including macrophage transplantation – are potential therapeutic options in this disorder.

5.3 Results

5.3.1 Transplant-derived macrophages compete with endogenous rnaset2 microglia for brain engraftment

When optimising the macrophage transplantation protocol in wild type animals, I noted greater engraftment efficiency in embryos which had their endogenous microglia-depleted – suggesting that clearing of the microglial niche was necessary for robust infiltration of transplanted cells into wild type brains (Figure 4.1). However, engraftment of transplanted macrophages is yet to be investigated in *rnaset2* mutant embryos. In particular, it remains unclear whether depletion of endogenous microglia will be required for transplanted cell engraftment in *rnaset2* mutant hosts, or whether the failure of rnaset2-deficient microglia to clear developmental apoptosis is sufficient to drive recruitment of transplant-derived cells to the brain without depletion (Hamilton *et al.*, 2020a). As such, I aimed to quantify engraftment of transplant-derived macrophages into the brains of *rnaset2* mutants, both with and without microglial depletion.

5.3.1.1 Microglia-depletion promotes transplanted cell recruitment to rnaset2 brains

To assess whether transplanted cell engraftment was affected by the presence of endogenous microglia in *rnaset2* embryos, 2dpf mutants and wild-type siblings – either microglia-depleted (*irf8* crRNA-injected) or non-depleted (scrambled crRNA-injected) – were transplanted as per section 2.2.3. To ensure all hosts received a comparable number of macrophages during transplantation,

experimental groups were alternated such that ten embryos of each were injected at a single time, as described in section 2.2.4.1 and Figure 2.17.

Screening of embryos at 5dpf revealed that, as previously shown, microglia-depletion increased the number of transplant-derived cells in the brains of wild type hosts (Figure 5.1). Interestingly, the same was true of *rnaset2* mutants – with a ~5-fold increase in the number of GFP-positive cells in the brain across both microglia-depleted groups relative to the genotype-specific non-depleted controls (**Figure 1a, b**). There was no significant difference in engraftment between non-depleted *rnaset2* hosts and wild type controls – suggesting lack of functioning rnaset2 in the endogenous microglia is insufficient to promote robust recruitment of transplant-derived macrophages to the brain. Nonetheless, a small proportion (~10%) of non-depleted *rnaset2* mutant hosts were able to achieve the criteria for successful engraftment (10 or more cells in the brain). As such, subsequent experiments explored the downstream impact of transplantation in both microglia-depleted and non-depleted *rnaset2* hosts, acknowledging that sample collection was likely to be more challenging for the non-depleted group.

5.3.1.2 Transplanted cells adopt microglia-like phenotypes in the absence of endogenous microglia in rnaset2 mutant hosts

After establishing that transplant-derived cells were able to reach the brains of *rnaset2* hosts, I next sought to investigate the phenotype of these cells. To assess the ability of transplant-derived macrophages to adapt to their new CNS environment, immunohistochemistry against the microglia specific marker 4C4 was performed. Co-localisation of 4C4 and anti-GFP staining revealed robust expression of this microglia marker by transplant-derived cells in microglia-depleted hosts at both 5- and 8dpf (59% and 77%, respectively) (Figure 5.2). However, in non-depleted embryos, expression of microglia-specific markers by transplant-derived cells was significantly poorer (23% at 5dpf; 49% at 8dpf). Interestingly, in both groups, the percentage of 4C4 expression by GFP-positive cells increased from 5- to 8dpf (no statistics performed; experiments performed on separate biological repeats) – suggesting that increased time since transplantation may induce greater expression of 4C4 by transplant-derived cells. Nonetheless, 4C4-GFP co-localisation remained much poorer in non-depleted hosts relative to microglia-depleted larvae, suggesting fewer transplant-derived cells adopt microglia-like phenotypes in non-depleted *rnaset2* mutants.

5.3.2 Transplantation rescues uncleared apoptotic cell burden in rnaset2 embryos

After demonstrating that transplant-derived cells differed both in number and 4C4-expression status in microglia-depleted and non-depleted hosts, I next sought to assess the functionality of these cells – namely their ability to clear apoptotic debris. Previous work has demonstrated that macrophage

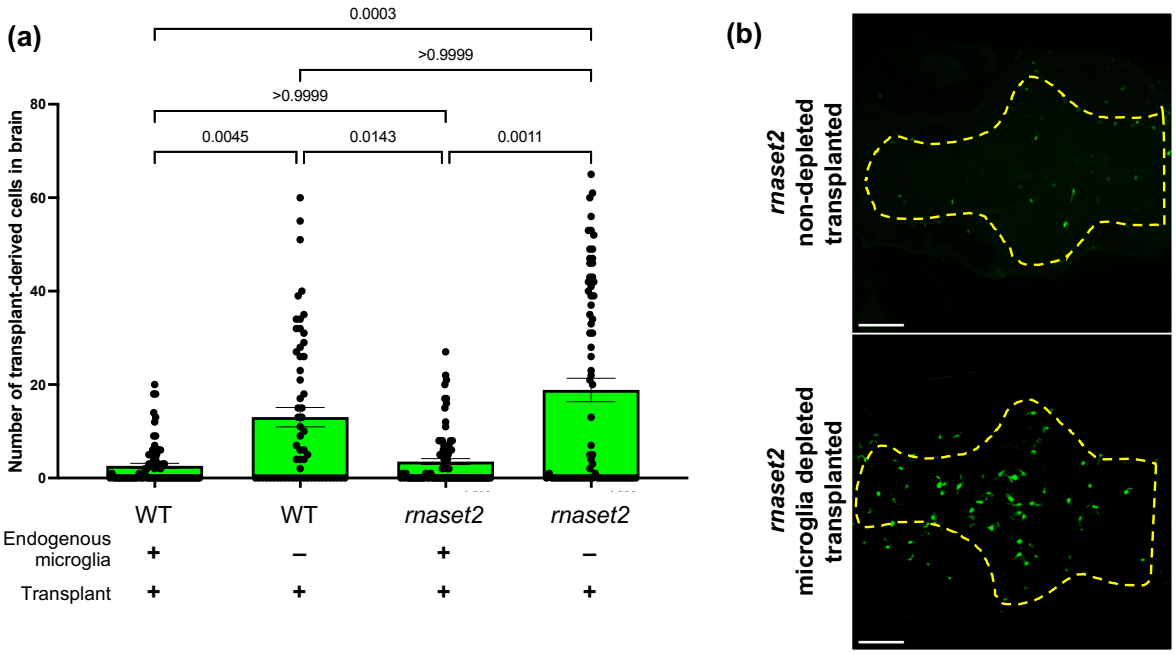

Figure 5.1. Transplanted macrophages compete with endogenous cells to fill the microglia niche in *rnaset2* mutants.

a. Quantification of the number of GFP-positive cells within *rnaset2* mutant and wild type host brains with and without microglia-depletion via knockout of *irf8*. Kruskal-Wallis test with Dunn's multiple comparisons, 3 biological replicates, n=60–90. **b.** Representative images of *rnaset2* transplanted hosts with and without microglia depletion. Red dashed line indicates outline of the brain. Scale bar represents 100µm.

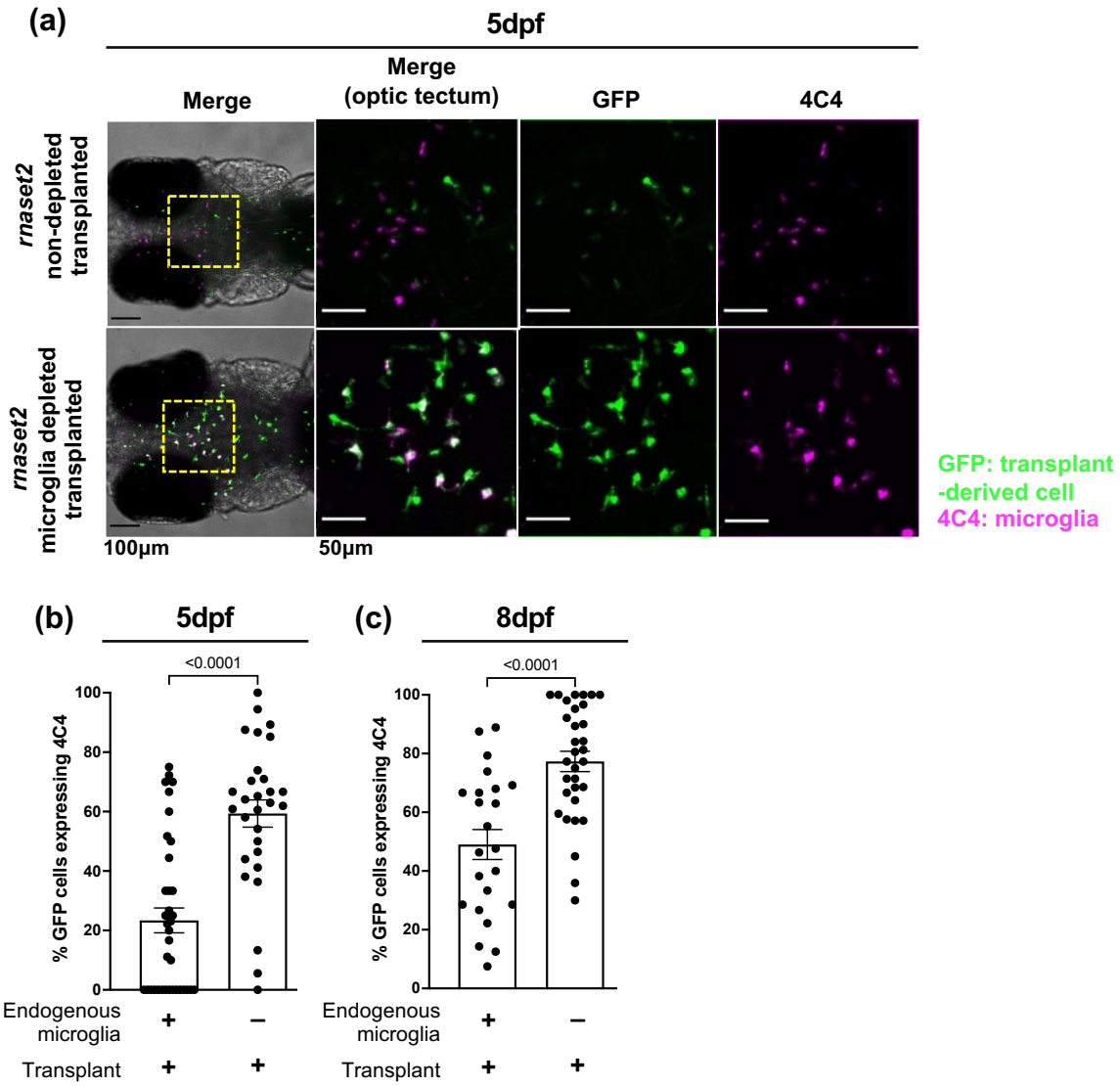

Figure 5.2. Transplanted macrophages express microglia-specific markers in microglia-depleted hosts.

Quantification of 4C4-expression of transplant-derived cells in microglia-depleted versus non-depleted *rnaset2* hosts at 5– (a, b) and 8dpf (c) reveals reduced expression of 4C4 by transplanted cells in non-depleted hosts. Mann Whitney test. 3 biological replicates, n=29–37 (a, b). 3 biological replicates, n=23–32 (c).

transplantation rescues the number of uncleared apoptotic cells in microglia-depleted wild type hosts in a dose-dependent manner (Figure 4.2). As a failure of *rnaset2* mutant microglia to digest dying cells during development is thought to be one of the central features of early neuropathology in this model, I investigated if this ability of transplanted macrophages to clear apoptotic debris was conserved in *rnaset2* mutants. Indeed, TUNEL staining revealed that transplanted animals exhibited significantly fewer uncleared apoptotic cells at 5– and 8dpf, with a complete rescue to wild type levels at 8dpf (Figure 5.3). Interestingly, this clearance of apoptotic cells was comparable across transplanted animals regardless of endogenous microglia depletion at both ages (Figure 5.3a,b). Crucially, this data demonstrates the ability of transplant-derived cells to undertake a key microglia function – clearance of apoptotic debris – in our disease model, both with and without microglia depletion, and suggests macrophage transplantation may rescue neuropathology in *rnaset2* larvae.

5.3.3 Transplantation rescues antiviral response in larvae

Previous publications have hypothesised that the failure of *rnaset2* mutant microglia to clear developmental apoptosis may trigger downstream neuropathology – in particular, the antiviral response which is prominently upregulated in mutants during larval and adult stages (Hamilton *et al.*, 2020a). Accordingly, I next sought to investigate whether the presence of transplant-derived cells in the brain could reduce the antiviral responses in larvae. Quantification of relative gene expression in the heads of 8dpf larvae revealed an approximately four-fold downregulation of the interferon response gene *isg15* in transplanted mutants, both with and without microglia depletion (Figure 5.4a). A similar pattern of rescue was observed for another interferon-induced antiviral response gene, *mxa*, although notably this was not significant (Figure 5.4b). Interestingly, no differences in expression were identified for the antiviral gene, *ifnφ1 secreted,* or a marker of more general inflammation, *il1β* (although, for *ifnφ1 secreted*, it should be noted that expression levels were so low across all groups for this transcript that a Cq value could only be identified for two repeats and so no statistical comparisons could be performed) (Figure 5.4c,d). Nonetheless, these data suggest normalisation of at least some aspects of the antiviral response following transplantation, even at this early stage (just 6 days post-transplant).

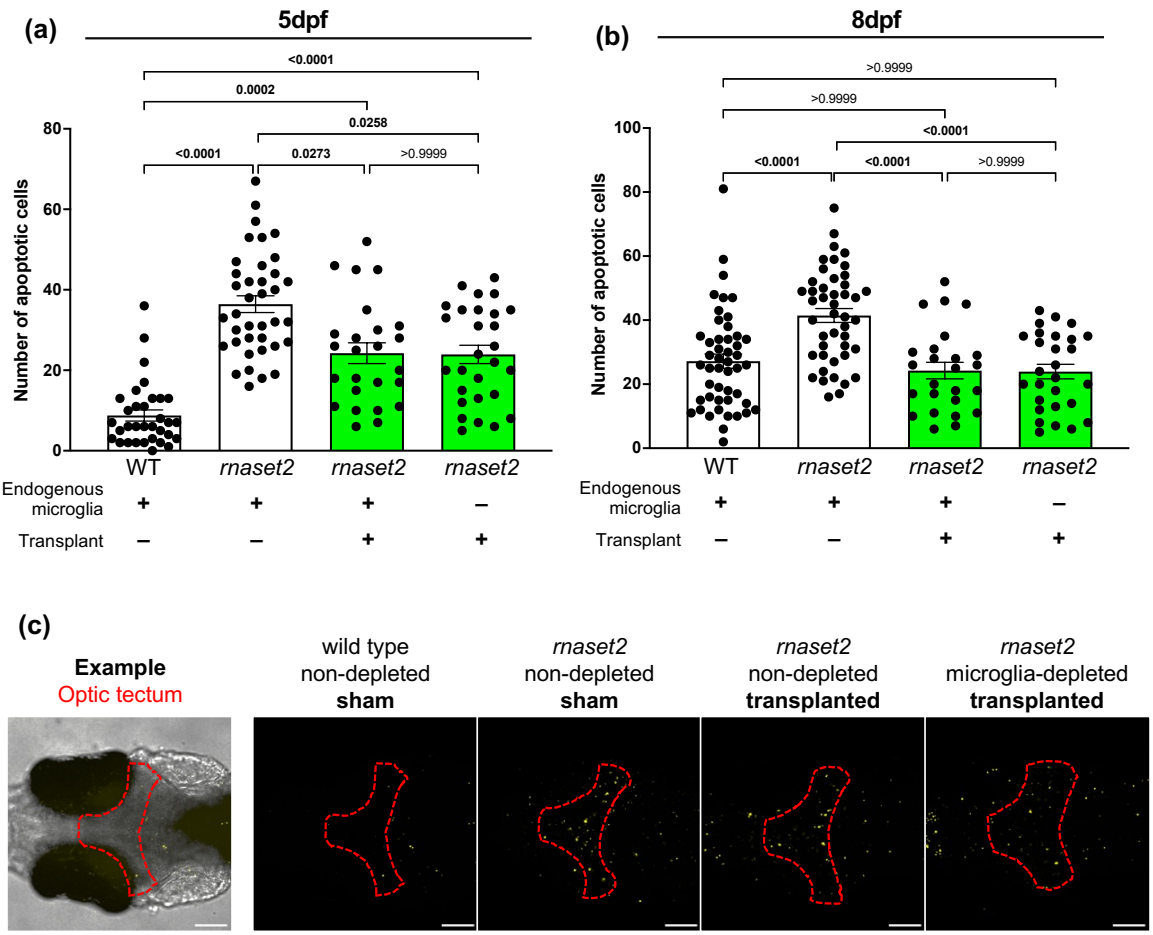

Figure 5.3. Macrophage transplantation promotes clearance of apoptotic cells in *rnaset2* mutants. **a, b.** Macrophage transplantation reduces the number of uncleared apoptotic cells in the optic tectum of 5– (a) and 8dpf (b) *rnaset2* mutants. Kruskal-Wallis test with Dunn's multiple comparisons. 4 biological replicates, n=25–38 (a). 3 biological replicates, n=25–48 (b). **c.** Representative images of TUNEL counts in the optic tectum of 8dpf animals (red dashed line). Scale bar represents 100µm.

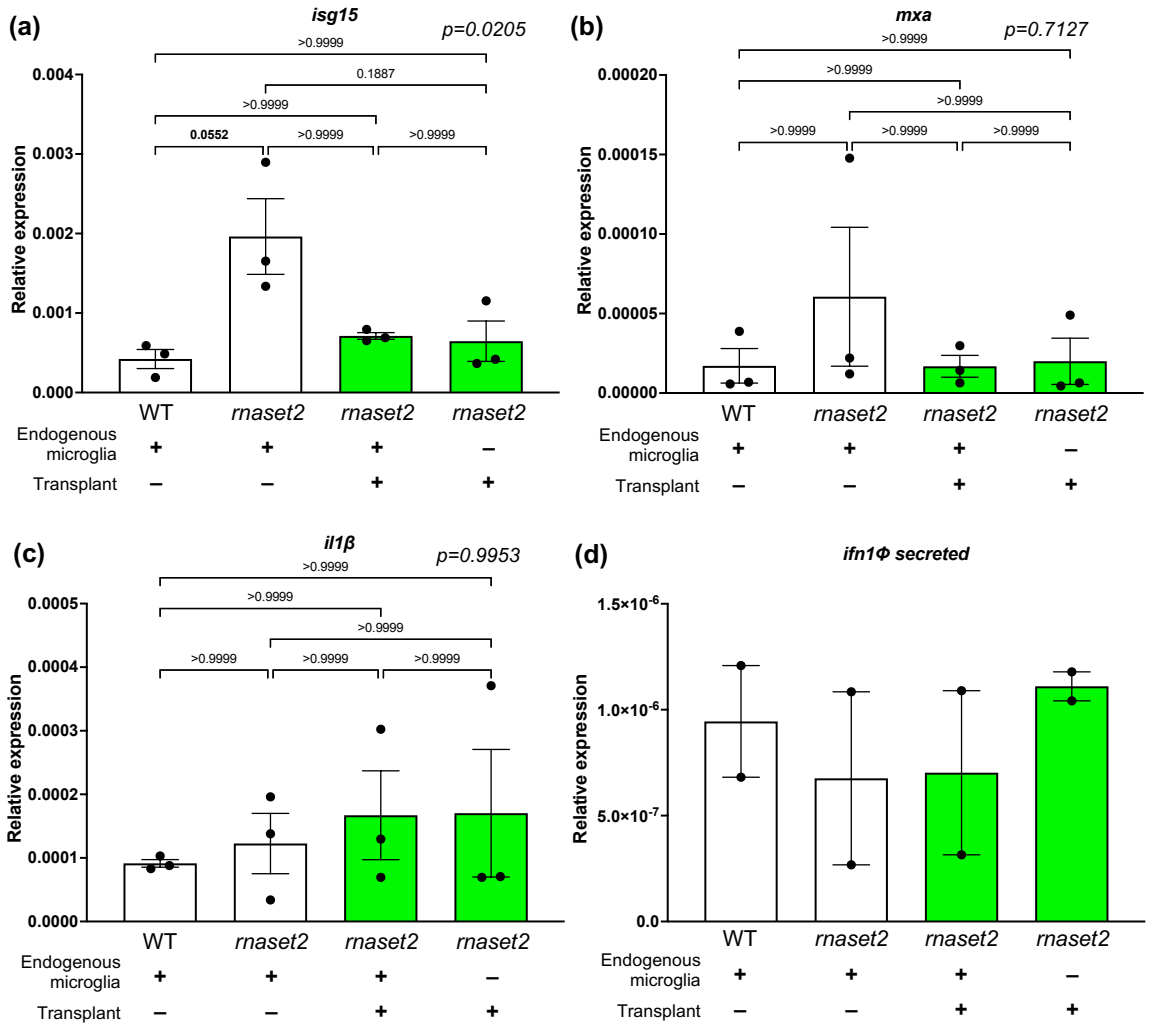

Figure 5.4. Macrophage transplantation reduces antiviral response in 8dpf *rnaset2* embryos. qPCR of *isg15* (a), *mxa* (b), *il1β* (c) and *ifnΦ1 secreted* (d) expression in the heads of transplanted animals and non-transplanted controls. Kruskal-Wallis test with Dunn's multiple comparisons. Kruskal-Wallis test p-value is indicated at top right of each figure. 3 (a,b,c) or 2 (d) biological replicates, 15 embryos pooled per replicate.

5.3.4 Transplantation does not increase global expression of rnaset2 in transplanted brains

Following the finding that transplantation can both reduce the number of uncleared apoptotic cells and the antiviral response in *rnaset2* mutant larvae, I next sought to understand whether this rescue was due to a global increase in the levels of functioning rnaset2 in transplanted brains, derived from *rnaset2*-competent transplanted cells. As such, I assessed the expression of *rnaset2* within transplanted brains by qPCR, as a proxy for enzyme levels across the entire tissue. Interestingly, *rnaset2* transcript levels remained downregulated in transplanted mutants compared to wild type controls (Figure 5.5), suggesting that normalisation of the antiviral response was unlikely to be due to elevated levels of functional, transplant-derived rnaset2 throughout the brain.

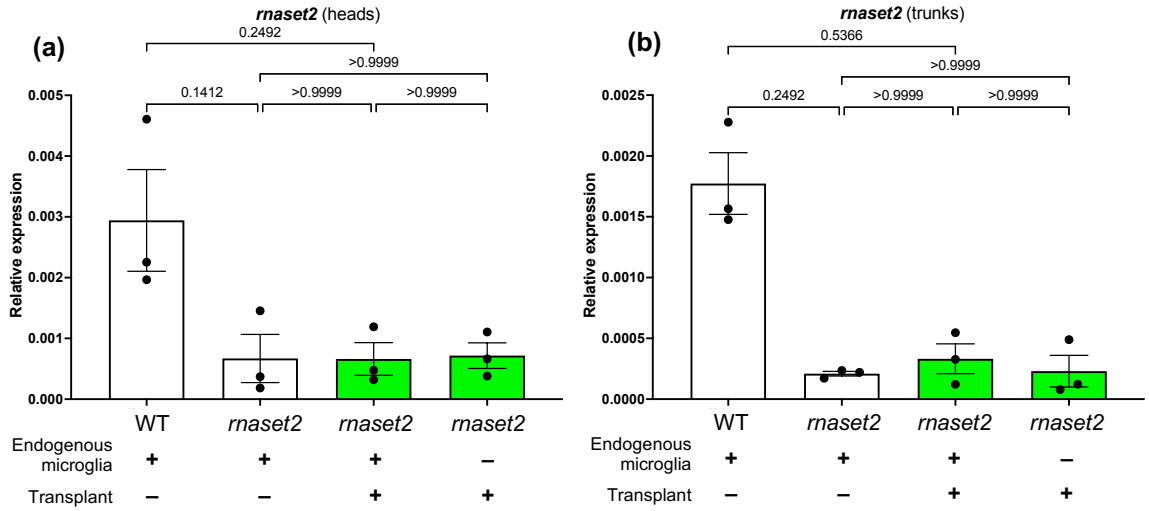

Figure 5.5. Transplantation of healthy macrophages does not increase global *rnaset2* expression in *rnaset2* mutant heads (a) nor trunks (b).
Kruskal-Wallis test with Dunn's multiple comparisons. 3 biological replicates, 15 embryos pooled per replicate.

5.3.5 Transplantation does not affect expression of myelin-associated genes

Given that RNASET2-deficient leukodystrophy is primarily a white matter disorder, I next sought to assess the impact of transplantation on myelin levels in *rnaset2* mutants. However, transplantation did not rescue the expression of myelin-associated transcripts – *mbpa*, *mbpb*, *mpz* or *plp1a* – in neither the trunks nor the heads of *rnaset2* hosts at 8dpf (Figure 5.6). As discussed in section 3.3.1, *mbpa* expression is significantly reduced in *rnaset2* mutant relative to wild type controls when quantifying transcripts at a whole organism level. This experiment extends this finding, demonstrating a prominent difference in *mbpa* expression in *rnaset2* mutant heads but not the trunks – suggesting most of this difference is likely to be due to reduced expression in the brain. However, these levels were not increased in either transplant group (with or without microglia depletion) – indicating that the presence of healthy macrophages may not be sufficient to rescue myelin pathology at this age.

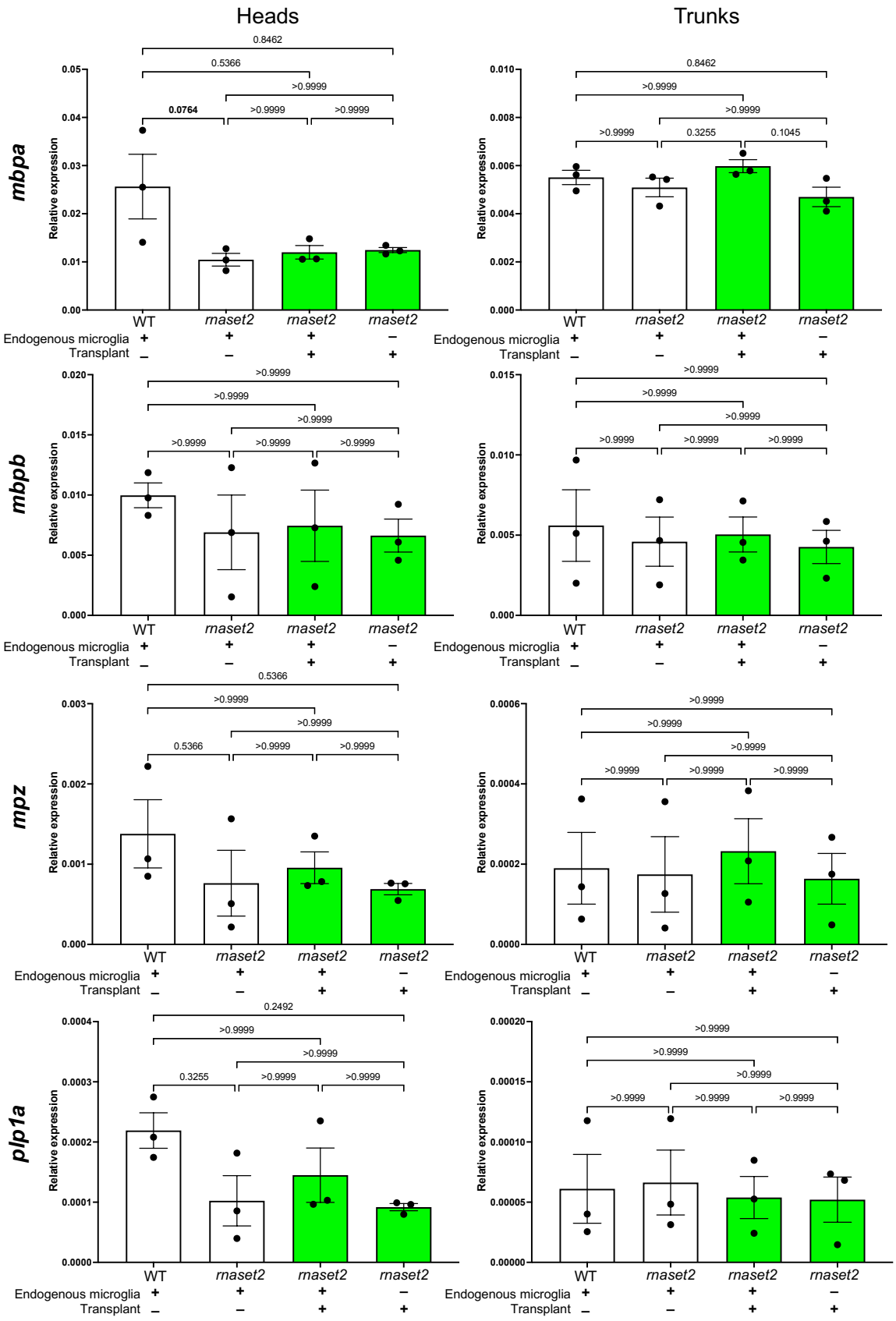

Figure 5.6. Transplantation does not rescue expression of myelin-associated genes in *rnaset2* mutant heads nor trunks.

Kruskal-Wallis test with Dunn's multiple comparisons. 3 biological replicates, 15 embryos pooled per replicate.

5.3.6 Transplantation rescues larval locomotor behaviours

After demonstrating that macrophage transplantation was able to rescue neuroinflammation, but not expression of myelin-associated transcripts, I next sought to investigate the impact of transplantation on larval behaviour. In alignment with findings in section 3.3.2.1, larval swimming analysis revealed that *rnaset2* mutants were hypoactive relative to wild type controls, with microglia-depleted mutants showing the greatest impairment of swimming behaviour (Figure 5.7). However, transplanted mutants swam greater distances over a 20-minute period at 8dpf compared to non-transplanted controls. While not all of these comparisons were statistically significant, analysis revealed a biologically relevant increase in distance travelled: +11% for non-depleted transplanted mutants versus non-depleted controls and +21% for microglia-depleted transplanted mutants versus microglia depleted controls. Interestingly, transplantation also appeared to increase swimming activity of *rnaset2* mutants in response to stimuli in acoustic startle assays (see Appendix 1. Acoustic startle response in transplanted *rnaset2* mutants). Therefore, transplantation of healthy phagocytes appears to increase the motor output of *rnaset2* mutant larvae – suggesting this intervention may rescue behavioural deficits in this disease model.

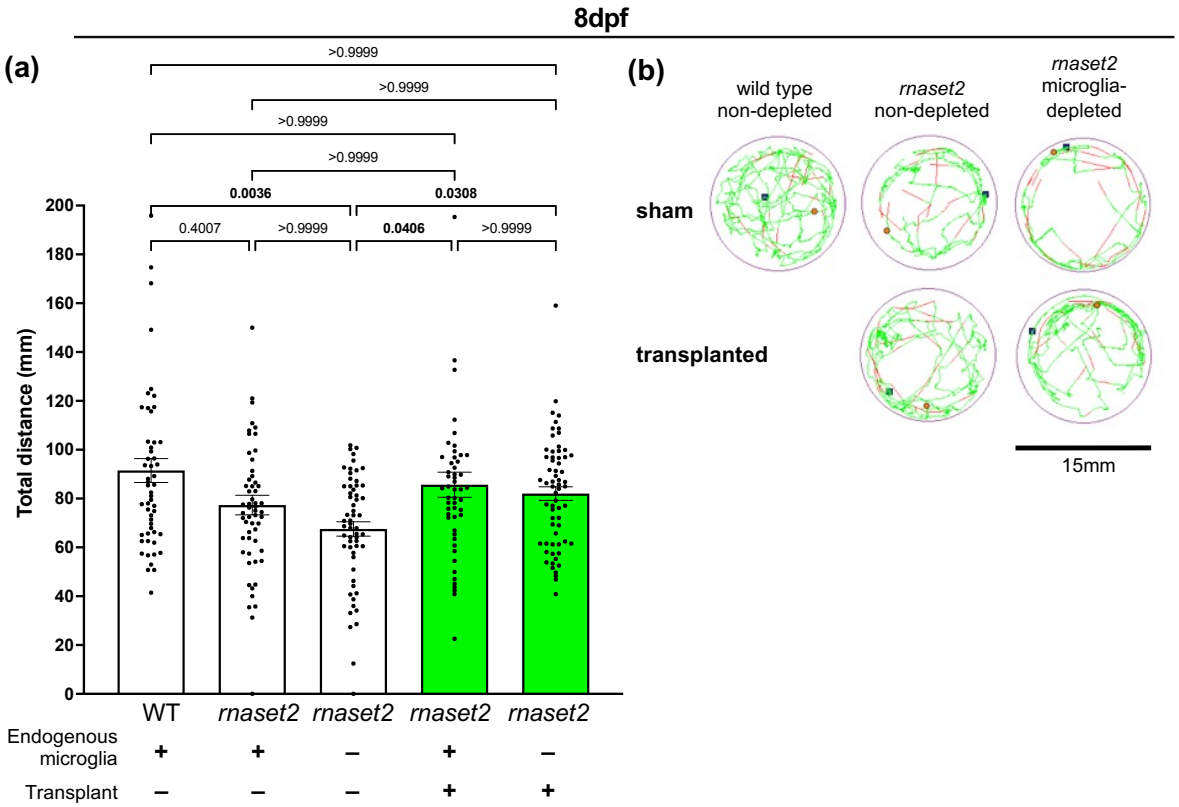

Figure 5.7. Transplantation rescues *rnaset2* mutant larval free-swimming behaviour.
a. Live tracking of larval swimming behaviour reveals that transplanted *rnaset2* mutants swim greater distances than non-transplanted controls. Kruskal-Wallis test with Dunn's multiple comparisons. 3 biological replicates, n=52–60. **b.** Representative traces of free-swimming behaviour of zebrafish larvae. Green line represents slow movements (3.0–6.6mm/s), red line represents fast movements (>6.6mm/s).

5.3.7 Transplanted cell numbers peak at 4wpf in rnaset2 mutants

After characterising the impact of transplantation in *rnaset2* mutant larvae, I next sought to investigate the impact of transplant-derived macrophages beyond larval stages. As discussed in section 4.3.3, transplant-derived cells initially increased in number in wild type microglia-depleted host brains – peaking at 4wpf – but were no longer detectable by 14wpf. Hence, I next investigated these key timepoints in transplanted *rnaset2* mutants to assess the longevity of transplanted cells in this disease model and establish whether engraftment dynamics were comparable to those seen in wild type hosts.

Interestingly, like in microglia-depleted wild type hosts, tissue clearing revealed robust engraftment of transplanted cells in microglia-depleted *rnaset2* brains at 4wpf – accounting for ~40% of the total microglial population at this age (Figure 5.8). However, in non-depleted *rnaset2* mutants, transplanted cells were present in only small numbers by 4wpf – suggesting that these cells do not persist to this age when host microglia are present. Across both groups, transplant-derived macrophages were absent at 14wpf, consistent with findings in wild type animals (Figure 5.8a,b). Nonetheless, these data suggest that transplant-derived cells are able to maintain engraftment for the month of life in hosts lacking endogenous microglia during early development, regardless of genotype. I therefore decided to use this time point – 4wpf – to investigate the impact of transplantation on *rnaset2* pathology beyond larval stages.

5.3.8 RNA sequencing reveals downregulation of antiviral signalling in transplanted rnaset2 mutants at 4wpf

To assess the impact of transplantation on *rnaset2* pathology at a whole brain level, RNA sequencing was performed on dissected brains from transplanted *rnaset2* mutants at 4wpf, along with age-matched sham-transplanted mutants and wild type. To minimise the need for multiple comparisons (and therefore the stringency of p value correction, which may mask biologically relevant changes), two separate analyses were performed for transplanted animals with their corresponding controls: firstly, comparing wild type sham, *rnaset2* sham and *rnaset2* transplanted non-depleted animals, with a second analysis comparing wild type sham, *rnaset2* sham and *rnaset2* transplanted microglia-depleted animals.

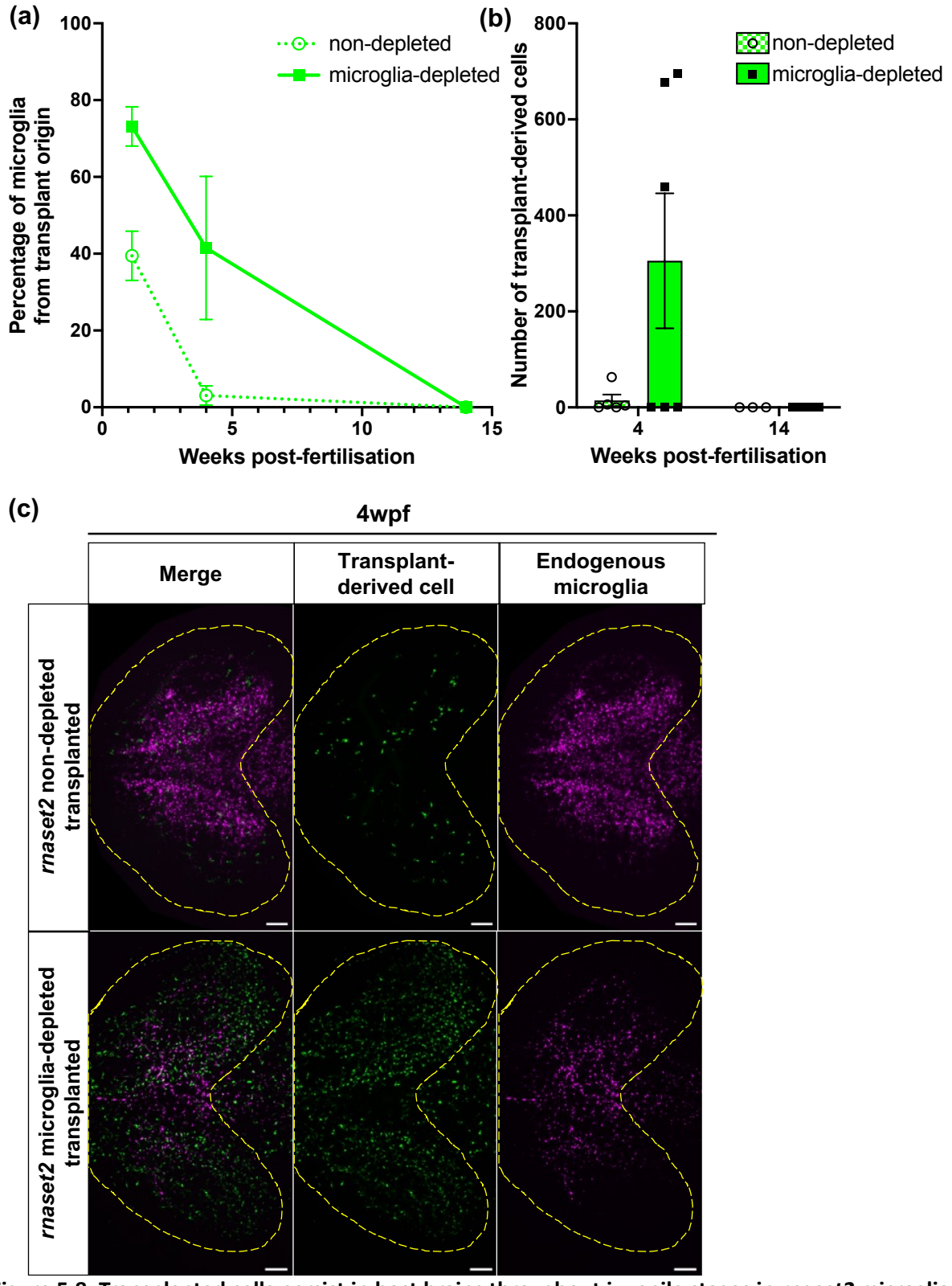

Figure 5.8. Transplanted cells persist in host brains throughout juvenile stages in *rnaset2* microglia-depleted mutants.

a, b. Tissue clearing and immunohistochemistry reveal reduced numbers of transplant-derived cells in non-depleted *rnaset2* animals compared with microglia-depleted siblings. Cells are no longer visible in both host groups by 14wpf. **c.** Representative image of transplant-derived cell engraftment at 4wpf in non-depleted and microglia-depleted *rnaset2* hosts. Yellow line indicates optic tectum outline. Scale bar represents 100µm.

5.3.8.1 Sequencing of non-depleted animals

Sequencing of non-depleted *rnaset2* mutants versus non-depleted wild types revealed 171 significantly differentially expressed genes (DEGs), while comparison of transplanted versus sham *rnaset2* mutants revealed just 72 DEGs. This relatively small number of significant DEGs may be attributed to high intra-group variability, as visualised by principal component analysis (PCA) (Figure 5.9a). Gene ontology analysis of DEGs identified in transplanted mutants versus untreated controls revealed 33 significantly enriched pathways in *rnaset2* transplanted animals compared with sham controls (Figure 5.9d). Interestingly, several of these pathways relate to nucleic acid metabolism – including "regulation of nucleobase-containing compound metabolic process", "regulation of RNA metabolic process" and "regulation of RNA biosynthetic process" – which may be of particular interest given the role of rnaset2 as a ribonuclease. Nonetheless, RNA sequencing of non-depleted samples failed to identify any pathways related to neuropathology, providing limited insight into the effects (if any) of transplantation on pathogenesis in non-depleted hosts.

5.3.8.2 Sequencing of microglia-depleted animals

In contrast, sequencing of microglia-depleted animals identified a greater number of differentially expressed genes (DEGS): 331 for *rnaset2* mutants versus wild type, and 117 for transplanted versus sham *rnaset2* mutants. PCA analysis revealed clustering of *rnaset2* transplanted samples – suggesting minimal variability within this group – although substantial intragroup variability was present in the wild type group (Figure 5.10a). Interestingly, transplanted *rnaset2* mutants cluster more closely to wild type samples than non-transplanted mutants – suggesting that transplanted brains may be more transcriptionally similar to wild type brains. Gene ontology analysis identified 31 significantly enriched pathways in *rnaset2* transplanted animals compared with *rnaset2* sham controls (Figure 5.10d). Strikingly, 25/31 of these pathways were related to immune, and specifically antiviral, response (Figure 5.11a). Antiviral-associated pathways were downregulated in transplanted animals relative to non-transplanted *rnaset2* mutants, with several of these pathways – including "Response to virus" and "ISG15 antiviral mechanisms" – restored to wild type levels (Figure 5.11b,c; see also Appendix 2. RNA sequencing of transplanted *rnaset2* mutants). These findings were supported by gene set enrichment analysis, which revealed that the greatest number of downregulated genes were found in the "Innate Immune Response" pathway for transplanted animals relative to sham controls. These results, therefore, suggest that antiviral signalling may be normalised by transplantation in *rnaset2* mutants.

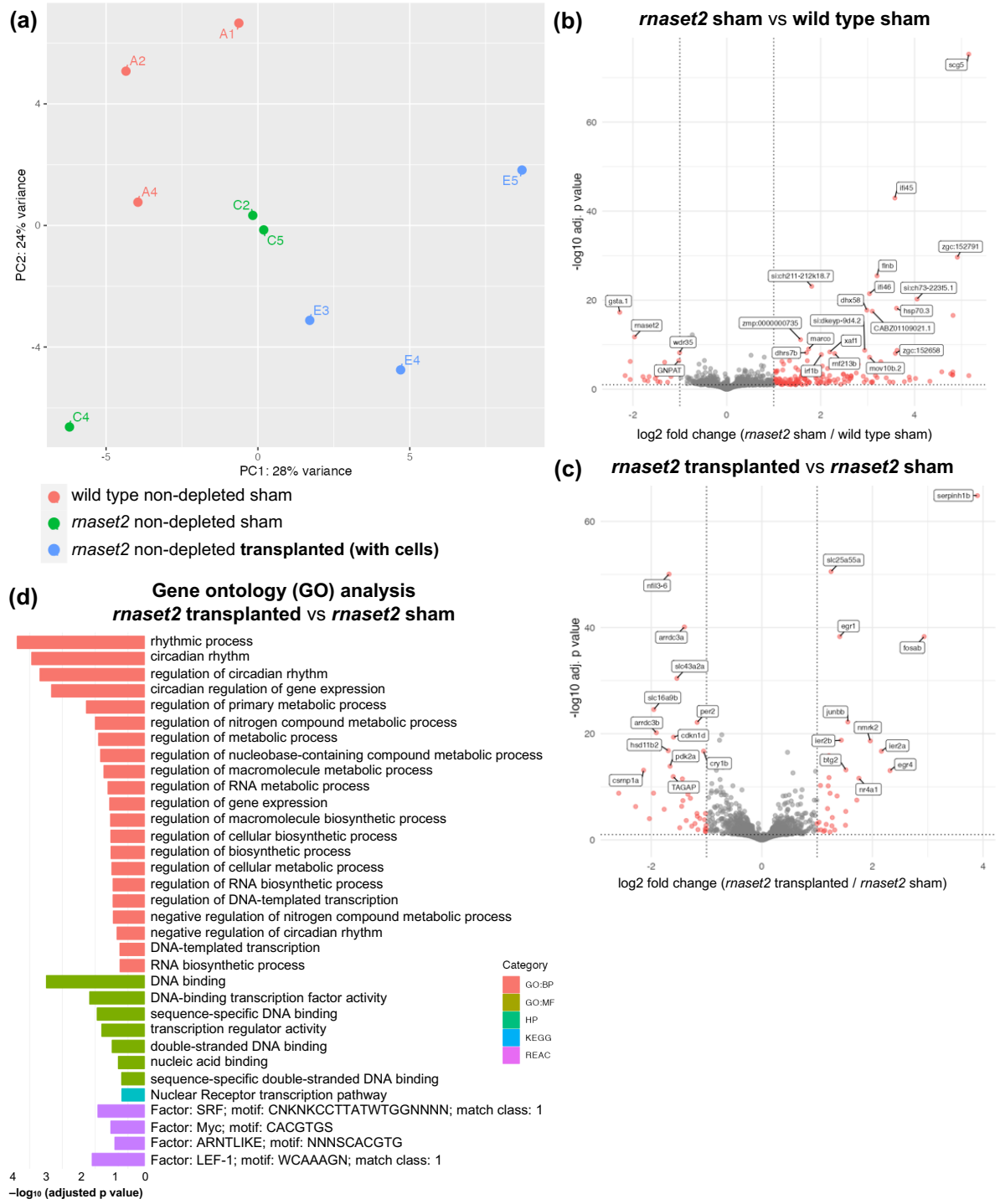

Figure 5.9. RNA sequencing of non-depleted wild type sham, *rnaset2* sham and *rnaset2* transplanted brains.

a. Principal component analysis (PCA) plot reveals clustering of brains within each group. **b, c.** Volcano plot of differentially expressed genes between *rnaset2* sham versus wild type sham (b) and *rnaset2* transplanted versus *rnaset2* sham groups (c) (all non-depleted). Significantly differentially regulated genes are shown in red. The top 25 differentially expressed genes are annotated. **d.** Gene ontology (GO) plot showing significantly enriched pathways in *rnaset2* non-depleted transplanted animals compared with non-depleted sham controls. Enriched pathways identified by gProfiler (https://biit.cs.ut.ee/gprofiler/gost).

Figure 5.10. RNA sequencing of microglia-depleted wild type sham, *rnaset2* sham and *rnaset2* transplanted brains.

a. Principal component analysis (PCA) plot reveals clustering of brains within each group. **b, c.** Volcano plot of differentially expressed genes between *rnaset2* sham versus wild type sham (b) and *rnaset2* transplanted versus *rnaset2* sham groups (c) (all microglia-depleted). Significantly differentially regulated genes are shown in red. The top 25 differentially expressed genes are annotated. **d.** Gene ontology (GO) plot showing significantly enriched pathways in *rnaset2* microglia-depleted transplanted animals compared with microglia-depleted sham controls. Enriched pathways identified by gProfiler (https://biit.cs.ut.ee/gprofiler/gost).

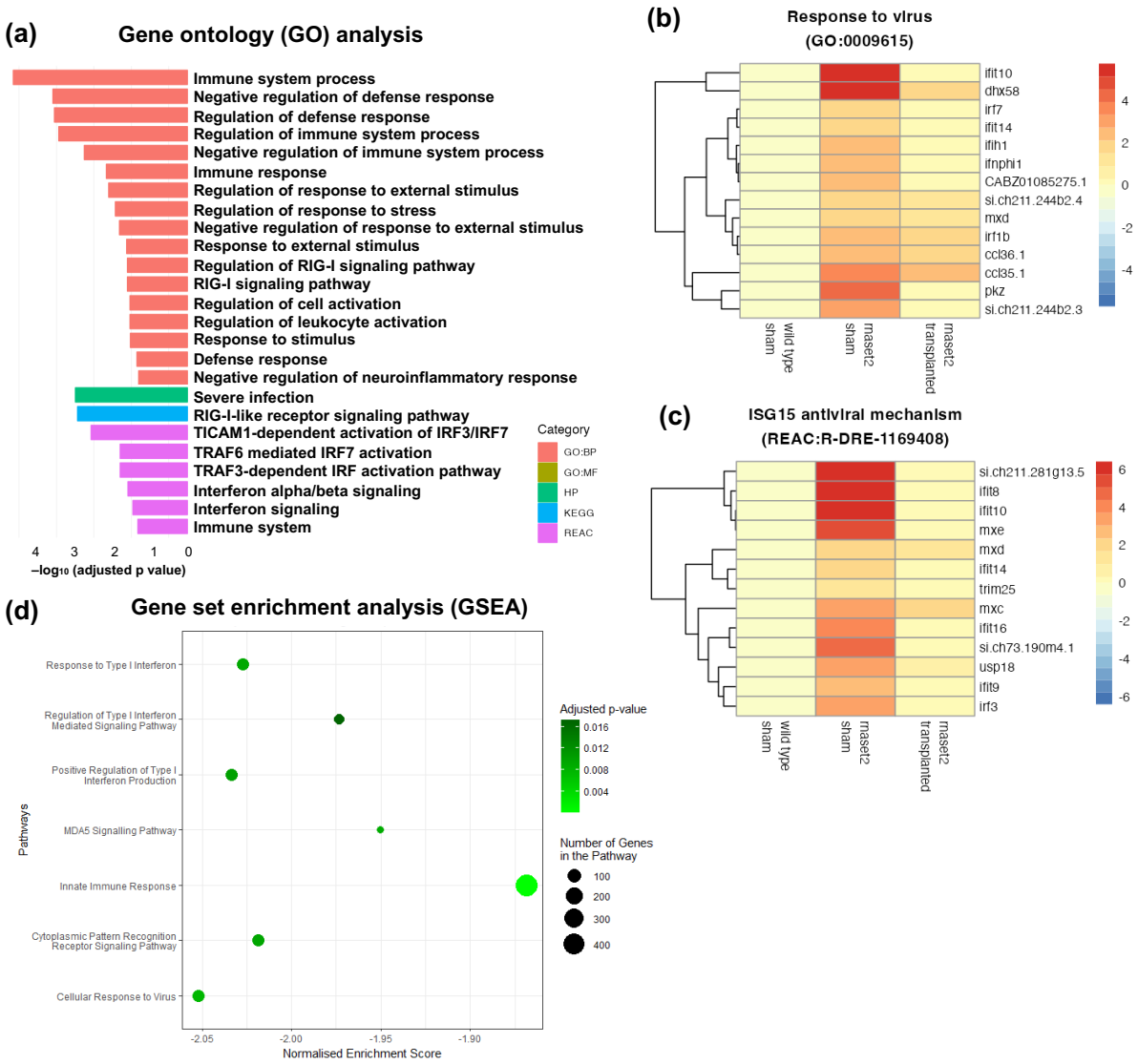

Figure 5.11. Pathway enrichment analysis reveals that microglia replacement recues antiviral immune response in 4wpf *rnaset2* microglia-depleted mutants.

a. Gene ontology (GO) plot showing significantly enriched pathways related to immune function in *rnaset2* microglia-depleted transplanted animals compared with microglia-depleted sham controls. **b, c.** Heatmap of genes belonging to response to virus (b) and ISG15 antiviral mechanism (c) GO pathways for all genes significantly upregulated in *rnaset2* microglia-depleted sham animals. Fold change relative to wild type microglia-depleted sham is indicated by color, with red indicating higher expression. For full heatmaps, see Appendix 1. Acoustic startle response in transplanted *rnaset2* mutants. **d.** GSEA in *rnaset2* microglia-depleted transplanted animals compared with microglia-depleted sham controls.

5.3.8.3 Validation of RNA sequencing

To validate the finding that transplantation reduces the expression of antiviral-associated genes in *rnaset2* mutants, qPCR expression analysis was performed on selected transcripts. In order to select candidates for validation, I first identified any genes that were differentially regulated in *rnaset2* sham relative to wild type sham samples and in *rnaset2* transplanted relative *rnaset2* sham samples. A total of 69 genes met these criteria, with 67 genes which were upregulated in mutants relative to wild type and downregulated following transplant (Figure 5.12). As expected, over half of these genes are involved in the interferon response (as identified by ZFIN (https://zfin.org/) or published in Levraud *et al.,* 2019). From this list, I selected two of the most differentially expressed antiviral transcripts – *isg15* and *cmpk2* – as well as a candidate which is not directly involved in interferon signalling but is highly expressed in macrophages – *cd68*. Gene expression analysis with qPCR confirmed the changes in expression identified by RNA sequencing – with the expression of each of these genes rescued to wild type levels following transplantation (Figure 5.13a–c). As an additional validation step, the expression of *rnaset2* was also investigated – revealing reduced expression in both sham and transplanted *rnaset2* mutants relative to wild type, in alignment with the expected biological effect (Figure 5.13d). Therefore, these findings validate the transcriptomic analysis described above, and demonstrate that transplantation is sufficient to rescue the brain-wide antiviral response in microglia-depleted *rnaset2* mutants.

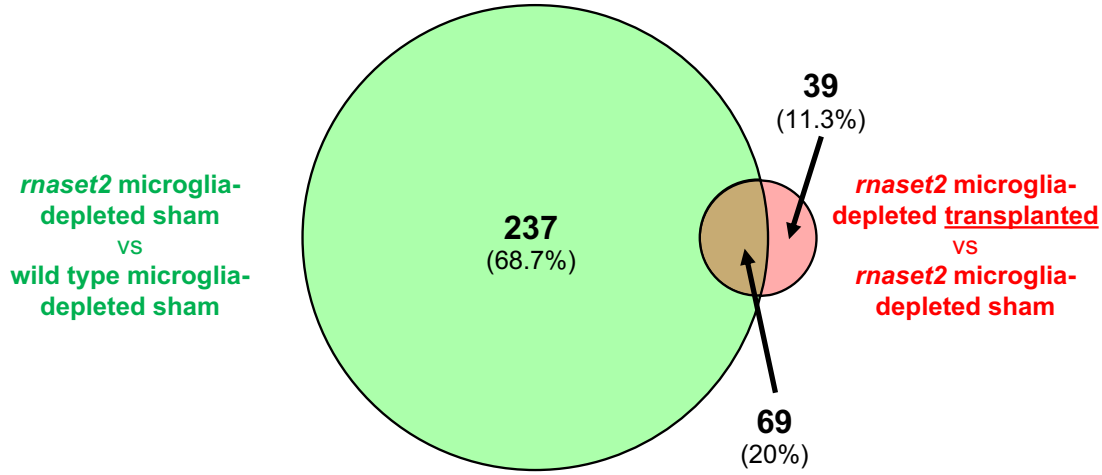

	log2 fold change	
Common differentially expressed genes	*rnaset2* microglia-depleted sham vs wild type microglia-depleted sham	*rnaset2* microglia-depleted transplanted vs *rnaset2* microglia-depleted sham
ftr80	9.734771053	-2.7050295
si:dkey-211g8.8	6.791982865	-4.8118329
zmp:0000000912	6.736902691	-2.4313241
cmpk2	6.729529312	-2.7283764
CU984600.2	6.040004913	-3.6758515
ifi46	5.934532527	-3.1266304
isg15	5.833056288	-3.181229
mov10b.1	5.699653344	-3.0490961
zgc:152658	5.479452948	-4.0613336
si:dkeyp-9d4.2 (ifi44a1)	5.30102727	-2.186786
dhx58	5.214060777	-2.92646
trim35-14	5.182714674	-4.0046973
si:ch211-281g13.4 (herc56.2)	4.942170629	-2.8388821
mov10b.2	4.606354374	-2.6521576
FO704622.1	4.469645605	-2.3452211
xaf1	4.285399773	-2.5620554
hsp70.3	4.146380055	-2.3012348
LO018432.1 (xgb)	3.95857414	-2.5438836
btr26	3.942383544	-2.2256046
rsad2	3.917832754	-2.4056179
si:ch211-197g15.6 (ifi44f5)	3.904010159	-3.0199251
irf3	3.589750287	-2.8217238
ssuh2.2	3.575589793	-2.2700297
ftr93	3.464423116	-2.367106
phf11	3.426258873	-2.1587056
ftr56	3.415073863	-1.3615268
stat2	3.409763995	-2.6807286
si:dkey-97a13.6 (helz2b)	3.365244839	-2.028989
hsp70.1	3.311416329	-1.9570956
hsp70.2	3.306355604	-1.7937952
helz2	3.278124862	-2.1689576
si:ch211-244b2.3	3.264983436	-1.622009
zmp:0000000735 (samd9l)	3.201433611	-1.7224258
usp18	3.115524079	-1.574364
ascl1b	3.053732505	-2.0993539

	log2 fold change	
Common differentially expressed genes	*rnaset2* microglia-depleted sham vs wild type microglia-depleted sham	*rnaset2* microglia-depleted transplanted vs *rnaset2* microglia-depleted sham
znfx1	3.023742855	-1.5612951
cxcl18b	2.899569143	-1.313528
si:ch211-197g15.8 (ifi44f3)	2.798576655	-1.2636454
marco	2.789623785	-1.8726118
lgals9l3	2.691465729	-1.9772003
si:dkey-40c23.2	2.645419737	-1.4840802
si:dkey-188i13.10 (ifi27.7)	2.59042203	-1.8404827
cd68	2.549490612	-1.6337118
parp12a	2.485393421	-1.842633
ifih1	2.476245201	-1.5977307
si:ch73-252i11.1	2.335544566	-1.7819006
gig2o	2.326392938	-1.2622741
sp100.2	2.287616663	-1.2877068
si:ch211-199g17.2	2.230788079	-1.2547993
irgq1	2.159294065	-2.070377
wu:fj29h11	2.005729167	-1.6744582
tdp2a	1.939905723	-2.0282283
irf7	1.876073997	-1.4807902
socs1a	1.8693998	-1.7641159
ftr14	1.822357757	-1.3329678
si:ch211-219a4.3 (parp14rs1)	1.736755442	-1.019893
adgrg1	1.690968383	-1.5723322
rnf213a	1.59629438	-1.0801253
grna	1.579351884	-1.1215752
trim25	1.528511297	-1.234642
sp100.1	1.51715915	-1.5638502
si:ch73-233k15.2 (apol)	1.457052876	-1.814265
si:dkeyp-1h4.6	1.380053105	-2.1120016
rxfp1	1.356435264	-1.0345777
nr1d4b	1.215517963	-1.2514786
si:ch211-1a19.3	1.185023286	-1.3604966
dhrs13b.2	1.17052979	-1.4392125
si:ch211-1f22.1	-3.02711094	2.21717627
mlpha	-4.910745915	4.2607506

Figure 5.12. Common differentially expressed genes between *rnaset2* transplanted versus *rnaset2* sham, and *rnaset2* sham vs wild type sham samples (with microglia depletion).
Adapted from Venny 2.1.0. Highlighted genes indicate those involved in interferon response as identified by ZFIN (https://zfin.org/) or Levraud *et al.,* 2019. Bold genes were taken forward for validation.

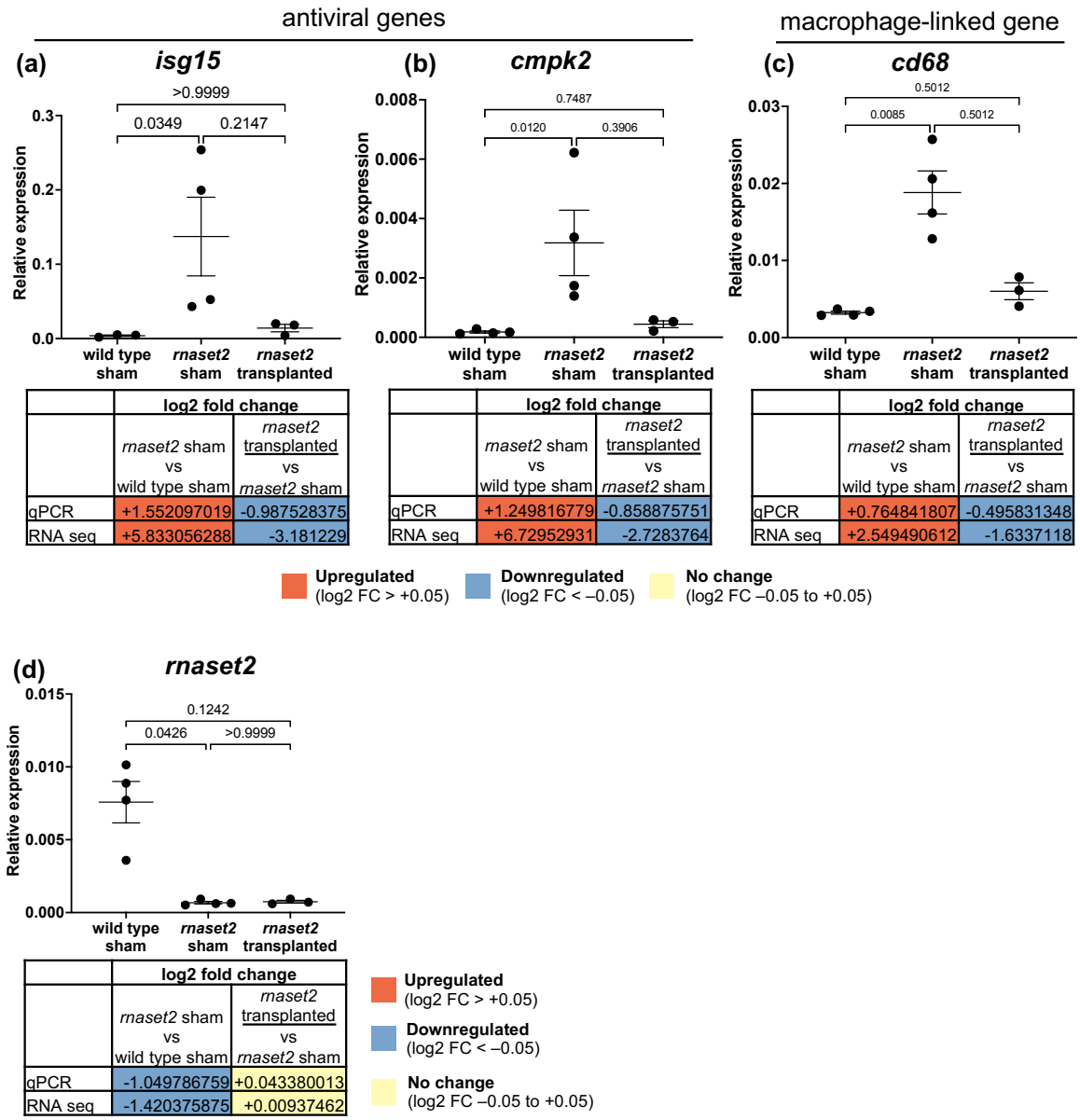

Figure 5.13. Validation of RNA sequencing hits by qPCR confirms rescue of antiviral- and macrophage-associated transcripts.

qPCR of antiviral genes *isg15* (a) and *cmpk2* (b), macrophage-associated gene *cd68* (c) and *rnaset2* (d) confirms changes in gene expression identified by RNA sequencing for microglia-depleted wild type sham, *rnaset2* sham and *rnaset2* transplanted brains. Plots show relative expression, 3–4 biological replicates, Kruskal-Wallis test with Dunn's multiple comparisons. Tables indicate fold change identified by qPCR and RNA sequencing.

5.3.9 Transplantation rescues juvenile free-swimming behaviour deficits in rnaset2 mutants

Considering the finding that transplantation rescues the brain-wide antiviral response at 4wpf, I next sought to assess the impact of these cells on swimming activity to establish whether the functional rescue seen in transplanted larvae persisted into juvenile stages.

To estimate the number of fish that would be required to test the hypothesis that transplantation will improve the swimming activity of *rnaset2* mutants at 4wpf, a power calculation was performed based on the data presented in Chapter 3. For this experiment, four groups were required: wild type non-depleted sham, *rnaset2* non-depleted sham, *rnaset2* microglia-depleted sham and *rnaset2* microglia-depleted transplanted. The estimated sample size to detect a meaningful difference in the swimming distance of transplanted and non-transplanted *rnaset2* mutants was calculated data from free swimming assessment of wild type and *rnaset2* 4wpf animals (see Chapter 3, section 3.3.2.3), based on the following assumptions:

1. *rnaset2* non-depleted sham and *rnaset2* microglia-depleted sham will be comparable to untouched *rnaset2* from free-swimming experiment in Chapter 3, Figure 3.11
2. The transplanted group will show ~50% rescue of swimming distances

To assess overall differences between the four treatment groups, one-way ANOVA (or equivalent non-parametric test) was selected as the appropriate statistical test. Using the estimates above, the anticipated effect size for this analysis was 0.43. As such, the total sample size required to detect this effect size (α=0.05, 1–β=0.80), was 64, meaning 16 animals per group would be required to detect any meaningful differences between all groups. However, given that this is the sample size required to detect power at a group level in the ANOVA, rather than for the multiple comparisons (which will require a greater n for comparable statistical power), I aimed to exceed this number with sample collection – particularly for the transplanted group in which variability is likely to be higher.

In confirmation with previous findings (Chapter 3, section 3.3.2.3; Figure 3.11), *rnaset2* mutants were significantly less active than their wild type counterparts at 4wpf. However, in alignment with the behavioural rescue at 8dpf, transplanted microglia-depleted 4wpf *rnaset2* mutants showed greater motor activity over a 10-minute period of free-swimming, compared with sham controls (Figure 5.14a). Notably, at this timepoint, non-depleted transplanted *rnaset2* animals were not assayed due to a failure of persistent engraftment in these animals by 4wpf (see section 5.3.7). Interestingly, in microglia-depleted transplanted hosts, the extent of motor recovery was similar between juveniles which had persistent cell engraftment and those which did not – suggesting that there may be some residual benefits of transplantation shortly after these cells disappear from the brain (Figure 5.14b). Most strikingly, this behavioural improvement appeared to be accompanied by an increase in survival

of transplanted *rnaset2* mutants at 4wpf relative to microglia-depleted sham controls (Figure 5.14c,d). As such, macrophage transplantation appears to have therapeutic benefits beyond embryonic stages lasting into juvenile stages in *rnaset2* mutants at a transcriptional to a cellular level.

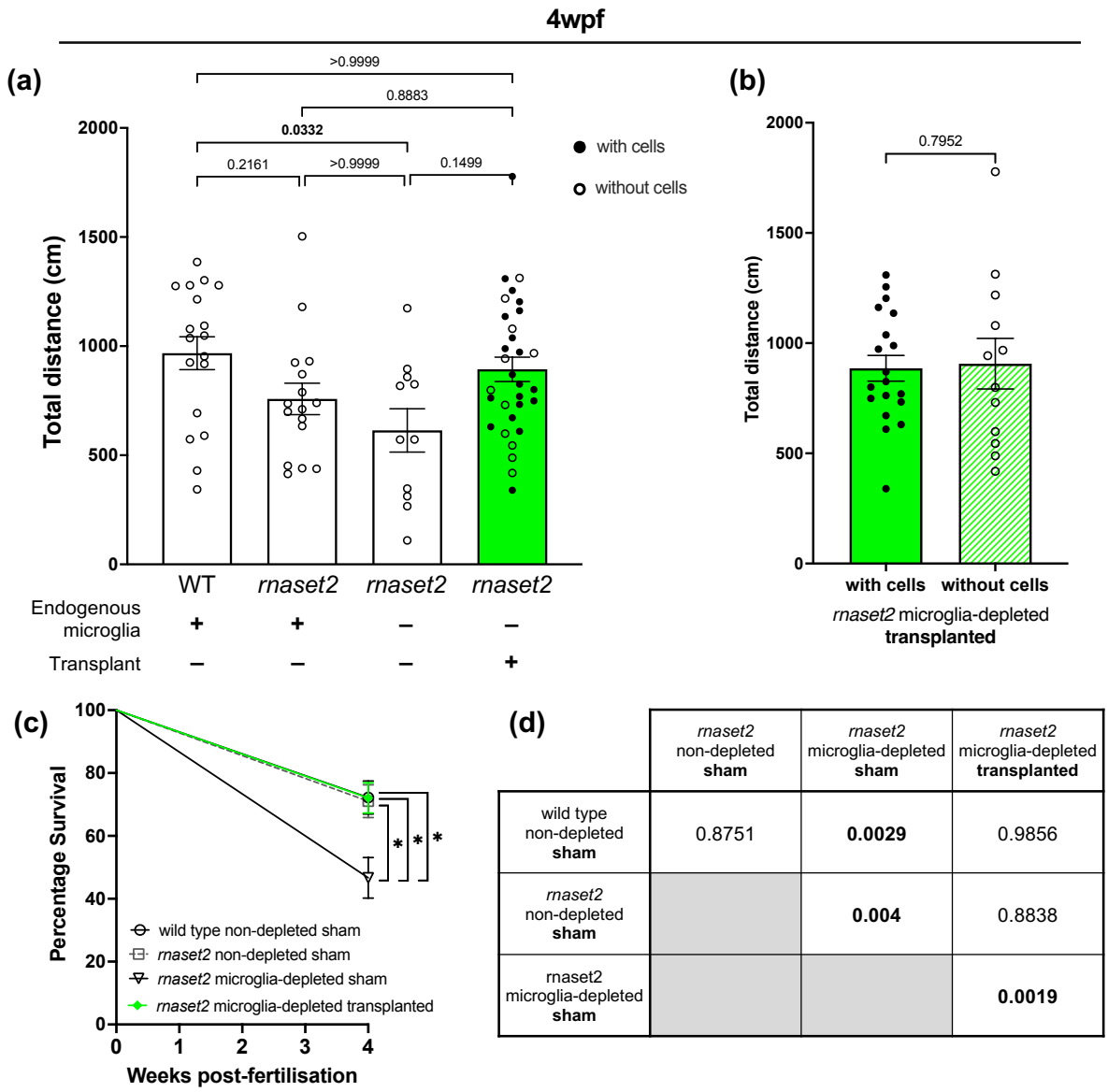

	rnaset2 non-depleted **sham**	*rnaset2* microglia-depleted **sham**	*rnaset2* microglia-depleted **transplanted**
wild type non-depleted **sham**	0.8751	**0.0029**	0.9856
rnaset2 non-depleted **sham**		**0.004**	0.8838
rnaset2 microglia-depleted **sham**			**0.0019**

Figure 5.14. Transplantation rescues *rnaset2* mutant swimming behaviour and survival at 4 weeks post-fertilisation.

a. Tracking of 4wpf juvenile behaviour reveals that transplantation restores *rnaset2* swimming behaviour to wild type levels. Kruskal-Wallis test with Dunn's multiple comparisons, n=11–31. **b.** Swimming behaviour was comparable between *rnaset2* microglia-depleted transplanted animals that had persistent engraftment of transplanted cells and those which did not. Mann-Whitney U test, n=12–19. **c, d.** Percentage survival of transplanted *rnaset2* mutants is greater than microglia-depleted sham controls at 4wpf. Pairwise comparisons and corresponding p values shown in (d), bold indicates significance. Log rank Mantel-Cox test with Bonferroni's multiple comparison correction (Bonferroni-corrected threshold: p<0.00833; family-wise significance threshold: P<0.05). Three biological replicates, n=60–86.

5.4 Discussion

A growing body of evidence has demonstrated that deficient microglia may drive the pathogenesis in RNASET2-deficient leukodystrophy and, therefore, that these neuroimmune cells may be a powerful therapeutic target (Chapter 3) (Hamilton *et al.*, 2020a; Weber *et al.*, 2020; Kettwig *et al.*, 2021). In this chapter, I have demonstrated that replacement of these diseased microglia with healthy cells is sufficient to rescue *rnaset2* mutant zebrafish pathology at a molecular, cellular and behavioural level. In alignment with findings in wild type hosts, I have demonstrated that transplant-derived cells reach *rnaset2* mutant brains during embryogenesis, compete with endogenous microglia for brain engraftment, undertake a microglial phenotype and persist in hosts until at least 4wpf. Transplantation was able to normalise the antiviral response and rescue behavioural phenotypes in *rnaset2* mutant larvae and juveniles – despite failing to alter the expression of myelin-associated transcripts. As such, this work supports the hypothesis that replacing microglia via macrophage transplantation can rescue aspects of neuropathology in *rnaset2* mutant zebrafish and provides further support for therapeutic targeting of microglia in the development of treatments for leukodystrophy.

5.4.1 Transplant-derived cells compete with rnaset2 mutant microglia for brain engraftment

The data presented in this chapter extend the findings of Chapter 4, demonstrating that transplant-derived cells are able to engraft within the brains of *rnaset2* mutant embryonic hosts, and express microglia specific markers. Intriguingly, brain engraftment was much more efficient in microglia-depleted *rnaset2* mutants relative to their non-depleted counterparts – with significantly fewer cells in non-depleted *rnaset2* mutants. This was a somewhat unexpected finding, as we had initially speculated that the increased number of uncleared apoptotic cells in *rnaset2* mutant brains (with or without microglial depletion) would be sufficient to drive robust transplant-derived cell recruitment. Developmental apoptosis is thought to be among the first triggers of microglial colonisation into the brain and so we had reasoned that *rnaset2* mutants – with their three-fold increase in the number of uncleared apoptotic cells at 5dpf – would have better engraftment than non-depleted wildtype (Casano, Albert and Peri, 2016a; Hamilton *et al.*, 2020a). However, no statistical difference was found for the number of transplant-derived cells in the brains of non-depleted wild type and *rnaset2* larvae, suggesting that a failure of *rnaset2*-deficient microglia to clear apoptosis alone does not promote brain engraftment.

There are several potential explanations for this. Firstly, it is possible that the location of this uncleared apoptotic debris – within microglia – limits the chemoattractant effects of apoptotic cells in recruiting microglia precursors to the brain. One of the key mechanisms by which developmental apoptosis is

thought to trigger brain colonisation is through nucleotide signalling – with blocking of these essential "find me" signals known to reduce the number of infiltrating microglia precursors infiltrating the brain (Elliott *et al.*, 2009; Casano, Albert and Peri, 2016a). In non-depleted *rnaset2* mutants, almost all of the uncleared apoptotic cells are found within the microglia – reflecting a failure of these cells to digest, but not phagocytose, debris (Li et al., 2012; Hamilton et al., 2020a). Perhaps, therefore, the containment of apoptotic debris within microglia in non-depleted animals blunts this nucleotide signalling and impairs recruitment to the brain, whereas the accumulation of apoptotic cells throughout the parenchyma allows transmission of "find me" signals and attracts transplant-derived cells into the brain. Additionally, the engraftment of transplant-derived cells in non-depleted animals may also be partially restricted by space availability. A variety of studies have demonstrated that microglia divide until they are spatially constrained, ultimately preventing the division of nearby cells through a process which is similar to contact inhibition (Bruttger et al., 2015; Zhan et al., 2019; Barry-Carroll et al., 2023; Barry-Carroll and Gomez-Nicola, 2024). This is likely particularly relevant to the failure of transplant-derived cells to persist in non-depleted *rnaset2* mutants at 4wpf, where transplanted cells are already in the minority compared to endogenous microglia, and their ability to divide is hindered by nearby, rapidly expanding host cells. Thus, this suggests the ability of *rnaset2* mutant microglia to phagocytose – but not clear – apoptotic cells may be sufficient to prevent transplanted cell recruitment during larval stages, and their retained ability to proliferate within the brain may prevent transplant-derived colonisation of non-depleted host brains.

It is particularly striking, however, that the extent of pathological rescue was similar between microglia-depleted and non-depleted larvae following transplantation. Across both transplanted groups, clearance of apoptotic debris, normalisation of the antiviral response and improvements in motor function were comparable in larvae – despite the differences in the number of transplant-derived cells in the brain and the expression of microglial markers by these cells. This suggests that the presence of any extra phagocytes in the brain may improve in *rnaset2* pathology, regardless of microglial identity, even in small numbers. Previous literature has suggested that circulation-derived macrophages may have increased capacity of phagocytosis relative to tissue-resident cells in zebrafish tail-fin injury models – thus, it is possible that transplant-derived cells are primed to act as professional phagocytes due to their haematopoietic origin (Li *et al.*, 2012). Nonetheless, these findings demonstrate that transplant-derived cells are able to ameliorate early neuropathology in *rnaset2* mutants, with or without the presence of endogenous microglia.

5.4.2 Transplantation rescues markers of neuroinflammation in rnaset2 mutants

5.4.2.1 Macrophage transplantation normalises antiviral immune response in larvae

One of the most prominent phenotypes found in patients with RNASET2-deficient leukodystrophy is upregulation of the antiviral response, particularly within the CNS (Henneke *et al.*, 2009b; Tonduti *et al.*, 2016b). In order to investigate the impact of transplantation on the antiviral response, I utilised a panel of four genes for qPCR – three antiviral response genes (*isg15*, *mxa*, *ifnφ1 secreted*) and the pro-inflammatory cytokine, *il1β*, which serves as a measure of general inflammation. – known to be upregulated in 3-month-old *rnaset2* brains (Hamilton *et al.*, 2020a). Strikingly, in *rnaset2* larvae, the expression of interferon-response genes *isg15* and *mxa* in *rnaset2* mutants was rescued following transplantation – suggesting that the presence of transplant-derived cells in the CNS may normalise the antiviral response.

However, it should be noted that each of the antiviral genes investigated do not follow the same expression pattern – both in their upregulation in mutants, and rescue by transplantation. While qPCR revealed a significant upregulation of *isg15* in mutants compared with wild type which was mirrored (albeit not significantly) by *mxa*, no differences in *ifnφ1* were observed at larval stages. This raises two key questions. Firstly, why is a significant difference observed for *isg15* but not *mxa*, especially given that *mxa* is widely considered to be a reliable readout of antiviral, and in particular interferon, response in zebrafish and humans (Aebi *et al.*, 1989; Altmann *et al.*, 2003; Lutfalla *et al.*, 2003; Holzinger *et al.*, 2007)? This may be explained by differing magnitudes of interferon-stimulated gene (ISG) upregulation in response for different stimuli within the zebrafish. In mammals, interferons (IFNs) are separated into three distinct groups: type I (IFNα and IFNβ), type III (IFNλ) – both of which are directly induced by viral infections – and type II (IFNγ) which has some antiviral effects but is also a key player in the adaptive immune response (Zhang *et al.*, 2008). While IFN-α, -β, and -λ are widespread across many species, neither of these subtypes possess direct homology with the IFNs identified in the zebrafish, which are instead referred to as ifnϕ1–4, and show clear antiviral activity with a combination of mammalian type I and III features (Stein *et al.*, 2007). The most detailed characterisation of the zebrafish ISG repertoire to date revealed that genes which are most robustly upregulated following direct inoculation with *ifnφ1* were induced to vastly differing extents after viral infection (Levraud *et al.*, 2019). Interestingly, in response to both stimuli, *isg15* showed increase over 400-fold from baseline, while *mxa* showed a lesser increase (160–262-fold). Hence, the lack of significance for *mxa* in the current study may be due to a smaller effect size in *rnaset2* mutants versus wild type which may limit the power of statistical analysis performed.

Secondly, the presence of multiple zebrafish IFNs explains why *isg15* and *mxa* – both widely researched ISGs – may be upregulated in the absence of increased *ifnφ1* in *rnaset2* mutants. It is possible that *isg15* and *mxa* in this instance are upregulated in response to the *ifnφ3* cascade, rather than *ifnφ1*. Of the four zebrafish IFNs, both *ifnφ1* and *ifnφ3* are expressed at larval stages and interact with different receptors: *ifnφ1* binds to a receptor complex containing CRFB5 and CRFB1, while *ifnφ3* binds to a complex of CFRB5 and CFRB2 (summarised in Figure 5.15a,b) (Aggad *et al.*, 2009; Levraud *et al.*, 2019). Additionally, these IFNs can be induced to differing extents in response to different viruses – demonstrating that their downstream effects may be, at least partly, distinct (Aggad *et al.*, 2009). Thus, it is possible that *ifnφ3* mediates the antiviral response in *rnaset2* mutant larvae. It may, therefore, be informative to assess *ifnφ3* expression in *rnaset2* larval brains through qPCR to explore this hypothesis.

Alternatively, it is possible that *isg15* and *mxa* are upregulated in an IFN-independent manner. While IFNs are certainly key regulators of the antiviral response, some ISGs can be induced by alternative signalling pathways such as the cGAS-STING or RIG-I pathways in response to the detection of viral nucleic acids in the cytoplasm (Figure 5.15c) (Perng and Lenschow, 2018). Indeed, subsequent RNA sequencing of 4wpf transplanted animals revealed downregulation of both type I IFN and RIG-I signalling, suggesting overlapping components of each pathway may contribute (Figure 5.11). It remains unclear whether *mxa* and *isg15* are among the ISGs which can be induced in the absence of IFN-signalling. Previous studies have suggested that MxA activation by influenza A virus in human cells is IFN-dependent and abolished in the absence of STAT-1 (Holzinger *et al.*, 2007). However, subsequent work has demonstrated that both MxA and ISG15 are in fact independent of IFNs – with persistent upregulation, albeit to a lesser extent, in IFN-non-responsive human cells – following infection with cytomegalovirus (CMV) (Ashley *et al.*, 2019). The latter is a particularly interesting finding, given the phenotype of RNASET2-deficient leukodystrophy so closely mirrors CMV in patients (Henneke *et al.*, 2009b). CMV is thought to activate the antiviral response via the cGAS-STING pathway in an IRF3-dependent manner – suggesting this pathway may also contribute to RNASET2-linked pathology. Thus, it does seem possible there may be interferon-independent activation of the antiviral response in larval stages, which could serve to increase downstream *ifnφ1* production into adult ages (Hamilton *et al.*, 2020a). To unpack this distinction, future work may seek disrupt key modulators of the cGAS-STING and RIG-I pathways, with and without knockdown of CFRB5 (the ubiquitous subunit of the receptors of both ifnϕ1 and ifnϕ3) to investigate the contribution of these pathways in the *rnaset2* immune response. Nonetheless, the finding that both *isg15* and *mxa* expression are reduced in transplanted

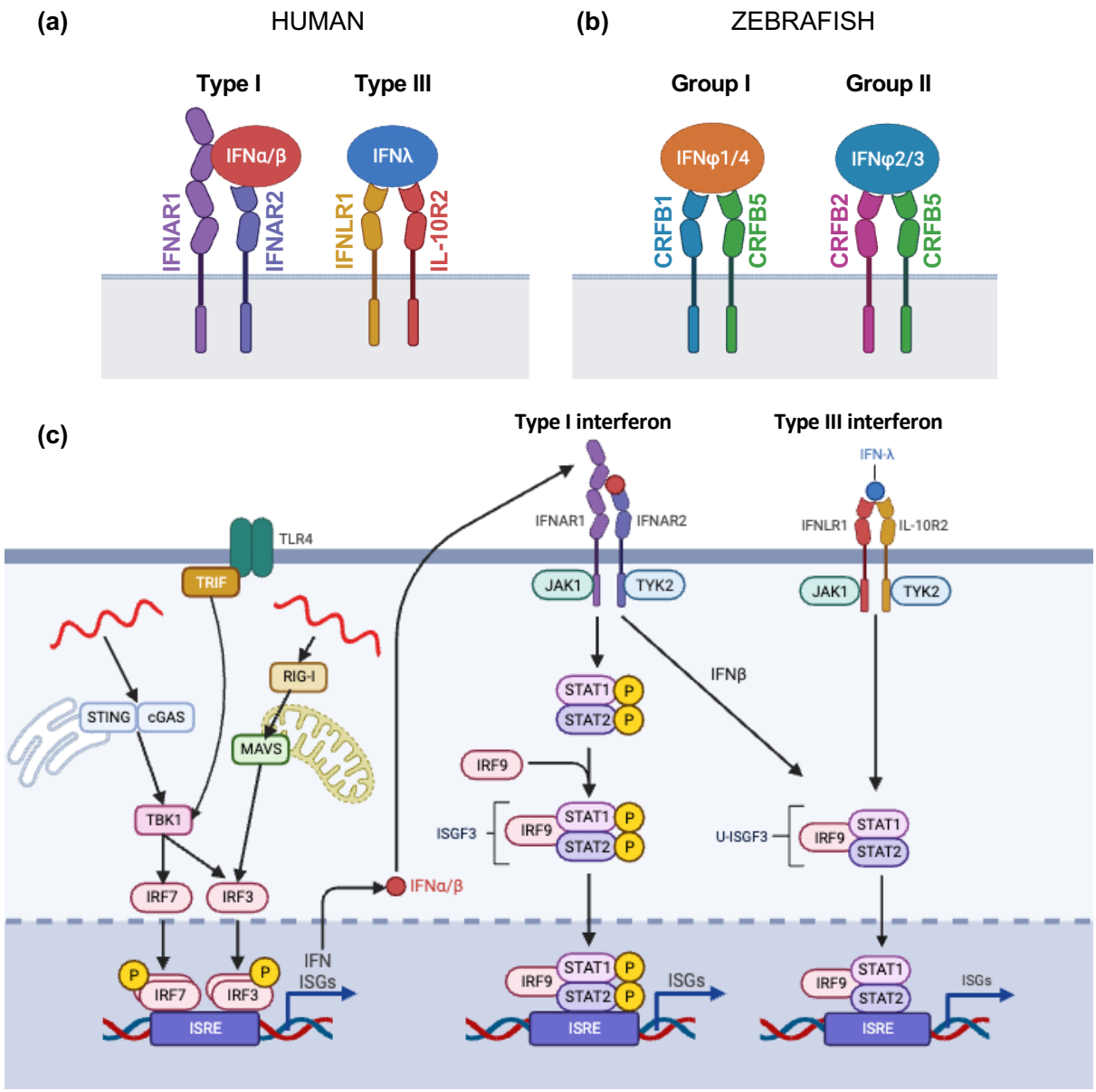

Figure 5.15. Induction of interferon stimulated genes.

a, b. Schematic representation of virus-induced IFNs and their receptors in human (a) and zebrafish (b). Adapted from Levraud *et al., J Immunol* 2019. **c.** Simplified schematic depicting the induction of interferon stimulated genes (ISGs) in mammals. Following type I interferon stimulation, IRF9 interacts with phosphorylated STAT1 and STAT2 to form the ISGF3 complex, which then binds to interferon-sensitive response element (ISRE) promoters to induce expression of ISGs (including ISG15 and MxA). During chronic viral infection, IFNβ and type III interferons can induce the formation of an unphosphorylatyed ISGF3 (U-ISGF3) complex, which can induce expression of a different ISG signature, also including ISG15 and MxA. Alternatively, foreign nucleic may also cause induction of ISG15 expression in an interferon-independent manner. For example, double-stranded RNA can act via RIG-1 and MAVS to induce expression of ISGs and IFNα/β. Figure adapted from Perng and Lenschow, 2018. Figure created with BioRender.

animal suggests that transplantation can stabilise the otherwise overactive immune response in *rnaset2* mutant larvae.

Notably, a key limitation in assessing transplantation effects in zebrafish larvae is the high variability in clutch sizes across repeats. Throughout this chapter, a minimum of three biological replicates were used for each assay – where each replicate reflects a clutch of embryos born from distinct parents on different dates. These embryos were checked for fertilisation and healthy development, then chosen at random for transplantation. Following transplantation, larvae were screened to ensure robust engraftment of transplant-derived cells before being selected for raising and later assessment of the effects of transplant in *rnaset2* mutant pathology. As such, there are multiple potential sources of variability in this experimental set-up: from the number of fertilised embryos to the number of animals which were successfully transplanted. To minimise the impact of this variability, I ensured embryos were housed at consistent densities throughout – in plates of 60 embryos before 5dpf, then in plates of 20 larvae to 8dpf. This ensured that the availability of space and nutrients were comparable from clutch to clutch, regardless of the number of successfully transplanted animals which could be raised. Additionally, the number of embryos used for each experimental group and assay was matched as much as possible, with this number stated within the figure legend for transparency. Finally, key experiments – such as assessing the impact of transplantation on the antiviral response or behavioural deficits in *rnaset2* mutants – were repeated in juvenile animals, where each fish was considered a biological replicate, and fewer animals were required. As such, this approach allows us to take advantage of the inherent advantages of using zebrafish embryos as a model – including their large clutch sizes – while accounting for variability as much as possible.

5.4.2.2 RNA sequencing confirms restoration of antiviral response in transplanted animals

Further to the rescued expression of some ISGs in transplanted *rnaset2* larvae, RNA sequencing revealed downregulation of a plethora of immune, and specifically antiviral, pathways in microglia-depleted transplanted animals at 4wpf. Many of the genes upregulated in non-transplanted mutants were restored entirely to wild type levels in transplanted animals, including *isg15* and *cmpk2* which were validated by qPCR. As such, the downregulation antiviral pathways downregulated in transplanted microglia-depleted animals - identified by non-biased transcriptomic analysis – lends support to the hypothesis that microglial replacement is sufficient to rescue *rnaset2*-deficient pathology.

However, it must be noted that no such antiviral pathways were identified in comparing the transcriptomes of non-depleted animals, both comparing untreated mutant to wild types, and

transplanted mutants to untreated *rnaset2* animals. This may, in part, be attributed to increased intra-group variability within the non-depleted transplanted group. Non-depleted, transplanted *rnaset2* mutant brains were briefly screened before RNA extraction to ensure some transplant-derived cells were present – however, as shown in Figure 5.8, the number of these cells was low and variable at 4wpf. Similarly, the low proportion of non-depleted animals which still contained transplant-derived cells at 4wpf limited the number of samples that could be collected to 3 biological repeats (compared with 4 repeats for the microglia-depleted group). As such, relatively few differentially expressed genes reached significance for these comparisons. Nonetheless, *rnaset2* was among the strongest downregulated genes for non-depleted *rnaset2* mutants relative to wild type controls, suggesting that robust changes in gene expression could still be identified. Similarly, several interferon-stimulated genes were significantly upregulated in non-depleted *rnaset2* brains relative to wild type, including *ifih1*, *cmpk2* and *rsad2* among others (see Appendix 2. RNA sequencing of transplanted *rnaset2* mutants). However, these genes were not significantly downregulated in transplanted animals – suggesting rescue of antiviral signalling may not be so robust in non-depleted transplanted animals, likely due to the low number of transplant-derived cells in their brains. However, several pathways relating to metabolism of nucleotides (and particularly RNA) were differentially regulated in transplanted animals, which is particularly of interest given the role of rnaset2 as a ribonuclease (Campomenosi *et al.*, 2006; Lübke, Lobel and Sleat, 2009b; Haud *et al.*, 2011b). Previous studies have revealed accumulation of rRNA in engorged lysosomes throughout the brains of *rnaset2* mutants – thus, the finding that nucleic acid metabolism may be altered in transplanted animals may suggest transplant-derived cells may respond to this accumulated RNA (Haud *et al.*, 2011b). As such, future work may wish to assess lysosome number and rRNA aggregates in transplanted animals – both with and without microglia depletion – to assess the ability of transplanted cells to clear this pathology.

5.4.3 Macrophage transplantation increases motor function in rnaset2 mutants

5.4.3.1 Transplanted animals show improved locomotion in free swimming assays

In addition to normalisation of various aspects of neuropathology, perhaps the most striking rescue observed in transplanted *rnaset2* mutants was the restoration of locomotor activity. In free swimming assays, transplanted mutants swam further than non-transplanted controls during both larval and adult stages, restored close to wild type levels. Interestingly, behavioural recovery was comparable between animals with persistent transplant-derived cell engraftment and those that had no visible cells at 4wpf, suggesting there may be residual benefits shortly after transplant-derived cells are cleared from host brains. Future work may investigate the duration of this beneficial effect after transplanted cell clearance, to see if this delays or even entirely prevents the onset of subsequent

pathology. Nonetheless, the behavioural recovery of transplanted animals provides compelling support to the hypothesis that replacement of deficient microglia can rescue *rnaset2*-deficient pathology.

In addition to providing support for the efficacy of transplantation in rescuing *rnaset2* mutant neuropathology, these behavioural studies provide further support to the idea that it is a loss of homeostatic microglial function that drives *rnaset2*-deficient pathogenesis, rather than a toxic gain-of-function. In Chapter 3, I demonstrated that depletion of microglia alone is insufficient to improve *rnaset2* mutant survival outcomes – instead, seemingly increasing mortality in larval and adult stages (**see Figures**). Similarly, in this chapter, free swimming analysis revealed that microglia-depleted *rnaset2* mutants show even greater reductions in locomotion relative to non-depleted controls during both larval and juvenile stages, with *rnaset2* microglia-depleted sham animals showing mortality rates almost double that of non-depleted siblings at 4wpf. As such, it seems that rnaset2-deficient microglia have some role in minimising neuropathology in *rnaset2* mutants, and that removing endogenous microglia – without replacement – is not a therapeutic avenue that should be explored in this disorder.

There are some key differences in the study of transplanted animal behaviour relative to the studies described in Chapter 3 which characterised *rnaset2* motor impairment. Firstly, for assessment of transplanted larvae swimming behaviour, larvae were recorded for 20- rather than 60-minutes as in section 3.3.2.1. This protocol was shortened to allow higher throughput of transplanted larvae and controls, which included five experimental groups per plate (4 animals per group) rather than two (12 animals per group). Reassuringly, analysis revealed ~3-fold reduction in overall distance swum between the 60- and 20-minute assays for both wild type and *rnaset2* mutants – suggesting that free swimming assessment is a robust assay of *rnaset2* pathology, even over shorter durations. Secondly, for juvenile assays, different behavioural tracking systems were used across the separate experiments to quantify the behaviour of untreated animals (Chapter 3) and transplanted fish (Chapter 5). Interestingly, across a 10-minute window, the ViewPoint software reported wild type animals swimming an average of ~250cm, whereas the EthoVision software reported swimming distances of ~1000cm for the same group. Each recording software was calibrated against the same ruler prior to recording and each tracking trace appeared faithful to the animals' movements when investigated by eye. Hence, this raises questions about the reproducibility of behavioural experiments where differing recording software is used. Nonetheless, both analyses were able to detect the hypoactivity of *rnaset2* fish compared with wild type siblings, giving some reassurance of the robustness of the biological effect.

As such, free swimming analysis provides compelling support to the hypothesis that macrophage transplantation rescues *rnaset2* mutant behavioural deficits up to 4wpf.

5.4.4 Potential mechanisms of rescue by macrophage transplantation in rnaset2 mutants

The data presented in this chapter demonstrate that replacement of deficient microglia is sufficient to rescue a variety of neuropathological markers in *rnaset2* mutant zebrafish. In the clinic, HSCT may provide a means of microglial replacement – although the arrival of microglia-like cells delays the onset of clinical improvements, with highly variable efficacy across patients (Krivit, 1995; Priller *et al.*, 2001; Asheuer *et al.*, 2004; Yamada *et al.*, 2004; Schönberger *et al.*, 2007; Cronk *et al.*, 2018; Bonkowsky *et al.*, 2021). Macrophage transplantation itself has been explored in a small subset of patients who had experienced stroke but is yet to be widely trialled in the leukodystrophies (Chernykh *et al.*, 2014; Na, Kim and Seok, 2023). A more detailed consideration of the feasibility of macrophage transplantation in patients with RNASET2-deficient leukodystrophy is provided in Section 6.3.1 – however, such an intervention remains highly experimental in this disorder. Therefore, a more detailed understanding of the mechanisms by which transplant-derived cells are able to rescue pathology may inform the development of targeted therapies, either to supplement cell replacement strategies or be used independently.

5.4.4.1 Transplantation does not increase global levels of rnaset2 expression

One mechanism by which HSCT has been proposed to exert beneficial effects in leukodystrophy patients and animal models is by cross-correction – whereby healthy donor cells provide functioning enzyme to neighbouring cells in the brain (Beck, 2010; Page *et al.*, 2019). However, several studies in both human tissue and animal models have suggested that enzymatic cross-correction contributes minimally, if at all, to HSCT success *in vivo* (Weinstock *et al.*, 2020; Wolf *et al.*, 2020). In the current study, transplantation of healthy macrophages into *rnaset2* mutant hosts did not elevate *rnaset2* expression in the heads or trunks of larvae, nor the brains of juvenile animals. This suggests that transplantation was insufficient to induce brain-wide increases of *rnaset2* transcripts, and therefore may be unlikely to be a robust source of functioning enzyme of the CNS. It must be noted, however, that this gene expression data is only a proxy for tissue-wide rnaset2 levels, and that assessment of both protein levels and function at global and local levels would be required to truly confirm an absence of cross-correction. Unfortunately, no antibodies are available for the detection of zebrafish rnaset2 to enable immunohistochemistry or western blot analysis of expression to validate these findings at a protein level. It is possible that the transfer of rnaset2 from competent, transplant-derived

cells to deficient neighbouring cells only replaces rnaset2 at a very local level – restricted to the cells in direct contact with transplant-derived macrophages/microglia. Previous studies have demonstrated that transfer large proteins occurs through direct lysosomal exchange and is dependent on cell-to-cell contacts, rather than transmission of enzymes through the extracellular space (Yamada *et al.*, 2004; Naphade *et al.*, 2015). As such, local increases in levels of functioning rnaset2 – which may be sufficient to rescue pathology – may be dwarfed at a brain-wide level. Therefore, it is not possible to rule out transfer of rnaset2 enzyme from healthy macrophages to mutant cells in this assay. Nonetheless, the current study provides no evidence of robust, global increases in *rnaset2* expression in transplanted *rnaset2* mutants.

5.4.4.2 Transplantation is unlikely to act by restoration of myelin-associated genes

Given that white matter abnormalities are central to leukodystrophy pathology, one might expect that a gold-standard treatment for such a disorder would rescue myelin integrity. However, in the current study, no evidence of rescue of myelin pathology was identified in transplanted *rnaset2* mutants. In larval stages, expression of the myelin-associated transcript *mbpa* was unchanged in transplanted animals relative to untransplanted *rnaset2* mutants, which themselves showed expression well below wild type levels. At 4wpf, no significant changes in the expression of myelin-associated transcripts were identified by RNA sequencing – again, suggesting no change in the expression of myelin genes.

However, as discussed in section 3.3.1, quantification of myelin transcripts alone is insufficient to infer changes at a protein, cellular or structural level. Due to lack of a reliable antibody for myelin labelling, the amount and distribution of myelin could sadly not be quantified. It is theoretically possible that the presence of healthy transplant-derived cells may promote myelin integrity through phagocytosis of debris without the production of any additional protein and, therefore, limited changes in gene expression, which would likely not be picked up by this assay. Sadly, I was also unable to take advantage of many of the transgenic reporter lines labelling oligodendrocytes (such as *Tg(mbpa:GFP)*) as these fluoresce in the same spectra as my GFP-positive transplant-derived cells, making it impossible to distinguish between transplant-derived cells and oligodendrocytes. Myelin transgenics are available in other fluorophores – however, there was insufficient time to acquire these in Sheffield, cross into the *rnaset2* background and perform transplantation in the duration of my PhD. Finally, the failure of transplant-derived cells to persist in host brains beyond juvenile stages meant MRIs could not be performed on transplanted animals, as the logistics of the MRI set up require fish to be relatively large (minimum of ~1 year old) (Hamilton *et al.*, 2020a). As such, the full effects of macrophage transplantation on white matter pathology remain unclear, with the current study failing to demonstrate any benefits of this intervention on myelin integrity or oligodendrocyte cell number.

If transplantation truly does not rescue myelin pathology, while still normalising antiviral response and behavioural deficits, this raises several key questions about *rnaset2*-deficient pathology. Firstly, the finding that transplantation is sufficient to rescue antiviral signalling without direct evidence of improvements in myelination suggests that independent mechanisms may drive these two potentially distinct pathologies. Indeed, elegant characterisation of the cell-specific roles of GALC in a mouse model of Krabbe disease has demonstrated that loss of this lysosomal hydrolase exerts distinct and independent effects in myelin-producing cells and macrophages (Weinstock *et al.*, 2020). Using the sciatic nerve as a model, these authors demonstrated that loss of GALC from Schwann cells (the myelin-producing cells of the peripheral nervous system) is sufficient to induce some myelin abnormalities but does not fully recapitulate the phenotypes seen in in global knockouts, including axon degeneration, myelin loss and the recruitment of engorged macrophages proximal to the nerve. In contrast, macrophage-specific GALC knockout was not sufficient to induce myelination but was associated with reduced expression of genes associated with phagocytosis and increased inflammatory markers. Strikingly, crossing Schwann cell- and macrophage-specific GALC knockouts was sufficient to recapitulate global knockout phenotypes – suggesting that a combination of cell autonomous dysfunction due to GALC deficiency in macrophages and myelin-producing cells accounts for peripheral neuropathology in Krabbe disease mouse models. While it remains unclear whether this paradigm also occurs in the CNS, this study demonstrates that macrophage- and myelin-associated pathology may occur via independent – but highly interactive – mechanisms in leukodystrophy. Thus, the finding that transplantation rescues expression of antiviral, but not myelin transcripts, suggests that similarly distinct mechanisms may be at play in *rnaset2* mutants, and demonstrates that myelin pathology is unlikely be the sole driver of pathogenesis in this leukodystrophy model.

Secondly, the finding that *rnaset2* swimming impairments are rescued following transplantation without restoration of myelin expression suggests that it is not these white matter abnormalities which underpin the behavioural phenotypes of these mutants. Instead, it seems that neuroinflammation is likely to be the main contributor to locomotor dysfunction – further adding support to the hypothesis that aberrant activation of the antiviral response induces hypoactivity and general sickness behaviours in *rnaset2* mutant larvae and juveniles (Kirsten *et al.*, 2018; Mojzesz *et al.*, 2021; Maleski *et al.*, 2022). As such, these findings further validate the growing movement to consider leukodystrophy pathology beyond myelin and oligodendrocytes, suggesting distinct neuroinflammatory mechanisms are likely contribute to pathogenesis.

5.4.4.3 *Transplantation may act by increasing the number of competent phagocytes in rnaset2 mutant brains*

One final mechanism by which macrophage transplantation may improve *rnaset2*-deficient pathology is through simply increasing the number of competent phagocytes within the CNS, which may have cell autonomous roles in reducing inflammation and promoting homeostasis (Nicholas, Wing and Compston, 2001a; Fuhrmann *et al.*, 2010a; Yeo *et al.*, 2012a; Healy *et al.*, 2016a; Hickman *et al.*, 2018a). As previously discussed, the presence of any additional phagocytes in *rnaset2* mutant brains is sufficient to normalise the antiviral response and improve motor dysfunction in larvae, as demonstrated by comparable rescue of these phenotypes in transplanted animals with or without microglial depletion. Strikingly, the extent of apoptotic debris clearance was identical in transplanted animals regardless of microglia-depletion status, despite non-depleted hosts having ~5-fold fewer transplant-derived cells in their brains relative to microglia-depleted transplanted hosts. This is the earliest pathological rescue we observed in the current study, with significant reductions in the number of uncleared apoptotic cells as early at 3 days post-transplant (5dpf). Thus, it is possible that transplantation may exert beneficial effects through increasing the capacity of the total phagocytic population in the brain to clear accumulated debris.

We have previously hypothesised that accumulation of apoptotic cells within *rnaset2*-deficient microglia may trigger downstream neuroinflammation and degeneration in *rnaset2* mutants (Hamilton *et al.*, 2020a). While apoptotic cells are themselves are thought to be immunologically silent, it is possible that the accumulation of undigested storage material in *rnaset2* mutant microglia following phagocytosis causes a phenotypic shift of these cells – whereby these cells lose their homeostatic function and, therefore, contribute to downstream pathology. Indeed, studies in Krabbe disease mouse models have demonstrated that loss of GALC leads to accumulation of galactosylceramidase (the substrate of GALC) within macrophages (Weinstock *et al.*, 2020). This causes a transcriptomic shift of these GALC-deficient macrophages – with reduced expression of homeostasis- and phagocytosis-associated genes, and upregulation of TNF-a and IL-1b. Strikingly, following HSCT in human patients, the number of macrophages expressing homeostatic genes is increased, with fewer engorged, pro-inflammatory macrophages observed. As such, this suggests a model whereby substrate accumulation due to GALC deficiency within macrophages drives a loss of homeostatic function in Krabbe disease, causing a pro-inflammatory environment which further drives both macrophage abnormalities and myelin dysfunction (Weinstock *et al.*, 2020).

A similar mechanism may occur in *rnaset2* mutants. Like GALC, RNASET2 is a lysosomal hydrolase, and patients with Krabbe disease and RNASET2-deficient leukodystrophy both develop pathology

indicative of lysosomal storage disorder ((Suzuki and Suzuki, 1970; Haud *et al.*, 2011b). While the precise substrate has yet to be fully characterised in RNASET2, accumulation of rRNA is visible in lysosomes of microglia and neurons in both animal models and patients with RNASET2-deficient leukodystrophy (Haud *et al.*, 2011b). Thus, it is entirely possible that a bottleneck of rRNA digestion within *rnaset2*-deficient microglia also drive a phenotypic shift of these cells away from homeostasis, towards a pro-inflammatory state, which may trigger subsequent neuroinflammation. The presence of competent, donor-derived phagocytes may clear this undigested substrate, restore microglial homeostasis and therefore prevent aberrant activation of the inflammatory response. Indeed, RNA sequencing revealed enrichment of genes involved in nucleic acid processing in some transplanted animals, supporting this potential mechanism. Thus, in the absence of evidence supporting enzymatic cross-correction or rescued myelin integrity in transplanted animals, restoration of substrate clearance appears to be the most likely mechanism by which macrophage transplantation exerts its beneficial effects. Future work may therefore seek to investigate the single cell transcriptomes of transplant-derived cells relative to endogenous microglia and other brain cell populations, to further understand the mechanisms underpinning both disease and rescue in this disorder.

5.4.5 Chapter summary

In conclusion, the data presented in this chapter demonstrate that macrophage transplantation rescues *rnaset2* mutant pathology by replacing deficient microglia. Transplant-derived cells compete with endogenous microglia for brain engraftment in *rnaset2* larvae and persist up to at least 4wpf in microglia-depleted *rnaset2* mutant hosts. Transplantation restored antiviral signalling to wild type levels, mirrored by rescue of free-swimming behaviours in larval through to juvenile ages. Hence, these findings support the hypothesis that microglial replacement is sufficient to rescue *rnaset2* pathology and provides further support that deficient microglia are the cellular drivers of pathology in this disease model.

Chapter 6. General Discussion and Future Perspectives

6.1 Summary of major findings

Due to the growing appreciation of the global impact of rare diseases, the past decade has seen an exponential increase in leukodystrophy research, with numerous ongoing clinical trials and the recent approval of novel therapies for subset of these disorders. However, the ultra-rare leukodystrophies – including RNASET2-deficient leukodystrophy – remain largely overlooked. Despite the severity of this disorder, there remain no disease-modifying therapies for patients with RNASET2-deficient leukodystrophy. A variety of animal models have begun to explore pathogenic mechanisms in this disorder – however, none have yielded a therapeutic intervention to date (Haud et al., 2011b; Sinkevicius et al., 2018; Hamilton et al., 2020a; Weber et al., 2020; Kettwig et al., 2021). As such, the unmet clinical need remains vast for patients and families living with this disorder.

The overarching aims of this thesis were to further characterise the neuropathology of *rnaset2* mutant zebrafish – a leading animal model of RNASET2-deficient leukodystrophy – and develop an intervention which could ameliorate pathology in this model. In combination with published literature, the characterisation of *rnaset2* mutants in Chapter 3 identified microglia, the brain-resident immune cells, as a likely driver of *rnaset2*-deficient neuropathology and a potential target for therapy development. Chapter 4 showed that functional replacement of zebrafish microglia could be achieved by transplantation of WKM-derived macrophages, providing a powerful tool which could be used to target these neuroimmune cells in disease models. Finally, the data presented in Chapter 5 demonstrate that transplantation is sufficient to rescue *rnaset2* mutant pathology at a molecular, cellular and behavioural level, by replacing deficient microglia in larval and juvenile hosts (summarised in Figure 6.1). Together, these findings demonstrate that microglia are powerful modulators of pathogenesis in this animal model, and that these cells are a promising target for therapy development in RNASET2-deficient neuropathology.

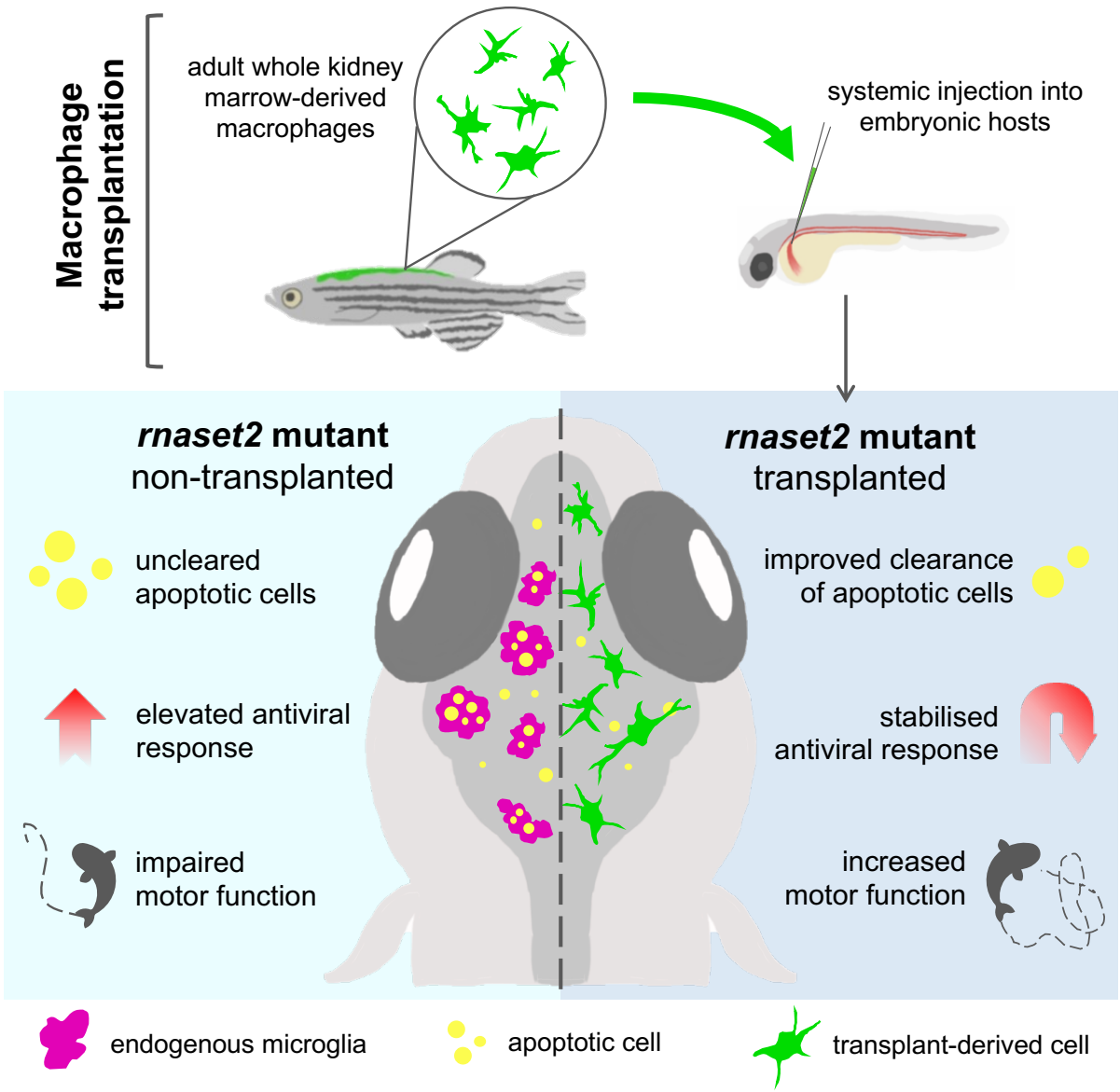

Figure 6.1. Summary: Macrophage transplantation rescues markers of RNASET2-deficient leukodystrophy pathology through microglia replacement in a zebrafish model.

6.2 The *rnaset2* mutant zebrafish has informed our understanding of RNASET2-deficient leukodystrophy

In ultra-rare diseases where patient material is scarce, animal models are a particularly vital tool to increase our understanding of the mechanisms of disease pathogenesis. To date, five animal models of RNASET2-deficient leukodystrophy have been published, including mouse, rat and zebrafish models (Haud et al., 2011b; Sinkevicius et al., 2018; Hamilton et al., 2020a; Weber et al., 2020; Kettwig et al., 2021). However, several of these models fail to recapitulate the white matter pathology and motor deficits central to RNASET2-deficient pathology (Sinkevicius *et al.*, 2018; Weber *et al.*, 2020; Kettwig *et al.*, 2021). Together with published literature, the data presented within this thesis further supports the claim that the *rnaset2*^{sh532} mutant zebrafish is the only animal model of this disorder to recapitulate a broad range of patient phenotypes, including myelin abnormalities, locomotor deficits, learning and memory abnormalities and upregulation of antiviral response (Hamilton et al., 2020a). As such, this model shows unique face validity in recapitulating the patient condition, has increased our understanding of potential disease mechanisms and provided a tool in which to study the impact of therapeutic interventions for RNASET2-deficient leukodystrophy.

6.2.1 Why do zebrafish better recapitulate RNASET2-deficient leukodystrophy pathology relative to mammalian models?

Upon first consideration, it may seem surprising that zebrafish models of RNASET2-deficient leukodystrophy appear to recapitulate patient phenotypes more faithfully than mammalian models, given the evolutionary divergence of fish and humans (Howe *et al.*, 2013). However, several zebrafish models of interferon-related leukodystrophies also appear to better recapitulate neuropathology relative to mouse and rat equivalents (Rutherford, Kasher and Hamilton, 2021). There are several potential explanations for this in the case of RNASET2-deficient animal models.

Firstly, the genetic strategy used to generate the *rnaset2*^{sh532} zebrafish model may have greater similarity to the human condition relative to rodent models. Typically, patients with RNASET2-deficient leukodystrophy present with single base pair substitutions or deletions (although some larger deletions have been reported), often inducing nonsense mutations and the production of a truncated, catalytically inactive RNASET2 protein (Kameli *et al.*, 2019). Accordingly, a similar genotype was generated by CRISPR/Cas9 gene editing in *rnaset2*^{sh532} mutant zebrafish, leading to an 8 base pair deletion in exon 5, induction of a premature stop codon and, ultimately, truncation of the rnaset2 protein with loss of catalytic activity (Hamilton et al., 2020a). In this zebrafish model, *rnaset2* transcripts are reduced – likely due to nonsense-mediated RNA decay – but not entirely ablated, as

might be expected in the human condition (Kameli et al., 2019; Hamilton et al., 2020a). In contrast, both mouse and rat models of this disorder have used genetic approaches which fully ablated protein production. In the case of the *RNaseT2*$^{-/-}$ rat, the use of two pairs of CRISPR gRNAs were used to delete all 9 exons of *RNaseT2* (Sinkevicius *et al.*, 2018). Generation of the *Rnaset2*$^{-/-}$ mouse required a dual approach due to the presence of two *Rnaset2* orthologues in mice (*Rnaset2a* and *Rnaset2b*), with targeting of *Rnaset2a* achieved by integration of a transgenic cassette deleting exons 2–4 and inducing an early stop in exon 5, and CRISPR/Cas9 targeting of exon 2 of *Rnaset2b* inducing an early stop codon (Kettwig *et al.*, 2021). Western blot confirmed complete lack of Rnaset2 protein in these double mutants. As such, these animal models do not fully recapitulate the genetics of many patients, which likely retain some (albeit reduced) level of functioning or malfunctioning protein. It is unclear why these mammalian models – with a complete loss of RNASET2 expression – seem to present with milder phenotypes relative to zebrafish models and patients (where some RNASET2 expression may be preserved); however, this is a phenomenon which has also been reported across animal models of AGS (Behrendt *et al.*, 2013; Rehwinkel *et al.*, 2013; Wu, 2013; Kasher *et al.*, 2015; Withers *et al.*, 2023). As such, the genetic strategy used to generate animal models requires careful consideration and may well affect the relevance of model phenotypes to the human condition.

The second key factor which must be considered when comparing zebrafish and mammalian models is the differing exposure of these laboratory animals to pathogens in their environment. Laboratory rodents are exposed to very few pathogens due to routine sterilisation of bedding, food, and water, which alters their immune composition relative to wild counterparts (Rosshart *et al.*, 2017). In contrast, zebrafish in aquaria across the world are known to be exposed to pathogens, including viruses, throughout their lifespan due to inherent features of their aquatic environment (Balla *et al.*, 2020). Arguably, this is more similar to the experience of human patients, for whom pathogen exposure begins during early life, or even *in utero* (Wenstrom *et al.*, 1998; Baschat *et al.*, 2003; Virgin, 2014; Xu *et al.*, 2015). This is particularly relevant to modelling interferonopathies like RNASET2-deficient leukodystrophy, which has a prominent immune component. It is possible that the naïve immune system of rodent animal models may alter the neuroinflammatory cascade such that pathological phenotypes are blunted in rat or mouse models, while raising zebrafish in pathogen-rich environments may further trigger the antiviral cascade and worsen pathology (Rutherford, Kasher and Hamilton, 2021). In Chapter 3, qPCR failed to reveal any differences in expression of a single ISG following sterile raising of *rnaset2* mutant zebrafish, although complete ablation of pathogen exposure was not confirmed. However, future work may investigate the role of pathogen exposure in rodent models of

RNASET2-deficient leukodystrophy to see if non-sterile raising may better recapitulate patient phenotypes in these disease models.

6.2.2 Study of rnaset2 mutants confirms that pathogenesis begins during developmental stages and is driven by microglial dysfunction

In addition to the recapitulation of a breadth of disease-associated phenotypes, characterisation of *rnaset2* mutant zebrafish has also informed our understanding the timing of, and potential triggers for, pathogenesis. Across almost every disease-associated phenotype assessed, abnormalities were evident in *rnaset2* mutants at 8dpf or earlier – suggesting that pathogenesis may begin during early development in this disorder. In patients, symptoms typically emerge within the first few months of life – however, the emergence of neuropathology and behavioural impairments as early as 5dpf in this zebrafish model suggests that disease processes likely begin even earlier (Henneke et al., 2009b; Kameli et al., 2019; Hamilton et al., 2020a). This has two main implications for patients. Firstly, this adds further evidence to the hypothesis that RNASET2-deficient leukodystrophy is a neurodevelopmental, rather than neurodegenerative, disorder – where a failure of normal brain development appears to drive pathology. Consequently, these findings also suggest that any therapeutic interventions which aim to entirely rescue pathology likely need to be administered into very young children, as is the case with approved therapies in other leukodystrophies (Libmeldy, 2024; Skysona, 2024). Indeed, the rescue of neuropathology by macrophage transplantation in *rnaset2* mutants was achieved by transplantation of embryos at 2dpf – an incredibly early developmental stage. As such, characterisation of *rnaset2* mutant zebrafish suggests the window for therapeutic intervention is narrow and early in RNASET2-deficient leukodystrophy.

Furthermore, the current study extends our understanding of the potential drivers of pathology in RNASET2-deficient leukodystrophy, adding to published evidence which suggests microglial dysfunction triggers pathogenesis in *rnaset2* mutants (Hamilton et al., 2020a). Several lines of evidence support the hypothesis that a loss of microglial homeostasis – particularly, the ability of these cells to clear debris within the brain – is the principle pathogenic event driving disease. Firstly, the data presented in this thesis confirms published findings that microglial dysfunction is among the earliest pathology to emerge in *rnaset2* mutants, with accumulation of apoptotic bodies within the brain indicative of reduced clearance of debris by microglia (Hamilton et al., 2020a). Secondly, despite the abnormal function of these cells, depletion of embryonic microglia appears to impair survival and swimming behaviour of microglia-depleted *rnaset2* mutants during both larval and juvenile stages. These findings suggest that microglia do not adopt a toxic gain-of-function in *rnaset2* mutants, but that loss of microglial homeostatic functions appears to be critical to the development of *rnaset2*-deficient

pathology. Finally, and perhaps most convincingly, functional replacement of deficient *rnaset2* microglia with healthy donor cells rescues almost all aspects of neuropathology for at least as long as these healthy phagocytes persist in host brains. As such, these three lines of evidence implicate microglia as powerful modulators of *rnaset2* mutant pathology and highlight these neuroimmune cells as a promising target for future therapeutic development.

6.3 Implications for therapeutic development in RNASET2-deficient leukodystrophy

6.3.1 Is macrophage transplantation a viable treatment in human patients?

In the *rnaset2* mutant zebrafish, transplantation of healthy macrophages was sufficient to replace host microglia and rescue neuroinflammation, behavioural impairment and survival deficits. While this certainly demonstrates that targeting microglia has the potential to ameliorate pathology in RNASET2-deficient leukodystrophy, the utility of macrophage transplantation remains unclear in human patients.

There is certainly a growing precedent for macrophage transplantation in the clinic, with an exponential increase in the number of macrophage transplantation methodologies which have been granted patents in the past decade (Na, Kim and Seok, 2023). However, the majority of these interventions have been explored only in non-neurological disorders, including cardiomyopathy, liver cirrhosis, and renal failure (Moroni *et al.*, 2019; Na, Kim and Seok, 2023). To date, just two reported clinical trials have explored macrophage transplantation in neurological disorders. Autologous macrophage transplantation appeared to induce functional improvements in patients who had suffered acute ischemic and haemorrhagic stroke, as well as leading to robust improvements in motor and cognitive function in children with cerebral palsy (Chernykh *et al.*, 2014, 2016). However, neither study validated the engraftment of transplant-derived cells in the brain (and thus, microglia replacement), meaning the mechanism of their beneficial effects remains unclear. Nonetheless, macrophage transplantation was not associated with any serious adverse events either trial, suggesting that this intervention may be well tolerated even in childhood patients. However, there remain several key drawbacks to the translation of macrophage transplantation in RNASET2-deficient leukodystrophy specifically.

Firstly, as discussed above, the window for treatment of RNASET2-deficient leukodystrophy is likely to be very early in development. Patients with this disorder present with pathogenic clinical and

radiological changes within the early months of life followed by a non-progressive clinical course, suggesting that the period in which pathogenesis is most active – and therefore, when treatments would be most impactful – is during newborn if not foetal stages (Henneke *et al.*, 2009b; Weber *et al.*, 2020). As such, transplantation would likely need to occur very soon after birth, if not *in utero*, due to the early onset of pathogenesis. *In utero* HSCT has been performed with some success across several diseases, this is a highly risky procedure; as such, rapid post-natal transplantation may present a better risk-benefit profile (Wengler *et al.*, 1996; Flake *et al.*, 2002; Le Blanc *et al.*, 2005). Nonetheless, early treatment also relies on early diagnosis, which is challenging for ultrarare diseases like RNASET2-deficient leukodystrophy – with some patients waiting up to a decade for definitive diagnosis (Parikh *et al.*, 2015). However, the monogenic nature of this disorder means it could feasibly be added to newborn screening panels, which could identify patients asymptomatically and facilitate a rapid intervention if a diagnosis was identified (Hong *et al.*, 2021).

A second consideration which may limit the translational potential of macrophage transplantation in RNASET2-deficient leukodystrophy is the time required to find a donor for an allogenic macrophage graft. In the transplantation set-up performed in this thesis, healthy non-related donor fish were used to obtain the transplant graft. This was possible due to the lack of adaptive immune system in zebrafish embryos, which meant that rejection of non-self-cells or emergence of graft-versus-host disease was unlikely (Miao *et al.*, 2021). However, for macrophage transplants in humans, donors would need to be carefully selected to ensure human leukocyte antigen (HLA)-matching (Page *et al.*, 2019). This process can be time consuming, particularly if non-affected family members are not suitable donors, which could mean patients progress beyond the window of therapeutic potential. However, there is a growing precedent for the use of genetically corrected autologous cells for transplantation grafts. To date, two *ex vivo* gene therapies have utilised genetically corrected autologous HSCT to achieve clinical benefits in leukodystrophies (Libmeldy, 2024; Skysona, 2024). Although not strictly genetically corrected, trials exploring macrophage transplantation in neurological disorders have reprogrammed patient-derived macrophages into a regenerative state through culturing with cytokines known to induce M2-like phenotypes (Chernykh *et al.*, 2014, 2016). It is conceivable that patient-derived cells – either HSCs, monocytes of fibroblasts reprogrammed into induced pluripotent stem cells (iPSCs) – could be genetically corrected and used to generate a source of RNASET2-competent macrophages for transplantation (Ackermann *et al.*, 2022). This work would require substantial further development – including a reliable transfection method for patient-derived cells, as well as *ex vivo* macrophage culture – but could, theoretically circumvent the need for a graft donor. As such, there are potential solutions

to many of the logistical barriers for implementation of macrophage transplantation in the treatment of RNASET2-deficient leukodystrophy.

However, one final barrier to the use of macrophage transplantation as a therapeutic strategy in RNASET2-deficient leukodystrophy is the failure of transplant-derived cells to persist in host brains beyond a few weeks post-transplantation. In *rnaset2* mutant zebrafish, transplant-derived cells appear to be cleared after several weeks, in parallel to the arrival of a second, adult wave of microglia (Chapter 4 and 5). It is unclear whether a distinct wave of infiltrating cells occurs in humans and, as such, how long transplant-derived cells could persist in patients (Priller *et al.*, 2001; Biffi *et al.*, 2004; Miyake *et al.*, 2010; Capotondo *et al.*, 2017). However, for maximum therapeutic benefits, one might expect life-long engraftment of transplant-derived cells to be required. Perhaps, therefore, a combination of macrophage transplantation and HSCT could circumvent the disadvantages of each individual intervention. Transplantation of macrophages could give rise to microglia-like cells in the brain within a relatively short-timescale, while HSCs could engraft within the haematopoietic niche to produce a potentially life-long source of healthy microglia-like cells. Future work may seek to combine transplant modalities to investigate the viability of this dual approach. The zebrafish may once again provide a useful model for such studies, where donor cells could be obtained from transgenic animals such that HSCs and macrophages are labelled with different fluorescent reporters to investigate the ability of transplant-derived cells to replace microglia throughout life. Therefore, there is precedent for the use of macrophage transplantation in the clinic, but more work is needed in order to increase the translational potential of macrophage transplantation in RNASET2-deficient leukodystrophy.

6.3.2 Further strategies for targeting of microglial function in RNASET2-deficient leukodystrophy

Beyond transplantation, there are several other strategies which could be used to target microglia in leukodystrophy, with a view of mimicking the rescue obtained by macrophage transplantation. Pharmacological approaches are a particularly promising intervention, with several compounds targeting the neuroimmune response currently in development for other leukodystrophies (Rice *et al.*, 2018; Deczkowska, Weiner and Amit, 2020; Vanderver *et al.*, 2020; Rodríguez-Pascau *et al.*, 2021; Larson *et al.*, 2024; Lynch *et al.*, 2024). It is possible that several of these may have clinical benefits in RNASET2-deficient leukodystrophy – in particular, small molecules targeting the antiviral response. Both RTIs and JAK-STAT inhibitors have shown some promise in AGS – another interferonopathy with comparable clinical presentation to patients with *RNASET2* mutations (Rice *et al.*, 2018; Vanderver *et al.*, 2020). However, the current study did not identify any evidence of ERV upregulation in *rnaset2* mutants, and so the clinical effectiveness of RTIs remain unclear in this disorder. Additionally, RNA

sequencing did not identify any upregulation of the JAK-STAT pathway in *rnaset2* mutants, nor downregulation following transplant, potentially limiting the utility of inhibitors of this signalling cascade in RNASET2-deficient leukodystrophy. Interestingly, bulk RNA sequencing revealed that transplantation led to downregulation of the RIG-I pathway in treated *rnaset2* mutants, suggesting this pathway may be a useful target for therapeutic development. Antagonists of RIG-I signalling are available and have been shown to prevent production of interferon stimulated genes in viral infection models (Rawling *et al.*, 2020; Fu *et al.*, 2023). Therefore, future work may seek to characterise the molecular basis of inflammation and microglial dysfunction, in order to develop more targeted therapies for the treatment of RNASET2-deficient leukodystrophy.

6.4 Future directions

As discussed above, in order to create a truly translational therapy for RNASET2-deficient leukodystrophy, a greater understanding of the mechanisms by which microglial dysfunction contributes to pathology, and how transplantation leads to rescue, is required. Bulk RNA sequencing has already identified one potential pathway which may be a useful target for subsequent drug development (the RIG-I pathway). As a next step, single cell RNA sequencing could be explored to compare cell-specific transcriptomic changes between *rnaset2* mutants and wild type brains, as well as in transplanted mutants relative to non-treated controls. Such an approach could yield specific targets for drug development, which could then be tested in a candidate screen (Van de Sande *et al.*, 2023). Not only are zebrafish generally well suited to high throughput screening, but the *rnaset2* mutant presents with several specific phenotypes which could be easily adapted to a drug screen. Firstly, the accumulation of uncleared apoptotic cells – indicative of impaired clearance of debris by microglia – can be easily visualised in *rnaset2* mutant brains with acridine orange staining, or by crossing *rnaset2* mutants into the *Tg(ubiq:secAnnexinV-mVenus)* background which labels apoptotic cells (Haud et al., 2011b; Hamilton et al., 2020a). Secondly, the hypoactive phenotype of *rnaset2* larvae can be easily quantified with automated tracking software. Together, these phenotypes could provide a valuable tool to identify candidates that rescue pathology at a cellular and behavioural level, which could be taken forward for subsequent characterisation. This approach should also include JAK-STAT inhibitors and RTIs, which have demonstrated efficacy in similar disorders, as well as antagonists of RIG-I signalling, which was identified as a potential modulator of RNASET2-deficient pathology in the current study (Rice *et al.*, 2018; Vanderver *et al.*, 2020). As such, continued investigation of pathogenic mechanisms and potential therapies is warranted in the *rnaset2* mutant zebrafish.

Moreover, future work should consider using a collaborative approach with multiple animal models to provide further insights into RNASET2-deficient pathogenesis and potential therapies. Although rodent models are limited in their ability to recapitulate disease-associated white matter and behavioural phenotypes, the *RNaseT2*$^{-/-}$ rat and *Rnaset2*$^{-/-}$ mouse still present with memory deficits and neuroinflammation, with the latter showing robust upregulation of interferon signalling throughout the brain which is particularly enriched in microglia (Sinkevicius *et al.*, 2018; Kettwig *et al.*, 2021). As such, it would be interesting to investigate the ability of macrophage transplant, or any other experimental therapy, to rescue these markers of pathology in rodent models. Furthermore, comparing single cell transcriptomics from *rnaset2* mutant zebrafish with already published data from the *Rnaset2*$^{-/-}$ mouse may provide further insights into disease pathways and ensure these mechanisms are applicable in mammalian models. As such, a collaborative approach using multiple animal models, with careful consideration of their individual limitations, should be employed for future research in RNASET2-deficient leukodystrophy.

In addition to animal models, further insights into pathogenesis could be obtained using patient-derived tissue. Due to the rarity of RNASET2-deficient leukodystrophy, no post-mortem tissue is currently available to study this disorder. However, the use of patient-derived induced pluripotent stem cells (iPSCs) may provide a non-invasive alternative to the study of human disease processes. Briefly, iPSC generation occurs by culturing human fibroblasts with specific transcription factors known to induce a stem cell state (Takahashi *et al.*, 2006). These iPSCs can then be differentiated to produce a variety of cell types – including neurons, microglia and astrocytes – which can be co-cultured to mimic cell-cell interactions (Abud *et al.*, 2017; Bianchi *et al.*, 2018; Autar *et al.*, 2022; Voulgaris, Nikolakopoulou and Herland, 2022). As such, this protocol allows observation of patient- and cell type-specific pathogenesis throughout various disease stages, with limited use of invasive procedures in patients, and has been employed across a variety of neurological disorders (Valadez-Barba *et al.*, 2020). In RNASET2-deficient leukodystrophy, iPSC-derived cells could provide three potential applications. Firstly, as discussed above, this protocol can provide insights into disease pathophysiology in human cells, which is likely to increase the translational output of any mechanistic insights obtained from this model. Secondly, iPSC-derived cells can also provide a useful tool for high-throughput drug screening, so long as a robust cellular phenotype has been characterised for a given model (Lamas and Roybon, 2021). In RNASET2-deficient leukodystrophy, it is conceivable that iPSC-derived microglia may fail to clear apoptotic debris (as is observed in zebrafish model) – as such, a drug screen in this model investigate the ability of candidates to increase clearance of undigested material by these cells. Further work is needed to generate and characterise phenotypes of patient-derived

iPSCs before drug screening could be performed in this disorder. Thirdly, patient-derived iPSCs could even provide a source of “donor” cells for transplantation, whereby reprogrammed patient fibroblasts are used for autologous transplantation. Several ongoing trials are investigating the regenerative capacity of iPSC transplantation across a variety of disorders, including iPSC-derived dopaminergic neuron transplantation in Parkinson’s disease and iPSC-derived inhibitory interneurons in epilepsy (ClinicalTrials.gov, 2022; Aspen Neuroscience, 2024; Neurona Therapeutics, 2024). As such, the use of genetically corrected patient-specific iPSC-derived macrophages as a transplant graft could potentially circumvent some of the limitations of allogenic transplantation – including donor identification – although significant further research is needed before this intervention would be ready for the clinic. Nonetheless, integrating patient-derived cells alongside animal model research may provide further insights into disease mechanisms and provide novel therapeutic strategies in RNASET2-deficient leukodystrophy.

Finally, to increase the feasibility of therapeutic development in such a rare disorder, future research may seek to consider a development pipeline that includes other similar, but perhaps more common, leukodystrophies with similar pathogenic mechanisms (Zanello *et al.*, 2023). In the rare disease field, there is a growing push for novel trial strategies which allow pooling of resources, including funding, research expertise, and access to small patient populations. One such approach is the use of basket trials to investigate single therapy across multiple disorders which share similar aetiology (Woodcock and LaVange, 2017). As an ultrarare disorder, RNASET2-deficient leukodystrophy may benefit from being grouped with other interferon-stimulated leukodystrophies such as AGS, which shares many of RNASET2-associated clinical phenotypes and molecular signalling pathways (Rutherford, Kasher and Hamilton, 2021). Therefore, future work may consider exploring shared disease mechanisms between these similar disorders in animal models to facilitate potential basket trials in the clinic. Similarly, ultra-rare diseases like RNASET2-deficient leukodystrophy could benefit from scalable technology platforms used in N-of-1 trials. This approach involves production of a generalised intervention which can be easily modified based on patient specific needs – for example, an ASO that can be modified to target a patient-specific mutation, conjugated drug-delivery systems which can be adapted to transport disease-specific compounds into the CNS or even individualised *ex vivo* gene therapy strategies (where patient HSCs are harvested, corrected for specific mutations and then transplanted back into the patient) (Soni, Gowthamarajan and Radhakrishnan, 2018; Synofzik *et al.*, 2022). While further work is required before RNASET2-deficient leukodystrophy could be included in such approaches, future research should bear in mind practical considerations when developing potential therapies for this disorder, to ensure maximum translational potential.

6.5 Concluding remarks

In conclusion, this thesis has demonstrated that the *rnaset2* mutant zebrafish is a valuable model of RNASET2-deficient leukodystrophy, and provided further evidence that microglial dysfunction is among the first markers of pathogenesis to trigger downstream pathology in this model. Macrophage transplantation was sufficient to rescue *rnaset2*-associated pathology at a molecular, cellular, and behavioural level, suggesting that microglial replacement is sufficient to ameliorate pathogenesis in *rnaset2* mutants. Together, these findings identify microglia as the cellular drivers of neuropathology in RNASET2-deficient leukodystrophy and suggest that microglia-directed interventions – macrophage transplant or otherwise – may have therapeutic benefits in this ultra-rare disorder.

Bibliography

Aboul-Enein, F. *et al.* (2003) 'Preferential Loss of Myelin-Associated Glycoprotein Reflects Hypoxia-Like White Matter Damage in Stroke and Inflammatory Brain Diseases', *Journal of Neuropathology & Experimental Neurology*, 62(1), pp. 25–33. Available at: https://doi.org/10.1093/jnen/62.1.25.

Abud, E.M. *et al.* (2017) 'iPSC-Derived Human Microglia-like Cells to Study Neurological Diseases', *Neuron*, 94(2), pp. 278-293.e9. Available at: https://doi.org/10.1016/j.neuron.2017.03.042.

Achleitner, M. *et al.* (2017) 'Lack of Trex1 Causes Systemic Autoimmunity despite the Presence of Antiretroviral Drugs', *The Journal of Immunology*, 199(7), pp. 2261–2269. Available at: https://doi.org/10.4049/jimmunol.1700714.

Ackerman, S.D. and Monk, K.R. (2016) 'The scales and tales of myelination: using zebrafish and mouse to study myelinating glia', *Brain Research*. Elsevier B.V., pp. 79–91. Available at: https://doi.org/10.1016/j.brainres.2015.10.011.

Ackermann, M. *et al.* (2022) 'Continuous human iPSC-macrophage mass production by suspension culture in stirred tank bioreactors', *Nature Protocols*, 17(2), pp. 513–539. Available at: https://doi.org/10.1038/s41596-021-00654-7.

Acquati, F. *et al.* (2019) 'Innate Immune Response Regulation by the Human RNASET2 Tumor Suppressor Gene', *Frontiers in Immunology*, 10. Available at: https://doi.org/10.3389/fimmu.2019.02587.

Aebi, M. *et al.* (1989) 'cDNA Structures and Regulation of Two Interferon-Induced Human Mx Proteins', *Molecular and Cellular Biology*, 9(11), pp. 5062–5072. Available at: https://doi.org/10.1128/mcb.9.11.5062-5072.1989.

Aggad, D. *et al.* (2009) 'The Two Groups of Zebrafish Virus-Induced Interferons Signal via Distinct Receptors with Specific and Shared Chains', *The Journal of Immunology*, 183(6), pp. 3924–3931. Available at: https://doi.org/10.4049/jimmunol.0901495.

Ahmed, S.S. *et al.* (2016) 'rAAV Gene Therapy in a Canavan's Disease Mouse Model Reveals Immune Impairments and an Extended Pathology Beyond the Central Nervous System', *Molecular Therapy*, 24(6), pp. 1030–1041. Available at: https://doi.org/10.1038/mt.2016.68.

Ainger, K. *et al.* (1993) 'Transport and localization of exogenous myelin basic protein mRNA microinjected into oligodendrocytes.', *The Journal of cell biology*, 123(2), pp. 431–441. Available at: https://doi.org/10.1083/jcb.123.2.431.

Ajami, B. *et al.* (2007a) 'Local self-renewal can sustain CNS microglia maintenance and function throughout adult life', *Nature Neuroscience*, 10(12), pp. 1538–1543. Available at: https://doi.org/10.1038/nn2014.

Ajami, B. *et al.* (2007b) 'Local self-renewal can sustain CNS microglia maintenance and function throughout adult life', *Nature Neuroscience*, 10(12), pp. 1538–1543. Available at: https://doi.org/10.1038/nn2014.

Almeida, R.G. *et al.* (2011) 'Individual axons regulate the myelinating potential of single oligodendrocytes in vivo', *Development*, 138(20), pp. 4443–4450. Available at: https://doi.org/10.1242/dev.071001.

Altmann, S.M. *et al.* (2003) 'Molecular and Functional Analysis of an Interferon Gene from the Zebrafish, *Danio rerio*', *Journal of Virology*, 77(3), pp. 1992–2002. Available at: https://doi.org/10.1128/JVI.77.3.1992-2002.2003.

Aradjanski, M. *et al.* (2017) 'DARS2 protects against neuroinflammation and apoptotic neuronal loss, but is dispensable for myelin producing cells', *Human Molecular Genetics*, 26(21), pp. 4181–4189. Available at: https://doi.org/10.1093/hmg/ddx307.

Armstrong, N. *et al.* (2023) 'A systematic review of clinical effectiveness and safety for historical and current treatment options for metachromatic leukodystrophy in children, including atidarsagene autotemcel', *Orphanet Journal of Rare Diseases*, 18(1), p. 248. Available at: https://doi.org/10.1186/s13023-023-02814-2.

Asheuer, M. *et al.* (2004) 'Human CD34 + cells differentiate into microglia and express recombinant therapeutic protein', *Proceedings of the National Academy of Sciences*, 101(10), pp. 3557–3562. Available at: https://doi.org/10.1073/pnas.0306431101.

Ashley, C.L. *et al.* (2019) 'Interferon-Independent Upregulation of Interferon-Stimulated Genes during Human Cytomegalovirus Infection is Dependent on IRF3 Expression', *Viruses*, 11(3), p. 246. Available at: https://doi.org/10.3390/v11030246.

Askew, K. *et al.* (2017) 'Coupled Proliferation and Apoptosis Maintain the Rapid Turnover of Microglia in the Adult Brain', *Cell Reports*, 18(2), pp. 391–405. Available at: https://doi.org/10.1016/j.celrep.2016.12.041.

Aspen Neuroscience (2024) *Aspen's Clinical Pipeline*, *https://aspenneuroscience.com/technology/pipeline/*.

Attili, S. and Hughes, S.M. (2014) 'Anaesthetic Tricaine Acts Preferentially on Neural Voltage-Gated Sodium Channels and Fails to Block Directly Evoked Muscle Contraction', *PLoS ONE*, 9(8), p. e103751. Available at: https://doi.org/10.1371/journal.pone.0103751.

Autar, K. *et al.* (2022) 'A functional hiPSC-cortical neuron differentiation and maturation model and its application to neurological disorders', *Stem Cell Reports*, 17(1), pp. 96–109. Available at: https://doi.org/10.1016/j.stemcr.2021.11.009.

Avila, R.L. *et al.* (2007) 'Myelin Structure and Composition in Zebrafish', *Neurochemical Research*, 32(2), pp. 197–209. Available at: https://doi.org/10.1007/s11064-006-9136-5.

Balla, K.M. *et al.* (2020) 'Linking Virus Discovery to Immune Responses Visualized during Zebrafish Infections', *Current Biology*, 30(11), pp. 2092-2103.e5. Available at: https://doi.org/10.1016/j.cub.2020.04.031.

Barbarese, E., Carson, J.H. and Braun, P.E. (1978) 'ACCUMULATION OF THE FOUR MYELIN BASIC PROTEINS IN MOUSE BRAIN DURING DEVELOPMENT 1', *Journal of Neurochemistry*, 31(4), pp. 779–782. Available at: https://doi.org/10.1111/j.1471-4159.1978.tb00110.x.

Baron, W. and Hoekstra, D. (2010) 'On the biogenesis of myelin membranes: Sorting, trafficking and cell polarity', *FEBS Letters*, 584(9), pp. 1760–1770. Available at: https://doi.org/10.1016/j.febslet.2009.10.085.

Barry-Carroll, L. *et al.* (2023) 'Microglia colonize the developing brain by clonal expansion of highly proliferative progenitors, following allometric scaling', *Cell Reports*, 42(5), p. 112425. Available at: https://doi.org/10.1016/j.celrep.2023.112425.

Barry-Carroll, L. and Gomez-Nicola, D. (2024) 'The molecular determinants of microglial developmental dynamics', *Nature Reviews Neuroscience*, 25(6), pp. 414–427. Available at: https://doi.org/10.1038/s41583-024-00813-1.

Barton, N.W. *et al.* (1991) 'Replacement Therapy for Inherited Enzyme Deficiency — Macrophage-Targeted Glucocerebrosidase for Gaucher's Disease', *New England Journal of Medicine*, 324(21), pp. 1464–1470. Available at: https://doi.org/10.1056/NEJM199105233242104.

Baschat, A.A. *et al.* (2003) 'Prevalence of viral DNA in amniotic fluid of low-risk pregnancies in the second trimester', *Journal of Maternal-Fetal and Neonatal Medicine*, 13(6), pp. 381–384. Available at: https://doi.org/10.1080/jmf.13.6.381.384.

Baudry, M. *et al.* (2003) 'Postnatal development of inflammation in a murine model of Niemann–Pick type C disease: immunohistochemical observations of microglia and astroglia', *Experimental Neurology*, 184(2), pp. 887–903. Available at: https://doi.org/10.1016/S0014-4886(03)00345-5.

Beck, M. (2010) 'Therapy for lysosomal storage disorders', *IUBMB Life*, pp. 33–40. Available at: https://doi.org/10.1002/iub.284.

Beck-Engeser, G.B., Eilat, D. and Wabl, M. (2011) 'An autoimmune disease prevented by anti-retroviral drugs.', *Retrovirology*, 8, p. 91. Available at: https://doi.org/10.1186/1742-4690-8-91.

Becker, C.G. and Becker, T. (2008) 'Adult zebrafish as a model for successful central nervous system regeneration.', *Restorative neurology and neuroscience*, 26(2–3), pp. 71–80.

Becker, T. *et al.* (1998) 'Readiness of Zebrafish Brain Neurons to Regenerate a Spinal Axon Correlates with Differential Expression of Specific Cell Recognition Molecules', *The Journal of Neuroscience*, 18(15), pp. 5789–5803. Available at: https://doi.org/10.1523/JNEUROSCI.18-15-05789.1998.

Becker, T. and Becker, C. (2001) 'Regenerating descending axons preferentially reroute to the gray matter in the presence of a general macrophage/microglial reaction caudal to a spinal transection in adult zebrafish', *Journal of Comparative Neurology*, 433(1), pp. 131–147. Available at: https://doi.org/10.1002/cne.1131.

Behrendt, R. *et al.* (2013) 'Mouse SAMHD1 has antiretroviral activity and suppresses a spontaneous cell-intrinsic antiviral response', *Cell Reports*, 4(4), pp. 689–696. Available at: https://doi.org/10.1016/j.celrep.2013.07.037.

Benitez-Guijarro, M. *et al.* (2018) 'RNase H2, mutated in Aicardi-Goutières syndrome, promotes LINE-1 retrotransposition', *The EMBO Journal*, 7(15), p. e98506. Available at: https://doi.org/10.15252/embj.201798506.

Bennett, F.C. *et al.* (2018) 'A Combination of Ontogeny and CNS Environment Establishes Microglial Identity', *Neuron*, 98(6), pp. 1170-1183.e8. Available at: https://doi.org/10.1016/j.neuron.2018.05.014.

Bennett, M.L. (2023) 'A polarizing answer — microglia in Nasu-Hakola disease', *Nature Immunology*, 24(3), pp. 379–381. Available at: https://doi.org/10.1038/s41590-023-01440-1.

Beppi, C., Straumann, D. and Bögli, S.Y. (2021) 'A model-based quantification of startle reflex habituation in larval zebrafish', *Scientific Reports*, 11(1), p. 846. Available at: https://doi.org/10.1038/s41598-020-79923-6.

Berdowski, W.M. *et al.* (2022) 'Dominant-acting CSF1R variants cause microglial depletion and altered astrocytic phenotype in zebrafish and adult-onset leukodystrophy', *Acta Neuropathologica*, 144(2), pp. 211–239. Available at: https://doi.org/10.1007/s00401-022-02440-5.

Bergner, C.G. *et al.* (2019) 'Microglia damage precedes major myelin breakdown in X-linked adrenoleukodystrophy and metachromatic leukodystrophy', *GLIA*, 67(6), pp. 1196–1209. Available at: https://doi.org/10.1002/glia.23598.

Bergner, C.G. *et al.* (2023) 'Case report: Treatment of advanced CSF1-receptor associated leukoencephalopathy with hematopoietic stem cell transplant', *Frontiers in Neurology*, 14. Available at: https://doi.org/10.3389/fneur.2023.1163107.

Bermejo, A.V. *et al.* (2020) 'Cancer associated endogenous retroviruses: Ideal immune targets for adenovirus-based immunotherapy', *International Journal of Molecular Sciences*. MDPI AG, pp. 1–21. Available at: https://doi.org/10.3390/ijms21144843.

Bermúdez, R. *et al.* (2018) 'First description of a natural infection with spleen and kidney necrosis virus in zebrafish', *Journal of Fish Diseases*, 41(8), pp. 1283–1294. Available at: https://doi.org/10.1111/jfd.12822.

Bérouti, M. *et al.* (2024) 'Lysosomal endonuclease RNase T2 and PLD exonucleases cooperatively generate RNA ligands for TLR7 activation', *Immunity*, 57(7), pp. 1482-1496.e8. Available at: https://doi.org/10.1016/j.immuni.2024.04.010.

Bianchi, F. *et al.* (2018) 'Rapid and efficient differentiation of functional motor neurons from human iPSC for neural injury modelling', *Stem Cell Research*, 32, pp. 126–134. Available at: https://doi.org/10.1016/j.scr.2018.09.006.

Biffi, A. *et al.* (2004) 'Correction of metachromatic leukodystrophy in the mouse model by transplantation of genetically modified hematopoietic stem cells', *Journal of Clinical Investigation*, 113(8), pp. 1118–1129. Available at: https://doi.org/10.1172/JCI200419205.

Björkhem, I. (2013) 'Cerebrotendinous xanthomatosis', *Current Opinion in Lipidology*, 24(4), pp. 283–287. Available at: https://doi.org/10.1097/MOL.0b013e328362df13.

Bjornevik, K. *et al.* (2022) *MULTIPLE SCLEROSIS Longitudinal analysis reveals high prevalence of Epstein-Barr virus associated with multiple sclerosis*, *Science*. Available at: https://www.science.org.

Le Blanc, K. *et al.* (2005) 'Fetal mesenchymal stem-cell engraftment in bone after in utero transplantation in a patient with severe osteogenesis imperfecta', *Transplantation* [Preprint]. Available at: https://doi.org/10.1097/01.TP.0000159029.48678.93.

BluebirdBio (2022) *bluebird bio Receives FDA Accelerated Approval for SKYSONA® Gene Therapy for Early, Active Cerebral Adrenoleukodystrophy (CALD)*, *https://investor.bluebirdbio.com/*.

BluebirdBio (2024) 'Skysona, Summary of Product Characteristics'.

Blume, Z.I. *et al.* (2020) 'Microglia in the developing retina couple phagocytosis with the progression of apoptosis via P2RY12 signaling', *Developmental Dynamics*, 249(6), pp. 723–740. Available at: https://doi.org/10.1002/dvdy.163.

Bojarczuk, A. *et al.* (2016) 'Cryptococcus neoformans Intracellular Proliferation and Capsule Size Determines Early Macrophage Control of Infection', *Scientific Reports*, 6, p. 21489. Available at: https://doi.org/10.1038/srep21489.

Bonkowsky, J.L. *et al.* (2010) 'The burden of inherited leukodystrophies in children', *Neurology*, 75(8), pp. 718–725. Available at: https://doi.org/10.1212/WNL.0b013e3181eee46b.

Bonkowsky, J.L. *et al.* (2021) 'Leukodystrophies in Children: Diagnosis, Care, and Treatment', *Pediatrics*, 148(3). Available at: https://doi.org/10.1542/peds.2021-053126.

Boucher, A.A. *et al.* (2015) 'Long-term outcomes after allogeneic hematopoietic stem cell transplantation for metachromatic leukodystrophy: the largest single-institution cohort report',

Orphanet Journal of Rare Diseases, 10, p. 94. Available at: https://doi.org/10.1186/s13023-015-0313-y.

Bourque, G. *et al.* (2018) 'Ten things you should know about transposable elements 06 Biological Sciences 0604 Genetics', *Genome Biology*, 19(1). Available at: https://doi.org/10.1186/s13059-018-1577-z.

Brösamle, C. and Halpern, M.E. (2002) 'Characterization of myelination in the developing zebrafish', *Glia*, 39(1), pp. 47–57. Available at: https://doi.org/10.1002/glia.10088.

Bruton, F.A. *et al.* (2022) 'Macrophages trigger cardiomyocyte proliferation by increasing epicardial vegfaa expression during larval zebrafish heart regeneration', *Developmental Cell*, 57(12), pp. 1512-1528.e5. Available at: https://doi.org/10.1016/j.devcel.2022.05.014.

Buckley, C.E., Goldsmith, P. and Franklin, R.J.M. (2008) 'Zebrafish myelination: a transparent model for remyelination?', *Disease Models & Mechanisms*, 1(4–5), pp. 221–228. Available at: https://doi.org/10.1242/dmm.001248.

Bugiani, M. *et al.* (2010) 'Leukoencephalopathy with vanishing white matter: a review.', *Journal of neuropathology and experimental neurology*, 69(10), pp. 987–96. Available at: https://doi.org/10.1097/NEN.0b013e3181f2eafa.

Bugiani, M. *et al.* (2018) 'Vanishing white matter: a leukodystrophy due to astrocytic dysfunction', *Brain Pathology*, 28(3), pp. 408–421. Available at: https://doi.org/10.1111/bpa.12606.

Buglo, E. *et al.* (2020) 'Genetic compensation in a stable slc25a46 mutant zebrafish: A case for using F0 CRISPR mutagenesis to study phenotypes caused by inherited disease.', *PloS one*, 15(3), p. e0230566. Available at: https://doi.org/10.1371/journal.pone.0230566.

Buntinx, M. *et al.* (2004) 'Cytokine-induced cell death in human oligodendroglial cell lines. II: Alterations in gene expression induced by interferon-γ and tumor necrosis factor-α', *Journal of Neuroscience Research*, 76(6), pp. 846–861. Available at: https://doi.org/10.1002/jnr.20117.

Burgess, H.A. and Burton, E.A. (2023) 'A Critical Review of Zebrafish Neurological Disease Models−1. The Premise: Neuroanatomical, Cellular and Genetic Homology and Experimental Tractability', *Oxford Open Neuroscience*, 2. Available at: https://doi.org/10.1093/oons/kvac018.

Campomenosi, P. *et al.* (2006) 'Characterization of RNASET2, the first human member of the Rh/T2/S family of glycoproteins', *Archives of Biochemistry and Biophysics*, 449(1–2), pp. 17–26. Available at: https://doi.org/10.1016/j.abb.2006.02.022.

Capotondo, A. *et al.* (2017) 'Intracerebroventricular delivery of hematopoietic progenitors results in rapid and robust engraftment of microglia-like cells', *Science Advances*, 3, p. e1701211. Available at: https://doi.org/10.1126/sciadv.1701211.

Casano, A.M., Albert, M. and Peri, F. (2016a) 'Developmental Apoptosis Mediates Entry and Positioning of Microglia in the Zebrafish Brain', *Cell Reports*, 16(4), pp. 897–906. Available at: https://doi.org/10.1016/j.celrep.2016.06.033.

Casano, A.M., Albert, M. and Peri, F. (2016b) 'Developmental Apoptosis Mediates Entry and Positioning of Microglia in the Zebrafish Brain', *Cell Reports*, 16(4), pp. 897–906. Available at: https://doi.org/10.1016/j.celrep.2016.06.033.

Cattalini, M. *et al.* (2021) 'Case Report: The JAK-Inhibitor Ruxolitinib Use in Aicardi-Goutieres Syndrome Due to ADAR1 Mutation', *Frontiers in Pediatrics*, 9. Available at: https://doi.org/10.3389/fped.2021.725868.

Chen, S.-K. *et al.* (2010) 'Hematopoietic Origin of Pathological Grooming in Hoxb8 Mutant Mice', *Cell*, 141(5), pp. 775–785. Available at: https://doi.org/10.1016/j.cell.2010.03.055.

Chernykh, E.R. *et al.* (2014) 'Clinical Experience with Autologous M2 Macrophages in Children with Severe Cerebral Palsy', *Cell Transplantation*, 23(1_suppl), pp. 97–104. Available at: https://doi.org/10.3727/096368914X684925.

Chernykh, E.R. *et al.* (2016) 'Safety and Therapeutic Potential of M2 Macrophages in Stroke Treatment', *Cell Transplantation*, 25(8), pp. 1461–1471. Available at: https://doi.org/10.3727/096368915X690279.

Chiang, J.J. *et al.* (2018) 'Viral unmasking of cellular 5S rRNA pseudogene transcripts induces RIG-I-mediated immunity', *Nature Immunology*, 19(1), pp. 53–62. Available at: https://doi.org/10.1038/s41590-017-0005-y.

Chiappinelli, K.B. *et al.* (2015) 'Inhibiting DNA Methylation Causes an Interferon Response in Cancer via dsRNA Including Endogenous Retroviruses.', *Cell*, 162(5), pp. 974–86. Available at: https://doi.org/10.1016/j.cell.2015.07.011.

Chitu, V. *et al.* (2015) 'Phenotypic characterization of a Csf1r haploinsufficient mouse model of adult-onset leukodystrophy with axonal spheroids and pigmented glia (ALSP)', *Neurobiology of Disease*, 74, pp. 219–228. Available at: https://doi.org/10.1016/j.nbd.2014.12.001.

Chitu, V. *et al.* (2020) 'Microglial Homeostasis Requires Balanced CSF-1/CSF-2 Receptor Signaling', *Cell Reports*, 30(9), pp. 3004-3019.e5. Available at: https://doi.org/10.1016/j.celrep.2020.02.028.

ClinicalTrials.gov (2022) *Phase 1 Safety and Tolerability Study of MSK-DA01 Cell Therapy for Advanced Parkinson's Disease*, *https://clinicaltrials.gov/study/NCT04802733*.

Cologna, S.M. *et al.* (2014) 'Human and mouse neuroinflammation markers in Niemann-Pick disease, type C1', *Journal of Inherited Metabolic Disease*, 37(1), pp. 83–92. Available at: https://doi.org/10.1007/s10545-013-9610-6.

Contreras, M. *et al.* (1994) 'The protein coded by the X-adrenoleukodystrophy gene is a peroxisomal integral membrane protein', *FEBS Letters*, 344(2–3), pp. 211–215. Available at: https://doi.org/10.1016/0014-5793(94)00400-5.

Coraci, I.S. *et al.* (2002) 'CD36, a class B scavenger receptor, is expressed on microglia in Alzheimer's disease brains and can mediate production of reactive oxygen species in response to β-amyloid fibrils', *American Journal of Pathology*, 160(1), pp. 101–112. Available at: https://doi.org/10.1016/S0002-9440(10)64354-4.

Cougnoux, A. *et al.* (2018) 'Microglia activation in Niemann–Pick disease, type C1 is amendable to therapeutic intervention', *Human Molecular Genetics*, 27(12), pp. 2076–2089. Available at: https://doi.org/10.1093/hmg/ddy112.

Cougnoux, A. *et al.* (2019) 'Unique molecular signature in mucolipidosis type IV microglia', *Journal of Neuroinflammation*, 16(1), p. 276. Available at: https://doi.org/10.1186/s12974-019-1672-4.

Cronk, J.C. *et al.* (2018) 'Peripherally derived macrophages can engraft the brain independent of irradiation and maintain an identity distinct from microglia', *The Journal of Experimental Medicine*, 215(6), pp. 1627–1647. Available at: https://doi.org/10.1084/jem.20180247.

Crow, Y.J. *et al.* (2006) 'Mutations in the gene encoding the 3'-5' DNA exonuclease TREX1 cause Aicardi-Goutières syndrome at the AGS1 locus', *Nature Genetics*, 38(8), pp. 917–920. Available at: https://doi.org/10.1038/ng1845.

Crow, Y.J., Shetty, J. and Livingston, J.H. (2020) 'Treatments in Aicardi–Goutières syndrome', *Developmental Medicine and Child Neurology*, 175(1), pp. 1–8. Available at: https://doi.org/10.1111/dmcn.14268.

Daghagh, H. *et al.* (2022) 'Homozygous mutation in *CSF1R* causes brain abnormalities, neurodegeneration, and dysosteosclerosis (BANDDOS)', *BioImpacts* [Preprint]. Available at: https://doi.org/10.34172/bi.2022.23528.

Dai, X.-M. *et al.* (2002) 'Targeted disruption of the mouse colony-stimulating factor 1 receptor gene results in osteopetrosis, mononuclear phagocyte deficiency, increased primitive progenitor cell frequencies, and reproductive defects', *Blood*, 99(1), pp. 111–120. Available at: https://doi.org/10.1182/blood.V99.1.111.

Deczkowska, A., Weiner, A. and Amit, I. (2020) 'The Physiology, Pathology, and Potential Therapeutic Applications of the TREM2 Signaling Pathway', *Cell*, 181(6), pp. 1207–1217. Available at: https://doi.org/10.1016/j.cell.2020.05.003.

Dee, C.T. *et al.* (2016) 'CD4-Transgenic Zebrafish Reveal Tissue-Resident Th2- and Regulatory T Cell–like Populations and Diverse Mononuclear Phagocytes', *The Journal of Immunology*, 197(9), pp. 3520–3530. Available at: https://doi.org/10.4049/jimmunol.1600959.

Derksen, A. *et al.* (2021) 'Variants in LSM7 impair LSM complexes assembly, neurodevelopment in zebrafish and may be associated with an ultra-rare neurological disease', *Human Genetics and Genomics Advances*, 2(3), p. 100034. Available at: https://doi.org/10.1016/j.xhgg.2021.100034.

Distéfano-Gagné, F. *et al.* (2023) 'Roles and regulation of microglia activity in multiple sclerosis: insights from animal models', *Nature Reviews Neuroscience*, 24(7), pp. 397–415. Available at: https://doi.org/10.1038/s41583-023-00709-6.

Dobin, A. *et al.* (2013) 'STAR: Ultrafast universal RNA-seq aligner', *Bioinformatics*, 29(1), pp. 15–21. Available at: https://doi.org/10.1093/bioinformatics/bts635.

Dong, J. *et al.* (2021) 'Inhibiting NLRP3 inflammasome activation prevents copper-induced neuropathology in a murine model of Wilson's disease', *Cell Death & Disease*, 12(1), p. 87. Available at: https://doi.org/10.1038/s41419-021-03397-1.

Doszyn, O., Dulski, T. and Zmorzynska, J. (2024) 'Diving into the zebrafish brain: exploring neuroscience frontiers with genetic tools, imaging techniques, and behavioral insights', *Frontiers in Molecular Neuroscience*, 17. Available at: https://doi.org/10.3389/fnmol.2024.1358844.

D'Rozario, M., Monk, K.R. and Petersen, S.C. (2017) 'Analysis of myelinated axon formation in zebrafish', in, pp. 383–414. Available at: https://doi.org/10.1016/bs.mcb.2016.08.001.

Duffner, P.K. *et al.* (2009) 'The long-term outcomes of presymptomatic infants transplanted for Krabbe disease: Report of the workshop held on July 11 and 12, 2008, Holiday Valley, New York', *Genetics in Medicine*, 11(6), pp. 450–454. Available at: https://doi.org/10.1097/GIM.0b013e3181a16e04.

Dumas, A.A., Borst, K. and Prinz, M. (2021) 'Current tools to interrogate microglial biology', *Neuron*, 109(18), pp. 2805–2819. Available at: https://doi.org/10.1016/j.neuron.2021.07.004.

Earley, A.M., Graves, C.L. and Shiau, C.E. (2018) 'Critical Role for a Subset of Intestinal Macrophages in Shaping Gut Microbiota in Adult Zebrafish', *Cell Reports*, 25(2), pp. 424–436. Available at: https://doi.org/10.1016/j.celrep.2018.09.025.

Efthymiou, A.G. and Goate, A.M. (2017) 'Late onset Alzheimer's disease genetics implicates microglial pathways in disease risk', *Molecular Neurodegeneration*, 12(1), p. 43. Available at: https://doi.org/10.1186/s13024-017-0184-x.

Eichler, F.S. *et al.* (2008) 'Is microglial apoptosis an early pathogenic change in cerebral X-linked adrenoleukodystrophy?', *Annals of Neurology*, 63(6), pp. 729–742. Available at: https://doi.org/10.1002/ana.21391.

Elabd, S. *et al.* (2019) 'Delay in development and behavioural abnormalities in the absence of p53 in zebrafish', *PLOS ONE*, 14(7), p. e0220069. Available at: https://doi.org/10.1371/journal.pone.0220069.

El-Brolosy, M.A. and Stainier, D.Y.R. (2017) 'Genetic compensation: A phenomenon in search of mechanisms.', *PLoS genetics*, 13(7), p. e1006780. Available at: https://doi.org/10.1371/journal.pgen.1006780.

Elitt, M.S. *et al.* (2020) 'Suppression of proteolipid protein rescues Pelizaeus–Merzbacher disease', *Nature*, 585(7825), pp. 397–403. Available at: https://doi.org/10.1038/s41586-020-2494-3.

Elliott, M.R. *et al.* (2009) 'Nucleotides released by apoptotic cells act as a find-me signal to promote phagocytic clearance', *Nature*, 461(7261), pp. 282–286. Available at: https://doi.org/10.1038/nature08296.

Elmer, J.L. and Ferguson-Smith, A.C. (2020) 'Strain-specific epigenetic regulation of endogenous retroviruses: The role of Trans-acting modifiers', *Viruses*. MDPI AG. Available at: https://doi.org/10.3390/v12080810.

Erblich, B. *et al.* (2011) 'Absence of colony stimulation factor-1 receptor results in loss of microglia, disrupted brain development and olfactory deficits', *PLoS ONE*, 6(10). Available at: https://doi.org/10.1371/journal.pone.0026317.

Escolar, M. *et al.* (2023) 'P014: First-in-human phase 1/2 trial of intravenous FBX-101 with cord blood transplantation increases GALC, brain and motor development in infantile Krabbe', *Genetics in Medicine Open*, 1(1), p. 100024. Available at: https://doi.org/10.1016/j.gimo.2023.100024.

Escolar, M.L. *et al.* (2005) *Transplantation of Umbilical-Cord Blood in Babies with Infantile Krabbe's Disease From the Program for Neurodevelopmen-tal Function in Rare Disorders, Clinical Cen-ter for the Study of Development and Learn-ing (M*, *N Engl J Med*. Available at: www.nejm.org.

EURORDIS (2021) *About Rare Diseases*.

Faught, E. and Vijayan, M.M. (2018) 'The mineralocorticoid receptor is essential for stress axis regulation in zebrafish larvae', *Scientific Reports*, 8, p. 18081. Available at: https://doi.org/10.1038/s41598-018-36681-w.

Favrais, G. *et al.* (2011) 'Systemic inflammation disrupts the developmental program of white matter', *Annals of Neurology*, 70(4), pp. 550–565. Available at: https://doi.org/10.1002/ana.22489.

Feng, L. *et al.* (2020) 'Cell-Based Therapy for Canavan Disease Using Human iPSC-Derived NPCs and OPCs', *Advanced Science*, 7(23). Available at: https://doi.org/10.1002/advs.202002155.

Ferrero, G. *et al.* (2018) 'Embryonic Microglia Derive from Primitive Macrophages and Are Replaced by cmyb-Dependent Definitive Microglia in Zebrafish', *Cell Reports*, 24(1), pp. 130–141. Available at: https://doi.org/10.1016/j.celrep.2018.05.066.

Ferrero, G. *et al.* (2021) 'A csf1rb mutation uncouples two waves of microglia development in zebrafish', *Development (Cambridge)*, 148(1), pp. 194241-undefined. Available at: https://doi.org/10.1242/dev.194241.

Filippi, A., Mueller, T. and Driever, W. (2014) '*vglut2* and *gad* expression reveal distinct patterns of dual GABAergic versus glutamatergic cotransmitter phenotypes of dopaminergic and noradrenergic neurons in the zebrafish brain', *Journal of Comparative Neurology*, 522(9), pp. 2019–2037. Available at: https://doi.org/10.1002/cne.23524.

Flake, A.W. *et al.* (2002) 'Treatment of X-Linked Severe Combined Immunodeficiency by in Utero Transplantation of Paternal Bone Marrow', *New England Journal of Medicine* [Preprint]. Available at: https://doi.org/10.1056/nejm199612123352404.

Fleming, A. *et al.* (2022) 'Unexpected Phenotype Reversion and Survival in a Zebrafish Model of Multiple Sulfatase Deficiency', *Frontiers in Cell and Developmental Biology*, 10. Available at: https://doi.org/10.3389/fcell.2022.843079.

Fleming, A., Diekmann, H. and Goldsmith, P. (2013) 'Functional Characterisation of the Maturation of the Blood-Brain Barrier in Larval Zebrafish', *PLoS ONE*, 8(10), p. e77548. Available at: https://doi.org/10.1371/journal.pone.0077548.

Fratantoni, J.C., Hall, C.W. and Neufeld, E.F. (1968) 'Hurler and Hunter Syndromes: Mutual Correction of the Defect in Cultured Fibroblasts', *Science*, 162(3853), pp. 570–572. Available at: https://doi.org/10.1126/science.162.3853.570.

Fu, L. *et al.* (2023) 'Dual mechanism: Epigenetic inhibitor apabetalone reduces SARS-CoV-2 Delta and Omicron variant spike binding and attenuates SARS-CoV-2 RNA induced inflammation', *International Immunopharmacology*, 117, p. 109929. Available at: https://doi.org/10.1016/j.intimp.2023.109929.

Fuhrmann, M. *et al.* (2010a) 'Microglial Cx3cr1 knockout prevents neuron loss in a mouse model of Alzheimer's disease', *Nature Neuroscience*, 13(4), pp. 411–413. Available at: https://doi.org/10.1038/nn.2511.

Fuhrmann, M. *et al.* (2010b) 'Microglial Cx3cr1 knockout prevents neuron loss in a mouse model of Alzheimer's disease', *Nature Neuroscience*, 13(4), pp. 411–413. Available at: https://doi.org/10.1038/nn.2511.

Fulton, D. *et al.* (2010) 'Regulation of L-type Ca ++ currents and process morphology in white matter oligodendrocyte precursor cells by golli-myelin proteins', *Glia*, 58(11), pp. 1292–1303. Available at: https://doi.org/10.1002/glia.21008.

Gahtan, E. and O'Malley, D.M. (2003) 'Visually guided injection of identified reticulospinal neurons in zebrafish: A survey of spinal arborization patterns', *Journal of Comparative Neurology*, 459(2), pp. 186–200. Available at: https://doi.org/10.1002/cne.10621.

Gall, A. *et al.* (2012) 'Autoimmunity Initiates in Nonhematopoietic Cells and Progresses via Lymphocytes in an Interferon-Dependent Autoimmune Disease', *Immunity*, 36(1), pp. 120–131. Available at: https://doi.org/10.1016/j.immuni.2011.11.018.

Garau, J. *et al.* (2019) 'Molecular Genetics and Interferon Signature in the Italian Aicardi Goutières Syndrome Cohort: Report of 12 New Cases and Literature Review', *Journal of Clinical Medicine*, 8(5), p. 750. Available at: https://doi.org/10.3390/jcm8050750.

Gauthier, P.T. and Vijayan, M.M. (2018) 'Nonlinear mixed-modelling discriminates the effect of chemicals and their mixtures on zebrafish behavior', *Scientific Reports*, 8, p. 1999. Available at: https://doi.org/10.1038/s41598-018-20112-x.

Gibson, E.M. *et al.* (2014) 'Neuronal Activity Promotes Oligodendrogenesis and Adaptive Myelination in the Mammalian Brain', *Science*, 344(6183). Available at: https://doi.org/10.1126/science.1252304.

Ginhoux, F. *et al.* (2010) 'Fate Mapping Analysis Reveals That Adult Microglia Derive from Primitive Macrophages', *Science*, 701(November), pp. 841–845.

Glass, C.K. *et al.* (2010) 'Mechanisms Underlying Inflammation in Neurodegeneration', *Cell*, 140(6), pp. 918–934. Available at: https://doi.org/10.1016/j.cell.2010.02.016.

Gogate, N. *et al.* (1994) 'Plasticity in the adult human oligodendrocyte lineage', *The Journal of Neuroscience*, 14(8), pp. 4571–4587. Available at: https://doi.org/10.1523/JNEUROSCI.14-08-04571.1994.

Gold, M. and El Khoury, J. (2015) 'β-amyloid, microglia, and the inflammasome in Alzheimer's disease', *Seminars in Immunopathology*. Springer Verlag, pp. 607–611. Available at: https://doi.org/10.1007/s00281-015-0518-0.

Gomez Perdiguero, E. *et al.* (2015) 'Tissue-resident macrophages originate from yolk-sac-derived erythro-myeloid progenitors', *Nature*, 518(7540), pp. 547–551. Available at: https://doi.org/10.1038/nature13989.

Gomez-Diaz, C. *et al.* (2025) 'RNase T2 restricts TLR13-mediated autoinflammation in vivo', *Journal of Experimental Medicine*, 222(3). Available at: https://doi.org/10.1084/jem.20241424.

Gong, Y. *et al.* (2017) 'Microglial dysfunction as a key pathological change in adrenomyeloneuropathy', *Annals of Neurology*, 82(5), pp. 813–827. Available at: https://doi.org/10.1002/ana.25085.

Gonzalez Melo, M. *et al.* (2021) 'The first knock-in rat model for glutaric aciduria type I allows further insights into pathophysiology in brain and periphery', *Molecular Genetics and Metabolism*, 133(2), pp. 157–181. Available at: https://doi.org/10.1016/j.ymgme.2021.03.017.

Green, L. *et al.* (2024) 'Biallelic mutations in SUPV3L1 cause an inherited neurodevelopmental disorder with variable leukodystrophy due to aberrant mitochondrial double stranded RNA processing'. Available at: https://doi.org/10.21203/rs.3.rs-4356120/v1.

Greulich, W. *et al.* (2019) 'TLR8 Is a Sensor of RNase T2 Degradation Products', *Cell*, 179(6), pp. 1264-1275.e13. Available at: https://doi.org/10.1016/j.cell.2019.11.001.

Guerrero, B.L. and Sicotte, N.L. (2020) 'Microglia in Multiple Sclerosis: Friend or Foe?', *Frontiers in Immunology*, 11, pp. 374-undefined. Available at: https://doi.org/10.3389/fimmu.2020.00374.

Hagemann, T.L. *et al.* (2018) 'Antisense suppression of glial fibrillary acidic protein as a treatment for Alexander disease', *Annals of Neurology*, 83(1), pp. 27–39. Available at: https://doi.org/10.1002/ana.25118.

Hagemeyer, N. *et al.* (2017) 'Microglia contribute to normal myelinogenesis and to oligodendrocyte progenitor maintenance during adulthood', *Acta Neuropathologica*, 134(3), pp. 441–458. Available at: https://doi.org/10.1007/s00401-017-1747-1.

Haideri, S.S. *et al.* (2017) 'Injection of embryonic stem cell derived macrophages ameliorates fibrosis in a murine model of liver injury', *npj Regenerative Medicine*, 2, p. 14. Available at: https://doi.org/10.1038/s41536-017-0017-0.

Hale, M.E. *et al.* (2016) 'Neural circuits that drive startle behavior, with a focus on the Mauthner cells and spiral fiber neurons of fishes', *Journal of Neurogenetics*, 30(2), pp. 89–100. Available at: https://doi.org/10.1080/01677063.2016.1182526.

Halley, M.C. *et al.* (2022) 'A call for an integrated approach to improve efficiency, equity and sustainability in rare disease research in the United States', *Nature Genetics*, 54(3), pp. 219–222. Available at: https://doi.org/10.1038/s41588-022-01027-w.

Hamilton, N. *et al.* (2020a) 'The failure of microglia to digest developmental apoptotic cells contributes to the pathology of RNASET2-deficient leukoencephalopathy', *GLIA*, 68(7), pp. 1531–1545. Available at: https://doi.org/10.1002/glia.23829.

Hamilton, N. *et al.* (2020b) 'The failure of microglia to digest developmental apoptotic cells contributes to the pathology of RNASET2-deficient leukoencephalopathy', *GLIA*, 68(7), pp. 1531–1545. Available at: https://doi.org/10.1002/glia.23829.

Hamilton, N., Allen, C. and Reynolds, S. (2023) 'Longitudinal MRI brain studies in live adult zebrafish', *NMR in Biomedicine*, 36(7), pp. 1–11. Available at: https://doi.org/10.1002/nbm.4891.

Hamilton, S.P. and Rome, L.H. (1994) 'Stimulation of in vitro myelin synthesis by microglia', *Glia*, 11(4), pp. 326–335. Available at: https://doi.org/10.1002/glia.440110405.

Harrison, F. *et al.* (2013) 'Hematopoietic stem cell gene therapy for the multisystemic lysosomal storage disorder cystinosis', *Molecular Therapy*, 21(2), pp. 433–444. Available at: https://doi.org/10.1038/mt.2012.214.

Hatton, C.F. and Duncan, C.J.A. (2019a) 'Microglia Are Essential to Protective Antiviral Immunity: Lessons From Mouse Models of Viral Encephalitis', *Frontiers in Immunology*, 10(November). Available at: https://doi.org/10.3389/fimmu.2019.02656.

Hatton, C.F. and Duncan, C.J.A. (2019b) 'Microglia Are Essential to Protective Antiviral Immunity: Lessons From Mouse Models of Viral Encephalitis', *Frontiers in Immunology*, 10(November). Available at: https://doi.org/10.3389/fimmu.2019.02656.

Haud, N. *et al.* (2011a) 'rnaset2 mutant zebrafish model familial cystic leukoencephalopathy and reveal a role for RNase T2 in degrading ribosomal RNA', *Proceedings of the National Academy of Sciences*, 108(3), pp. 1099–1103. Available at: https://doi.org/10.1073/pnas.1009811107.

Haud, N. *et al.* (2011b) 'rnaset2 mutant zebrafish model familial cystic leukoencephalopathy and reveal a role for RNase T2 in degrading ribosomal RNA', *Proceedings of the National Academy of Sciences*, 108(3), pp. 1099–1103. Available at: https://doi.org/10.1073/pnas.1009811107.

Healy, L.M. *et al.* (2016a) 'MerTK Is a Functional Regulator of Myelin Phagocytosis by Human Myeloid Cells', *The Journal of Immunology*, 196(8), pp. 3375–3384. Available at: https://doi.org/10.4049/jimmunol.1502562.

Healy, L.M. *et al.* (2016b) 'MerTK Is a Functional Regulator of Myelin Phagocytosis by Human Myeloid Cells', *The Journal of Immunology*, 196(8), pp. 3375–3384. Available at: https://doi.org/10.4049/jimmunol.1502562.

Henneke, M. *et al.* (2009a) 'RNASET2-deficient cystic leukoencephalopathy resembles congenital cytomegalovirus brain infection', *Nature Genetics*, 41(7), pp. 773–775. Available at: https://doi.org/10.1038/ng.398.

Henneke, M. *et al.* (2009b) 'RNASET2-deficient cystic leukoencephalopathy resembles congenital cytomegalovirus brain infection', *Nature Genetics*, 41(7), pp. 773–775. Available at: https://doi.org/10.1038/ng.398.

Herbomel, P., Thisse, B. and Thisse, C. (2001) 'Zebrafish early macrophages colonize cephalic mesenchyme and developing brain, retina, and epidermis through a M-CSF receptor-dependent invasive process', *Developmental Biology*, 238(2), pp. 274–288. Available at: https://doi.org/10.1006/dbio.2001.0393.

Hickman, S. *et al.* (2018a) 'Microglia in neurodegeneration', *Nature Neuroscience*, 21(10), pp. 1359–1369. Available at: https://doi.org/10.1038/s41593-018-0242-x.

Hickman, S. *et al.* (2018b) 'Microglia in neurodegeneration', *Nature Neuroscience*, 21(10), pp. 1359–1369. Available at: https://doi.org/10.1038/s41593-018-0242-x.

Hildebrand, C. and Hahn, R. (1978) 'Relation between myelin sheath thickness and axon size in spinal cord white matter of some vertebrate species', *Journal of the Neurological Sciences*, 38(3), pp. 421–434. Available at: https://doi.org/10.1016/0022-510X(78)90147-8.

Hillen, A.E.J. *et al.* (2022) 'Therapeutic potential of human stem cell transplantations for Vanishing White Matter: A quest for the Goldilocks graft', *CNS Neuroscience and Therapeutics*, 28(9), pp. 1315–1325. Available at: https://doi.org/10.1111/cns.13872.

Hironaka, K. *et al.* (2015) 'Enzyme replacement in the CSF to treat metachromatic leukodystrophy in mouse model using single intracerebroventricular injection of self-complementary AAV1 vector', *Scientific Reports*, 5, p. 13104. Available at: https://doi.org/10.1038/srep13104.

Hoeffel, G. *et al.* (2015) 'C-Myb+ Erythro-Myeloid Progenitor-Derived Fetal Monocytes Give Rise to Adult Tissue-Resident Macrophages', *Immunity*, 42(4), pp. 665–678. Available at: https://doi.org/10.1016/j.immuni.2015.03.011.

Holzinger, D. *et al.* (2007) 'Induction of MxA Gene Expression by Influenza A Virus Requires Type I or Type III Interferon Signaling', *Journal of Virology*, 81(14), pp. 7776–7785. Available at: https://doi.org/10.1128/JVI.00546-06.

Hong, X. *et al.* (2021) 'Toward newborn screening of metachromatic leukodystrophy: results from analysis of over 27,000 newborn dried blood spots', *Genetics in Medicine*, 23(3), pp. 555–561. Available at: https://doi.org/10.1038/s41436-020-01017-5.

Hordeaux, J. *et al.* (2022) 'Efficacy and Safety of a Krabbe Disease Gene Therapy', *Human Gene Therapy*, 33(9–10), pp. 499–517. Available at: https://doi.org/10.1089/hum.2021.245.

Howe, K. *et al.* (2013) 'The zebrafish reference genome sequence and its relationship to the human genome', *Nature*, 496(7446), pp. 498–503. Available at: https://doi.org/10.1038/nature12111.

Huang, J., Liu, P. and Wang, G. (2018) 'Regulation of mitochondrion-associated cytosolic ribosomes by mammalian mitochondrial ribonuclease T2 (RNASET2)', *Journal of Biological Chemistry*, 293(51), pp. 19633–19644. Available at: https://doi.org/10.1074/jbc.RA118.005433.

Hughes, A.N. and Appel, B. (2020) 'Microglia phagocytose myelin sheaths to modify developmental myelination', *Nature Neuroscience*, 23(9), pp. 1055–1066. Available at: https://doi.org/10.1038/s41593-020-0654-2.

Hughes, E.G. *et al.* (2018) 'Myelin remodeling through experience-dependent oligodendrogenesis in the adult somatosensory cortex', *Nature Neuroscience*, 21(5), pp. 696–706. Available at: https://doi.org/10.1038/s41593-018-0121-5.

Ibhazehiebo, K. *et al.* (2018) 'A novel metabolism-based phenotypic drug discovery platform in zebrafish uncovers HDACs 1 and 3 as a potential combined anti-seizure drug target', *Brain*, 141(3), pp. 744–761. Available at: https://doi.org/10.1093/brain/awx364.

Jia, S. *et al.* (2020) 'Multiple Developmental Defects in *sox11a* Mutant Zebrafish with Features of Coffin-Siris Syndrome', *International Journal of Biological Sciences*, 16(15), pp. 3039–3049. Available at: https://doi.org/10.7150/ijbs.47510.

Johnston, J.B. *et al.* (2001) 'Monocyte activation and differentiation augment human endogenous retrovirus expression: Implications for inflammatory brain diseases', *Annals of Neurology*, 50(4), pp. 434–442. Available at: https://doi.org/10.1002/ana.1131.

Jones, R.A., Renshaw, M.J. and Barry, D.J. (2024) 'Automated staging of zebrafish embryos with deep learning', *Life Science Alliance*, 7(1), p. e202302351. Available at: https://doi.org/10.26508/lsa.202302351.

Jung, S. *et al.* (2010) 'Visualization of myelination in GFP-transgenic zebrafish', *Developmental Dynamics*, 239(2), pp. 592–597. Available at: https://doi.org/10.1002/dvdy.22166.

Jurga, A.M., Paleczna, M. and Kuter, K.Z. (2020) 'Overview of General and Discriminating Markers of Differential Microglia Phenotypes', *Frontiers in Cellular Neuroscience*, 14. Available at: https://doi.org/10.3389/fncel.2020.00198.

Kajitani, G.S. *et al.* (2021) 'Neurovascular dysfunction and neuroinflammation in a Cockayne syndrome mouse model', *Aging*, 13(19), pp. 22710–22731. Available at: https://doi.org/10.18632/aging.203617.

Kalueff, A. V. *et al.* (2013) 'Towards a Comprehensive Catalog of Zebrafish Behavior 1.0 and Beyond', *Zebrafish*, 10(1), pp. 70–86. Available at: https://doi.org/10.1089/zeb.2012.0861.

Kameli, R. *et al.* (2019) 'RNASET2-deficient leukoencephalopathy mimicking congenital CMV infection and Aicardi-Goutieres syndrome: A case report with a novel pathogenic variant', *Orphanet Journal of Rare Diseases*, 14(1). Available at: https://doi.org/10.1186/s13023-019-1155-9.

Karumuthil-Melethil, S. *et al.* (2016) 'Intrathecal administration of AAV/GALC vectors in 10–11-day-old twitcher mice improves survival and is enhanced by bone marrow transplant', *Journal of Neuroscience Research*, 94(11), pp. 1138–1151. Available at: https://doi.org/10.1002/jnr.23882.

Kasher, P.R. *et al.* (2015) 'Characterization of *samhd1* Morphant Zebrafish Recapitulates Features of the Human Type I Interferonopathy Aicardi-Goutières Syndrome', *The Journal of Immunology*, 194(6), pp. 2819–2825. Available at: https://doi.org/10.4049/jimmunol.1403157.

Keefe, M.D. *et al.* (2020) 'Vanishing white matter disease expression of truncated EIF2B5 activates induced stress response', *eLife*, 9. Available at: https://doi.org/10.7554/eLife.56319.

Kemp, S. *et al.* (2001) 'ABCD1 mutations and the X-linked adrenoleukodystrophy mutation database: Role in diagnosis and clinical correlations', *Human Mutation*, 18(6), pp. 499–515. Available at: https://doi.org/10.1002/humu.1227.

Kempthorne, L. *et al.* (2020) 'Loss of homeostatic microglial phenotype in CSF1R-related Leukoencephalopathy', *Acta Neuropathologica Communications*, 8(1), pp. 1–15. Available at: https://doi.org/10.1186/s40478-020-00947-0.

Keren-Shaul, H. *et al.* (2017) 'A Unique Microglia Type Associated with Restricting Development of Alzheimer's Disease', *Cell*, 169(7), pp. 1276-1290.e17. Available at: https://doi.org/10.1016/j.cell.2017.05.018.

Kettleborough, R.N.W. *et al.* (2013) 'A systematic genome-wide analysis of zebrafish protein-coding gene function', *Nature*, 496(7446), pp. 494–497. Available at: https://doi.org/10.1038/nature11992.

Kettwig, M. *et al.* (2021) 'Interferon-driven brain phenotype in a mouse model of RNaseT2 deficient leukoencephalopathy', *Nature Communications*, 12(1). Available at: https://doi.org/10.1038/s41467-021-26880-x.

Kierdorf, K. *et al.* (2013) 'Microglia emerge from erythromyeloid precursors via Pu.1-and Irf8-dependent pathways', *Nature Neuroscience*, 16(3), pp. 273–280. Available at: https://doi.org/10.1038/nn.3318.

Kimmel, C.B., Patterson, J. and Kimmel, R.O. (1974) 'The development and behavioral characteristics of the startle response in the zebra fish', *Developmental Psychobiology*, 7(1), pp. 47–60. Available at: https://doi.org/10.1002/dev.420070109.

Kirsten, K. *et al.* (2018) 'Characterization of sickness behavior in zebrafish', *Brain, Behavior, and Immunity*, 73, pp. 596–602. Available at: https://doi.org/10.1016/j.bbi.2018.07.004.

van der Knaap, M.S. and Bugiani, M. (2017a) 'Leukodystrophies: a proposed classification system based on pathological changes and pathogenetic mechanisms', *Acta Neuropathologica*, 134(3), pp. 351–382. Available at: https://doi.org/10.1007/s00401-017-1739-1.

van der Knaap, M.S. and Bugiani, M. (2017b) 'Leukodystrophies: a proposed classification system based on pathological changes and pathogenetic mechanisms', *Acta Neuropathologica*, 134(3), pp. 351–382. Available at: https://doi.org/10.1007/s00401-017-1739-1.

Köhler, W. *et al.* (2023) 'Safety and efficacy of leriglitazone for preventing disease progression in men with adrenomyeloneuropathy (ADVANCE): a randomised, double-blind, multi-centre, placebo-controlled phase 2–3 trial', *The Lancet Neurology*, 22(2), pp. 127–136. Available at: https://doi.org/10.1016/S1474-4422(22)00495-1.

Kolberg, L. *et al.* (2023) 'G:Profiler-interoperable web service for functional enrichment analysis and gene identifier mapping (2023 update)', *Nucleic Acids Research*, 51(W1), pp. W207–W212. Available at: https://doi.org/10.1093/nar/gkad347.

Kondagari, G.S., Yang, J. and Taylor, R.M. (2011) 'Investigation of cerebrocortical and cerebellar pathology in canine fucosidosis and comparison to aged brain', *Neurobiology of Disease*, 41(3), pp. 605–613. Available at: https://doi.org/10.1016/j.nbd.2010.10.026.

Konno, T. *et al.* (2018) 'Diagnostic criteria for adult-onset leukoencephalopathy with axonal spheroids and pigmented glia due to *<scp>CSF</scp> 1R* mutation', *European Journal of Neurology*, 25(1), pp. 142–147. Available at: https://doi.org/10.1111/ene.13464.

Koudelka, S. *et al.* (2016) 'Individual Neuronal Subtypes Exhibit Diversity in CNS Myelination Mediated by Synaptic Vesicle Release', *Current Biology*, 26(11), pp. 1447–1455. Available at: https://doi.org/10.1016/j.cub.2016.03.070.

Krivit, W. (1995) 'Microglia: The effector cell for reconstitution of the central nervous system following bone marrow transplantation for lysosomal and peroxisomal storage diseases', *Cell Transplantation*, 4(4), pp. 385–392. Available at: https://doi.org/10.1016/0963-6897(95)00021-O.

Kucenas, S. *et al.* (2009) 'A selective glial barrier at motor axon exit points prevents oligodendrocyte migration from the spinal cord', *Journal of Neuroscience*, 29(48), pp. 15187–15194. Available at: https://doi.org/10.1523/JNEUROSCI.4193-09.2009.

Lamas, N.J. and Roybon, L. (2021) 'Harnessing the Potential of Human Pluripotent Stem Cell-Derived Motor Neurons for Drug Discovery in Amyotrophic Lateral Sclerosis: From the Clinic to the Laboratory and Back to the Patient', *Frontiers in Drug Discovery*, 1. Available at: https://doi.org/10.3389/fddsv.2021.773424.

Lander, S. *et al.* (2001) *Initial sequencing and analysis of the human genome International Human Genome Sequencing Consortium* The Sanger Centre: Beijing Genomics Institute/Human Genome Center*, *NATURE*. Available at: www.nature.com.

Larson, K. *et al.* (2024) 'VGL101: A TREM2 Immunotherapy that Enhances Microglial Survival for Adult-Onset Leukoencephalopathy with Axonal Spheroids and Pigmented Glia (ALSP)', *American Academy of Neurology (AAN) Annual Meeting* [Preprint].

Lasselin, J. (2021) 'Back to the future of psychoneuroimmunology: Studying inflammation-induced sickness behavior', *Brain, Behavior, & Immunity - Health*, 18, p. 100379. Available at: https://doi.org/10.1016/j.bbih.2021.100379.

Lee, Y.-R. *et al.* (2021) 'Eif2b3 mutants recapitulate phenotypes of vanishing white matter disease and validate novel disease alleles in zebrafish.', *Human molecular genetics*, 30(5), pp. 331–342. Available at: https://doi.org/10.1093/hmg/ddab033.

Levraud, J.-P. *et al.* (2019) 'IFN-Stimulated Genes in Zebrafish and Humans Define an Ancient Arsenal of Antiviral Immunity', *The Journal of Immunology*, 203(12), pp. 3361–3373. Available at: https://doi.org/10.4049/jimmunol.1900804.

Li, J. *et al.* (2006) 'Conditional deletion of the colony stimulating factor-1 receptor (c-fms proto-oncogene) in mice', *genesis*, 44(7), pp. 328–335. Available at: https://doi.org/10.1002/dvg.20219.

Li, L. *et al.* (2011a) 'Irf8 regulates macrophage versus neutrophil fate during zebrafish primitive myelopoiesis', *Blood*, 117(4), pp. 1359–1369. Available at: https://doi.org/10.1182/blood-2010-06-290700.

Li, L. *et al.* (2011b) 'Irf8 regulates macrophage versus neutrophil fate during zebrafish primitive myelopoiesis', *Blood*, 117(4), pp. 1359–1369. Available at: https://doi.org/10.1182/blood-2010-06-290700.

Li, L. *et al.* (2012) 'Live imaging reveals differing roles of macrophages and neutrophils during zebrafish tail fin regeneration', *Journal of Biological Chemistry*, 287(30), pp. 25353–25360. Available at: https://doi.org/10.1074/jbc.M112.349126.

Li, W. *et al.* (2015) 'Human endogenous retrovirus-K contributes to motor neuron disease', *Science Translational Medicine*, 7(307). Available at: https://doi.org/10.1126/scitranslmed.aac8201.

Li, W. *et al.* (2022) 'Janus Kinase Inhibitors in the Treatment of Type I Interferonopathies: A Case Series From a Single Center in China', *Frontiers in Immunology*, 13. Available at: https://doi.org/10.3389/fimmu.2022.825367.

Li, X. *et al.* (2019) 'Zebrafish neurobehavioral phenomics applied as the behavioral warning methods for fingerprinting endocrine disrupting effect by lead exposure at environmentally relevant level', *Chemosphere*, 231, pp. 315–325. Available at: https://doi.org/10.1016/j.chemosphere.2019.05.146.

Libmeldy (2024) *LIBMELDY clinical study design*, *https://www.libmeldy.eu/clinical-results/*.

Lin, W. and Lin, Y. (2010) 'Interferon-γ inhibits central nervous system myelination through both STAT1-dependent and STAT1-independent pathways', *Journal of Neuroscience Research*, 88(12), pp. 2569–2577. Available at: https://doi.org/10.1002/jnr.22425.

Liu, A. and Ying, S. (2023) '<scp>Aicardi–Goutières</scp> syndrome: A monogenic type I interferonopathy', *Scandinavian Journal of Immunology*, 98(4). Available at: https://doi.org/10.1111/sji.13314.

Liu, F. *et al.* (2019) 'Evolution of IFN subgroups in bony fish - 1:Group I-III IFN exist in early ray-finned fish, with group II IFN subgroups present in the Holostean spotted gar, Lepisosteus oculatus', *Fish & Shellfish Immunology*, 95, pp. 163–170. Available at: https://doi.org/10.1016/j.fsi.2019.10.032.

Liu, K.S. and Fetcho, J.R. (1999) 'Laser Ablations Reveal Functional Relationships of Segmental Hindbrain Neurons in Zebrafish', *Neuron*, 23(2), pp. 325–335. Available at: https://doi.org/10.1016/S0896-6273(00)80783-7.

Liu, S. *et al.* (2021) 'A GM1 gangliosidosis mutant mouse model exhibits activated microglia and disturbed autophagy', *Experimental Biology and Medicine*, 246(11), pp. 1330–1341. Available at: https://doi.org/10.1177/1535370221993052.

López-Schier, H. (2019) 'Neuroplasticity in the acoustic startle reflex in larval zebrafish', *Current Opinion in Neurobiology*, 54, pp. 134–139. Available at: https://doi.org/10.1016/j.conb.2018.10.004.

Love, M.I., Huber, W. and Anders, S. (2014) 'Moderated estimation of fold change and dispersion for RNA-seq data with DESeq2', *Genome Biology*, 15(12), pp. 1–21. Available at: https://doi.org/10.1186/s13059-014-0550-8.

Lübke, T., Lobel, P. and Sleat, D.E. (2009a) 'Proteomics of the lysosome', *Biochimica et Biophysica Acta (BBA) - Molecular Cell Research*, 1793(4), pp. 625–635. Available at: https://doi.org/10.1016/j.bbamcr.2008.09.018.

Lübke, T., Lobel, P. and Sleat, D.E. (2009b) 'Proteomics of the lysosome', *Biochimica et Biophysica Acta (BBA) - Molecular Cell Research*, 1793(4), pp. 625–635. Available at: https://doi.org/10.1016/j.bbamcr.2008.09.018.

Lucchinetti, C.F. *et al.* (2002) 'A role for humoral mechanisms in the pathogenesis of Devic's neuromyelitis optica.', *Brain : a journal of neurology*, 125(Pt 7), pp. 1450–61. Available at: https://doi.org/10.1093/brain/awf151.

Lutfalla, G. *et al.* (2003) 'Comparative genomic analysis reveals independent expansion of a lineage-specific gene family in vertebrates: The class II cytokine receptors and their ligands in mammals and fish', *BMC Genomics*, 4(1), p. 29. Available at: https://doi.org/10.1186/1471-2164-4-29.

Lynch, D. *et al.* (2024) 'IGNITE Phase 2 Trial of Iluzanebart (VGL101) in Adult-Onset Leukoencephalopathy With Axonal Spheroids and Pigmented Glia (ALSP)', *American Academy of Neurology (AAN) Annual Meeting* [Preprint].

Lyons, D.A. *et al.* (2005) 'erbb3 and erbb2 Are Essential for Schwann Cell Migration and Myelination in Zebrafish', *Current Biology*, 15(6), pp. 513–524. Available at: https://doi.org/10.1016/j.cub.2005.02.030.

Lyons, D.A. *et al.* (2009) 'Kif1b is essential for mRNA localization in oligodendrocytes and development of myelinated axons', *Nature Genetics*, 41(7), pp. 854–858. Available at: https://doi.org/10.1038/ng.376.

Ma, S. *et al.* (2017) '*L2hgdh* Deficiency Accumulates <scp>l</scp> -2-Hydroxyglutarate with Progressive Leukoencephalopathy and Neurodegeneration', *Molecular and Cellular Biology*, 37(8). Available at: https://doi.org/10.1128/MCB.00492-16.

MacIntosh, G.C. (2011) 'RNase T2 Family: Enzymatic Properties, Functional Diversity, and Evolution of Ancient Ribonucleases', in, pp. 89–114. Available at: https://doi.org/10.1007/978-3-642-21078-5_4.

Madden, M.E. *et al.* (2021) 'CNS Hypomyelination Disrupts Axonal Conduction and Behavior in Larval Zebrafish', *The Journal of Neuroscience*, 41(44), pp. 9099–9111. Available at: https://doi.org/10.1523/JNEUROSCI.0842-21.2021.

Mahmood, A. *et al.* (2007) 'Survival analysis of haematopoietic cell transplantation for childhood cerebral X-linked adrenoleukodystrophy: a comparison study'. Available at: https://doi.org/10.1016/S1474.

Maier, T., Güell, M. and Serrano, L. (2009) 'Correlation of mRNA and protein in complex biological samples', *FEBS Letters*, 583(24), pp. 3966–3973. Available at: https://doi.org/10.1016/j.febslet.2009.10.036.

Maksakova, I.A., Mager, D.L. and Reiss, D. (2008) 'Endogenous retroviruses - Keeping active endogenous retroviral-like elements in check: The epigenetic perspective', *Cellular and Molecular Life Sciences*, pp. 3329–3347. Available at: https://doi.org/10.1007/s00018-008-8494-3.

Maleski, A.L.A. *et al.* (2022) 'Recapitulation of Retinal Damage in Zebrafish Larvae Infected with Zika Virus', *Cells*, 11(9), p. 1457. Available at: https://doi.org/10.3390/cells11091457.

Mameli, G. *et al.* (2007) 'Brains and peripheral blood mononuclear cells of multiple sclerosis (MS) patients hyperexpress MS-associated retrovirus/HERV-W endogenous retrovirus, but not human herpesvirus 6', *Journal of General Virology*, 88(1), pp. 264–274. Available at: https://doi.org/10.1099/vir.0.81890-0.

Marshall, M.S. *et al.* (2018) 'Long-Term Improvement of Neurological Signs and Metabolic Dysfunction in a Mouse Model of Krabbe's Disease after Global Gene Therapy', *Molecular Therapy*, 26(3), pp. 874–889. Available at: https://doi.org/10.1016/j.ymthe.2018.01.009.

Martin, H.R. *et al.* (2013) 'Neurodevelopmental Outcomes of Umbilical Cord Blood Transplantation in Metachromatic Leukodystrophy', *Biology of Blood and Marrow Transplantation*, 19(4), pp. 616–624. Available at: https://doi.org/10.1016/j.bbmt.2013.01.010.

Martin, M. (2011) 'Cutadapt removes adapter sequences from high-throughput sequencing reads', *EMBnet.journal*, 17(1), pp. 10–12.

Martínez Cerdeño, V. *et al.* (2018) 'Microglial cell activation and senescence are characteristic of the pathology FXTAS', *Movement Disorders*, 33(12), pp. 1887–1894. Available at: https://doi.org/10.1002/mds.27553.

März, M. *et al.* (2011) 'Regenerative response following stab injury in the adult zebrafish telencephalon', *Developmental Dynamics*, 240(9), pp. 2221–2231. Available at: https://doi.org/10.1002/dvdy.22710.

Mazaheri, F. *et al.* (2014) 'Distinct roles for BAI1 and TIM-4 in the engulfment of dying neurons by microglia', *Nature Communications*, 5(1), p. 4046. Available at: https://doi.org/10.1038/ncomms5046.

Mazzolini, J. *et al.* (2020) 'Gene expression profiling reveals a conserved microglia signature in larval zebrafish', *Glia*, 68(2), pp. 298–315. Available at: https://doi.org/10.1002/glia.23717.

McNamara, N.B. *et al.* (2023) 'Microglia regulate central nervous system myelin growth and integrity', *Nature*, 613(7942), pp. 120–129. Available at: https://doi.org/10.1038/s41586-022-05534-y.

Medline Plus (2024) *RNAse T2-deficient leukoencephalopathy*, *https://medlineplus.gov/genetics/condition/rnase-t2-deficient-leukoencephalopathy/*.

Menassa, D.A. *et al.* (2022) 'The spatiotemporal dynamics of microglia across the human lifespan', *Developmental Cell*, 57(17), pp. 2127-2139.e6. Available at: https://doi.org/10.1016/j.devcel.2022.07.015.

Mercuri, E. *et al.* (2018) 'Nusinersen versus Sham Control in Later-Onset Spinal Muscular Atrophy', *New England Journal of Medicine*, 378(7), pp. 625–635. Available at: https://doi.org/10.1056/NEJMoa1710504.

Miao, K.Z. *et al.* (2021) 'Tipping the Scales With Zebrafish to Understand Adaptive Tumor Immunity', *Frontiers in Cell and Developmental Biology*, 9. Available at: https://doi.org/10.3389/fcell.2021.660969.

Mildner, A. *et al.* (2007a) 'Microglia in the adult brain arise from Ly-6ChiCCR2+ monocytes only under defined host conditions', *Nature Neuroscience*, 10(12), pp. 1544–1553. Available at: https://doi.org/10.1038/nn2015.

Mildner, A. *et al.* (2007b) 'Microglia in the adult brain arise from Ly-6ChiCCR2+ monocytes only under defined host conditions', *Nature Neuroscience*, 10(12), pp. 1544–1553. Available at: https://doi.org/10.1038/nn2015.

Miller, T.M. *et al.* (2022) 'Trial of Antisense Oligonucleotide Tofersen for *SOD1* ALS', *New England Journal of Medicine*, 387(12), pp. 1099–1110. Available at: https://doi.org/10.1056/NEJMoa2204705.

Miller, W.P. *et al.* (2011) 'Outcomes after allogeneic hematopoietic cell transplantation for childhood cerebral adrenoleukodystrophy: The largest single-institution cohort report', *Blood*, 118(7), pp. 1971–1978. Available at: https://doi.org/10.1182/blood-2011-01-329235.

Minoryx Therapeutics (2023) *Minoryx presents positive interim results from NEXUS registration study for leriglitazone targeting pediatric ALD patients with cerebral adrenoleukodystrophy (cALD)*, *https://www.minoryx.com/media/minoryx-presents-positive-interim-results-from-nexus/*.

Mitew, S. *et al.* (2018) 'Pharmacogenetic stimulation of neuronal activity increases myelination in an axon-specific manner', *Nature Communications*, 9(1), p. 306. Available at: https://doi.org/10.1038/s41467-017-02719-2.

Miyake, N. *et al.* (2010) 'Successful treatment of metachromatic leukodystrophy using bone marrow transplantation of HoxB4 overexpressing cells', *Molecular Therapy*, 18(7), pp. 1373–1378. Available at: https://doi.org/10.1038/mt.2010.74.

MLD Support Association UK (2024) *Clinical trial update from Takeda*, *https://www.mldsupportuk.org.uk/*.

Möbius, W. *et al.* (2008) 'Phylogeny of proteolipid proteins: divergence, constraints, and the evolution of novel functions in myelination and neuroprotection', *Neuron Glia Biology*, 4(2), pp. 111–127. Available at: https://doi.org/10.1017/S1740925X0900009X.

Mojzesz, M. *et al.* (2021) 'Tilapia Lake Virus-Induced Neuroinflammation in Zebrafish: Microglia Activation and Sickness Behavior', *Frontiers in Immunology*, 12. Available at: https://doi.org/10.3389/fimmu.2021.760882.

Moravec, C.E. *et al.* (2015) 'Rest mutant zebrafish swim erratically and display atypical spatial preferences', *Behavioural Brain Research*, 284, pp. 238–248. Available at: https://doi.org/10.1016/j.bbr.2015.02.026.

Morell, P. (1984) 'A correlative synopsis of the leukodystrophies.', *Neuropediatrics*, 15(Suppl), pp. 62–65. Available at: https://doi.org/10.1055/s-2008-1052383.

Morgan, J.T. *et al.* (2010) 'Microglial Activation and Increased Microglial Density Observed in the Dorsolateral Prefrontal Cortex in Autism', *Biological Psychiatry*, 68(4), pp. 368–376. Available at: https://doi.org/10.1016/j.biopsych.2010.05.024.

Morita, M. *et al.* (2004) 'Gene-Targeted Mice Lacking the Trex1 (DNase III) 3'-5' DNA Exonuclease Develop Inflammatory Myocarditis', *Molecular and Cellular Biology*, 24(15), pp. 6719–6727. Available at: https://doi.org/10.1128/MCB.24.15.6719-6727.2004.

Moroni, F. *et al.* (2019) 'Safety profile of autologous macrophage therapy for liver cirrhosis', *Nature Medicine*, 25(10), pp. 1560–1565. Available at: https://doi.org/10.1038/s41591-019-0599-8.

Morris, J.K. *et al.* (2004) 'The 36K protein of zebrafish CNS myelin is a short-chain dehydrogenase', *Glia*, 45(4), pp. 378–391. Available at: https://doi.org/10.1002/glia.10338.

Münzel, E.J. *et al.* (2014) 'Zebrafish regenerate full thickness optic nerve myelin after demyelination, but this fails with increasing age', *Acta Neuropathologica Communications*, 2(1), p. 77. Available at: https://doi.org/10.1186/s40478-014-0077-y.

Mura, E. *et al.* (2021) 'Ruxolitinib in Aicardi-Goutières syndrome', *Metabolic Brain Disease*, 36(5), pp. 859–863. Available at: https://doi.org/10.1007/s11011-021-00716-5.

Na, Y.R., Kim, S.W. and Seok, S.H. (2023) 'A new era of macrophage-based cell therapy', *Experimental & Molecular Medicine*, 55(9), pp. 1945–1954. Available at: https://doi.org/10.1038/s12276-023-01068-z.

Nandi, S. *et al.* (2012) 'The CSF-1 receptor ligands IL-34 and CSF-1 exhibit distinct developmental brain expression patterns and regulate neural progenitor cell maintenance and maturation', *Developmental Biology*, 367(2), pp. 100–113. Available at: https://doi.org/10.1016/j.ydbio.2012.03.026.

Naphade, S. *et al.* (2015) 'Brief Reports: Lysosomal Cross-Correction by Hematopoietic Stem Cell-Derived Macrophages Via Tunneling Nanotubes', *Stem Cells*, 33(1), pp. 301–309. Available at: https://doi.org/10.1002/stem.1835.

Neely, S.A. *et al.* (2022) 'New oligodendrocytes exhibit more abundant and accurate myelin regeneration than those that survive demyelination', *Nature Neuroscience*, 25(4), pp. 415–420. Available at: https://doi.org/10.1038/s41593-021-01009-x.

Neurona Therapeutics (2024) *A Phase I/II Clinical Trial of NRTX-1001 Nerve Cell Therapy in Drug-Resistant Unilateral Mesial Temporal Lobe Epilepsy*, *https://www.neuronatherapeutics.com/nte001/#NRTX1001*.

Neuwelt, E.A. *et al.* (2004) 'Mechanisms of Disease: The Blood-Brain Barrier', *Neurosurgery*, 54(1), pp. 131–142. Available at: https://doi.org/10.1227/01.NEU.0000097715.11966.8E.

Nguengang Wakap, S. *et al.* (2020) 'Estimating cumulative point prevalence of rare diseases: analysis of the Orphanet database', *European Journal of Human Genetics*, 28(2), pp. 165–173. Available at: https://doi.org/10.1038/s41431-019-0508-0.

Nguyen, L.T.M. *et al.* (2024) 'Interplay of Zeb2a, Id2a and Batf3 regulates microglia and dendritic cell development in the zebrafish brain', *Development*, 151(3). Available at: https://doi.org/10.1242/dev.201829.

Nicaise, A.M., Bongarzone, E.R. and Crocker, S.J. (2016) 'A microglial hypothesis of globoid cell leukodystrophy pathology', *Journal of Neuroscience Research*, 94(11), pp. 1049–1061. Available at: https://doi.org/10.1002/jnr.23773.

Nicholas, R.S.T.J., Wing, M.G. and Compston, A. (2001a) 'Nonactivated microglia promote oligodendrocyte precursor survival and maturation through the transcription factor NF-κB', *European Journal of Neuroscience*, 13(5), pp. 959–967. Available at: https://doi.org/10.1046/j.0953-816X.2001.01470.x.

Nicholas, R.S.T.J., Wing, M.G. and Compston, A. (2001b) 'Nonactivated microglia promote oligodendrocyte precursor survival and maturation through the transcription factor NF-κB', *European Journal of Neuroscience*, 13(5), pp. 959–967. Available at: https://doi.org/10.1046/j.0953-816X.2001.01470.x.

Niescierowicz, K. *et al.* (2022) 'Adar-mediated A-to-I editing is required for embryonic patterning and innate immune response regulation in zebrafish', *Nature Communications*, 13(1), p. 5520. Available at: https://doi.org/10.1038/s41467-022-33260-6.

Nimmerjahn, A., Kirchhoff, F. and Helmchen, F. (2005) 'Resting microglial cells are highly dynamic surveillants of brain parenchyma in vivo', *Neuroforum*, 11(3), pp. 95–96. Available at: https://doi.org/10.1515/nf-2005-0304.

O'Brien, C.A., Bennett, F.C. and Bennett, M.L. (2022) 'Microglia in antiviral immunity of the brain and spinal cord', *Seminars in Immunology*. Academic Press. Available at: https://doi.org/10.1016/j.smim.2022.101650.

Ogawa, Y. *et al.* (2017) 'FcRγ-dependent immune activation initiates astrogliosis during the asymptomatic phase of Sandhoff disease model mice', *Scientific Reports*, 7(1), p. 40518. Available at: https://doi.org/10.1038/srep40518.

Oliveira, D. V *et al.* (2023) 'Active immunotherapy reduces <scp>NOTCH3</scp> deposition in brain capillaries in a <scp>CADASIL</scp> mouse model', *EMBO Molecular Medicine*, 15(2). Available at: https://doi.org/10.15252/emmm.202216556.

O'Malley, D.M., Kao, Y.-H. and Fetcho, J.R. (1996) 'Imaging the Functional Organization of Zebrafish Hindbrain Segments during Escape Behaviors', *Neuron*, 17(6), pp. 1145–1155. Available at: https://doi.org/10.1016/S0896-6273(00)80246-9.

Oosterhof, N. *et al.* (2017) 'Identification of a conserved and acute neurodegeneration-specific microglial transcriptome in the zebrafish', *Glia*, 65(1), pp. 138–149. Available at: https://doi.org/10.1002/glia.23083.

Oosterhof, N. *et al.* (2018) 'Colony-Stimulating Factor 1 Receptor (CSF1R) Regulates Microglia Density and Distribution, but Not Microglia Differentiation In Vivo', *Cell Reports*, 24(5), pp. 1203-1217.e6. Available at: https://doi.org/10.1016/j.celrep.2018.06.113.

Oosterhof, N. *et al.* (2019) 'Homozygous Mutations in CSF1R Cause a Pediatric-Onset Leukoencephalopathy and Can Result in Congenital Absence of Microglia', *American Journal of Human Genetics*, 104(5), pp. 936–947. Available at: https://doi.org/10.1016/j.ajhg.2019.03.010.

Ostendorf, T. *et al.* (2020) 'Immune Sensing of Synthetic, Bacterial, and Protozoan RNA by Toll-like Receptor 8 Requires Coordinated Processing by RNase T2 and RNase 2', *Immunity*, 52(4), pp. 591-605.e6. Available at: https://doi.org/10.1016/j.immuni.2020.03.009.

Oyanagi, K. *et al.* (2017) 'Adult onset leukoencephalopathy with axonal spheroids and pigmented glia (ALSP) and Nasu–Hakola disease: lesion staging and dynamic changes of axons and microglial subsets', *Brain Pathology*, 27(6), pp. 748–769. Available at: https://doi.org/10.1111/bpa.12443.

Padilla, S. *et al.* (2011) 'Assessing locomotor activity in larval zebrafish: Influence of extrinsic and intrinsic variables', *Neurotoxicology and Teratology*, 33(6), pp. 624–630. Available at: https://doi.org/10.1016/j.ntt.2011.08.005.

Page, K.M. *et al.* (2019) 'Hematopoietic Stem Cell Transplantation to Treat Leukodystrophies: Clinical Practice Guidelines from the Hunter's Hope Leukodystrophy Care Network', *Biology of Blood and Marrow Transplantation*, 25(12), pp. e363–e374. Available at: https://doi.org/10.1016/j.bbmt.2019.09.003.

Paloneva, J. *et al.* (2000) 'Loss-of-function mutations in TYROBP (DAP12) result in a presenile dementia with bone cysts', *Nature Genetics*, 25(3), pp. 357–361. Available at: http://ovidsp.ovid.com/ovidweb.cgi?T=JS&PAGE=reference&D=emed5&NEWS=N&AN=2000239944.

Panahi, M. *et al.* (2023) 'ER stress induced immunopathology involving complement in CADASIL: implications for therapeutics', *Acta Neuropathologica Communications*, 11(1), p. 76. Available at: https://doi.org/10.1186/s40478-023-01558-1.

Pant, D.C., Boespflug-Tanguy, O. and Pujol, A. (2019) 'Loss of the sphingolipid desaturase DEGS1 causes hypomyelinating leukodystrophy', *Journal of Clinical Investigation*, 129(3), pp. 1240–1256. Available at: https://doi.org/10.1172/JCI123959.

Papapetropoulos, S. *et al.* (2022) 'Adult-Onset Leukoencephalopathy With Axonal Spheroids and Pigmented Glia: Review of Clinical Manifestations as Foundations for Therapeutic Development', *Frontiers in Neurology*, 12. Available at: https://doi.org/10.3389/fneur.2021.788168.

Parichy, D.M. *et al.* (2000) 'An orthologue of the kit-related gene fms is required for development of neural crest-derived xanthophores and a subpopulation of adult melanocytes in the zebrafish, Danio rerio', *Development*, 127(14), pp. 3031–3044. Available at: https://doi.org/10.1242/dev.127.14.3031.

Parikh, S. *et al.* (2015) 'A clinical approach to the diagnosis of patients with leukodystrophies and genetic leukoencephelopathies', *Molecular Genetics and Metabolism*, 114(4), pp. 501–515. Available at: https://doi.org/10.1016/j.ymgme.2014.12.434.

Perng, Y.-C. and Lenschow, D.J. (2018) 'ISG15 in antiviral immunity and beyond', *Nature Reviews Microbiology*, 16(7), pp. 423–439. Available at: https://doi.org/10.1038/s41579-018-0020-5.

Pesch, M.H. *et al.* (2021) 'Congenital cytomegalovirus infection', *The BMJ*. BMJ Publishing Group. Available at: https://doi.org/10.1136/bmj.n1212.

Peters, C. *et al.* (2004) 'Cerebral X-linked adrenoleukodystrophy: The international hematopoietic cell transplantation experience from 1982 to 1999', *Blood*, 104(3), pp. 881–888. Available at: https://doi.org/10.1182/blood-2003-10-3402.

Phillips, J.A. *et al.* (1997) 'Pharmacokinetics, metabolism, and elimination of a 20-mer phosphorothioate oligodeoxynucleotide (CGP 69846A) after intravenous and subcutaneous administration', *Biochemical Pharmacology*, 54(6), pp. 657–668. Available at: https://doi.org/10.1016/S0006-2952(97)00190-1.

van den Pol, A.N. (2009) 'Viral Infection Leading to Brain Dysfunction: More Prevalent Than Appreciated?', *Neuron*, 64(1), pp. 17–20. Available at: https://doi.org/10.1016/j.neuron.2009.09.023.

Poliani, P.L. *et al.* (2015) 'TREM2 sustains microglial expansion during aging and response to demyelination', *Journal of Clinical Investigation*, 125(5), pp. 2161–2170. Available at: https://doi.org/10.1172/JCI77983.

Potter, G.B. *et al.* (2013) 'Missense mutation in mouse GALC mimics human gene defect and offers new insights into krabbe disease', *Human Molecular Genetics*, 22(12), pp. 3397–3414. Available at: https://doi.org/10.1093/hmg/ddt190.

Preston, M.A. *et al.* (2019) 'A novel myelin protein zero transgenic zebrafish designed for rapid readout of in vivo myelination', *Glia*, 67(4), pp. 650–667. Available at: https://doi.org/10.1002/glia.23559.

Preston, M.A. and Macklin, W.B. (2015) 'Zebrafish as a model to investigate CNS myelination', *GLIA*. John Wiley and Sons Inc., pp. 177–193. Available at: https://doi.org/10.1002/glia.22755.

Priller, J. *et al.* (2001) 'Targeting gene-modified hematopoietic cells to the central nervous system: Use of green fluorescent protein uncovers microglial engraftment', *Nature Medicine*, 7(12), pp. 1356–1361. Available at: https://doi.org/10.1038/nm1201-1356.

Prineas, J.W. and Parratt, J.D.E. (2012) 'Oligodendrocytes and the early multiple sclerosis lesion.', *Annals of neurology*, 72(1), pp. 18–31. Available at: https://doi.org/10.1002/ana.23634.

Putri, G.H. *et al.* (2022) 'Analysing high-throughput sequencing data in Python with HTSeq 2.0', *Bioinformatics*, 38(10), pp. 2943–2945. Available at: https://doi.org/10.1093/bioinformatics/btac166.

Raas, Q. *et al.* (2021) 'Metabolic rerouting via SCD1 induction impacts X-linked adrenoleukodystrophy', *Journal of Clinical Investigation*, 131(8). Available at: https://doi.org/10.1172/JCI142500.

Raas, Q. *et al.* (2024) 'Generation and characterization of a zebrafish gain-of-function ACOX1 Mitchell disease model', *Frontiers in Pediatrics*, 12. Available at: https://doi.org/10.3389/fped.2024.1326886.

Rademakers, R. *et al.* (2012) 'Mutations in the colony stimulating factor 1 receptor (CSF1R) gene cause hereditary diffuse leukoencephalopathy with spheroids', *Nature Genetics*, 44(2), pp. 200–205. Available at: https://doi.org/10.1038/ng.1027.

Rafi, M.A. *et al.* (2015) 'Long-term Improvements in Lifespan and Pathology in CNS and PNS After BMT Plus One Intravenous Injection of AAVrh10-GALC in Twitcher Mice', *Molecular Therapy*, 23(11), pp. 1681–1690. Available at: https://doi.org/10.1038/mt.2015.145.

Rajani, R.M. *et al.* (2021) 'Characterisation of early ultrastructural changes in the cerebral white matter of CADASIL small vessel disease using high-pressure freezing/freeze-substitution', *Neuropathology and Applied Neurobiology*, 47(5), pp. 694–704. Available at: https://doi.org/10.1111/nan.12697.

Rankin, C.H. *et al.* (2009) 'Habituation revisited: An updated and revised description of the behavioral characteristics of habituation', *Neurobiology of Learning and Memory*, 92(2), pp. 135–138. Available at: https://doi.org/10.1016/j.nlm.2008.09.012.

Rawling, D.C. *et al.* (2020) 'Small-Molecule Antagonists of the RIG-I Innate Immune Receptor', *ACS Chemical Biology*, 15(2), pp. 311–317. Available at: https://doi.org/10.1021/acschembio.9b00810.

Rehwinkel, J. *et al.* (2013) 'SAMHD1-dependent retroviral control and escape in mice', *EMBO Journal*, 32(18), pp. 2454–6242. Available at: https://doi.org/10.1038/emboj.2013.163.

Rehwinkel, J. and Gack, M.U. (2020) 'RIG-I-like receptors: their regulation and roles in RNA sensing', *Nature Reviews Immunology*, 20(9), pp. 537–551. Available at: https://doi.org/10.1038/s41577-020-0288-3.

Ren, X. *et al.* (2019) 'RIG-I Selectively Discriminates against 5'-Monophosphate RNA', *Cell Reports*, 26(8), pp. 2019-2027.e4. Available at: https://doi.org/10.1016/j.celrep.2019.01.107.

Réu, P. *et al.* (2017) 'The Lifespan and Turnover of Microglia in the Human Brain', *Cell Reports*, 20(4), pp. 779–784. Available at: https://doi.org/10.1016/j.celrep.2017.07.004.

Rice, G.I. *et al.* (2018) 'Reverse-Transcriptase Inhibitors in the Aicardi–Goutières Syndrome', *New England Journal of Medicine*, 37(23), pp. 2275–2277. Available at: https://doi.org/10.1056/nejmc1810983.

Richardson, D.S. *et al.* (2021) 'Tissue clearing', *Nature Reviews Methods Primers*, 1(1), p. 84. Available at: https://doi.org/10.1038/s43586-021-00080-9.

Roberts, A.C. *et al.* (2011) 'Habituation of the C-Start Response in Larval Zebrafish Exhibits Several Distinct Phases and Sensitivity to NMDA Receptor Blockade', *PLoS ONE*, 6(12), p. e29132. Available at: https://doi.org/10.1371/journal.pone.0029132.

Roberts, A.C. *et al.* (2016) 'Long-term habituation of the C-start escape response in zebrafish larvae', *Neurobiology of Learning and Memory*, 134, pp. 360–368. Available at: https://doi.org/10.1016/j.nlm.2016.08.014.

Robinson, A.C. *et al.* (2020) 'Neuropathology of a case of fragile <scp>X</scp> -associated tremor ataxia syndrome without tremor', *Neuropathology*, 40(6), pp. 611–619. Available at: https://doi.org/10.1111/neup.12674.

Robinson, M.B. *et al.* (1995) 'Evidence of excitotoxicity in the brain of the ornithine carbamoyltransferase deficient sparse fur mouse', *Developmental Brain Research*, 90(1–2), pp. 35–44. Available at: https://doi.org/10.1016/0165-3806(96)83484-5.

Rodríguez-Pascau, L. *et al.* (2021) 'The brain penetrant PPARγ agonist leriglitazone restores multiple altered pathways in models of X-linked adrenoleukodystrophy', *Science Translational Medicine*, 13(596). Available at: https://doi.org/10.1126/scitranslmed.abc0555.

Rosshart, S.P. *et al.* (2017) 'Wild Mouse Gut Microbiota Promotes Host Fitness and Improves Disease Resistance', *Cell*, 171,(5), pp. 1015–1028. Available at: https://doi.org/10.1016/j.cell.2017.09.016.

Rouf, M.A. *et al.* (2023) 'The recent advances and future perspectives of genetic compensation studies in the zebrafish model.', *Genes & diseases*, 10(2), pp. 468–479. Available at: https://doi.org/10.1016/j.gendis.2021.12.003.

Rovira, M. *et al.* (2023) 'Zebrafish Galectin 3 binding protein is the target antigen of the microglial 4C4 monoclonal antibody', *Developmental Dynamics*, 252(3), pp. 400–414. Available at: https://doi.org/10.1002/dvdy.549.

Rovira, M. *et al.* (2024) 'A single-cell transcriptomic atlas reveals resident dendritic-like cells in the zebrafish brain parenchyma', *eLife*, 13, p. RP91427.

Rowe, H.M. *et al.* (2010) 'KAP1 controls endogenous retroviruses in embryonic stem cells', *Nature*, 463(7278), pp. 237–240. Available at: https://doi.org/10.1038/nature08674.

Rutherford, H.A. *et al.* (2022) 'A zebrafish reporter line reveals immune and neuronal expression of endogenous retrovirus.', *Disease models & mechanisms*, 15(4). Available at: https://doi.org/10.1242/dmm.048921.

Rutherford, H.A. and Hamilton, N. (2019a) 'Animal models of leukodystrophy: a new perspective for the development of therapies', *FEBS Journal*, 286(21), pp. 4176–4191. Available at: https://doi.org/10.1111/febs.15060.

Rutherford, H.A. and Hamilton, N. (2019b) 'Animal models of leukodystrophy: a new perspective for the development of therapies', *FEBS Journal*, 286(21), pp. 4176–4191. Available at: https://doi.org/10.1111/febs.15060.

Rutherford, H.A., Kasher, P.R. and Hamilton, N. (2021) 'Dirty Fish Versus Squeaky Clean Mice: Dissecting Interspecies Differences Between Animal Models of Interferonopathy', *Frontiers in Immunology*, 11(January), pp. 1–12. Available at: https://doi.org/10.3389/fimmu.2020.623650.

Salter, M.W. and Stevens, B. (2017) 'Microglia emerge as central players in brain disease', *Nature Medicine*, 23(9), pp. 1018–1027. Available at: https://doi.org/10.1038/nm.4397.

Sanchez, G.A.M. *et al.* (2018) 'JAK1/2 inhibition with baricitinib in the treatment of autoinflammatory interferonopathies', *Journal of Clinical Investigation*, 128(7), pp. 3041–3052. Available at: https://doi.org/10.1172/JCI98814.

Sanchez, J.M.S. *et al.* (2019) 'Microglial cell depletion is fatal with low level picornavirus infection of the central nervous system', *Journal of NeuroVirology*, 25(3), pp. 415–421. Available at: https://doi.org/10.1007/s13365-019-00740-3.

Van de Sande, B. *et al.* (2023) 'Applications of single-cell RNA sequencing in drug discovery and development', *Nature Reviews Drug Discovery*, 22(6), pp. 496–520. Available at: https://doi.org/10.1038/s41573-023-00688-4.

Sariol, A. *et al.* (2020) 'Microglia depletion exacerbates demyelination and impairs remyelination in a neurotropic coronavirus infection', *Proceedings of the National Academy of Sciences*, 117(39), pp. 24464–24474. Available at: https://doi.org/10.1073/pnas.2007814117.

Schaefer, K. and Brosamle, C. (2008) 'Zwilling-A and -B, Two Related Myelin Proteins of Teleosts, Which Originate from a Single Bicistronic Transcript', *Molecular Biology and Evolution*, 26(3), pp. 495–499. Available at: https://doi.org/10.1093/molbev/msn298.

Schönberger, S. *et al.* (2007) 'Genotype and Protein Expression After Bone Marrow Transplantation for Adrenoleukodystrophy', *Arch Neurol*, 64(5), pp. 651–7. Available at: www.archneurol.com.

Schwartz, L. *et al.* (2018) 'The Immunomodulatory and Antimicrobial Properties of the Vertebrate Ribonuclease A Superfamily', *Vaccines*, 6(4), p. 76. Available at: https://doi.org/10.3390/vaccines6040076.

Scott-Hewitt, N., Folts, C. and Noble, M. (2018) 'Heterozygous carriers of galactocerebrosidase mutations that cause Krabbe disease have impaired microglial function and defective repair of myelin damage', *Neural Regeneration Research*, 13(3), p. 393. Available at: https://doi.org/10.4103/1673-5374.228712.

Seitz, S., Clarke, P. and Tyler, K.L. (2018) 'Pharmacologic Depletion of Microglia Increases Viral Load in the Brain and Enhances Mortality in Murine Models of Flavivirus-Induced Encephalitis', *Journal of Virology*, 92(16). Available at: https://doi.org/10.1128/jvi.00525-18.

Settembre, C. *et al.* (2007) 'Systemic inflammation and neurodegeneration in a mouse model of multiple sulfatase deficiency', *Proceedings of the National Academy of Sciences*, 104(11), pp. 4506–4511. Available at: https://doi.org/10.1073/pnas.0700382104.

She, J. *et al.* (2019) 'Genetic compensation by *epob* in pronephros development in *epoa* mutant zebrafish', *Cell Cycle*, 18(20), pp. 2683–2696. Available at: https://doi.org/10.1080/15384101.2019.1656019.

Shiau, C.E. *et al.* (2015) 'Differential requirement for irf8 in formation of embryonic and adult macrophages in zebrafish', *PLoS ONE*, 10(1), pp. 1–15. Available at: https://doi.org/10.1371/journal.pone.0117513.

Shih, H.Y., Raas, Q. and Bonkowsky, J.L. (2024) 'Progress in leukodystrophies with zebrafish', *Development Growth and Differentiation*. John Wiley and Sons Inc, pp. 21–34. Available at: https://doi.org/10.1111/dgd.12907.

Sieger, D. *et al.* (2012) 'Long-Range Ca2+ Waves Transmit Brain-Damage Signals to Microglia', *Developmental Cell*, 22(6), pp. 1138–1148. Available at: https://doi.org/10.1016/j.devcel.2012.04.012.

Siems, S.B. *et al.* (2021) 'Proteome Profile of Myelin in the Zebrafish Brain', *Frontiers in Cell and Developmental Biology*, 9. Available at: https://doi.org/10.3389/fcell.2021.640169.

Sieweke, M.H. and Allen, J.E. (2013) 'Beyond stem cells: Self-renewal of differentiated macrophages', *Science*, 342(6161). Available at: https://doi.org/10.1126/science.1242974.

Simonian, R. *et al.* (2023) 'Methylenetetrahydrofolate reductase deficiency and high-dose FA supplementation disrupt embryonic development of energy balance and metabolic homeostasis in zebrafish', *Human Molecular Genetics*, 32(9), pp. 1575–1588. Available at: https://doi.org/10.1093/hmg/ddac308.

Sinkevicius, K.W. *et al.* (2018) 'RNaseT2 knockout rats exhibit hippocampal neuropathology and deficits in memory', *Disease Models & Mechanisms*, 11(6), p. dmm032631. Available at: https://doi.org/10.1242/dmm.032631.

Skysona (2024) *Skysona, Results from clinical studies*, *https://www.skysona.com/clinical-results-safety*.

Snook, E.R. *et al.* (2014) 'Innate immune activation in the pathogenesis of a murine model of globoid cell leukodystrophy', *American Journal of Pathology*, 184(2), pp. 382–396. Available at: https://doi.org/10.1016/j.ajpath.2013.10.011.

Soni, A., Gowthamarajan, K. and Radhakrishnan, A. (2018) 'Personalized Medicine and Customized Drug Delivery Systems: The New Trend of Drug Delivery and Disease Management.', *International journal of pharmaceutical compounding*, 22(2), pp. 108–121.

de Sousa Abreu, R. *et al.* (2009) 'Global signatures of protein and mRNA expression levels', *Molecular BioSystems* [Preprint]. Available at: https://doi.org/10.1039/b908315d.

Speirs, Z.C. *et al.* (2024) 'What can we learn about fish neutrophil and macrophage response to immune challenge from studies in zebrafish', *Fish and Shellfish Immunology*, 148. Available at: https://doi.org/10.1016/j.fsi.2024.109490.

Sperling, R.A. *et al.* (2001) 'Regional Magnetic Resonance Imaging Lesion Burden and Cognitive Function in Multiple Sclerosis', *Archives of Neurology*, 58(1). Available at: https://doi.org/10.1001/archneur.58.1.115.

Squarzoni, P. *et al.* (2014) 'Microglia Modulate Wiring of the Embryonic Forebrain', *Cell Reports*, 8(5), pp. 1271–1279. Available at: https://doi.org/10.1016/j.celrep.2014.07.042.

Stein, C. *et al.* (2007) 'Conservation and divergence of gene families encoding components of innate immune response systems in zebrafish', *Genome Biology*, 8(11), p. R251. Available at: https://doi.org/10.1186/gb-2007-8-11-r251.

Stellingwerff, M.D. *et al.* (2021) 'MRI Natural History of the Leukodystrophy Vanishing White Matter', *Radiology*, 300(3), pp. 671–680. Available at: https://doi.org/10.1148/radiol.2021210110.

Stellitano, L.A. *et al.* (2016) 'Leukodystrophies and genetic leukoencephalopathies in childhood: a national epidemiological study', *Developmental Medicine and Child Neurology*, 58(7), pp. 680–689. Available at: https://doi.org/10.1111/dmcn.13027.

Stetson, D.B. *et al.* (2008) 'Trex1 Prevents Cell-Intrinsic Initiation of Autoimmunity', *Cell*, 134(4), pp. 587–598. Available at: https://doi.org/10.1016/j.cell.2008.06.032.

Strachan, L.R. *et al.* (2017) 'A zebrafish model of X-linked adrenoleukodystrophy recapitulates key disease features and demonstrates a developmental requirement for abcd1 in oligodendrocyte patterning and myelination', *Human Molecular Genetics*, 26(18), pp. 3600–3614. Available at: https://doi.org/10.1093/HMG/DDX249.

Sundal, C. *et al.* (2015) 'Hereditary diffuse leukoencephalopathy with spheroids with phenotype of primary progressive multiple sclerosis', *European Journal of Neurology*, 22(2), pp. 328–333. Available at: https://doi.org/10.1111/ene.12572.

Susaki, E.A. *et al.* (2015) 'Advanced CUBIC protocols for whole-brain and whole-body clearing and imaging', *Nature Protocols*, 10(11), pp. 1709–1727. Available at: https://doi.org/10.1038/nprot.2015.085.

Suzuki, K. *et al.* (2013) 'Microglial Activation in Young Adults With Autism Spectrum Disorder', *JAMA Psychiatry*, 70(1), p. 49. Available at: https://doi.org/10.1001/jamapsychiatry.2013.272.

Suzuki, K. and Suzuki, Y. (1970) 'Globoid Cell Leucodystrophy (Krabbe's Disease): Deficiency of Galactocerebroside -Galactosidase', *Proceedings of the National Academy of Sciences*, 66(2), pp. 302–309. Available at: https://doi.org/10.1073/pnas.66.2.302.

Suzuki, T. *et al.* (2014) 'Pulmonary macrophage transplantation therapy', *Nature*, 514(7523), pp. 450–445. Available at: https://doi.org/10.1038/nature13807.

Svahn, A.J. *et al.* (2013) 'Development of ramified microglia from early macrophages in the zebrafish optic tectum', *Developmental Neurobiology*, 73(1), pp. 60–71. Available at: https://doi.org/10.1002/dneu.22039.

Swire, M. *et al.* (2019) 'Endothelin signalling mediates experience-dependent myelination in the CNS', *eLife*, 8. Available at: https://doi.org/10.7554/eLife.49493.

Synofzik, M. *et al.* (2022) 'Preparing n-of-1 Antisense Oligonucleotide Treatments for Rare Neurological Diseases in Europe: Genetic, Regulatory, and Ethical Perspectives', *Nucleic Acid Therapeutics*, 32(2), pp. 83–94. Available at: https://doi.org/10.1089/nat.2021.0039.

Tada, Mari *et al.* (2016) 'Characteristic microglial features in patients with hereditary diffuse leukoencephalopathy with spheroids', *Annals of Neurology*, 80(4), pp. 554–565. Available at: https://doi.org/10.1002/ana.24754.

Takahashi, K. *et al.* (2006) 'Induction of Pluripotent Stem Cells from Mouse Embryonic and Adult Fibroblast Cultures by Defined Factors', *Cell*, 126(4), pp. 663–676. Available at: https://doi.org/10.1016/j.cell.2006.07.024.

Takashima, S. *et al.* (2021) 'Zebrafish model of human Zellweger syndrome reveals organ-specific accumulation of distinct fatty acid species and widespread gene expression changes', *Molecular Genetics and Metabolism*, 133(3), pp. 307–323. Available at: https://doi.org/10.1016/j.ymgme.2021.05.002.

The Lancet Diabetes Endocrinology (2019) 'Spotlight on rare diseases', *Lancet Diabetes Endocrinology*, 7(2), pp. 75-. Available at: https://doi.org/10.1016/S2213.

Tonduti, D. *et al.* (2016a) 'Clinical, radiological and possible pathological overlap of cystic leukoencephalopathy without megalencephaly and Aicardi-Goutières syndrome', *European Journal of Paediatric Neurology*, 20(4), pp. 604–610. Available at: https://doi.org/10.1016/j.ejpn.2016.03.009.

Tonduti, D. *et al.* (2016b) 'Clinical, radiological and possible pathological overlap of cystic leukoencephalopathy without megalencephaly and Aicardi-Goutières syndrome', *European Journal of Paediatric Neurology*, 20(4), pp. 604–610. Available at: https://doi.org/10.1016/j.ejpn.2016.03.009.

Torvund-Jensen, J. *et al.* (2018) 'The 3'UTRs of Myelin Basic Protein mRNAs Regulate Transport, Local Translation and Sensitivity to Neuronal Activity in Zebrafish', *Frontiers in Molecular Neuroscience*, 11. Available at: https://doi.org/10.3389/fnmol.2018.00185.

Traver, D. *et al.* (2003) 'The Zebrafish as a Model Organism to Study Development of the Immune System', in, pp. 254–330. Available at: https://doi.org/10.1016/S0065-2776(03)81007-6.

Tress, O. *et al.* (2011) 'Pathologic and Phenotypic Alterations in a Mouse Expressing a Connexin47 Missense Mutation That Causes Pelizaeus-Merzbacher–Like Disease in Humans', *PLoS Genetics*, 7(7), p. e1002146. Available at: https://doi.org/10.1371/journal.pgen.1002146.

Troy, S. *et al.* (2020) 'Pharmacokinetic Modeling of Intrathecally Administered Recombinant Human Arylsulfatase A (TAK-611) in Children With Metachromatic Leukodystrophy', *Clinical Pharmacology & Therapeutics*, 107(6), pp. 1394–1404. Available at: https://doi.org/10.1002/cpt.1752.

Turelli, P. *et al.* (2014) 'Interplay of TRIM28 and DNA methylation in controlling human endogenous retroelements', *Genome Research*, 24(8), pp. 1260–1270. Available at: https://doi.org/10.1101/gr.172833.114.

Ueda, H.R. *et al.* (2020) 'Tissue clearing and its applications in neuroscience', *Nature Reviews Neuroscience*, 21(2), pp. 61–79. Available at: https://doi.org/10.1038/s41583-019-0250-1.

Ulland, T.K. and Colonna, M. (2018) 'TREM2 — a key player in microglial biology and Alzheimer disease', *Nature Reviews Neurology*, 14(11), pp. 667–675. Available at: https://doi.org/10.1038/s41582-018-0072-1.

United Leukodystrophy Foundation (2021) *What is leukodystrophy?*

Vajn, K. *et al.* (2013) 'Axonal regeneration after spinal cord injury in zebrafish and mammals: differences, similarities, translation', *Neuroscience Bulletin*, 29(4), pp. 402–410. Available at: https://doi.org/10.1007/s12264-013-1361-8.

Valadez-Barba, V. *et al.* (2020) 'iPSC for modeling neurodegenerative disorders', *Regenerative Therapy*, 15, pp. 332–339. Available at: https://doi.org/10.1016/j.reth.2020.11.006.

Vanderver, A. *et al.* (2013) 'More Than Hypomyelination in Pol-III Disorder', *Journal of Neuropathology & Experimental Neurology*, 72(1), pp. 67–75. Available at: https://doi.org/10.1097/NEN.0b013e31827c99d2.

Vanderver, A. *et al.* (2015) 'Early-Onset Aicardi-Goutières Syndrome: Magnetic Resonance Imaging (MRI) Pattern Recognition', *Journal of Child Neurology*, 30(10), pp. 1343–1348. Available at: https://doi.org/10.1177/0883073814562252.

Vanderver, A. *et al.* (2020) 'Janus Kinase Inhibition in the Aicardi–Goutières Syndrome', *New England Journal of Medicine*, 383(10), pp. 986–989. Available at: https://doi.org/10.1056/NEJMc2001362.

Venegas, C. *et al.* (2017) 'Microglia-derived ASC specks crossseed amyloid-β in Alzheimer's disease', *Nature*, 552(7685), pp. 355–361. Available at: https://doi.org/10.1038/nature25158.

Verrips, A. *et al.* (2020) 'The safety and effectiveness of chenodeoxycholic acid treatment in patients with cerebrotendinous xanthomatosis: two retrospective cohort studies', *Neurological Sciences*, 41(4), pp. 943–949. Available at: https://doi.org/10.1007/s10072-019-04169-8.

Villamizar, N. *et al.* (2014) 'Effect of Lighting Conditions on Zebrafish Growth and Development', *Zebrafish*, 11(2), pp. 173–181. Available at: https://doi.org/10.1089/zeb.2013.0926.

Virgin, H.W. (2014) 'The virome in mammalian physiology and disease', *Cell*, 157(1), pp. 142–150. Available at: https://doi.org/10.1016/j.cell.2014.02.032.

Vogel, C. and Marcotte, E.M. (2012) 'Insights into the regulation of protein abundance from proteomic and transcriptomic analyses', *Nature Reviews Genetics*, 13(4), pp. 227–232. Available at: https://doi.org/10.1038/nrg3185.

Volkman, H.E. and Stetson, D.B. (2014) 'The enemy within: Endogenous retroelements and autoimmune disease', *Nature Immunology*, 15(5), pp. 415–422. Available at: https://doi.org/10.1038/ni.2872.

Voss, A.K. and Strasser, A. (2020) 'The essentials of developmental apoptosis', *F1000Research*. F1000 Research Ltd, pp. 148-undefined. Available at: https://doi.org/10.12688/f1000research.21571.1.

Voulgaris, D., Nikolakopoulou, P. and Herland, A. (2022) 'Generation of Human iPSC-Derived Astrocytes with a mature star-shaped phenotype for CNS modeling', *Stem Cell Reviews and Reports*, 18(7), pp. 2494–2512. Available at: https://doi.org/10.1007/s12015-022-10376-2.

Wada, R., Tifft, C.J. and Proia, R.L. (2000) 'Microglial activation precedes acute neurodegeneration in Sandhoff disease and is suppressed by bone marrow transplantation', *Proceedings of the National Academy of Sciences*, 97(20), pp. 10954–10959. Available at: https://doi.org/10.1073/pnas.97.20.10954.

Walsh, F. (2023) *UK's most expensive drug Libmeldy saved Teddi Shaw, but is too late for her sister*, *BBC News*.

Walsh, J. *et al.* (2021) 'Microglial activation and blood–brain barrier permeability in cerebral small vessel disease', *Brain*, 144(5), pp. 1361–1371. Available at: https://doi.org/10.1093/brain/awab003.

Walterfang, M. *et al.* (2020) 'Imaging of neuroinflammation in adult Niemann-Pick type C disease', *Neurology*, 94(16). Available at: https://doi.org/10.1212/WNL.0000000000009287.

Wang, Y. *et al.* (2014) 'Interleukin-1β induces blood-brain barrier disruption by downregulating sonic hedgehog in astrocytes', *PLoS ONE*, 9(10), pp. e110024-undefined. Available at: https://doi.org/10.1371/journal.pone.0110024.

Waxman, S.G. (1980) 'Determinants of conduction velocity in myelinated nerve fibers', *Muscle & Nerve*, 3(2), pp. 141–150. Available at: https://doi.org/10.1002/mus.880030207.

Weber, T. *et al.* (2020) 'Zebrafish disease model of human RNASET2 deficient cystic leukoencephalopathy displays abnormalities in early microglia', *Biology Open* [Preprint]. Available at: https://doi.org/10.1242/bio.049239.

Weber, T. and Köster, R. (2013) 'Genetic tools for multicolor imaging in zebrafish larvae', *Methods*, 62(3), pp. 279–291. Available at: https://doi.org/10.1016/j.ymeth.2013.07.028.

Weinstock, N.I. *et al.* (2020) 'Brainstem development requires galactosylceramidase and is critical for pathogenesis in a model of Krabbe disease', *Nature Communications*, 11(1), p. 5356. Available at: https://doi.org/10.1038/s41467-020-19179-w.

Wengler, G.S. *et al.* (1996) 'In-utero transplantation of parental CD34 haematopoietic progenitor cells in a patient with X-linked severe combined immunodeficiency (SCIDXI)', *Lancet* [Preprint]. Available at: https://doi.org/10.1016/S0140-6736(96)09392-0.

Wenstrom, K.D. *et al.* (1998) 'Elevated second-trimester amniotic fluid interleukin-6 levels predict preterm delivery', *American Journal of Obstetrics and Gynecology*, 178(3), pp. 546–550. Available at: https://doi.org/10.1016/S0002-9378(98)70436-3.

Wheeler, D.L. *et al.* (2018) 'Microglia are required for protection against lethal coronavirus encephalitis in mice', *Journal of Clinical Investigation*, 128(3), pp. 931–943. Available at: https://doi.org/10.1172/JCI97229.

Whitfield, T.T. (2002) 'Zebrafish as a model for hearing and deafness', *Journal of Neurobiology*, 53(2), pp. 157–171. Available at: https://doi.org/10.1002/neu.10123.

Wishnew, J. *et al.* (2014) 'Umbilical cord blood transplantation to treat Pelizaeus-Merzbacher disease in 2 young boys', *Pediatrics*, 134(5), pp. e1451–e1457. Available at: https://doi.org/10.1542/peds.2013-3604.

Withers, S.E. *et al.* (2023) 'Characterization of a mutant samhd1 zebrafish model implicates dysregulation of cholesterol biosynthesis in Aicardi-Goutières syndrome', *Frontiers in Immunology*, 14. Available at: https://doi.org/10.3389/fimmu.2023.1100967.

Wolf, H. *et al.* (2016) 'A mouse model for fucosidosis recapitulates storage pathology and neurological features of the milder form of the human disease', *Disease Models & Mechanisms*, 9(9), pp. 1015–1028. Available at: https://doi.org/10.1242/dmm.025122.

Wolf, N.I. *et al.* (2014) 'Clinical spectrum of 4H leukodystrophy caused by *POLR3A* and *POLR3B* mutations', *Neurology*, 83(21), pp. 1898–1905. Available at: https://doi.org/10.1212/WNL.0000000000001002.

Wolf, N.I. *et al.* (2020) 'Metachromatic leukodystrophy and transplantation: remyelination, no cross-correction', *Annals of Clinical and Translational Neurology*, 7(2), pp. 169–180. Available at: https://doi.org/10.1002/acn3.50975.

Woodcock, J. and LaVange, L.M. (2017) 'Master Protocols to Study Multiple Therapies, Multiple Diseases, or Both', *New England Journal of Medicine*, 377(1), pp. 62–70. Available at: https://doi.org/10.1056/NEJMra1510062.

Wright, T. *et al.* (2018) 'Nonclinical comparability studies of recombinant human arylsulfatase A addressing manufacturing process changes', *PLOS ONE*, 13(4), p. e0195186. Available at: https://doi.org/10.1371/journal.pone.0195186.

Wu, L. (2013) 'Samhd1 knockout mice: Modeling retrovirus restriction in vivo', *Retrovirology*, 10, p. 142. Available at: https://doi.org/10.1186/1742-4690-10-142.

Wu, X. *et al.* (2022) 'Development and clinical translation of ex vivo gene therapy', *Computational and Structural Biotechnology Journal*, 20, pp. 2986–3003. Available at: https://doi.org/10.1016/j.csbj.2022.06.015.

Xu, G.J. *et al.* (2015) 'Comprehensive serological profiling of human populations using a synthetic human virome', *Science*, 348(6239), p. aaa0698. Available at: https://doi.org/10.1126/science.aaa0698.

Xu, J. *et al.* (2016) 'Microglia Colonization of Developing Zebrafish Midbrain Is Promoted by Apoptotic Neuron and Lysophosphatidylcholine', *Developmental Cell*, 38(2), pp. 214–222. Available at: https://doi.org/10.1016/j.devcel.2016.06.018.

Yamada, T. *et al.* (2004) 'Therapeutic effects of normal cells on ABCD1 deficient cells in vitro and hematopoietic cell transplantation in the X-ALD mouse model', *Journal of the Neurological Sciences*, 218(1–2), pp. 91–97. Available at: https://doi.org/10.1016/j.jns.2003.11.006.

Yan, H. *et al.* (2022) 'Functional Study of TMEM163 Gene Variants Associated with Hypomyelination Leukodystrophy', *Cells*, 11(8), p. 1285. Available at: https://doi.org/10.3390/cells11081285.

Yang, F. *et al.* (2023) 'Identification of *POLR3B* biallelic mutations-associated hypomyelinating leukodystrophy-8 in two siblings', *Clinical Genetics*, 103(5), pp. 596–602. Available at: https://doi.org/10.1111/cge.14300.

Yeo, Y.A. *et al.* (2012a) 'CD137 ligand activated microglia induces oligodendrocyte apoptosis via reactive oxygen species', *Journal of Neuroinflammation*, 9, p. 173. Available at: https://doi.org/10.1186/1742-2094-9-173.

Yeo, Y.A. *et al.* (2012b) 'CD137 ligand activated microglia induces oligodendrocyte apoptosis via reactive oxygen species', *Journal of Neuroinflammation*, 9, p. 173. Available at: https://doi.org/10.1186/1742-2094-9-173.

Zanello, G. *et al.* (2023) 'Targeting shared molecular etiologies to accelerate drug development for rare diseases', *EMBO Molecular Medicine*, 15(7). Available at: https://doi.org/10.15252/emmm.202217159.

Zhang, S. *et al.* (2008) 'Inborn errors of interferon (IFN)-mediated immunity in humans: insights into the respective roles of IFN-α/β, IFN-γ, and IFN-λ in host defense', *Immunological Reviews*, 226(1), pp. 29–40. Available at: https://doi.org/10.1111/j.1600-065X.2008.00698.x.

Zhao, C. *et al.* (2024) 'Macrophages in tissue repair and regeneration: insights from zebrafish', *Cell Regeneration*. Springer. Available at: https://doi.org/10.1186/s13619-024-00195-w.

Zhao, M. *et al.* (2022) 'Knockdown of myorg leads to brain calcification in zebrafish', *Molecular Brain*, 15(1), p. 65. Available at: https://doi.org/10.1186/s13041-022-00953-4.

Zhou, Y. *et al.* (2023) 'Human early-onset dementia caused by DAP12 deficiency reveals a unique signature of dysregulated microglia', *Nature Immunology*, 24(3), pp. 545–557. Available at: https://doi.org/10.1038/s41590-022-01403-y.

Zizioli, D. *et al.* (2014) 'Molecular cloning and knockdown of galactocerebrosidase in zebrafish: New insights into the pathogenesis of Krabbe's disease', *Biochimica et Biophysica Acta (BBA) - Molecular Basis of Disease*, 1842(4), pp. 665–675. Available at: https://doi.org/10.1016/j.bbadis.2014.01.008.

Zottoli, S.J. *et al.* (1995) 'Comparative studies on the Mauthner cell of teleost fish in relation to sensory input.', *Brain, behavior and evolution*, 46(3), pp. 151–64. Available at: https://doi.org/10.1159/000113268.

Appendices

Appendix 1. Acoustic startle response in transplanted *rnaset2* mutants

Data presented in Chapter 3 (section 3.3.2.2) demonstrates that untreated *rnaset2* mutants also show abnormal startle responses, whereby mutant larvae swim significantly further following exposure to acoustic stimuli. As such, I next sought to investigate the effects of transplantation on this startle reflex. Interestingly, in this assay, non-transplanted *rnaset2* mutants showed subtle reductions in both distance and displacement relative to wild type siblings following auditory stimulus (Figure S) – in opposition to previous findings. However, transplantation appeared to increase response distance and displacement in *rnaset2* mutants – with transplanted *rnaset2* larvae swimming even further distances than wild types (wild type non-depleted sham: 71.19±4.861; *rnaset2* non-depleted transplanted: 109.8±14.98; *rnaset2* microglia-depleted transplanted: 218.0±32.38 [mean ± SEM]). Trial-by-trial analysis confirmed a general trend for transplanted animals to travel increased distances following each auditory stimulus (particularly for microglia-depleted, transplanted *rnaset2* mutants) (Figure S). Notably, all comparisons are exploratory as no statistical analysis could be performed due to insufficient biological repeats. Nonetheless, macrophage transplantation appears to increase the motor output of *rnaset2* mutant larvae in this startle response assay.

However, several factors make this experiment difficult to interpret. Firstly, this assay was only repeated twice, marking any statistical comparisons impossible. This is particularly important to consider given the broad spread of the data, suggesting large variability in this assay.

Secondly, the behaviour of untreated mutants in this experiment – whereby they appear to swim slighter lesser distances relative to wild type – is in direct contrast to the data described in section 3.3.2.2, where *rnaset2* mutants swam further than wild type controls. However, this may be explained by differences in the treatment of these larvae across the two studies. As a control for transplantation, *rnaset2* mutants were sedated at both 2dpf (for sham transplantation) and 5dpf (for screening of endogenous microglia-depletion), as well as undergoing the procedure for sham transplantation itself (injection of cell-free buffer into the duct of Cuvier). Each of these factors may have affected larval behaviour across all groups – as demonstrated by slight reductions in swimming distance of wild type sham animals in this experiment (71.19±4.861 [mean ± SEM]) relative to untreated wild types (93.62±14.46 [mean ± SEM]), which were completely untouched other than daily welfare checks and feeds from 5– to 8dpf. Given the neuropathology already present in *rnaset2* mutants by 8dpf, it is possible that these larvae were particularly susceptible to the effects of anaesthesia and the small injection site injury, which reduced their swimming behaviour (*rnaset2* untreated: 105.6±10.59;

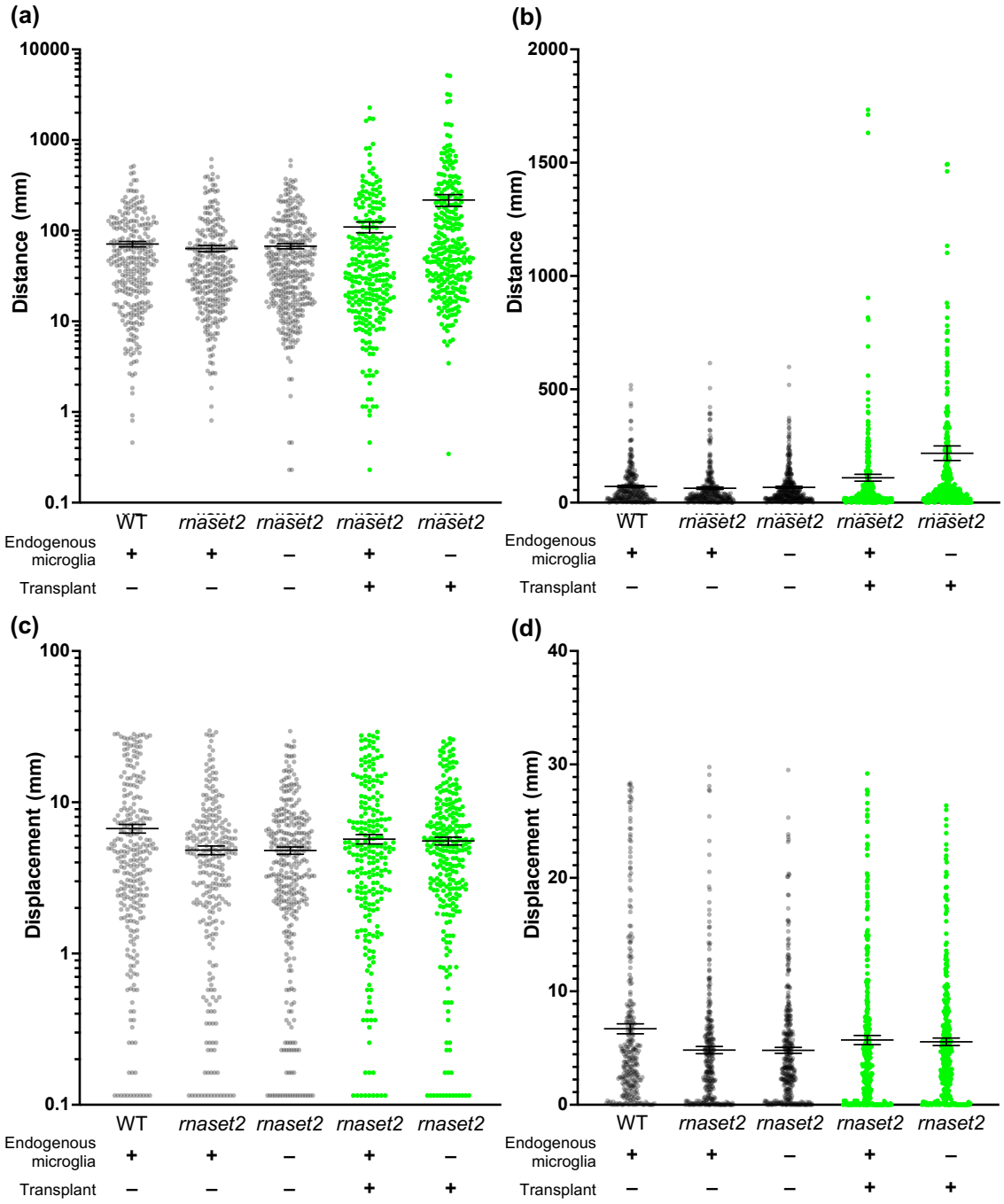

Figure S1. Transplanted *rnaset2* mutants may swim increased distances in response to acoustic stimuli, relative to non-transplanted controls.

Fast-cam analysis suggests transplanted *rnaset2* mutants show increased swimming distance (a, b) and displacement (c, d) by relative to non-transplanted mutants in acoustic startle assay at 8dpf. Data are shown with a linear (a, c) and logarithmic scale (b, d) for clarity. Two biological repeats, n=30 per group. Each data point reflects the movements of each fish in a single trial. No statistical analysis performed.

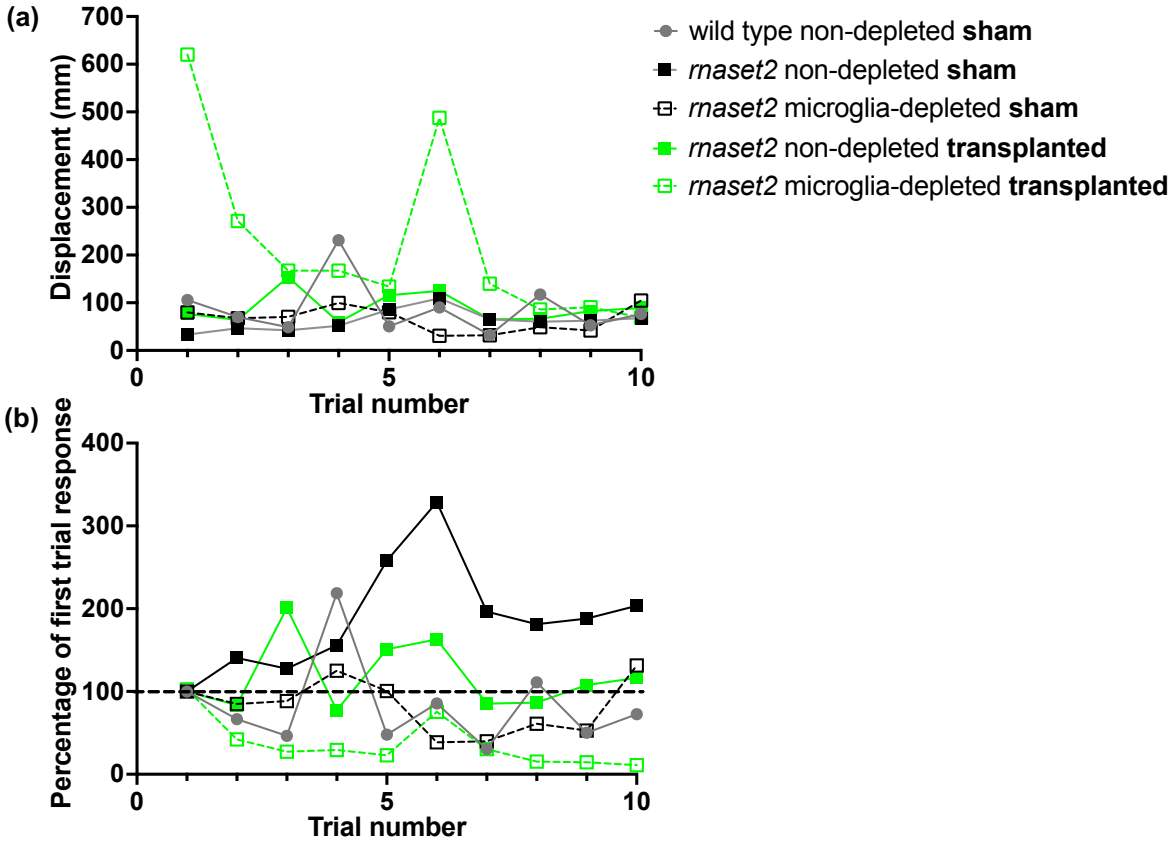

Figure S2. Trial-by-trial comparison of transplanted larvae startle displacement.
a, b. Startle response of 8dpf embryos as total displacement (a) and percentage of first trial response (b) across all ten trials. Dashed line indicates 100% of first trial response (b).

rnaset2 non-depleted sham: 63.60±4.990 [mean ± SEM]). As such, these groups may not be entirely comparable, and future work should consider including an untreated wild type and mutant group as an additional control.

Finally, it is unclear what such a drastic increase in startle response may mean in transplanted animals, if it is indeed a real biological effect. In Chapter 3, trial-by-trial analysis suggested that increased startle response of *rnaset2* mutant larvae may be due to a failure to habituate to the auditory stimulus (see section 3.3.2.2). To some extent, the current study supports this finding – with *rnaset2* non-depleted sham larvae seemingly swimming increasing distances with each stimulus repeat. However, there is little convincing evidence in this data to suggest that the increased swimming distance by transplanted animals is due to a failure of auditory habituation, for several reasons. Firstly, it must be noted that habituation by wild type larvae in this assay is much less pronounced than in untreated animals, perhaps because of anaesthesia or injection as discussed above. Secondly, while the magnitude of startle response in *rnaset2* non-depleted transplanted larvae remains largely similar throughout – which could be interpreted as a failure to habituate – this contrasts with the increasing response of their sham counterparts with each passing stimulus, suggesting a distinct behavioural response. Finally, microglia-depleted transplanted *rnaset2* mutants do seemingly show a reduced startle response with each subsequent exposure to auditory stimulus as quantified by percentage of first response, the absolute magnitude of response is far greater – with transplanted animals swimming distances over six times further than microglia-depleted shams in the first trial. As such, the increase in swimming behaviour in transplanted larvae is unlikely to be due to failure to habituate but may rather reflect general hypersensitivity to acoustic stimuli or hyperactivity overall. Therefore, future work may explore further assays to understand whether transplantation is able to rescue the full range of *rnaset2* mutant behavioural deficits.

Nonetheless, the current study suggests that macrophage transplantation is sufficient to rescue the most robust behavioural phenotype observed in *rnaset2* mutants – free swimming deficits.

Appendix 2. RNA sequencing of transplanted *rnaset2* mutants

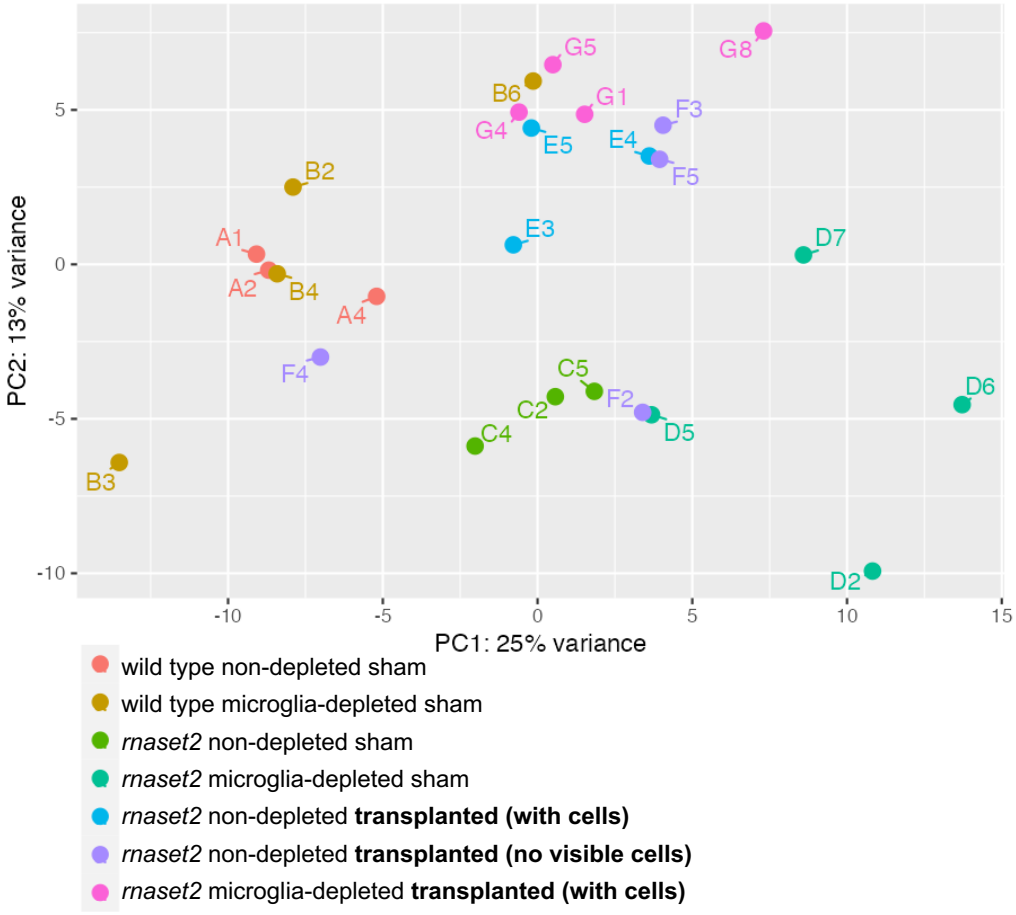

Figure S3. Principle component analysis (PCA) plot reveals clustering of all experimental groups.

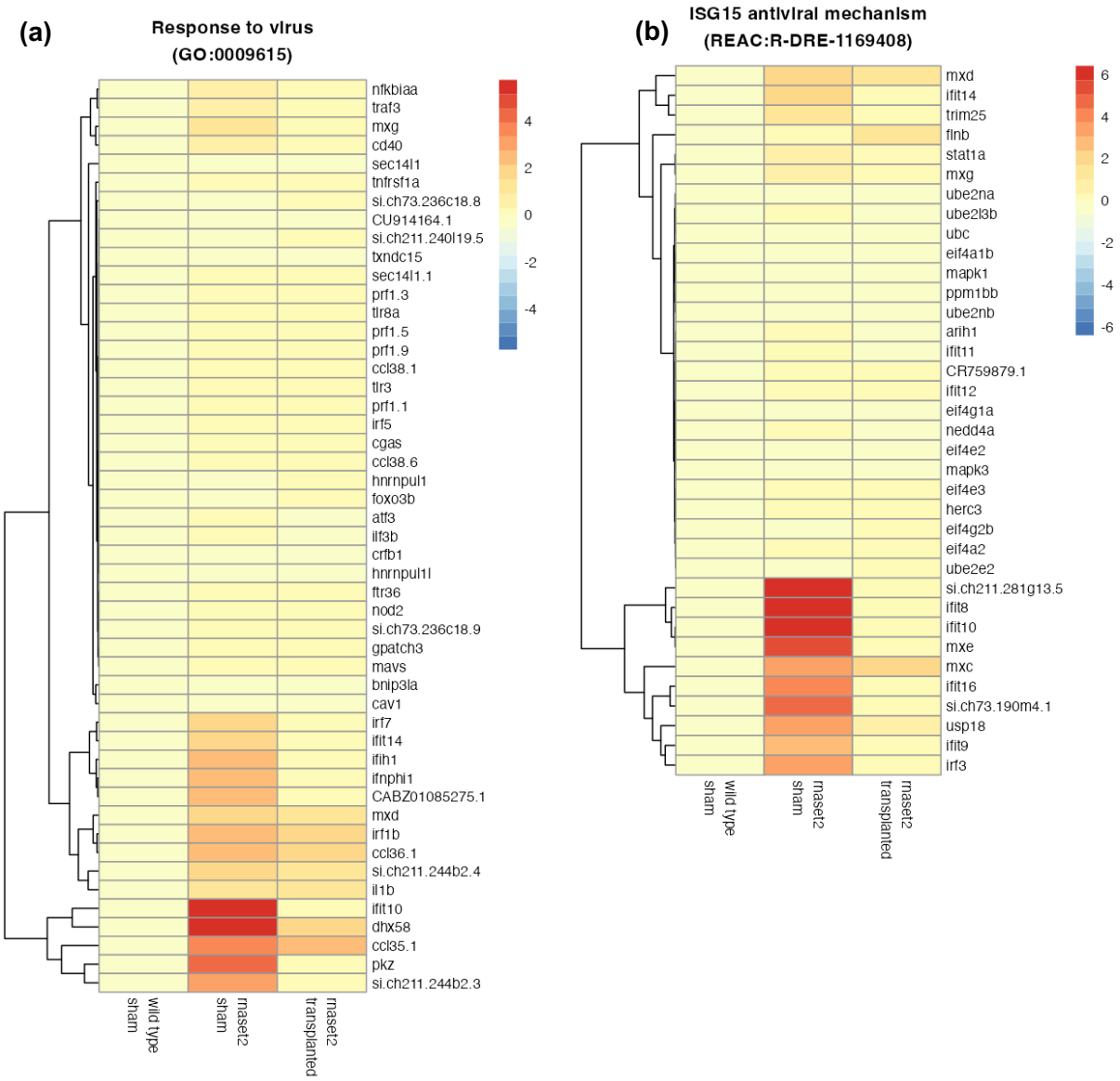

Figure S4. Complete heatmap of genes belonging to response to virus and ISG15 antiviral mechanism GO pathways for microglia-depleted animals.
Fold change relative to wild type sham is indicated by color, with red indicating higher expression.

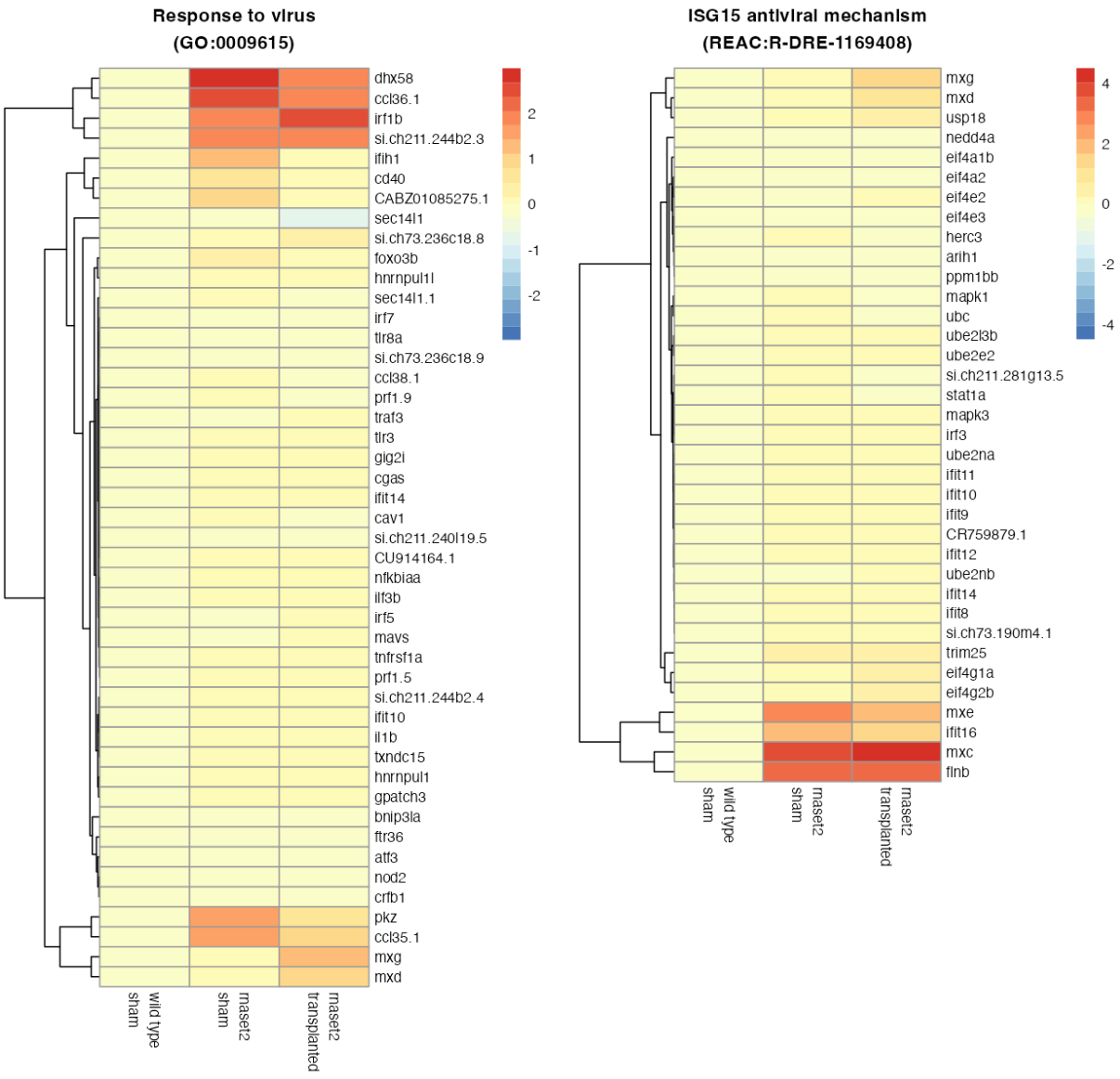

Figure S5. Complete heatmap of genes belonging to response to virus and ISG15 antiviral mechanism GO pathways for nondepleted animals.
Fold change relative to wild type sham is indicated by color, with red indicating higher expression.

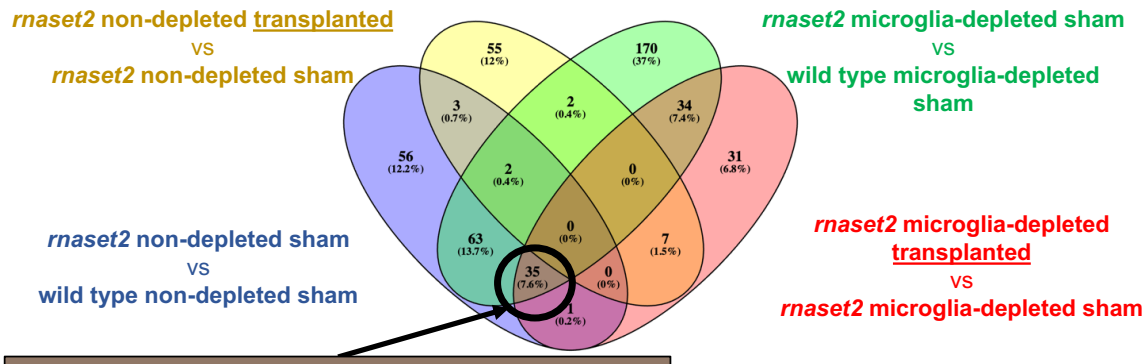

Common differentially expressed genes in "***rnaset2* sham versus wild type sham** (non-depleted)", "***rnaset2* sham versus wild type sham** (microglia-depleted)" and "***rnaset2 transplanted* versus *rnaset2* sham** (microglia depleted)"

Common differentially expressed genes		log2 fold change		
Gene ID	Gene name and description	rnaset2 non-depleted sham vs wild type non-depleted sham	rnaset2 microglia-depleted sham vs wild type microglia-depleted sham	rnaset2 microglia-depleted transplanted vs rnaset2 microglia-depleted sham
hsp70.3	heat shock cognate 70-kd protein, tandem duplicate 3	3.61483711	4.14638006	-2.3012348
zgc:152658		3.59026991	5.47945295	-4.0613336
ftr80	finTRIM family, member 80	3.20107317	9.73477105	-2.7050295
mov10b.2	Mov10 RNA helicase b, tandem duplicate 2	3.04125768	4.60635437	-2.6521576
ifi46	interferon alpha inducible protein 27.4; involved in apoptotic signaling	3.03974896	5.93453253	-3.1266304
dhx58	DEXH (Asp-Glu-X-His) box polypeptide 58	2.98355584	5.21406078	-2.92646
ifi44a1	interferon induced protein 44a1	2.93716862	5.30102727	-2.186786
cmpk2	cytidine monophosphate (UMP-CMP) kinase 2, mitochondrial	2.4852425	6.72952931	-2.7283764
zmp:0000000912	Orthologous to human GVINP1 (GTPase, very large interferon inducible pseudogene 1)	2.47786513	6.73690269	-2.4313241
xaf1	XIAP associated factor 1; predicted to be involved in apoptotic process	2.19397855	4.28539977	-2.5620554
hsp70.2	heat shock cognate 70-kd protein, tandem duplicate 2	2.14680551	3.3063556	-1.7937952
hsp70.1	heat shock cognate 70-kd protein, tandem duplicate 1	2.03927066	3.31141633	-1.9570956
mov10b.1	Mov10 RNA helicase b, tandem duplicate 1	2.03484176	5.69965334	-3.0490961
si:ch211-244b2.3		2.00580703	3.26498344	-1.622009
ifi44f5	interferon-induced protein 44f5	1.99240109	3.90401016	-3.0199251
cd68	Cluster of Differentiation 68; highly expressed by cells in the monocyte lineage including circulating macrophages and tissue macrophages	1.8089268	2.54949061	-1.6337118
btr26	bloodthirsty-related gene family, member 26	1.75722409	3.94238354	-2.2256046
marco	macrophage receptor with collagenous structure; involved in defense response to bacterium and phagocytosis	1.74334917	2.78962379	-1.8726118
LO018432.1 (xgb)	x globin	1.70350307	3.95857414	-2.5438836
CU984600.2		1.69895919	6.04000491	-3.6758515
cxcl18b	chemokine (C-X-C motif) ligand 18b	1.6685246	2.89956914	-1.313528
FO704622.1		1.66076255	4.46964561	-2.3452211
ifi44f3	interferon induced protein 44f3	1.57460269	2.79857666	-1.2636454
samd9l	sterile alpha motif domain containing 9 like	1.57132438	3.20143361	-1.7224258
rsad2	radical S-adenosyl methionine domain containing 2; response to virus	1.36573512	3.91783275	-2.4056179
si:dkey-97a13.6		1.3356579	3.36524484	-2.028989
ssuh2.2	ssu-2 homolog, tandem duplicate 2	1.21515593	3.57558979	-2.2700297
grna	granulin a; involved in axon extension	1.19313369	1.57935188	-1.1215752
lgals9l3	lectin, galactoside-binding, soluble, 9 (galectin 9)-like 3	1.17454096	2.69146573	-1.9772003
ifih1	interferon induced with helicase C domain 1; human ortholog(s) of this gene implicated in Aicardi-Goutieres syndrome	1.16207005	2.4762452	-1.5977307
gig2o	grass carp reovirus (GCRV)-induced gene 2o	1.13674167	2.32639294	-1.2622741
stat2	signal transducer and activator of transcription 2	1.13073422	3.409764	-2.6807286
phf11	PHD finger protein 11	1.09895054	3.42625887	-2.1587056
ifi27.7	interferon alpha inducible protein 27.7; involved in apoptotic signaling	1.04906825	2.59042203	-1.8404827
ascl1b	achaete-scute family bHLH transcription factor 1	1.01165743	3.05373251	-2.0993539

Figure S6. Common differentially expressed genes between rnaset2 transplanted versus *rnaset2* sham, and *rnaset2* sham vs wild type sham samples (with and without microglia depletion). Adapted from Venny 2.1.0. Adapted from Venny 2.1.0. Highlighted genes indicate those involved in interferon response as identified by ZFIN (https://zfin.org/) or Levraud *et al.,* 2019. Bold genes were taken forward for validation.